INTEGRATED CATALYSIS FOR UPGRADING MICROBIAL DERIVED CARBOXYLIC ACIDS TO RENEWABLE FUELS AND VALUE-ADDED CHEMICALS

BY

DEREK R. VARDON

DISSERTATION

Submitted in partial fulfillment of the requirements
for the degree of Doctor of Philosophy in Environmental Engineering in Civil Engineering
in the Graduate College of the
University of Illinois at Urbana-Champaign, 2015

Urbana, Illinois

Doctoral Committee:

Professor Timothy J. Strathmann, Chair and Director of Research
Professor Vijay Singh
Assistant Professor Jeremy S. Guest
Research Engineer Gregg T. Beckham

ABSTRACT

In order to transition to a renewable carbon society, economically and environmentally sustainable technologies are needed to displace our dependence on petroleum. Carboxylic acids are a diverse class of biological metabolites that can be converted to renewable fuels and chemicals to offset our consumption of petroleum. However, significant challenges occur when integrating catalysis with biological processes, which include: (1) biological conversion produces carboxylic acids at relatively dilute levels (<20 wt%) in broth that can contain residual impurities, creating separation and downstream process challenges, (2) microbial acids can contain unique chemical moieties (e.g., polyunsaturated bonds, hydroxyl groups, ester linkages) compared to aliphatic petroleum, requiring tailored catalytic upgrading strategies to produce fuels and chemicals, and (3) carboxylic acid valorization can occur through a multitude of unit process schemes, necessitating early-stage techno-economic analysis to identify key bottlenecks for further development. To address these challenges, this thesis investigates integrated catalysis for upgrading microbial derived acids to renewable fuels and value-added chemicals.

To target both renewable fuels and value-added chemicals from microbial acids, the following research objectives were pursued: (1) hydrothermal catalysis was investigated for deoxygenating monocarboxylic acids to diesel-grade hydrocarbons with *in situ* hydrogen production from renewable organic donors, (2) separation and catalysis was examined for recovering and *cis,cis*-muconic acid from culture broth and converting it to adipic acid, the latter compound being a high-value polymer precursor for nylon-6,6 production, and (3) key economic drivers and technical targets were identified for the downstream processing of muconic acid to adipic acid using preliminary techno-economic analysis.

Initially, hydrothermal catalysis was investigated for converting long chain saturated and unsaturated carboxylic acids to hydrocarbon fuels using a Pt-Re catalyst supported on activated carbon (AC). The addition of Re as a secondary metal was shown to enhance the rate of carboxylic acid deoxygenation and modify the chemisorption behavior of Pt, suggesting alloy formation. Decarboxylation/decarbonylation of the carboxylate group was observed as the primary reaction pathway, and characterization of the Pt-Re/AC catalyst by x-ray photoelectron spectroscopy determined that hydrogen in the headspace resulted in a reduced oxidation state of the metals after exposure to hydrothermal conditions. Lastly, the addition of glycerol as an *in situ* hydrogen donor proved effective at meeting process hydrogen demands through aqueous phase reforming reactions.

The application of the Pt-Re/AC catalyst system was then evaluated using a complex monocarboxylic acid feedstock derived biologically from lignin. The microorganism *Pseudomonas putida* KT2440 was initially used to biologically "funnel" lignin derived monomers to intracellular medium chain length polyhydroxyalkanoates (*mcl*-PHAs). Shake flask studies demonstrated that *P. putida* produces *mcl*-PHAs from both mixed model compounds and complex lignin derived monomers derived from corn stover. Extraction and characterization of lignin derived *mcl*-PHAs showed similar physicochemical properties compared to *mcl*-PHAs produced from clean glucose, and thermal depolymerization readily converted *mcl*-PHAs to alkenoic acid monomers. Subsequent catalytic processing of alkenoic acids in hydrothermal media with Pt-Re/AC produced linear hydrocarbons, similar to the model compound fatty acid study, demonstrating the integrated biological and catalytic conversion of lignin to hydrocarbon fuel.

In order to target value-added chemicals from microbial acids, the downstream separation and catalytic upgrading of *cis,cis*-muconic was evaluated for the production of adipic acid, the latter molecule being a high-value polymer precursor for nylon-6,6 production. Expanding on previous work, a metabolically engineered strain of *P. putida* KT2440 was used to produce muconic acid extracellularly from both model and lignin derived monomers. Following fed-batch biological conversion of *p*-coumaric acid, activated carbon purification was shown to effectively remove broth non-target upstream metabolites, color compounds, and unconverted substrate. Muconic acid was then recovered from culture broth by pH/temperature shift crystallization in high purity (>97%) and yield. Catalyst batch screening studies of commercial Pd, Pt, Ru identified Pd as a highly active metal for muconic acid hydrogenation, although leaching was observed.

As a follow-up, the downstream separation and catalysis of muconic acid was further examined to improve the separation purity, evaluate catalyst stability, and demonstrate bio-adipic acid polymerization to nylon-6,6. Following crystallization, dissolution of muconic acid crystals in ethanol with membrane filtration removed insoluble inorganic salts, producing muconic acid at 99.8% purity. In house catalysts were synthesized on both carbon and silica supports and tested in batch hydrogenation screening reactions. Pd and Rh were identified as highly active on both carbon and silica supports when compared to Ru and Pt, although Pd leached significantly, with a greater extent on silica. To further evaluate the stability of Rh/AC, continuous trickle bed hydrogenation demonstrated steady state partial conversion for 48 h, followed by complete conversion until 96 h, with a return to partial steady state conversion for 120 h of time on stream. Characterization of the post reaction Rh/AC catalyst showed a modest increase in support surface area and pore volume, moderate loss in active metal surface area, and minor increase in

metal crystallite size. Bio-adipic acid derived catalytically from muconic acid was then polymerized to nylon-6,6, and characterization of the polymer confirmed properties comparable to nylon produced from adipic acid of petrochemical origin.

Lastly, preliminary techno-economic analysis was conducted to evaluate key economic drivers and technical targets for the downstream processing of muconic acid to adipic acid. An n^{th}-generation downstream plant was modeled to produce 75 million kg of adipic acid per year. For the base-case process model, the following technical parameters were employed: cell free culture broth containing 50 g/L muconate and 2 g/L of non-target aromatic compounds was purified continuously with activated carbon. Muconic acid was then recovered by pH/temperature shift crystallization, dissolved in ethanol, and filtered to provide a condensed phase for catalytic processing. Muconic acid in ethanol was catalytically converted to adipic acid over a packed bed reactor containing 2%Rh/AC, and a second train of evaporative crystallization with rotary filtration and drying recovered adipic acid as the final product. The largest capital costs for the base case model were activated carbon regeneration kilns and the packed bed hydrogenation reactor. Variable operating costs were comparable throughout, excluding the cost of incoming muconate broth which was the largest variable expense by far. Economic analysis of the base case model determined a minimum selling price of bio-based adipic acid of $1.90/kg, within the 5-year historical range ($1.75-2.50/kg) for petroleum derived adipic acid. Lastly, single point sensitivity analysis determined that the broth ratio of muconate to non-target aromatic compounds was a major non-linear cost driver, as well as the required reactor throughput for the 2%Rh/AC catalyst.

Overall, this thesis demonstrated that integrated catalysis can convert both model and complex microbial acids derived from lignocellulosic feedstocks to renewable fuels and value-

added chemicals. Upstream biological funneling is uniquely suited to address the heterogeneity of complex biomass monomer streams, while tailored separation schemes have potential to produce carboxylate feedstocks of suitable purity for value-added chemical production. The unique functional moieties of microbial acids will require tuned reaction conditions and catalytic formulations depending when targeting renewable fuels and chemicals, while the challenges of substrate acidity, residual impurities, and potentially harsh reactions conditions will require robust catalyst development.

To Rejill and Kaleb

ACKNOWLEDGEMENTS

I would like to thank the many people who have helped me throughout my dissertation. First and foremost, I would like to thank my wife, Jill, and my son, Kaleb. Kaleb, you're awesome and the reason for my focus, drive, and dedication. I love you both. Certainly this would not have been possible without my advisor, Prof. Timothy Strathmann, and his willingness to support my efforts and offer critical feedback throughout my thesis. I am also especially grateful to Dr. Gregg Beckham at the National Renewable Energy Laboratory (NREL) for integrating me into his research group, encouraging me to set my scientific sights high, and sharing a never-ending enthusiasm for science. I would also like to thank Dr. BK Sharma and John Scott at the Illinois Sustainable Technology Center, for opening their laboratory doors, providing outstanding scientific insight and assistance, as well as for their personal support and encouragement. In addition, I am greatly indebted to all of my colleagues and team members at NREL, especially Dr. Eric Karp, Dr. Mary Biddy, Dr. Mary Ann Franden, Dr. Christopher Johnson, Dr. Jeffrey Linger, Dr. Michael Guarnieri, and Dr. Peter Ciesielski, as well as numerous others. I would also like to thank Prof. Vijay Singh for serving on my defense committee, as well as Prof. Jeremy Guest for both serving on my committee and supporting my teaching experience. Last, but not least, I would also like to thank Prof. David Ladner and Prof. Manish Kumar, who collectively inspired me to pursue a career in research after exiting the military, albeit at the expense of being an architect.

TABLE OF CONTENTS

CHAPTER 1

INTRODUCTION

1.1 Motivation

The need for sustainable carbon-based fuels and chemicals is increasingly evident with the growing population, energy demand, and associated environmental impact. Over 90 million barrels of petroleum are consumed daily, resulting in 57% of global greenhouse gas (GHG) emissions from fossil fuel use.[1] Likewise, catalytic processing of petroleum to chemicals and materials results in ~10% of the global energy demand and ~7% of global GHG emissions.[2] The conversion of lignocellulosic feedstocks offers a potential source of renewable carbon for offsetting our current petrochemical consumption, without competing for agricultural resources used for food production.[3–5] Significant technological strides have been made within recent decades to advance a lignocellulose biorefinery scheme, where incoming biomass is "refined" to produce renewable fuels, and more recently renewable chemicals.[6] Recent analysis has shown that as light-duty vehicles transition to electric and hybrid drivetrains, heavy-duty vehicle fuel consumption (e.g., diesel- and aviation-grade hydrocarbon fuels) is expected to grow.[7,8] As such, renewable hydrocarbon fuels are being targeted within a biorefinery.[9] Furthermore, the co-production of value-added chemicals can potentially offset the economic costs associated with renewable hydrocarbon production, providing a two-fold path for biomass valorization.[9] Therefore, this research examines the integrated catalytic upgrading of microbial derived carboxylic acids to target both hydrocarbon fuels and chemicals within the context of a biorefinery.

1.2 Background

Conventional technology pathways for valorizing biomass typically apply an "either-or" approach via biological or chemo-catalytic routes. For example, biological fermentation of cellulosic sugars to ethanol has been developed at the pilot scale, and more recently commercial scale.[10,11] In accord, academic research is pursuing novel engineered metabolic pathways to biologically produce fuels, such as bisobolene[12] and farnesol,[13] from sugars. Biological processing provides unique advantages since microorganisms have evolved highly efficient enzymatic pathways to convert heterogeneous lignocellulosic monomers to metabolites.[14,15] However, in many scenarios the high oxygen content and unique functionality of these biologically derived molecules limits their direct replacement of conventional petroleum derived products.[12,16,17] Conversely, chemo-catalytic processing can directly convert biomass to fuels through routes such as catalytic fast pyrolysis and bio-syngas reforming.[11] In parallel, academic researchers are pursing the direct catalytic conversion of sugars to hydrocarbon fuels and platform chemicals, such as γ-valerolactone.[18] Chemo-catalytic processing is advantageous due to the high throughput and targeted selectivity when starting with simple substrate molecules. However, the heterogeneity of biomass, high water content, and numerous poisons present significant challenges to catalysis. To overcome the limitations of single approach, we propose a hybrid biological and chemo-catalytic strategy that uses microorganisms to funnel diverse biomass monomers to target metabolites, and subsequently upgrade these metabolites catalytically to renewable fuels and chemicals with high throughput and selectivity.

Microorganisms produce and utilize carboxylic acids throughout central metabolism to generate and store energy, as shown in **Figure 1.1**. This includes (1) multiple intermediates along the citric acid cycle for energy production, such as succinic acid, (2) triglycerides and

polyhydroxyalkanoates for energy storage,[19,20] and (3) more novel acids, such as muconic acid, that are generated through the β-ketoadipate pathway when metabolizing aromatic molecules.[21,22] These acids can be produced with native and engineered microorganisms, generating a wide array of potential products for downstream catalytic upgrading. Energy storage acids, such as medium and long chain monocarboxylic acids, contain highly reduced aliphatic chains that can serve as precursors to renewable hydrocarbon fuels. In addition, highly oxygenated dicarboxylic acids are promising precursors for renewable polymers, since their dual terminal functionality allows for facile polymerization reactions.[23] Despite the potential of microbial acids, the aqueous environment of microbial conversion presents unique downstream processing challenges due to cost associated with separation, incompatibility of water with conventional petrochemical catalytic processes, and the elevated-boiling point of highly oxygenated bio-molecules.[24,25]

Subcritical hydrothermal media (250-374°C, 5-20 MPa) is a promising solvent for bio-based chemical reactions since it is compatible with high-moisture feedstocks. Heating water under saturation conditions avoids the significant latent heat of vaporization associated with drying, resulting in potential energy savings.[26,27] In hydrothermal media, polymerized lipids rapidly hydrolyze to form free fatty acids,[28,29] and in the case of acylglycerides, glycerol is liberated for further use as a potential renewable in situ hydrogen donor. Deoxygenation of the carboxylic group converts monocarboxylic acids to linear hydrocarbon, providing an ideal fuel replacement. Once fatty acids are deoxygenated, a self-separating hydrocarbon organic phase forms at ambient conditions, facilitating downstream separations. Despite the potential of hydrothermal catalysis, work on lipid deoxygenation has been limited to the conversion of saturated fatty acids with monometallic catalysts under inert atmospheres. Although saturated fatty acids rapidly deoxygenate under an inert atmosphere, unsaturated fatty acids are only hydrogenated to their

saturated counterpart, with no significant deoxygenation.[30,31] Significant work remains to determine the use of hydrogen to facilitate unsaturated fatty acid reduction and influence the reaction pathway and kinetics, as well as the potential for utilizing renewable hydrogen donors, such as glycerol, to support process hydrogen demand.

Bimetallic catalysts enhance multiple classes of reactions, but to our knowledge the impact on fatty acid deoxygenation with *in situ* hydrogen production has not been explored. Previous efforts to convert glycerol to hydrogen by aqueous phase reforming have demonstrated that enhanced production can be achieved by adding Re to Pt.[32,33] It has been proposed that the secondary metal addition produces an alloy with reduced affinity for CO, as supported by CO chemisorption.[34,35] CO is known to adsorb strongly to bare Pt surfaces, and its reduced affinity facilitates rapid turnover during the water gas shift (WGS) reaction to produce carbon dioxide and hydrogen. In a similar vain, past efforts by our group utilized the oxophilic character of Re to enhance the catalytic performance of Pd for perchlorate reduction for water treatment applications.[36] Re's preferential coordination with oxygenated moieties was proposed to be the key step,[37] although its ability to coordinate carboxylic acid functional groups for deoxygenation is unknown. In addition, the effect of hydrothermal water on the stability of bimetallic catalyst materials has been poorly studied. Previous reports using alumina and silica supports in hydrothermal media have shown dramatic reductions in surface area, lending preference to carbon-based supports.[38] Hydrothermal media can also greatly influence the oxidation state of metal catalysts,[39] which dramatically alters their performance. Control over the oxidation state of catalytic materials is key to promoting optimum turn over frequencies (TOFs),[36] since the interaction of active sites and chemical reactants can be dictated by the electronics of the upper few nanometers of metal crystallites.

In contrast to targeting hydrocarbon fuels from monocarboxylic acids, dicarboxylic acids possess dual terminal functionality for producing renewable polymers, with muconic acid being an ideal candidate. Dicarboxylic acids have received significant attention in recent years as renewable platform chemicals, since they are readily derived from glucose via the citric acid cycle (**Figure 1.1**). Our group has recently identified muconic acid as a promising dicarboxylic acid that can be produced biologically from lignin monomers, as shown in **Figure 1.2**. Within a biorefinery scheme, lignin is typically relegated to direct heat and on site power generation.[40,41] Recent techno-economic and life cycle analysis at NREL has determined that significant economic and GHG savings can result if lignin is diverted to value-added chemicals.[9] In particular, muconic acid can be readily hydrogenated to adipic acid, with the latter being the most commercially abundant dicarboxylic acid.[42] Adipic acid has a global market size of over 3 million tons per year and a value of $1700 USD per ton,[9] significantly greater than diesel fuel ($1080 USD per ton)[1] and ethanol ($610 USD per ton).[1] Conventional adipic acid production relies on the nitric acid oxidation of petroleum-derived cyclohexane, resulting in 5-8% of global N_2O emissions, a potent GHG.[43] By producing adipic acid renewably from lignin via muconic acid, significant environmental benefits result due to petrochemical product displacement. In addition, adipic acid can serve as a platform molecule for other renewable chemicals, including caprolactone, cylcopentanone, and hexanediol (**Figure 1.3**), with applications as polymer building blocks, solvents, and fuel precursors.[44–47]

Previous efforts to produce muconic acid have been limited to model glucose feedstocks, with cursory emphasis on downstream separations and catalysis. The use of glucose as a carbon source allows for facile downstream separation strategies, such as crystallization, that assume a high solubility of the initial carbon substrate (e.g., glucose) and non-target metabolites (e.g.,

acetic acid, formic acid) compared to the target product.[48] In the case of utilizing lignin-derived monomers as a carbon substrate (e.g., coumaric acid, caffeic acid, vanillic acid) for muconic acid production, the aromatic ring and carboxylic side chains results in solubilities highly sensitive to pH,[48] similar to the target product. As such, adsorptive separation using activated carbon is a promising approach for removing non-target aromatic metabolites unique to lignin valorization. Activated carbon is commonly used to remove color and protein compounds from fermentation broth,[49] and has a long history in environmental remediation applications for removing aromatic acids from aqueous streams.[50,51] However, to our knowledge the purification and crystallization of muconic acid derived from lignin has yet to be examined in the peer-reviewed literature.

Following recovery of muconic acid from the culture media, catalytic hydrogenation is required to produce renewable adipic acid. Downstream catalytic processing is greatly influenced by the presence of non-target constituents and catalyst poisons,[52] necessitating detailed characterization of the incoming feed stream; to date, catalytic hydrogenation of muconic acid has been limited to glucose derived feedstocks and demonstration reactions to complete conversion.[53,54] The impact of fermentation impurities on the final product quality was not addressed, and catalytic activity parameters were not evaluated. Further development is required advance downstream muconic acid processing, including catalyst activity screening, analysis of surface reaction controlled kinetics, influence of reaction conditions, and stability with time on stream.

In order for biomass valorization technologies to have a significant positive impact on society, the pathways must be environmentally sustainable and economically competitive with conventional processes. Techno-economic analysis has been used extensively for understanding the influence of key cost drivers within an integrated biorefinery scheme and estimating the final

product price.[55,56] For hybrid bio-catalytic processing, major cost drivers include feedstock utilization, biological conversion yields and titers, separations, catalytic upgrading, and capital equipment costs.[7,9] Biorefinery unit processes can be modeled using engineering plant design software, such as Aspen Plus, to account for the behavior and interaction of unit process "blocks" (e.g., biological conversion, separation, catalytic upgrading), including their mass and energy flows. Process flow balances are then used to determine the necessary equipment sizing, capital and operating costs, as well as the product minimum selling price (MSP).[57] The behavior of each unit process can be varied within anticipated performance bands to determine the sensitivity response of the MSP to a given parameter. This approach provides a powerful tool for identifying research areas for further cost reduction. With regards to muconic acid downstream processing, technical targets can be set for broth composition, feed stream purity requirements, continuous catalytic hydrogenation conditions, and catalysis stability requirements to improve the economic prospects for renewable adipic acid production.

1.3 Research Objectives

Our research goal is to advance the integrated catalytic upgrading of biologically derived carboxylic acids to renewable fuels and value-added chemicals. A research plan is designed to (1) evaluate aqueous phase deoxygenation of monocarboxylic acids to diesel-grade hydrocarbons, (2) assess the downstream separation and catalytic upgrading of muconic acid to adipic acid over noble metal hydrogenation catalysts, and (3) determine the economic viability of muconic acid production through techno-economic modeling with coupled catalytic experimentation. With this goal in mind, we propose the following research objectives and hypotheses:

Objective 1: *Evaluate aqueous-phase catalysis for deoxygenating monocarboxylic acids to diesel-grade hydrocarbons, with in situ hydrogen production from renewable donors.* Aqueous phase catalytic processing can potentially eliminate costly separation steps associated with recovering carboxylic acids from fermentation broth. Previous work has highlighted the challenge of unsaturated fatty acid decarboxylation,[30,31] while parallel efforts have highlighted the potential for aqueous phase reforming of renewable hydrogen donors *in situ*.[33] We hypothesize that hydrogen addition, either with conventional or renewable donors, can facilitate tandem fatty acid hydrogenation and deoxygenation in hydrothermal media. Further, we propose that the addition of Re as a secondary promoter can facilitate increased reactivity and reduced affinity for CO, a key water-gas-shift (WGS) intermediate.[32] To highlight the potential application with multiple classes of biologically-derived acids, this approach will be tested with both model and complex lipid feedstocks. We anticipate that highly active bimetallic catalysts can be identified for aqueous phase deoxygenation of monocarboxylic acids that simultaneously promote *in situ* hydrogen production.

Objective 2: *Assess the integrated downstream processing of muconic acid to adipic acid via separation of non-target metabolites, hydrogenation catalyst screening, and continuous time on stream testing.* Muconic acid is a polyunsaturated dicarboxylic acid that can be produced biologically from sugars[53,54] and potentially lignin monomers.[15] Subsequently, muconic acid can be catalytically hydrogenated to adipic acid,[53,54] a nylon precursor. However, little is information is known regarding the separation challenges when utilizing carbon substrates derived from lignin for muconic acid bioconversion, and their influence on downstream catalysis, product yield, and final purity. We hypothesize that facile adsorption with activated carbon can remove

non-target aromatic metabolites present in culture broth. We expect to identify separation strategies to recover muconic acid in high purity and yield, while gaining insight into the catalytic materials that are active and stable for continuous muconic acid hydrogenation.

Objective 3: *Determine the economic viability for the downstream processing of muconic acid using preliminary techno-economic analysis.* In order to be successful, renewable fuels and chemicals must be economically competitive with conventional petroleum-derived products.[55] Due to the multitude of unit process operations (e.g., biomass pretreatment, separations, biological conversion, catalytic processing) and their potential configurations within a biorefinery, preliminary techno-economic analysis can provide key insight regarding how plant design impacts the final unit price of fuel and chemical products, as well as process performance parameters (e.g., recovery yield, utility demand, product selectivity). We hypothesize that the downstream separation and catalysis of muconic acid derived from lignocellulosic biomass can economically compete with adipic acid produced from petroleum. To test this hypothesis, preliminary techno-economic analysis will be performed based on separation and unit process operations examined at the bench-scale. Major capital and operating expense will be identified, and single-point sensitivity analysis will assess the impact of unit process design parameters on the minimum selling price of adipic acid. We anticipate that key cost drivers will be identified to shape the future research objectives and accelerate commercial viability.

1.4 Thesis Outline

The research objectives were addressed in the following chapters described, with personal and joint contributions detailed:

- Chapter 2 contains a manuscript published in *Green Chemistry,* entitled "Hydrothermal catalytic processing of saturated and unsaturated fatty acids to hydrocarbon with glycerol for in production" with co-authors B.K. Sharma, J. Haramillo, D. Kim, J.K. Choe, P.N. Cisielski, and T.J. Strathmann. This work addresses research objective 1, evaluating hydrothermal media for renewable hydrocarbon production and the influence of hydrogen, bimetallic catalysts and their stability, and the use of glycerol as a renewable hydrogen donor.

- Chapter 3 contains a manuscript published in *Proceedings of the National Academy of Sciences* with co-lead authors J.G. Linger, M.T. Guarnieri, and E.M Karp, as well as co-authors G.B. Hunsinger, M.A. Franden, C.W. Johnson, G. Chupka, T.J. Strathmann, P.T. Pienkos, and G.T. Beckham. This work addresses the overall goal of examining integrated biological and catalytic processes with complex lignocellulosic feedstocks, as well as research objective 1 for catalytic hydrothermal processing. This chapter was a collaborative effort with the National Renewable Energy Laboratory (NREL), with an individual contribution that included (a) joint authoring of the manuscript, (b) integrated figure development, (c) extraction and characterization of intracellular polymer composition, molecular weight distribution, and thermal and physicochemical characteristics, (d) experimental design to verify uptake of ^{13}C-labled substrates by GC-IRMS, (e) polymer thermal depolymerization and product characterization, and (f) hydrothermal catalytic deoxygenation of alkenoic acids to hydrocarbons.

- Chapter 4 contains a manuscript published in *Energy & Environmental Science* with co-lead authors M.A. Franden, C.W. Johnson, and E.M Karp, as well as co-authors M.T. Guarnieri, J.G. Linger, M.J. Salm, T.J. Strathmann, and G.T. Beckham. This work addresses research objective 2 by evaluating the downstream separation and catalysis of muconic acid for polymer precursor production. This chapter was also a collaborative effort with NREL, with an individual contribution that included (a) joint authoring of the manuscript, (b) integrated figure development, (c) purification and separation of muconic acid from biological culture media, (d) catalyst synthesis and characterization, and (e) catalyst activity screening and rate evaluation.

- Chapter 5 contains a manuscript in preparation entitled "*cis,cis*-Muconic acid: Downstream separation and catalysis to bio-adipic acid for nylon-6,6 polymerization", with co-authors N. Rorrer, M.J. Menart, D. Salvachua, P.N. Ciesielski, J.R. Dorgan, G.T. G.T. Beckham, and T.J. Strathmann. This work further expands on research objective 2 by evaluating additional purification steps to meet polymer precursor specifications, examining the activity and stability of catalysts on multiple supports, testing promising catalysts continuously in a flow reactor, and demonstrating the polymerization of bio-adipic acid to nylon-6,6.

- Chapter 6 contains a manuscript in preparation entitled "Preliminary techno-economic analysis for the downstream processing of bio-based muconic acid to adipic acid", with co-authors T.J. Strathmann, G.T. Beckham, and M.J. Biddy. This work addresses

research objective 3 by evaluating key unit process cost drivers and technical targets for the downstream processing of muconic acid to adipic acid.

- Chapter 7 contains a final summary of the work conducted in this thesis, as well as implications for future research directions.

1.5 References Cited

1. U.S. EIA. International Energy Outlook. (2013). at <http://www.eia.gov/forecasts/ieo/transportation.cfm>
2. International Energy Agency. Technology Roadmap: Energy and GHG Reductions in the Chemical Industry via Catalytic Processes. (2013).
3. Melero, J. A., Iglesias, J. & Garcia, A. Biomass as renewable feedstock in standard refinery units. Feasibility, opportunities and challenges. *Energy Environ. Sci.* **5,** 7393–7420 (2012).
4. Serrano-Ruiz, J. C., West, R. M. & Dumesic, J. A. Catalytic Conversion of Renewable Biomass Resources to Fuels and Chemicals. *Annu. Rev. Chem. Biomol. Eng.* **1,** 79–100 (2010).
5. Wettstein, S. G., Alonso, D. M., Gürbüz, E. I. & Dumesic, J. A. A roadmap for conversion of lignocellulosic biomass to chemicals and fuels. *Curr. Opin. Chem. Eng.* **1,** 218–224 (2012).
6. Bozell, J. J. & Petersen, G. R. Technology development for the production of biobased products from biorefinery carbohydrates—the US Department of Energy's 'Top 10' revisited. *Green Chem.* **12,** 539 (2010).
7. Milbrandt, A., Kinchin, C. & McCormick, R. L. The Feasibility of Producing and Using Biomass-Based Diesel and Jet Fuel in the United States. *NREL Tech. Rep.* (2013).
8. National Research Council. Transitions to Alternative Vehicles and Fuels. *Natl. Acad. Press* (2013). at <http://www.nap.edu/openbook.php?record_id=18264>
9. Davis, R. *et al.* Process design and economics for the conversion of lignocellulosic biomass to hydrocarbons: Dilute-acid and enzymatic deconstruction of biomass to sugars and biological conversion of sugars to hydrocarbons. *NREL Tech. Rep.* 88–101 (2013).
10. Peplow, M. Cellulosic ethanol fights for life. *Nature* **507,** 152–153 (2014).

11. Brown, T. R. & Brown, R. C. A review of cellulosic biofuel commercial-scale projects in the United States. *Biofuels Bioprod. Biorefining* **7,** 235–245 (2013).
12. Peralta-Yahya, P. P. *et al.* Identification and microbial production of a terpene-based advanced biofuel. *Nat. Commun.* **2,** 483 (2011).
13. Wang, C., Kim, J.-Y., Choi, E.-S. & Kim, S.-W. Microbial production of farnesol (FOH): Current states and beyond. *Process Biochem.* **46,** 1221–1229 (2011).
14. Chundawat, S. P. S., Beckham, G. T., Himmel, M. E. & Dale, B. E. Deconstruction of Lignocellulosic Biomass to Fuels and Chemicals. *Annu. Rev. Chem. Biomol. Eng.* **2,** 121–145 (2011).
15. Fuchs, G., Boll, M. & Heider, J. Microbial degradation of aromatic compounds — from one strategy to four. *Nat. Rev. Microbiol.* **9,** 803–816 (2011).
16. Xiong, M. *et al.* A Bio-Catalytic Approach to Aliphatic Ketones. *Sci. Rep.* **2,** (2012).
17. Anbarasan, P. *et al.* Integration of chemical catalysis with extractive fermentation to produce fuels. *Nature* **491,** 235–239 (2012).
18. Braden, D. J., Henao, C. A., Heltzel, J., Maravelias, C. C. & Dumesic, J. A. Production of liquid hydrocarbon fuels by catalytic conversion of biomass-derived levulinic acid. *Green Chem.* **13,** 1755–1765 (2011).
19. Chen, G. G.-Q. *Plastics from Bacteria: Natural Functions and Applications*. (Springer Science & Business Media, 2009).
20. Wynn, J. P. & Ratledge, C. in *Bailey's Industrial Oil and Fat Products* (John Wiley & Sons, Inc., 2005). at <http://onlinelibrary.wiley.com/doi/10.1002/047167849X.bio006/abstract>
21. Kosa, M. & Ragauskas, A. J. Lignin to lipid bioconversion by oleaginous *Rhodococci*. *Green Chem.* **15,** 2070–2074 (2013).

22. Wells Jr, T. & Ragauskas, A. J. Biotechnological opportunities with the β-ketoadipate pathway. *Trends Biotechnol.* **30,** 627–637 (2012).

23. Yang, S.-T., El-Ensashy, H. & Thongchul, N. *Bioprocessing Technologies in Biorefinery for Sustainable Production of Fuels, Chemicals, and Polymers*. (John Wiley & Sons, 2013).

24. Ramaswamy, S., Huang, H.-J. & Ramarao, B. *Separation and Purification Technologies in Biorefineries*. (John Wiley and Sons Ltd, 2012).

25. Chheda, J. N., Huber, G. W. & Dumesic, J. A. Liquid-phase catalytic processing of biomass-derived oxygenated hydrocarbons to fuels and chemicals. *Angew. Chem. Int. Ed.* **46,** 7164–7183 (2007).

26. Peterson, A. A. *et al.* Thermochemical biofuel production in hydrothermal media: A review of sub- and supercritical water technologies. *Energy Environ. Sci.* **1,** 32–65 (2008).

27. Yeh, T. M. *et al.* Hydrothermal catalytic production of fuels and chemicals from aquatic biomass. *J. Chem. Technol. Biotechnol.* n/a–n/a (2012). doi:10.1002/jctb.3933

28. King, J. W., Holliday, R. L. & List, G. R. Hydrolysis of soybean oil. in a subcritical water flow reactor. *Green Chem.* **1,** 261–264 (1999).

29. Saeki, T., Tsukegi, T., Tsuji, H., Daimon, H. & Fujie, K. Hydrolytic degradation of poly[(R)-3-hydroxybutyric acid] in the melt. *Polymer* **46,** 2157–2162 (2005).

30. Fu, J., Lu, X. & Savage, P. E. Hydrothermal decarboxylation and hydrogenation of fatty acids over Pt/C. *ChemSusChem* **4,** 481–486 (2011).

31. Fu, J., Lu, X. & Savage, P. E. Catalytic hydrothermal deoxygenation of palmitic acid. *Energy Environ. Sci.* **3,** 311–317 (2010).

32. Kunkes, E. L. *et al.* The role of rhenium in the conversion of glycerol to synthesis gas over carbon supported platinum–rhenium catalysts. *J. Catal.* **260,** 164–177 (2008).

33. King, D. L. *et al.* Aqueous phase reforming of glycerol for hydrogen production over Pt–Re supported on carbon. *Appl. Catal. B Environ.* **99,** 206–213 (2010).

34. Simonetti, D. A., Kunkes, E. L. & Dumesic, J. A. Gas-phase conversion of glycerol to synthesis gas over carbon-supported platinum and platinum–rhenium catalysts. *J. Catal.* **247,** 298–306 (2007).

35. Isaacs, B. H. & Petersen, E. E. Surface area measurement of platinum/rhenium/alumina: I. Stoichiometry of hydrogen-oxygen chemisorptions and titrations. *J. Catal.* **85,** 1–7 (1984).

36. Choe, J. K., Shapley, J. R., Strathmann, T. J. & Werth, C. J. Influence of rhenium speciation on the stability and activity of Re/Pd bimetal catalysts used for perchlorate reduction. *Environ. Sci. Technol.* **44,** 4716–4721 (2010).

37. Hurley, K. D. & Shapley, J. R. Efficient Heterogeneous Catalytic Reduction of Perchlorate in Water. *Environ. Sci. Technol.* **41,** 2044–2049 (2007).

38. Pham, H. N., Anderson, A. E., Johnson, R. L., Schmidt-Rohr, K. & Datye, A. K. Improved hydrothermal stability of mesoporous oxides for reactions in the aqueous phase. *Angew. Chem. Int. Ed.* **51,** 13163–13167 (2012).

39. Zhang, L. *et al.* Correlation of Pt–Re surface properties with reaction pathways for the aqueous-phase reforming of glycerol. *J. Catal.* **287,** 37–43 (2012).

40. Himmel, M. E. *et al.* Biomass Recalcitrance: Engineering Plants and Enzymes for Biofuels Production. *Science* **315,** 804–807 (2007).

41. Ragauskas, A. J. *et al.* Lignin Valorization: Improving Lignin Processing in the Biorefinery. *Science* **344,** 1246843 (2014).

42. Vyver, S. V. de & Román-Leshkov, Y. Emerging catalytic processes for the production of adipic acid. *Catal. Sci. Technol.* **3,** 1465–1479 (2013).

43. Thiemens, M. H. & Trogler, W. C. Nylon production: An unknown source of atmospheric nitrous oxide. *Science* **251,** 932–934 (1991).

44. Hoyle, C. E., Cranford, M., Trapp, M., No, Y. G. & Kim, K.-J. Photopolymerization of 1,6-hexanediol diacrylate with deoxybenzoin as photoinitiator. *Polymer* **29,** 2033–2040 (1988).

45. Jiang, Z. & Zhang, J. Lipase-catalyzed synthesis of aliphatic polyesters via copolymerization of lactide with diesters and diols. *Polymer* **54,** 6105–6113 (2013).

46. Magano, J. & Dunetz, J. R. Large-Scale Applications of Transition Metal-Catalyzed Couplings for the Synthesis of Pharmaceuticals. *Chem. Rev.* **111,** 2177–2250 (2011).

47. Yang, J. *et al.* Synthesis of renewable high-density fuels using cyclopentanone derived from lignocellulose. *Chem. Commun.* (2014). doi:10.1039/C3CC46588H

48. Urbanus, J., Roelands, C. P. M., Verdoes, D. & ter Horst, J. H. Intensified crystallization in complex media: Heuristics for crystallization of platform chemicals. *Chem. Eng. Sci.* **77,** 18–25 (2012).

49. Lin, S. K. C. *et al.* Novel resin-based vacuum distillation-crystallisation method for recovery of succinic acid crystals from fermentation broths. *Green Chem.* **12,** 666 (2010).

50. Dąbrowski, A., Podkościelny, P., Hubicki, Z. & Barczak, M. Adsorption of phenolic compounds by activated carbon—a critical review. *Chemosphere* **58,** 1049–1070 (2005).

51. Franz, M., Arafat, H. A. & Pinto, N. G. Effect of chemical surface heterogeneity on the adsorption mechanism of dissolved aromatics on activated carbon. *Carbon* **38,** 1807–1819 (2000).

52. Bartholomew, C. H. & Farrauto, R. J. *Fundamentals of Industrial Catalytic Processes*. (Wiley-AIChE, 2005).

53. Draths, K. M. & Frost, J. W. Environmentally compatible synthesis of adipic acid from D-glucose. *J. Am. Chem. Soc.* **116,** 399–400 (1994).

54. Niu, W., Draths, K. M. & Frost, J. W. Benzene-Free Synthesis of Adipic Acid. *Biotechnol. Prog.* **18,** 201–211 (2002).

55. Klein-Marcuschamer, D. & Blanch, H. W. Survival of the fittest: An economic perspective on the production of novel biofuels. *AIChE J.* **59,** 4454–4460 (2013).

56. Claypool, J. T. & Raman, D. R. Development and validation of a technoeconomic analysis tool for early-stage evaluation of bio-based chemical production processes. *Bioresour. Technol.* **150,** 486–495 (2013).

57. Peters, M., Timmerhaus, K. & West, R. *Plant Design and Economics for Chemical Engineers*. (McGraw-Hill Science/Engineering/Math, 2002).

1.6 Figures

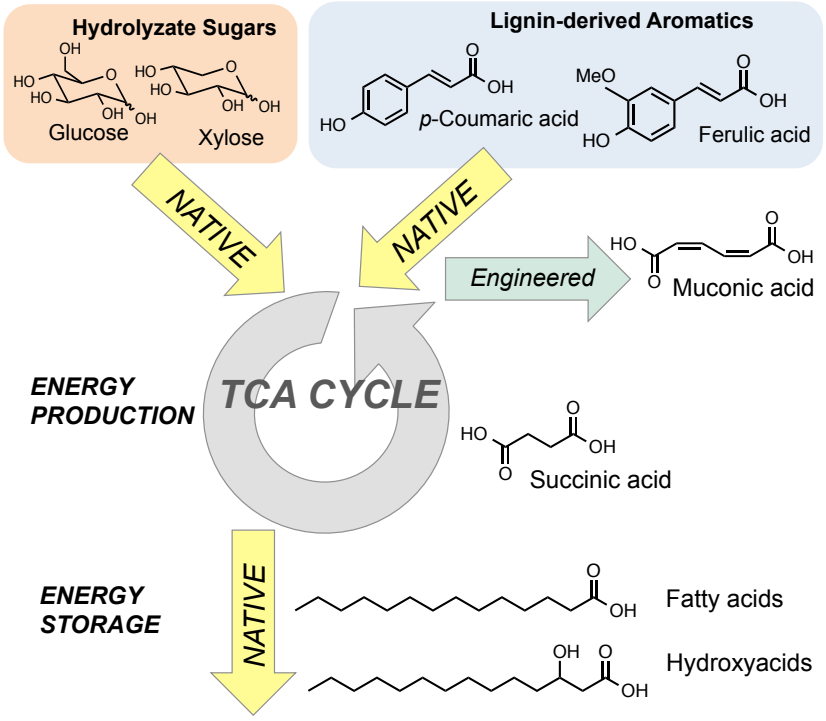

Figure 1.1 Biological production of carboxylic acids via native and engineered metabolic pathways. Key target acids are shown for renewable fuels and chemicals.

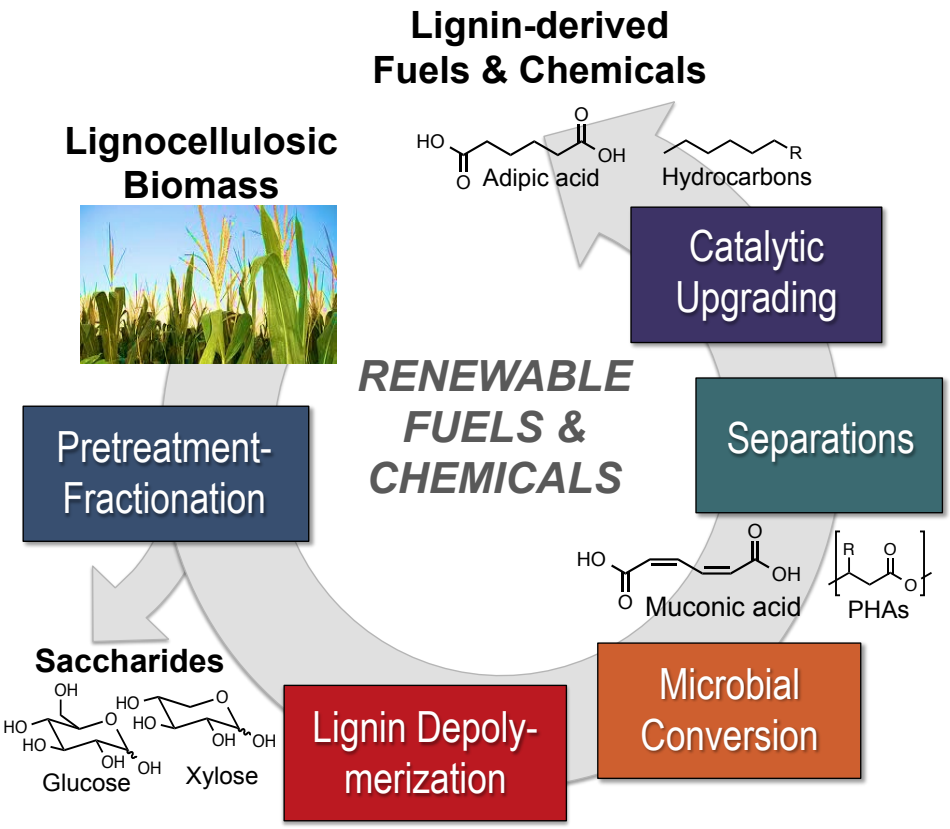

Figure 1.2 Renewable fuels and chemicals from lignocellulosic biomass through integrated biological-catalytic processing. Example scheme for valorizing biomass to fuel and polymer precursors.

.

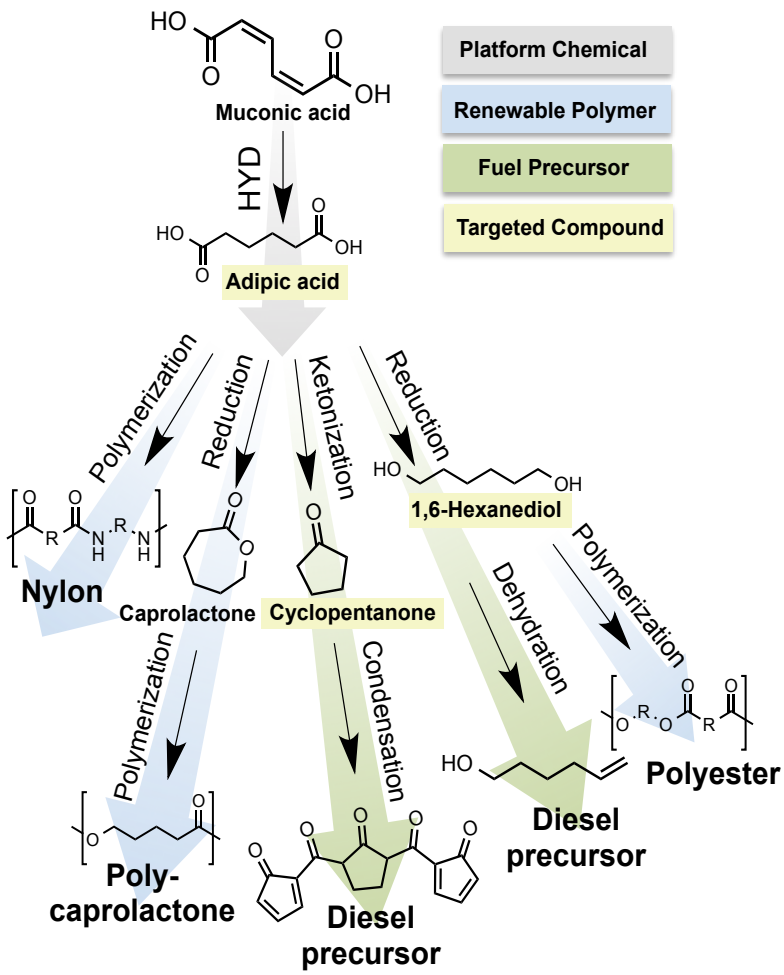

Figure 1.3 Downstream catalytic processing routes for upgrading muconic acid to renewable fuels and chemicals.

CHAPTER 2

HYDROTHERMAL CATALYTIC PROCESSING OF SATURATED AND UNSATURATED FATTY ACIDS TO HYDROCARBONS WITH GLYCEROL FOR IN SITU HYDROGEN PRODUCTION[1]

2.1 Abstract

Lipids are a promising feedstock to produce renewable hydrocarbon fuels and H_2 via catalytic hydrothermal processing. Upon exposure to hydrothermal media (e.g., 300°C, 8-11 MPa), lipids rapidly hydrolyze to produce saturated and unsaturated free fatty acids in varying ratios, depending on the feedstock, as well as glycerol. This report demonstrates the potential of Pt-Re/C for the hydrothermal conversion of saturated and unsaturated fatty acids to hydrocarbons, using glycerol reforming for in situ H_2 production to meet process demands. Experiments showed that deoxygenation of stearic acid, a model saturated fatty acid, was significantly enhanced with Pt-Re/C under a reducing atmosphere compared to Pt/C. The coupled hydrogenation and deoxygenation (HYD-DOX) of oleic aid, a model unsaturated fatty acid, was also moderately enhanced under an inert atmosphere using glycerol for in situ H_2 production, with DOX as the rate-limiting step. Characterization of Pt-Re/C showed that Re had a significant effect on CO:H uptake ratio (2.2) compared to commercial Pt/C (1.3), with the metals dispersed as small crystallites (~3-4 nm) throughout carbon support. Experiments revealed that the initial system H_2 headspace loading <3.45 MPa greatly enhances fatty acid DOX kinetics via decarboxylation/decarbonylation without net H_2 consumption. At higher initial H_2 loadings (≥3.45 MPa), fatty acid reduction was also observed as a minor DOX pathway.

[1] A modified version of Chapter 2 was published in Green Chemistry, 2014, 16, 1507-1520. (D.R. Vardon lead author with co-authors B.K. Sharma, J. Haramillo, D. Kim, J.K. Choe, P.N. Ciesielski, and T.J. Strathmann).

Experiments also showed that oleic acid HYD-DOX and glycerol reforming are affected by initial glycerol concentration and catalyst loading. Under optimized process conditions, complete HYD-DOX of oleic acid to heptadecane was achieved within 2 h with a net-zero H_2 consumption using a 1:3 glycerol-to-fatty acid ratio (i.e., the native ratio in triacylglycerides). X-ray photoelectron spectroscopy showed that H_2 in the reactor headspace results in lower oxidation states of Pt and Re, suggesting a possible mechanism for enhanced DOX kinetics. This approach holds promise for overcoming the high external H_2 demands of conventional lipid hydrotreatment processes.

2.2 Introduction

With the effect of global climate change increasingly evident, there is a pressing need to transition to renewable fuels and petrochemical substitutes. Green diesel (e.g., renewable diesel-grade hydrocarbons) produced from lipid feedstocks is a potential alternative for partially displacing the 46 billion gallons per year of petroleum diesel consumed in the United States.[1] Green diesel has several advantages over conventional fatty acid methyl esters (i.e., biodiesel), including their direct compatibility with existing refinery operations, full integration into the transportation infrastructure, and improved fuel performance properties.[2] Commercialization of green diesel by catalytic hydrodeoxygenation (HDO) has been pursued by Neste Oil's NExBTL and UOP/Eni's Ecofining processes. However, the high moisture content of many lipid-rich feedstocks (e.g., microalgae, waste grease) can be problematic for downstream processing operations, requiring energetic and costly pretreatment and separation steps. In addition, the HDO process has high H_2 process demands because oxygenated lipid functional groups are primarily removed by catalytic reduction.[3,4] For example, the Ecofining process requires 1.5-3.8

wt.% H_2 of the incoming feed stream for vegetable oil upgrading.[2] The large H_2 demand necessitates colocation with hydrogen production facilities and negatively impacts the process sustainability since H_2 is primarily derived from fossil fuels.[3,4] As a result, alternative lipid processing routes are being explored for green diesel production.

Catalytic hydrothermal processing is a promising method for producing renewable hydrocarbons from lipids by utilizing water as the reaction medium.[5–8] Under subcritical conditions (200-374°C, 5-20 MPa), water becomes a unique reaction medium with a reduced dielectric constant, providing lipid solubility similar to non-polar solvents.[9] The interphase mass transfer and water self-disassociation constant increase, creating a highly reactive processing environment.[9] Additionally, water as a solvent is well suited for high-moisture waste lipid feedstocks such as fish and animal fat processing residues,[10] sewage sludge,[11] and algal biomass.[12] Algae are a particularly promising feedstock due to their high lipid productivity rates compared to terrestrial biomass, potential integration with wastewater treatment, and ability to use non-arable land for cultivation.[12–14]

Triacylglycerides (TAGs), the predominant component of neutral lipids, rapidly hydrolyze in hydrothermal media to produce saturated and unsaturated free fatty acids (FFAs) (e.g., lauric, palmitic, palmitoleic, stearic, oleic, linoleic) in varying ratios, depending on the feedstock, as well as glycerol. Recent work has shown that saturated fatty acids (e.g., lauric, palmitic, stearic) rapidly undergo catalytic deoxygenation (DOX) to produce linear hydrocarbons and CO_2 via decarboxylation/decarbonylation without external H_2 addition over Pt/C and Pd/C catalysts, with Pt/C displaying significantly greater DOX activity.[5,6] In contrast, oleic acid (mono-unsaturated C18 fatty acid) does not readily undergo DOX under the same conditions. Instead, only partial hydrogenation (HYD) is observed, with stearic acid (saturated C18 fatty acid) being the primary

reaction product.[5,6] Complete conversion of unsaturated fatty acids to renewable hydrocarbons is not achieved, suggesting that olefin HYD (a H_2-consuming reaction) is necessary prior to DOX with noble metals on activated carbon.

In addition, other studies have examined hydrothermal catalytic reforming of glycerol, a by-product of TAG hydrolysis, to generate H_2, commonly referred to as aqueous phase reforming (APR).[15–20] Typically, glycerol is assumed to be derived as a by-product from biodiesel production. However, utilization of glycerol APR for in situ H_2 production may facilitate unsaturated fatty acid HYD, allowing for subsequent fatty acid DOX (HYD-DOX). Furthermore, the addition of Re to Pt/C has been shown to enhance glycerol APR by reducing the affinity for CO, [18,21] which may allow for improved turnover frequency. Increased CO turnover frequency may also potentially enhance fatty acid DOX via decarbonylation, since CO is a reaction by-product; [22,23] however, to our knowledge the use of Pt-Re/C for the conversion of saturated and unsaturated fatty acids to hydrocarbons with integrated glycerol APR for in situ H_2 production has not been investigated.

This study examines the use of Pt-Re/C for the hydrothermal deoxygenation of stearic acid, a model saturated fatty acid, as well as the coupled hydrogenation and deoxygenation (HYD-DOX) of oleic acid, a model unsaturated fatty acid, with in situ H_2 production from glycerol. Experiments were conducted to (i) evaluate the material properties of Pt-Re/C and its stability in hydrothermal media, (ii) determine the use of Re as a promoter metal to enhance saturated fatty acid DOX and generate H_2 in situ from glycerol to facilitate complete HYD-DOX of unsaturated fatty acids, (iii) investigate the influence of initial H_2 gas addition on fatty acid HYD-DOX kinetics, reaction pathways, catalyst oxidation state, and net H_2 consumption, and (iv) explore the impact of glycerol and catalyst loading on product yields. Results support a proposed

reaction scheme for one-pot hydrothermal catalytic conversion of TAGs to liquid hydrocarbon fuels, involving hydrolysis and catalytic reforming, hydrogenation, and deoxygenation reactions.

2.3 Results and Discussion

2.3.1 Catalyst characterization

Commercial Pt/C and as prepared Pt-Re/C catalysts were initially characterized to determine their material properties. The metal loading of commercial Pt/C as received was 5 wt.% nominal. Pt-Re/C was prepared by aqueous deposition of Re onto commercial Pt/C, followed by in situ reduction. This method produced a catalyst with a Pt loading of 5.2 wt.% and a Re loading of 4.2 wt.% (Pt-Re molar ratio of 1.2), as measured by ICP.

Multipoint N_2-physisoprtion provided additional information regarding the catalyst support properties, as shown in **Table 2.1**. BET analysis determined that commercial Pt/C had a support surface area of 1075 m^2/g, while BJH desorption analysis determined that the pore volume was 0.715 cm^3/g, with an average pore diameter of 10.23 Å. The addition of Re to commercial Pt/C reduced the support surface area to 750 m^2/g and the pore volume to 0.607 cm^3/g, while the average pore diameter remained fairly constant 10.06 Å. The reduction in surface area and pore volume is not atypical for high secondary metal loadings, which may result in pore blockage.[24] Recent work by our group to prepare Ru-Sn/C from commercial Ru/C by incipient wetness with $SnCl_2$ also resulted in a decrease in surface area by 268 m^2/g, without in situ reduction; however, for Pt-Re/C, the influence of hydrothermal in situ reduction may also be a factor.

CO and H_2 pulse chemisorption was then performed to evaluate catalyst metal site properties, as shown in **Table 2.1**. The measured value of irreversible CO uptake for

commercial Pt/C was 130 μmol/g, slightly greater than the value for H uptake (112 μmol/g). This resulted in a calculated metal dispersion of 51% for Pt/C, based on CO uptake and an assumed CO:M ratio of unity. The addition of Re moderately lowered the measured CO uptake by 13% (112 μmol/g), with a calculated metal dispersion of 42% based on Pt loading. This suggests an increase in particle size, similar to findings from XRD and SEM-EDS described below, or Re coverage of Pt sites during secondary metal loading. In contrast to CO uptake, the H uptake with Pt-Re/C was markedly reduced by 49% (52 μmol/g) compared to commercial Pt/C. The reduction of H uptake by nearly two-fold (CO:H uptake ratio of 2.2) is similar to previous findings by Simonetti et al. (CO:H uptake ratio of 2.3),[25] which confirms the significant influence of Re addition and suggests Pt-Re alloy formation.[26]

XRD analysis of unloaded activated carbon, commercial Pt/C, and Pt-Re/C as prepared was provided additional information regarding long-range order and average metal crystallite size, as shown in **Figure 2.1**. Distinct peaks were observed on the bare carbon support, while the lack of sharp, pronounced peaks with Pt/C and Pt-Re/C suggests that the metals were highly dispersed as small crystallites. In comparison to Pt/C, Pt-Re/C displayed a broad XRD peak near 40° (2θ value), with a bulk metal crystallite size of ~3.4 nm estimated by the Scherer equation.

Transmission electron microscopy (TEM) of Pt-Re/C revealed disperse metal crystallites <5 nm in diameter (**Figure 2.3A)**, consistent with crystallite size estimates from XRD. The distribution of Pt and Re within individual metal crystallites was also evaluated using scanning transmission electron microscopy coupled to energy dispersive X-ray spectroscopy (STEM-EDS), as shown in **Figure 2.3B** and **2.3C**. EDS analysis confirmed

that Pt and Re were present throughout the crystallites, but a fixed metallic ratio was not observed. Based on these results, it was evident that Pt and Re were well dispersed and largely co-localized throughout the support; however, a definitive assessment of the atomic scale, bimetallic crystallite composition (e.g., collocated mono-metallics, intermetallic alloys, core-shell bimetallics, etc.) could not be concluded from this data.

2.3.2 Catalyst activity

2.3.2.1 Stearic acid DOX with Pt/C and Pt-Re/C

The influence of Re on the activity of Pt/C for stearic acid DOX was initially investigated, as shown in **Rxn. 1**, since saturated fatty acids can comprise a significant component of lipids.

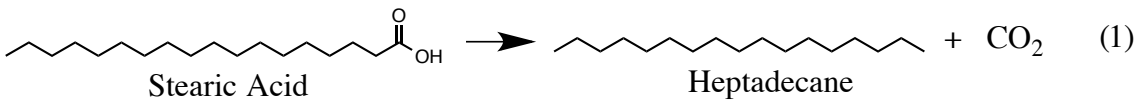

Experiments were performed with Pt/C and Pt-Re/C using a reducing H_2 headspace (<3.447 MPa /557 mmol H_2), as shown in **Figure 2.4**. The conversion of stearic acid to heptadecane at 300°C occurred with high selectively (>90% molar yield) to heptadecane for both Pt and Pt-Re/C, with octadecane observed in trace amounts (3-8% molar yield). The high selectivity to heptadecane suggests decarboxylation/decarbonylation as the primary DOX pathway,[3,4] similar to past findings by Fu et al. using Pt/C with an inert N_2 headspace.[5] The main reaction products from fatty acid decarbonylation (**Rxn. 2**),[22,23] terminal alkenes and CO, were not detected in significant amounts. However, CO can be rapidly converted to CO_2 by the WGS reaction, and terminal alkenes can be readily hydrogenated with a H_2 headspace, as shown in **Rxn. 3** and **Rxn. 4**, respectively.

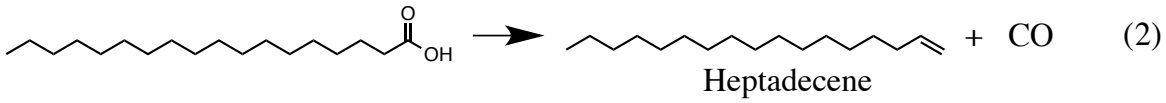

$$CO + H_2O \longrightarrow H_2 + CO_2 \quad (3)$$

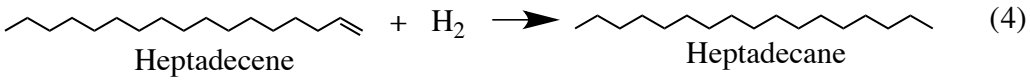

In contrast to hydrothermal media, organic solvents (e.g., dodecane) produce CO as the primary C-gas product during fatty acid DOX with a H_2 headspace, since the DOX pathway sharply shifts from decarboxylation to decarbonylation.[22,23] This may be problematic due to competitive adsorption of CO on active catalyst sites and the lack of H_2 regeneration by the WGS reaction in organic media.[27]

The addition of Re to Pt/C had a significant effect on the apparent stearic acid DOX kinetics at 300°C, as shown in **Figure 2.4A**. The Pt-Re/C pseudo-first order apparent rate constant for stearic acid DOX, normalized to catalyst loading ($k_{app\ Pt\text{-}Re/C\ DOX}$ = 2.72 ± 0.24 $\times 10^{-4}$ $s^{-1}g^{-1}$), was nearly 3-fold greater compared to Pt/C ($k_{app\ Pt/C\ DOX}$ = 0.94 ± 0.05 $\times 10^{-4}$ $s^{-1}g^{-1}$). Although multi-phase reaction kinetics are significantly more complex than a pseudo-first order assumption, this simplification allowed for generalized activity comparisons. In addition, Pt-Re/C also displayed improved DOX performance at low temperatures (i.e., <340°C), as indicated by the heptadecane 3-h molar yields shown in **Figure 2.4B**.

Due to the limitations of collecting accurate hydrothermal kinetic data in a large batch reactor, detailed kinetic analysis was not addressed. Multiple factors can potentially mask intrinsic catalytic activity in batch, including partial deactivation with time on stream, inhibition from reaction by-products, and artifacts introduced during the time delay for

batch reactor heat-up.[28] However, the effect of Re addition on catalyst activity was pronounced and in-depth kinetic analysis will be addressed in follow-up work.

The increased activity with Re addition may be due to a number of factors, including enhanced CO turnover for decarbonylation as a DOX pathway, alteration to active site morphology, or changes to active site electronic properties. Previous work has shown that addition of Re to Pt/C can significantly reduce CO adsorption affinity,[18,21] which may allow for greater active site turnover and availability for fatty acid DOX and glycerol reforming reactions. As a control, the activity of the Re precursor alone was tested for stearic acid DOX, with no conversion to heptadecane observed. This suggests that Re may only function as promoter metal with Pt, although further investigation into mechanism for stearic acid DOX in hydrothermal media is needed.

2.3.2.2 Glycerol for facilitating oleic acid HYD-DOX

The utilization of glycerol APR for in situ H_2 production (**Rxn. 5)** was then examined to facilitate HYD of oleic acid to stearic acid (**Rxn. 6**), and subsequent fatty acid DOX (**Rxn. 1**). Ideally, in situ H_2 production from glycerol would alleviate the need for external H_2 consumption, which is problematic for conventional lipid hydrotreatment processes.[3,4]

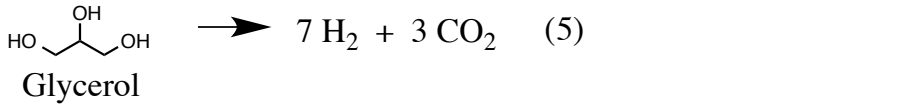

Glycerol

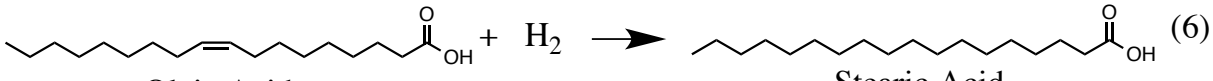

Oleic Acid Stearic Acid

Pt/C and Pt-Re/C catalysts were tested with a reactor headspace initially pressurized with N_2 gas (345 kPa/56 mmol) at a reaction temperature of 300°C, as shown in **Table 2.2**. With Pt/C and no glycerol addition, oleic acid was only partially hydrogenated (31% molar yield) to stearic acid, similar to findings by Fu et al.[5] Based on the oleic acid loading (71 mmol), 22 mmol of H_2 was required to account for hydrogenation of the single olefin bond in oleic acid. It has been suggested that water, the carbon support, or organic reactants may serve as potential H_2 sources in hydrothermal media.[5,6,29] Hydrocarbon products resulting from fatty acid DOX were not observed (e.g., heptadecane, octadecane, or lower hydrocarbons). Likewise, analysis of the reactor headspace gas following the reaction revealed no significant quantities (<1 mmol) of H_2 remaining. Therefore, it is presumed that the small amount of H_2 generated in situ was consumed by HYD of oleic acid.

In contrast, when glycerol (5 g/54 mmol) was added to the reactor with Pt/C, complete HYD of oleic acid was observed and partial DOX of the resulting stearic acid occurred (24% molar yield), producing heptadecane with high selectivity (>98%). However, heptadecane yields were significantly lower compared to initial experiments with stearic acid in a reducing headspace (**Figure 2.4**), suggesting that the system H_2 level greatly affects catalyst DOX performance. Residual H_2 was also detected in the headspace following the conversion (48 mmol), indicating significant in situ H_2 production with glycerol addition. It is estimated that 119 mmol of H_2 was produced in situ if the stoichiometric H_2 requirement for oleic acid HYD is added to the measured headspace residual.

Similar to findings with a reducing headspace, the use of Pt-Re/C enhanced the stearic acid DOX (38% heptadecane molar yield), although the extent of oleic acid HYD

was lower (92% molar yield). As with Pt/C, no significant levels of glycerol remained in the aqueous phase after 9 h for Pt-Re/C. The residual H_2 measured in the headspace (50 mmol) and estimated total in situ production (115 mmol; 30% of theoretical maximum APR yield) were also to Pt/C. As a control, glycerol APR with Pt-Re/C was tested without oleic acid, which produced a comparable level of H_2 (142 mmol; 37 % of theoretical), indicating no significant inhibition at the time scale investigated. Past work examining Pt-Re/C solely for glycerol APR found enhanced H_2 productivity (88.7% glycerol conversion, 24.5% H_2 selectivity) compared to Pt/C (5.3% conversion, 56.5% H_2 selectivity);[18] however, significantly lower temperatures were investigated (225°C).

Analysis of the aqueous phase following the conversion revealed that little residual glycerol remained (<1 wt.% of initial loading), suggesting complete decomposition at the elevated temperature (300°C) and extended reaction time (9 h). The estimated in situ production of H_2 represented 31% of the theoretical maximum H_2 yield for glycerol APR (7 H_2 per glycerol). Direct comparisons with previous results for glycerol APR are complicated due to differing temperature regimes, reactor configurations (batch vs. continuous), active metals, and catalyst supports. For example, initial investigations with Pt/Al_2O_3 for glycerol APR at 255°C demonstrated 100% C-conversion to the gas phase with 51% selectivity to H_2. The lower H_2 yield from glycerol observed in this study may be due to undesirable C-O bond cleavage pathways that generate H_2 consuming side-products and prevent CO formation.[18] High temperatures have also been shown to decrease H_2 selectivity during glycerol APR, despite increased conversion.[19] Likewise, higher temperatures can impair the water gas shift (WGS) reaction,[30] lowering H_2 yields. However, fatty acid DOX kinetics

increase with temperature, following Arrhenius parameters,[5] suggesting a tradeoff between optimum conditions for glycerol APR and fatty acid DOX.

Based on these results, Pt-Re/C was then chosen for further study due to enhanced acid DOX kinetics compared to Pt/C (**Figure 2.4** and **Table 2.2**), together with past reports of enhanced glycerol APR[18,20] and reduced affinity for binding CO (**Table 2.1**).[18] As noted, CO is produced during fatty acid decarbonylation and APR of glycerol, and is a known inhibitor of noble metal catalyst activity.[31]

2.3.2.3 Pt-Re/C activity with an inert and reducing headspace

The reactivity of Pt-Re/C for oleic acid HYD-DOX with in situ H_2 production from glycerol was further explored using a reactor headspace initially pressurized with either an inert gas (345 kPa/56 mmol N_2) or reducing gas (2.586 MPa/417 mmol H_2) (Figure 5). With an initial headspace of N_2 (**Figure 2.5A**), oleic acid HYD occurred to a significant extent (91%) after 1.5 h at temperature, followed by a slow progression until completion at 12 h. The H_2 level in the headspace remained fairly constant throughout the reaction (44 ± 4 mmol), and no significant quantities of glycerol were detected in the aqueous phase, indicating that decomposition was complete during reactor heatup to the setpoint temperature. The estimated total in situ production of H_2 (measured headspace + estimated stoichiometric demand for oleic acid HYD) was 115 mmol, consistent with findings from catalyst screening experiments. As the reaction progressed, DOX molar yields increased significantly from 7% after 3 h to 38% after 9 h, before leveling off at 41% after 12 h with heptadecane as the primary DOX product (>98% selectivity). The addition of glycerol at high levels (5 g) appeared to have an inhibitory effect on the rate of stearic acid DOX,

therefore pseudo-first order rate constants were not determined. The DOX process progressed much slower compared to HYD of oleic acid and the APR process for glycerol, suggesting that additional work should target increasing catalytic activity for the former.

With the initial headspace gas switched to H_2 (2.586 MPa/417 mmol), a dramatic enhancement was observed in the apparent rate of oleic acid HYD-DOX with glycerol, as shown in **Figure 2.5B**. Analysis of the reaction products after 1 h at temperature revealed complete HYD, as well as a small amount of DOX (13%). As the reaction progressed, the elevated initial H_2 level greatly enhanced fatty acid DOX kinetics, resulting in complete conversion within 7 h and high selectivity for heptadecane (>98%).

Enhancement of oleic acid HYD-DOX with the addition of H_2 to the headspace was not surprising since oleic acid HYD appears to be a necessary step prior to DOX in hydrothermal media with noble metal catalysts on activated carbon.[5,6,29] However, it was surprising that headspace analysis revealed a surplus of H_2 (479 ± 9 mmol) in the reactor compared to the initial external loading (417 mmol H_2). After accounting for the extent of oleic acid HYD and final headspace composition, it was estimated that 133 mmol of H_2 was produced in situ. Thus, while increased H_2 pressure provides a significant kinetic enhancement, in situ H_2 production from glycerol APR exceeded the H_2 consumption requirement for oleic acid HYD and yielded a net positive H_2 balance for the overall catalytic process. It follows that after initial pressurization with H_2, no additional external inputs of H_2 would be required for the catalytic hydrothermal conversion of lipids if H_2 can be captured and recycled in the process.

2.3.2.4 Influence of initial hydrogen loading

Due to the dramatic influence of H_2, the effect of varying initial H_2 loading (0-5.171 MPa/0-833 mmol) was investigated further by examining the 3-h DOX yields and resulting headspace gas composition. As the initial H_2 reactor loading increased, the 3-h yield of DOX products increased from 7% (0 Pa initial H_2) to 94% (5.171 MPa initial H_2) (**Figure 2.6A**). Heptadecane was observed as the only major DOX product at initial H_2 loadings <3.447 MPa. At higher initial H_2 loadings, fatty acid reduction products (e.g., octadecane, stearic alcohol) were observed (11.3%), indicating a minor shift towards reduction of the carboxylate group as a secondary DOX pathway (**Rxn. 7**).

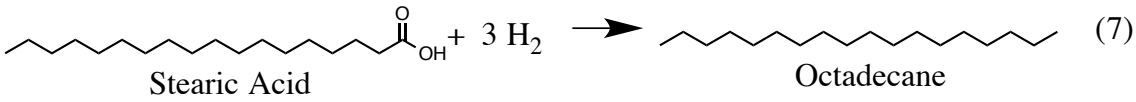

(7)

The high selectivity for heptadecane observed in hydrothermal media is in contrast to observations reported for organic solvent media (e.g., dodecane), where selectivity is highly sensitive to H_2 loading. In organic solvents, reaction products are observed from all three fatty acid DOX pathways (e.g., decarboxylation, decarbonylation, reduction) depending on the H_2 loading, with a sharp shift towards decarbonylation as the H_2 partial pressure is increased.[23,32,33]

Headspace analysis also revealed that the net process H_2 balance was affected by the initial external H_2 loading, as shown in **Figure 2.6B**. At lower initial H_2 loadings (<3.447 MPa/557 mmol), in situ H_2 production from glycerol provided a net surplus of system H_2 (net increase of 45 ± 12 mmol) despite the consumption of H_2 by oleic acid HYD (estimated requirement of 71 mmol H_2). However, at high initial loadings of H_2 (≥3.447 MPa/557 mmol), a net reduction in system H_2 was observed after 3 h. The net reduction was attributed to additional H_2 consumption by fatty acid reduction, which consumes 3 moles of H_2 to fully

reduce the carboxylate group. In addition, high H_2 pressures can suppress the WGS reaction,[34] lowering H_2 production.

Based on these results, the system H_2 pressure, either provided from external sources or produced by in situ APR of glycerol, was determined to be a key parameter influencing both fatty acid DOX kinetics and conversion product selectivity. It is also worth noting that the shift in DOX pathways at elevated H_2 pressure suggests that process H_2 levels will be self-limiting, since accumulation of H_2 pressure will shift conversion towards the H_2-consuming reduction processes, preventing further accumulation.

2.3.2.5 Effect of glycerol and catalyst loading

Additional experiments were then performed to determine the effect of varying glycerol concentrations (**Figure 2.7A**) and catalyst loadings (**Figure 2.7B**) on the 3-h oleic acid HYD-DOX molar yields with in situ H_2 production using an initial reducing headspace (2.586 MPa/417 mmol H_2). When no glycerol was added to the reactor, fatty acid HYD was complete and the DOX heptadecane molar yield was still significant (45%) due to the initial loading of H_2 in the system; however, the final measured H_2 level (345 mmol) decreased proportionally due to oleic acid HYD. With a glycerol loading (2.2 g) native to the TAG triolein (1 mol of glycerol for every 3 mol of oleic acid), the DOX molar yield increased modestly, resulting in a 3-h molar conversion to heptadecane of 55%. The final headspace H_2 level (394 mmol) dropped below the initial loading (417 mmol); however, to a lesser extent compared to the reaction with no added glycerol (345 mmol). After accounting for H_2 consumption estimated for oleic acid HYD, a total of 48 mmol of H_2 was produced in situ. Lastly, a glycerol loading of 5 g (54 mmol) resulted in surplus H_2 in the system (479 ± 9

mmol) compared to the initial loading, with a DOX heptadecane molar yield (55%) comparable to the native triolein loading (2.2 g/24 mmol). The estimated in situ H_2 yield was ~30% of the theoretical maximum yield for glycerol APR. After accounting for oleic acid HYD, 133 mmol of H_2 was produced in situ. Further enhancements in glycerol APR activity may be needed to facilitate net zero or net positive system H_2 levels for lipid feedstocks with greater degrees of unsaturation compared to triolein.

Figure 2.7B shows the effect of catalyst loading on the 3-h oleic acid HYD-DOX molar yields and in situ H_2 production from glycerol. As discussed earlier, the standard catalyst loading used throughout this study (0.5 g) resulted in complete HYD and partial DOX (55%) of oleic acid after 3 h, with a net surplus of H_2 in the headspace (478 mmol ± 51 mmol). At higher catalyst loadings, the increased number of active sites resulted in a greater degree of fatty acid conversion, as expected. With 1 g of catalyst, complete HYD-DOX of oleic acid to heptadecane occurred with high selectivity (>98%). The yield of in situ H_2 remained the same as that observed with 0.5 g catalyst loading, consistent with the observation that glycerol APR has gone to completion for the current sampling time scale. When the catalyst loading was increased further to 2 g (1:10 fatty acid to catalyst ratio by weight), however, a modest increase was also observed for in situ H_2 production (556 mmol), which resulted in an observed H_2 yield of 47% of the theoretical maximum. This suggest that the glycerol-to-fatty acid ratio for a given catalyst loading may influence in situ H_2 yields, although further study is needed.

2.3.2.6 Native triolein loading

As a demonstration, **Figure 8** shows a final time series experiment conducted for oleic acid using a glycerol loading representative of triolein, a TAG with oleic acid side chains (1:3 glycerol-to-oleic acid molar ratio), and an increased catalyst loading (2 g Pt-Re/C) due to enhanced in situ H_2 production from glycerol APR (**Figure 7B**). Analysis of the reaction products revealed that oleic acid HYD to stearic acid was complete within 15 min at 300°C (time at which first sample was collected), with a significant extent likely occurring during heat-up from ambient temperature. Despite H_2 consumption from oleic acid HYD, the headspace H_2 level remained fairly constant near the initial loading (417 mmol), suggesting rapid APR of glycerol and improved H_2 yields compared to earlier results with 0.5 g of catalyst. No significant quantities of glycerol were detected in the aqueous phase after 15 min at temperature. After 2 h at temperature, fatty acid DOX reached completion, significantly faster than the 7 h required with 0.5 g of catalyst despite a higher glycerol loading (5 g glycerol; **Figure 5B**). Analysis of the headspace at 2 h confirmed that the overall process was net zero in H_2 consumption (421 ± 25 mmol). The stearic acid pseudo-first order DOX rate constant, normalized to catalyst loading ($k_{app\ Pt\text{-}Re/C\ DOX}$ = 2.83 ± 0.38 $\times 10^{-4}$ s^{-1} g^{-1}) was comparable to previous results obtained with 0.5 g of catalyst under a reducing headspace without glycerol ($k_{app\ Pt\text{-}Re/C\ DOX}$ = 2.72 ± 0.24 $\times 10^{-4}$ s^{-1} g^{-1}; **Figure 4**). The rapid apparent DOX kinetics and lower glycerol loading may the mask inhibitory effects of glycerol and its degradation products noted previously. These results demonstrate an initial proof of concept for the catalytic hydrothermal processing of unsaturated TAGs with H_2 consumption requirements being met through APR of glycerol, a byproduct of TAG hydrolysis.

2.3.2.7 Influence of headspace composition on Pt-Re oxidation state

The influence headspace gas composition on the Pt-Re oxidation state during exposure to hydrothermal media was then examined due to the pronounced effect on fatty acid DOX kinetics (**Figures 5** and **6**). X-ray photoelectron spectroscopy (XPS) was used to characterize the oxidation states of Pt and Re after exposure to hydrothermal media (300°C, 3 h) with either an inert headspace (345 kPa/56 mmol N_2) or a reducing headspace (2.586 MPa/417 mmol H_2). Individual oxidation states of Pt and Re exhibit characteristic doublet pairs due to spin-orbit coupling effects. Metal oxidation states were assessed by comparing binding energy (BE) of the $4f_{7/2}$ peak against reference standards collected previsouly,[35] as shown in **Figure 9**. Following exposure to hydrothermal media with an inert N_2 headspace, Pt-Re/C was characterized by metals with a high BE and corresponding oxidation state, as shown in **Figure 9A** and **9B**, respectively. The Pt-Re surface atomic ratio (1.0) determined by XPS was comparable to the bulk ratio measured by ICP (1.2), suggesting a relatively uniform surface and bulk metal ratio throughout the metal crystallites, as opposed to a core-shell orientation. The BE of the $4f_{7/2}$ peak for Pt was fit with two peaks (71.7 eV, 73.9 eV), indicating a mixed oxidation state based on the range of values previously reported in literature for the NIST XPS database (Pt^0 = 70.7-71.3 eV; Pt-Re alloy = 71.6-71.8 eV; Pt^{II} = 72.4-74.6 eV;).[36] The BE of the $4f_{7/2}$ peak for Re was fit with a single peak (45.6 eV), consistent with a Re^{VI-VII} oxidation state based on Re^{VI} NIST database values (44.3-46.8 eV) and Re^{VII} reference standards previously collected by our group (45.4-46.7 eV),[35] despite in situ pre-reduction with H_2 at 1.379 MPa for 2 h prior switching the headspace gas over to N_2. This finding agrees with previous work analyzing the oxidation state of Pt-Re/C exposed to hydrothermal media at lower temperature (225°C) using in situ XPS.[20]

In contrast to the above, XPS indicated that Pt and Re were in more reduced states for following exposure to hydrothermal media with H_2 headspace (2.586 MPa/417 mmol), as shown in **Figure 2.9c** and 2.**9d**. The BE of the $4f_{7/2}$ peak for Pt (71.9 eV) was consistent with a highly reduced state, whereas the measured BE for Re (41.4 eV) was closest to +I reference standard previously collected by our group (41.9 eV).[35] Analysis of the Pt-Re surface atomic ratio under a reducing atmosphere (1.0) was identical to the inert headspace above, suggesting no significant changes in crystallite elemental distribution. To our knowledge, this is the first study to examine the effect of H_2 on the oxidation state of Pt-Re/C in hydrothermal media. The lower oxidation states observed with a H_2 headspace may account for the increased activity of the catalyst for DOX processes that are H_2 neutral. However, other factors such as coke minimization, saturation of reaction by-products,[32] alteration of carbon support functional groups,[29,37] or promotion of decarbonylation as a DOX pathway [22,38,39] may also contribute to the enhanced fatty acid DOX kinetics observed with H_2 reactor headspace.

It is also worth noting that the standard catalyst pre-reduction step used for all reactions in this study (catalyst exposed to 1.379 MPa H_2 for 2 h at 200°C prior to flushing the headspace and introducing reactants) had a significant effect on the Pt-Re/C fatty acid DOX activity, even when the headspace was initially pressurized with H_2 (2.586 MPa). With catalyst pre-reduction, the 3-h DOX molar yield of heptadecane from oleic acid was 34 ± 3%, compared to 7% without pre-reduction. This contrasts with past studies that reported no enhancement for DOX of saturated fatty acids when Pt/C was pre-reduced (Fu et al., 2010). The difference in DOX performance with Pt-Re/C may be due to rapid re-oxidation of the catalyst after exposure to hydrothermal media with an inert headspace[20] or

changes in the metal crystallite composition distribution (i.e., alloy formation), as indicated by H_2 chemisorption results.

2.3.2.8 Pt-Re/C hydrothermal stability

The stability of Pt-Re/C in hydrothermal media (300°C, 3 h) with a reducing headspace (2.586 MPa/417 mmol H_2) was then evaluated to determine changes in catalyst composition or morphology. ICP analysis of a representative Pt-Re/C catalyst sample after hydrothermal exposure showed no significant changes in metal loading. Subsequent analysis of the aqueous phase also confirmed that metal leaching was not prominent, although trace levels (< 1% of the total metal loading) of Pt and Re initially loaded were observed (Pt = 0.18 ppm; Re = 4.16 ppm).

Analysis of the carbon support by multipoint N_2 physisorption revealed pronounced changes in the surface area, as shown in **Table 2.1**. Following hydrothermal exposure, the support surface area of Pt-Re/C decreased by 11% (675 m^2/g), similar to past reports for activated carbon noble metal catalysts in hydrothermal media.[5,24] Although this decrease is not insignificant, the degree of degradation is much lesser compared to oxide supports which can degrade by over 90% hydrothermal media.[40] The support pore volume also decreased by 16% (0.507 cm^3/g), while the average pore diameter remained fairly constant (10.04 Å).

CO and H_2 chemisorption following hydrothermal exposure also revealed significant changes to the exposed metal area, as shown in **Table 2.1**. Irreversible CO uptake decreased by 25% (CO uptake 84 mol/g), resulting in a calculated dispersion of 31.5%. This indicates that high temperature hydrothermal exposure likely results in some sintering of the

immobilized metal crystallites, consistent with findings by XRD and SEM-EDS as described below. In addition, irreversible H uptake decreased by 42% (H uptake 30 mol/g), resulting in a CO:H uptake ratio of 2.8. The high CO:H uptake ratio indicates that Re continues to influence the chemisorption behavior of Pt, although significant morphological changes have occurred compared to as prepared Pt-Re/C.

XRD analysis of Pt-Re/C after hydrothermal media exposure showed support and crystallite peaks similar to the as prepared catalyst (**Figure 2.1**). Estimation of the metal crystallite size by XRD after hydrothermal exposure (3.8 nm compared with 3.4 nm for fresh catalyst) also suggested that a small degree of sintering had occurred. SEM-EDS elemental mapping of Pt and Re revealed that the majority metallic sites remained co-dispersed, but single-element crystallites were present to a greater degree, as shown in **Figure 2.2G-H**. These results indicate the need for additional investigation into the hydrothermal stability and activity of Pt-Re/C for fatty acid deoxygenation with time on stream. Although time on stream testing was beyond the scope of this initial study, evaluation of Pt-Re supported on activated carbon pellets for the hydrodeoxygenation of phenol in hydrothermal media demonstrated high stability and activity for over 140 h on stream in a packed bed flow reactor,[24] highlighting the potential of Pt-Re/C for facilitating hydrothermal chemistry.

2.3.2.9 Integrated reaction scheme

Experimental results support an integrated catalytic hydrothermal reaction scheme for the conversion of lipids to hydrocarbons, with in situ H_2 production from glycerol (**Figure 2.10)**. As mentioned, in hydrothermal media triacylglycerides rapidly hydrolyze to

produce free fatty acids and glycerol. This process is utilized at commercial scale, commonly referred to as fat-splitting.[41–43] The utilization of hydrolyzed lipids facilitates the use of low-quality lipid feedstocks which are typically high in free fatty acids and problematic for conventional biodiesel processing.[44] Polar lipids (e.g., phosphatidylcholine) are also known to rapidly hydrolyze to produce free fatty acids, glycerol, and P and N containing moieties,[45] potentially expanding the range of viable lipid feedstocks for hydrothermal conversion to hydrocarbons.

Following hydrolysis, liberated glycerol can undergo catalytic decomposition reactions to generate H_2 and CO, with CO undergoing the WGS reaction to produce additional H_2 over the appropriate catalyst (**Rxn. 5**).[30] Collectively, aqueous phase reforming can theoretically produce 7 moles of H_2 from 1 mole of glycerol.

As noted, free fatty acids generated from lipid hydrolysis can contain varying ratios of saturated, unsaturated, and polyunsaturated fatty acids, depending on the feedstock origin. For example, waste grease feedstocks (e.g., yellow grease, brown grease, tallow) may contain saturated fatty acids ranging from 39-52% of the total fatty acid profile. Algal lipid feedstocks, in contrast, may contain as low as 10% saturated fatty acids,[3] and over 30% polyunsaturated fatty acids depending on the strain.[46] Fatty acid unsaturation can impart a H_2 consumption demand since HYD to the corresponding saturated fatty acids (**Rxn. 6**) is necessary prior to DOX of the carboxylic acid group (**Rxn. 1** and **Rxn. 2**). The continuous H_2 demand can potentially be met by APR of glycerol released upon lipid hydrolysis, yielding a net neutral or net positive system H_2 balance. Lipid feedstocks can also be blended prior to processing to maintain an optimal degree of unsaturation during continuous

processing. Additional H_2 can initially be introduced to accelerate kinetics; however, unlike conventional hydrotreatment processes, continuous H_2 input may not be required.

Saturated fatty acids undergo DOX during catalytic hydrothermal processing to produce linear hydrocarbons with high selectivity. The DOX pathway may progress via decarboxylation (**Rxn. 1**), or decarbonylation (**Rxn. 2**) rapidly followed by HYD of the terminal alkene (**Rxn. 4**).

Although terminal alkene HYD includes consumption of H_2, the overall decarbonylation process is H_2 neutral because the CO produced from the initial decarbonylation yields additional H_2 via the WGS reaction (**Rxn. 3**). In contrast to H_2-neutral decarboxylation and decarbonylation pathways, fatty acid reduction pathways observed at higher initial H_2 loadings (Figure 3a) consume H_2. Complete fatty acid reduction to the corresponding hydrocarbon consumes 3 moles of H_2 (**Rxn. 7**).

2.4 Conclusion

In summary, catalytic hydrothermal processing is a promising method for converting unsaturated fatty acids into hydrocarbon fuels while using glycerol APR to meet process H_2 consumption needs. To our knowledge, this is the first report demonstrating complete HYD-DOX of unsaturated fatty acids with net zero H_2 consumption using glycerol. Experiments revealed that fatty acid DOX was influenced by the addition of Re to Pt/C, system H_2 level, and glycerol and catalyst loading. Fatty acid decarboxylation/decarbonylation was observed as the primary DOX pathway, with reduction being observed as a minor pathway at high initial H_2 loadings (≥3.447 MPa/557 mmol). Although several mechanisms may account for enhanced DOX yields with H_2 initially loaded into the system, the effect on catalyst activity

and oxidation state was pronounced. Characterization of Pt-Re/C determined that Re had a significant effect on CO:H uptake ratio (2.2) compared to commercial Pt/C (1.3), with metals dispersed as small crystallites (~ 3-4 nm) throughout carbon support. Optimized conditions were applied with a 1:3 glycerol-to-oleic acid molar ratio (i.e., native ratio formed upon hydrolysis of the TAG triolein), which resulted in complete DOX within 2 h at temperature and net-zero H_2 consumption. Catalyst characterization after hydrothermal exposure revealed that moderate sintering had occurred, suggesting additional work is needed to evaluate Pt-Re/C stability with time on stream. A H_2-neutral (or positive) scheme for hydrothermal catalytic conversion of TAGs is proposed, involving TAG hydrolysis, catalytic reforming of glycerol, and fatty acid hydrogenation and deoxygenation processes resulting in saturated hydrocarbon products. Results from this study suggest a promising strategy for overcoming some of the major limitations of conventional lipid-to-biofuel pathways.

2.5 Methods

2.5.1. Materials

Stearic acid (98%) was obtained from TCI Chemicals and oleic acid (90%) was obtained from Alfa Aesar. Glycerol (99.5%), activated carbon (Darco 100 mesh), powdered Pt/C (5 wt.%) catalyst, and ammonium perrhenate salt (NH_4ReO_4) were purchased from Sigma-Aldrich. Hydrocarbon standards (e.g., pentadecane, hexadecane, heptadecane, octadecane) were obtained from Chem Service Inc. Analytical-grade dichloromethane (DCM) and methanol were obtained from Fisher Scientific. For a typical experiment, Pt-Re/C (5 wt.% Pt, 5 wt.% Re) was prepared via aqueous adsorption of 38 mg of NH_4ReO_4 onto 0.5 g of Pt/C catalyst suspended in 50 g of

deionized (DI) water. The contents were loaded into a Parr 4575 500-mL high temperature/pressure reactor. Pt/C and Pt-Re/C catalysts were pre-reduced in situ prior to use by purging and venting the reactor with 1.379 MPa of H_2 over three cycles, followed by heating to 200°C with continuous mixing for 2 h at temperature. The reactor was then cooled to ambient temperature and maintained under positive pressure with either an inert (N_2) or reducing (H_2) gas.

2.5.2 Catalyst characterization

Catalyst metal loadings were measured using a Spector Arcos Inductively Couples Plasma Atomic Emission Spectrometer (ICP-AES) after digestion in concentrated acid. Support surface area, pore volume, and average pore diameter were determined by multipoint N_2 physisorption using a QuandraSorb SI analyzer. Catalyst specific surface area was calculated by BET, and pore volume and pore diameter were calculated by BJH desorption. Prior to analysis, catalysts were outgassed at 250°C for 18 h. Physisorption measurements were performed at the temperature of liquid N_2.

Catalyst metal dispersion and the influence of Re on Pt was determined by CO and H_2 chemisorption using a Micometrics Autochem II 2920 pulse analyzer. Prior to analysis, catalysts were degassed at 40°C for 0.2 h under Ar, dried at 100°C, and reduced at 280°C in flowing 10% H_2/Ar (50 mL/min) for 1 h. Catalysts were then purged at 280°C for 0.5 h with either He (for CO chemisorption) or Ar (for H_2 chemisorption). Chemisorption measurements were performed at 45°C and metal dispersion was calculated based on CO uptake with a CO:M ratio of unity.

Long-range catalyst material order was analyzed by XRD using a Rigaku Ultima IV X-ray diffractometer. The X-ray voltage was set to 40 kV and 44 ma, with a sampling width of

0.02° and scan speed of 5°/min. Metal crystallite size parameters were estimated using the Scherer equation with PDXL version 1.6.0.1 (Rigaku Corporation).

Imaging and elemental of mapping of multiple catalyst particles was performed by SEM-EDS using a FEI Quanta 400 FEG scanning electron microscope equipped with an EDAX X-ray detector. Samples were mounted onto aluminum stubs using a conductive carbon tape to adhere the particles to the stub and provide electrical conductivity. Elemental mapping was performed using an accelerated voltage of 30 kV. The signal was based on net X-ray intensity using a Z absorption florescence (ZAF) correction over a dwell time of 300 ms per pixel.

High-resolution TEM images of individual catalyst particles were collected using a JEOL 2010LAB$_6$ TEM instrument. Samples were dispersed in acetone and mounted onto holey carbon Cu grids prior to analysis. STEM-EDS elemental mapping of metallic crystallites was also performed using a JEOL 2010F field emission TEM instrument, coupled to an Oxford INCA EDS detector with a 1-nm probe size.

Catalyst surface oxidation states were examined using a Physical Electronics PHI 5400 X-ray photoelectron spectrometer equipped with a monochromatized Mg Kα source (1253.6 eV). The pass energy employed for high resolution Pt and Re XPS spectra was 35.8 eV. Pt-Re/C catalysts for XPS analysis were exposed to hydrothermal media (300°C, 3 h) using the Parr 4575 reactor loaded initially with either an inert (345 kPa/56 mmol N_2) or reducing (2.586 MPa/417 mmol H_2) headspace. After exposure, catalysts were sampled in situ using a Parr 4532-D collection attachment. The isolation valve on the reactor was briefly released to charge the sampling accessory, which was then cooled to ambient pressure using a water-cooling sleeve. To prevent air exposure, catalyst samples were dried inside an anoxic glove box and loaded onto conductive copper tape located inside an anoxic XPS-sample holder chamber, as described

previously.[35] High-resolution (i.e., 0.1 eV resolution) XPS spectra were collected from 38.0 eV to 58.0 eV for Re and 68.0 eV to 88.0 eV for Pt. Spectra were energy-normalized relative to the dominant C 1s peak from the activated carbon support (284.5 eV). Spectra were then normalized and fit with a convoluted Gaussian and Lorentzian function after constraining the separation distance and peak area ratio of contributing doublet peaks with CasaXPS version 2.3 (Casa Software Ltd).

2.5.3. Catalytic hydrothermal processing

Hydrothermal conversions were conducted in the Parr 4575 reactor. The reactor containing pre-reduced catalyst was loaded with the 20 g of oleic acid, and 5 g of glycerol dissolved in 30 g of DI (80 g DI total including water from catalyst pre-reduction). The reactor vessel was pressurized to 1.379 MPa with the desired headspace gas (N_2 or H_2) and purged for three cycles under constant stirring. The headspace pressure was then increased to the desired initial value corrected to 25°C. Reactor temperature was raised to 300°C at a rate of ~10°C/min (heat-up time ~1 h) with constant stirring at high speed (>1000 rpm) applied for the desired reaction time. Once the reaction time elapsed, the reactor was rapidly cooled to ambient temperature by initiating water flow through internal cooling coils. For time series studies, independent batch reactions were performed for each time point. Where indicated, triplicate reactions were performed independently to determine experimental variability, with error bars representing standard deviations.

2.5.4. Reaction product analysis

The total reactor contents were collected, fractionated, and analyzed gravimetrically to ensure mass balance closure of the aqueous and organic product phases. After confirming mass balance closure, the recovered reactor contents were heated while stirring to produce a bi-phase system for sampling. The top organic layer containing fatty acids and hydrocarbons was sampled, dissolved in DCM (1 wt.% sample), and filtered (0.45 μm PTFE) prior to analysis to remove catalyst particles. Dissolved glycerol in the bottom aqueous phase was sampled, dissolved in methanol (1 wt.% sample) and filtered (0.45-μm PTFE) prior to analysis. As a control, each complete bilayer was also dissolved in excess solvent and analyzed to ensure representative results from sampling.

Fatty acids, alkanes, alcohols, (e.g., stearyl alcohol), glycerol and glycol derivatives (e.g., ethylene glycol, propylene glycol) were quantified using a HP 5890 Series II FID gas chromatograph outfitted with a Restek Stabilwax-DA column (30m × 0.25 mm id, 0.25 μm film). Helium (6 mL/min column flow) was used as the carrier gas with the injector split flow set to 60 ml/min. The oven temperature was increased from 40°C to 250°C at 10°C/min. The injector volume was set to 1 μL and the inlet temperature set at 250°C. The detector temperature was set to 250°C, H_2 gas set to 32 ml/min, and airflow set to 400 ml/min. Compound retention times and FID-calibration response curves were conducted using fatty acid, glycerol, and alkane standards. Reaction products were also confirmed by GC-MS analysis using a Varian 3800 gas chromatograph with a Varian 2000 mass spectrometer and Restek RTX-5MS column and by ^1H NMR using a Varian Unity 400 MHz spectrometer with conditions described previously.[47]

Reactor headspace gas samples were collected after the reaction using 0.5-L Restek Tedlar sample bags, and analyzed for H_2, CH_4, CO, and CO_2 using a HP 5890 Series II TCD gas chromatograph outfitted with a Carboxen-1010 Supelco column. For the carrier gas, N_2 (1

mL/min) was used to analyze H_2, while He was used to analyze carbon-based gases (1 mL/min). A split flow of 10 mL/min was used with an inlet temperature of 225°C. An isothermal oven temperature profile was used to detect H_2 (35°C) and carbon-based gases (125°C). The TCD detector was set to 225°C at high sensitivity with a reference gas flow of 15 mL/min and auxiliary gas flow of 7 mL/min.

Hydrocarbon product molar yields were calculated by dividing the moles of recovered product by the moles of fatty acid initially loaded into the reactor. Hydrocarbon selectivities were calculated by dividing the moles of hydrocarbon product by the moles of converted fatty acid. In situ H_2 production yields were determined using the ideal gas law based on the final headspace gas pressure and compositional analysis determined by GC-TCD. Due to the low solubility of H_2 in water at ambient temperature compared to the gas loadings examined in this study, dissolved H_2 was assumed to be negligible. For this work, H_2 selectivity from glycerol APR is defined as the ratio of H_2 produced, divided by the theoretical amount of H_2 produced if the converted glycerol was completely reformed (e.g., decomposition and WGS) to generate H_2 and CO_2. Apparent reaction rate constants for stearic acid deoxygenation were estimated assuming pseudo-first order kinetics using nonlinear regression with GraphPad Prism version 6.00 (GraphPad Software).

2.6 References Cited

1. U.S. EIA. International Energy Outlook. (2013). at <http://www.eia.gov/forecasts/ieo/transportation.cfm>
2. Kalnes, T. N., Koers, K. P., Marker, T. & Shonnard, D. R. A technoeconomic and environmental life cycle comparison of green diesel to biodiesel and syndiesel. *Environ. Prog. Sustain. Energy* **28,** 111–120 (2009).
3. Berenblyum, A., Danyushevsky, V., Katsman, E., Podoplelova, T. & Flid, V. Production of engine fuels from inedible vegetable oils and fats. *Pet. Chem.* **50,** 305–311 (2010).
4. Santillan-Jimenez, E. & Crocker, M. Catalytic deoxygenation of fatty acids and their derivatives to hydrocarbon fuels via decarboxylation/decarbonylation. *J. Chem. Technol. Biotechnol.* **87,** 1041–1050 (2012).
5. Fu, J., Lu, X. & Savage, P. E. Catalytic hydrothermal deoxygenation of palmitic acid. *Energy Environ. Sci.* **3,** 311–317 (2010).
6. Fu, J., Lu, X. & Savage, P. E. Hydrothermal decarboxylation and hydrogenation of fatty acids over Pt/C. *ChemSusChem* **4,** 481–486 (2011).
7. Biller, P., Riley, R. & Ross, A. B. Catalytic hydrothermal processing of microalgae: Decomposition and upgrading of lipids. *Bioresour. Technol.* **102,** 4841–4848 (2011).
8. Yeh, T. M. *et al.* Hydrothermal catalytic production of fuels and chemicals from aquatic biomass. *J. Chem. Technol. Biotechnol.* **88,** 13–24 (2013).
9. Peterson, A. A. *et al.* Thermochemical biofuel production in hydrothermal media: A review of sub- and supercritical water technologies. *Energy Environ. Sci.* **1,** 32–65 (2008).
10. Jayasinghe, P. & Hawboldt, K. A review of bio-oils from waste biomass: Focus on fish processing waste. *Renew. Sustain. Energy Rev.* **16,** 798–821 (2012).

11. Siddiquee, M. N. & Rohani, S. Lipid extraction and biodiesel production from municipal sewage sludges: A review. *Renew. Sustain. Energy Rev.* **15,** 1067–1072 (2011).
12. Brennan, L. & Owende, P. Biofuels from microalgae—A review of technologies for production, processing, and extractions of biofuels and co-products. *Renew. Sustain. Energy Rev.* **14,** 557–577 (2010).
13. Pittman, J. K., Dean, A. P. & Osundeko, O. The potential of sustainable algal biofuel production using wastewater resources. *Bioresour. Technol.* **102,** 17–25 (2010).
14. Lercher, J. A., Zhao, C. & Brueck, T. Catalytic deoxygenation of microalgae oil to green hydrocarbons. *Green Chem.* **15,** 1720–1739 (2013).
15. Cortright, R. D., Davda, R. R. & Dumesic, J. A. Hydrogen from catalytic reforming of biomass-derived hydrocarbons in liquid water. *Nature* **418,** 964–967 (2002).
16. Shabaker, J. ., Huber, G. . & Dumesic, J. . Aqueous-phase reforming of oxygenated hydrocarbons over Sn-modified Ni catalysts. *J. Catal.* **222,** 180–191 (2004).
17. Luo, N., Fu, X., Cao, F., Xiao, T. & Edwards, P. P. Glycerol aqueous phase reforming for hydrogen generation over Pt catalyst – Effect of catalyst composition and reaction conditions. *Fuel* **87,** 3483–3489 (2008).
18. King, D. L. *et al.* Aqueous phase reforming of glycerol for hydrogen production over Pt–Re supported on carbon. *Appl. Catal. B Environ.* **99,** 206–213 (2010).
19. Özgür, D. Ö. & Uysal, B. Z. Hydrogen production by aqueous phase catalytic reforming of glycerine. *Biomass Bioenergy* **35,** 822–826 (2011).
20. Zhang, L. *et al.* Correlation of Pt–Re surface properties with reaction pathways for the aqueous-phase reforming of glycerol. *J. Catal.* **287,** 37–43 (2012).

21. Kunkes, E. L. *et al.* The role of rhenium in the conversion of glycerol to synthesis gas over carbon supported platinum–rhenium catalysts. *J. Catal.* **260,** 164–177 (2008).
22. Berenblyum, A. S., Podoplelova, T. A., Shamsiev, R. S., Katsman, E. A. & Danyushevsky, V. Y. On the mechanism of catalytic conversion of fatty acids into hydrocarbons in the presence of palladium catalysts on alumina. *Pet. Chem.* **51,** 336–341 (2011).
23. Rozmysłowicz, B. *et al.* Influence of hydrogen in catalytic deoxygenation of fatty acids and their derivatives over Pd/C. *Ind Eng Chem Res* **51,** 8922–8927 (2012).
24. Kim, Y. T., Dumesic, J. A. & Huber, G. W. Aqueous-phase hydrodeoxygenation of sorbitol: A comparative study of Pt/Zr phosphate and PtReOx/C. *J. Catal.* **304,** 72–85 (2013).
25. Simonetti, D. A., Kunkes, E. L. & Dumesic, J. A. Gas-phase conversion of glycerol to synthesis gas over carbon-supported platinum and platinum–rhenium catalysts. *J. Catal.* **247,** 298–306 (2007).
26. Isaacs, B. H. & Petersen, E. E. Surface area measurement of platinum/rhenium/alumina: I. Stoichiometry of hydrogen-oxygen chemisorptions and titrations. *J. Catal.* **85,** 1–7 (1984).
27. Rozmysłowicz, B., Mäki-Arvela, P. & Murzin, D. in *Biomass Conversion* (eds. Baskar, C., Baskar, S. & Dhillon, R. S.) 199–220 (Springer Berlin Heidelberg, 2012). at <http://dx.doi.org/10.1007/978-3-642-28418-2_6>
28. Behrens, M. & Datye, A. K. *Catalysis for the Conversion of Biomass and Its Derivatives*. (Max Planck Research Library for the History and Development of Knowledge, 2013). at <http://www.edition-open-access.de/proceedings/2/toc.html>
29. Fu, J., Shi, F., Thompson, L. T., Lu, X. & Savage, P. E. Activated carbons for hydrothermal decarboxylation of fatty acids. *ACS Catal.* **1,** 227–231 (2011).

30. Davda, R. R., Shabaker, J. W., Huber, G. W., Cortright, R. D. & Dumesic, J. A. A review of catalytic issues and process conditions for renewable hydrogen and alkanes by aqueous-phase reforming of oxygenated hydrocarbons over supported metal catalysts. *Appl. Catal. B Environ.* **56,** 171–186 (2005).

31. Soares, R. R., Simonetti, D. A. & Dumesic, J. A. Glycerol as a source for fuels and chemicals by low-temperature catalytic processing. *Angew. Chem.* **118,** 4086–4089 (2006).

32. Immer, J. G. & Lamb, H. H. Fed-batch catalytic deoxygenation of free fatty acids. *Energy Fuels* **24,** 5291–5299 (2010).

33. Immer, J. G., Kelly, M. J. & Lamb, H. H. Catalytic reaction pathways in liquid-phase deoxygenation of C18 free fatty acids. *Appl. Catal. Gen.* **375,** 134–139 (2010).

34. Shabaker, J. W. & Dumesic, J. A. Kinetics of aqueous-phase reforming of oxygenated hydrocarbons: Pt/Al_2O_3 and Sn-modified Ni catalysts. *Ind. Eng. Chem. Res.* **43,** 3105–3112 (2004).

35. Choe, J. K., Shapley, J. R., Strathmann, T. J. & Werth, C. J. Influence of rhenium speciation on the stability and activity of Re/Pd bimetal catalysts used for perchlorate reduction. *Environ. Sci. Technol.* **44,** 4716–4721 (2010).

36. NIST. *X-Ray Photoelectron Spectroscopy Database*. (2012). at <http://srdata.nist.gov/xps/Default.aspx>

37. Boehm, H. P. Some aspects of the surface chemistry of carbon blacks and other carbons. *Carbon* **32,** 759–769 (1994).

38. Lu, J., Behtash, S. & Heyden, A. Theoretical investigation of the reaction mechanism of the decarboxylation and decarbonylation of propanoic acid on Pd(111) model surfaces. *J. Phys. Chem. C* **116,** 14328–14341 (2012).

39. Lu, J., Behtash, S., Faheem, M. & Heyden, A. Microkinetic modeling of the decarboxylation and decarbonylation of propanoic acid over Pd(111) model surfaces based on parameters obtained from first principles. *J. Catal.* **305,** 56–66 (2013).

40. Pham, H. N., Anderson, A. E., Johnson, R. L., Schmidt-Rohr, K. & Datye, A. K. Improved hydrothermal stability of mesoporous oxides for reactions in the aqueous phase. *Angew. Chem. Int. Ed.* **51,** 13163–13167 (2012).

41. Lascaray, L. Mechanism of fat splitting. *Ind. Eng. Chem.* **41,** 786–790 (1949).

42. Patil, T. A., Butala, D. N., Raghunathan, T. S. & Shankar, H. S. Thermal hydrolysis of vegetable oils and fats. 1. Reaction kinetics. *Ind. Eng. Chem. Res.* **27,** 727–735 (1988).

43. Holliday, R. L., King, J. W. & List, G. R. Hydrolysis of vegetable oils in sub- and supercritical water. *Ind. Eng. Chem. Res.* **36,** 932–935 (1997).

44. Ma, F. & Hanna, M. A. Biodiesel production: A review. *Bioresour. Technol.* **70,** 1–15 (1999).

45. Changi, S., Matzger, A. J. & Savage, P. E. Kinetics and pathways for an algal phospholipid (1,2-dioleoyl-*sn*-glycero-3-phosphocholine) in high-temperature (175–350 °C) water. *Green Chem.* **14,** 2856 (2012).

46. Griffiths, M. J. & Harrison, S. T. L. Lipid productivity as a key characteristic for choosing algal species for biodiesel production. *J. Appl. Phycol.* **21,** 493–507 (2009).

47. Vardon, D. R. *et al.* Chemical properties of biocrude oil from the hydrothermal liquefaction of *Spirulina* algae, swine manure, and digested anaerobic sludge. *Bioresour. Technol.* **102,** 8295–8303 (2011).

2.7 Figures and Tables

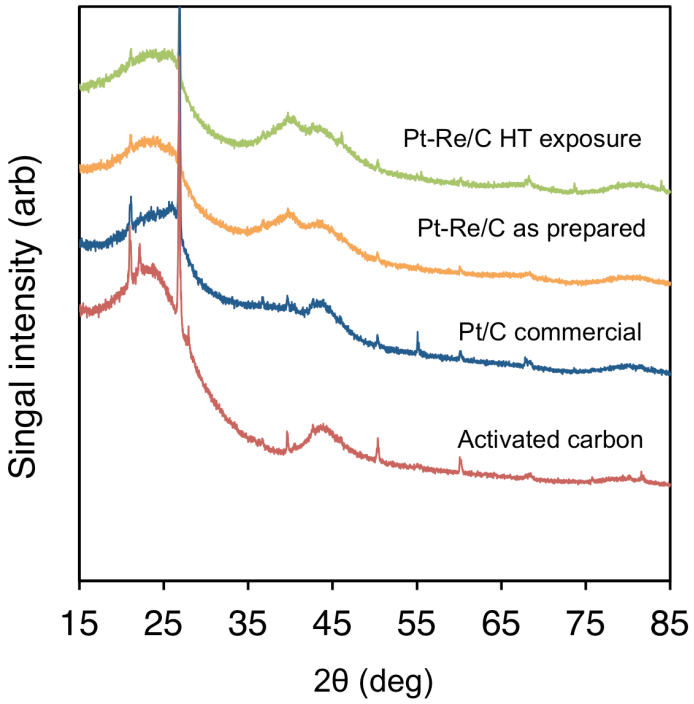

Figure 2.1 XRD spectra of unloaded activated carbon, commercial Pt/C as received, Pt-Re/C as prepared, and Pt-Re/C after exposure to hydrothermal media.

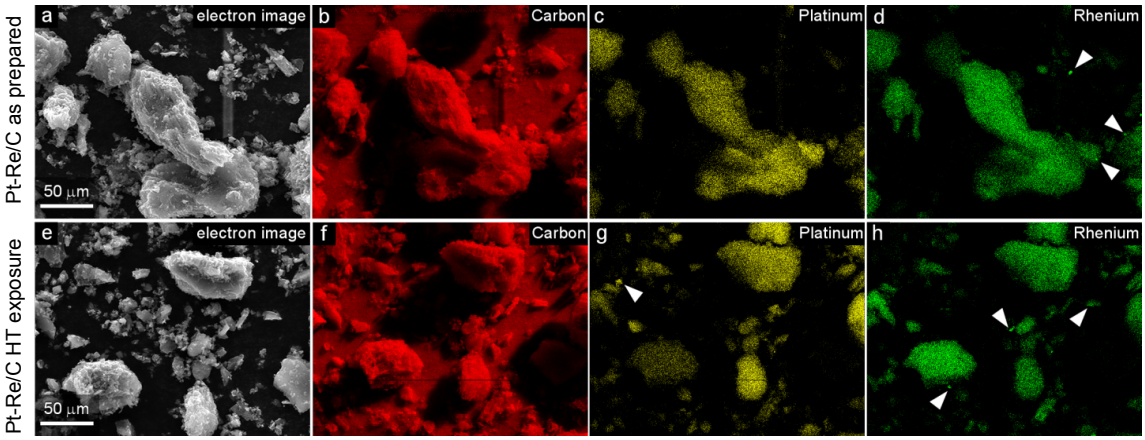

Figure 2.2 SEM images and EDS maps of Pt-Re/C catalyst particles as prepared (a-d) and post hydrothermal media exposure (e-f), with single-metal crystallites indicated by white arrowheads.

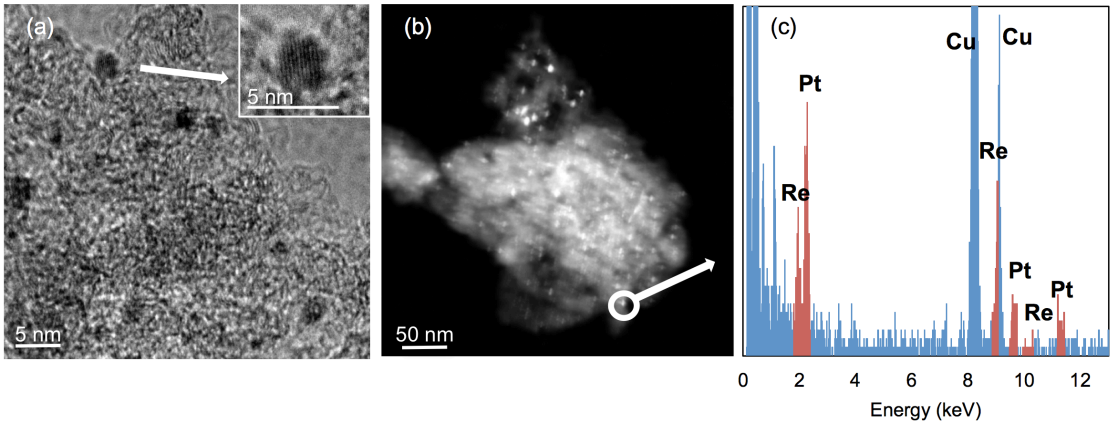

Figure 2.3 Pt-Re/C images of the catalyst as prepared by TEM (a) and STEM (b), with localized STEM-EDS spectra obtained from the region of an individual crystallite (c). Note that Cu peaks present due to STEM sample holder.

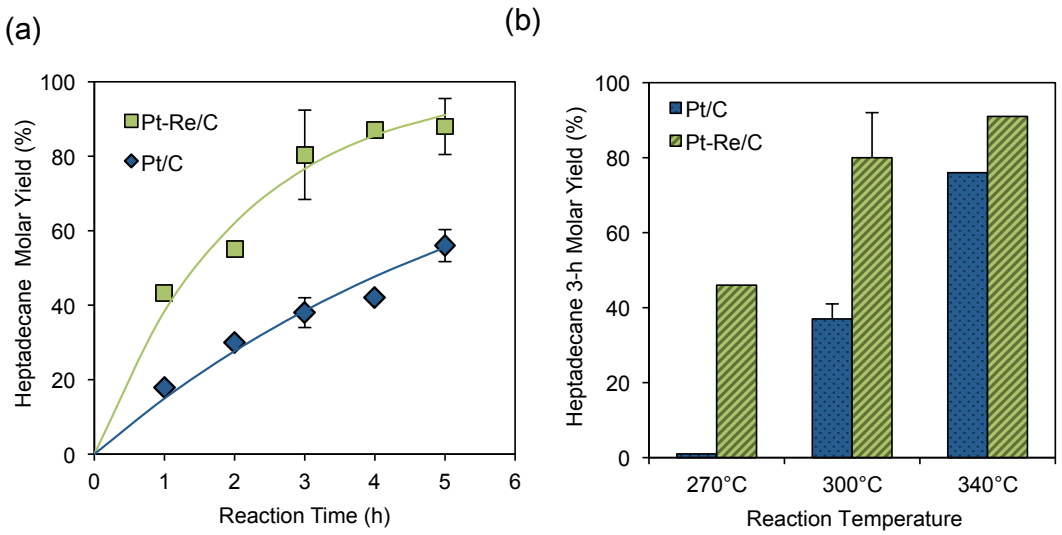

Figure 2.4 Timecourse for stearic acid DOX at 300°C with an initial H_2 reactor headspace using Pt/C and Pt-Re/C (a). Pseudo-first order kinetic parameter fits for heptadecane formation indicated by color solid lines for Pt-Re/C (green) and Pt/C (blue). Effect of temperature on stearic acid DOX 3-h heptadecane molar yields using Pt/C and Pt-Re/C with an initial H_2 reactor headspace (b). Reaction conditions: 20 g stearic acid, 0.5 g catalyst, 80 g H_2O, initial head-gas = 3.447 MPa H_2.

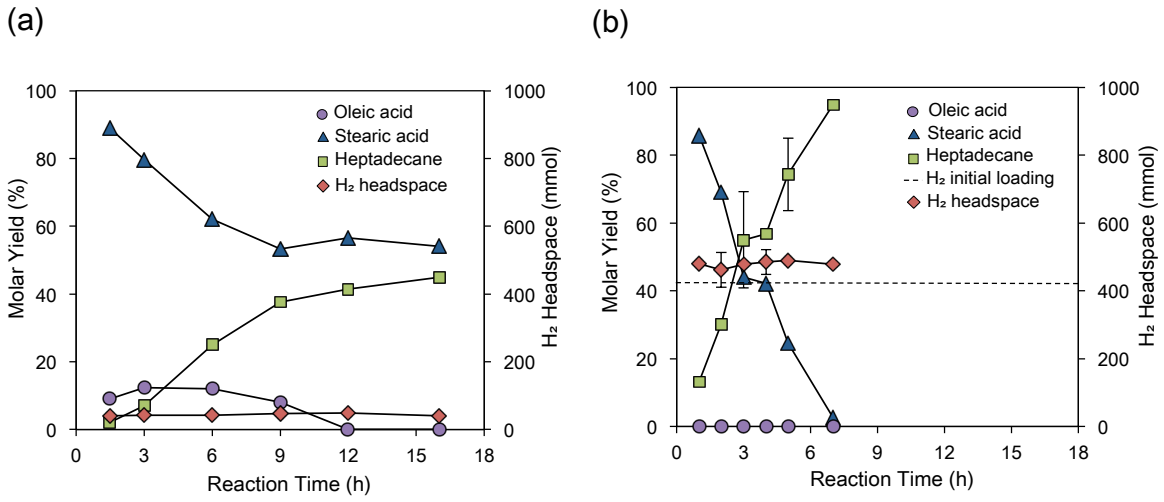

Figure 2.5 Hydrothermal catalytic HYD-DOX kinetics of oleic acid using glycerol as an in situ H_2 source and an initial reactor headspace containing N_2 (a) and H_2 (b). Reaction conditions: 300°C, 20 g oleic acid, 5 g glycerol, 0.5 g Pt-Re/C, 80 g H_2O, 345 kPa N_2 or 2.586 MPa H_2.

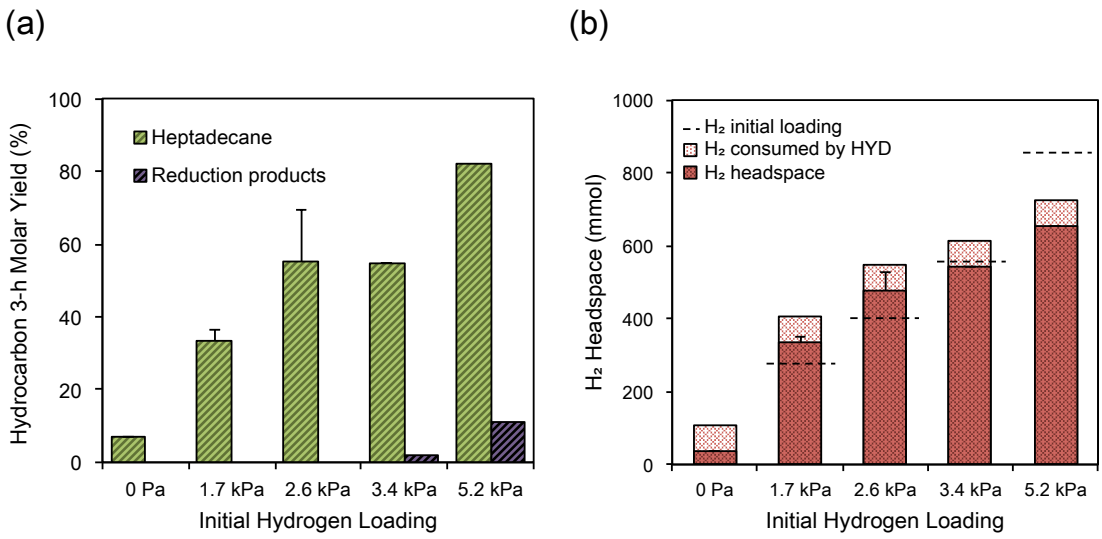

Figure 2.6 Influence of initial headspace H_2 loading on oleic acid HYD-DOX (a) and in situ H_2 production by glycerol APR (b). Reaction conditions: t = 3 h, 300°C, 20 g oleic acid, 5 g glycerol, 0.5 g Pt-Re/C, 80 g H_2O. H_2 consumed by HYD is estimated based on the observed saturated compounds derived from oleic acid.

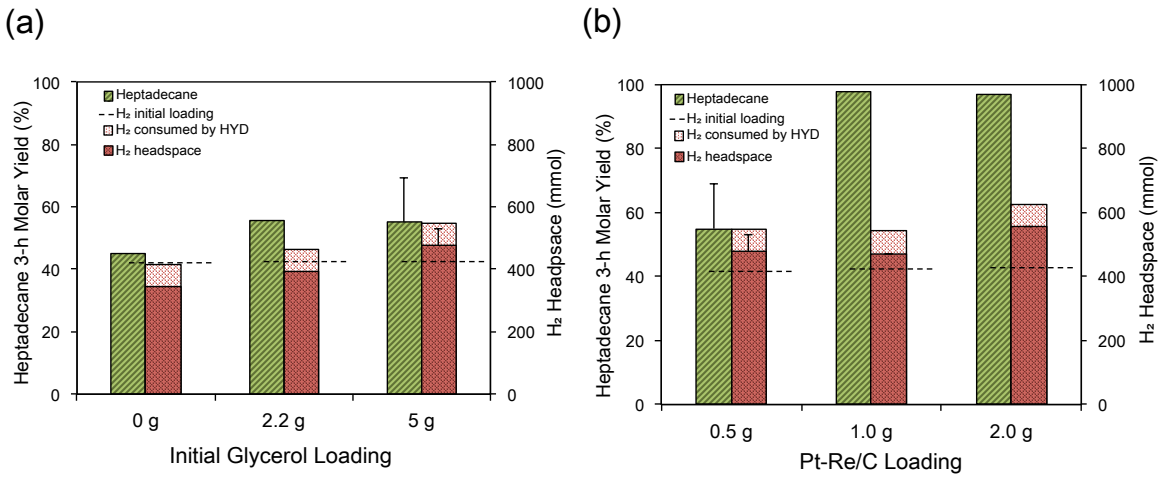

Figure 2.7 Influence of glycerol loading (a) and Pt-Re/C loading (b) on 3-h oleic acid HYD-DOX yields and H_2 headspace concentrations. Reaction conditions: 300°C, 20 g oleic acid, 18 g H_2O, initial H_2 loading = 2.586 MPa, 0.5 g Pt-Re/C loading (for panel a), 5 g glycerol (for panel b).

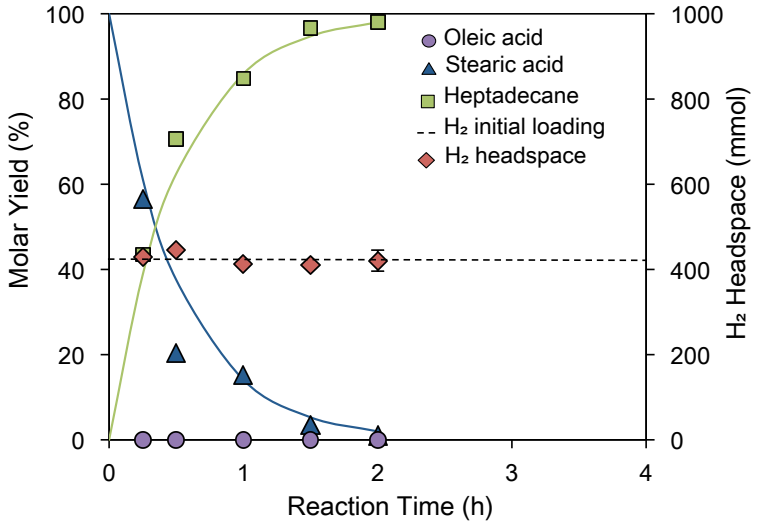

Figure 2.8 Timecourse yields for oleic acid HYD-DOX using a glycerol loading native to triolein (1:3 glycerol-to-oleic acid molar ratio) and an elevated loading of Pt-Re/C (2.0 g). Other reaction conditions: 300°C, 20 g oleic acid, 2.2 g glycerol, 18 g H_2O, initial H_2 headspace = 2.586 MPa. Pseudo-first order kinetic parameter fits for stearic acid DOX (blue) to produce heptadecane (green) are shown with solid color lines.

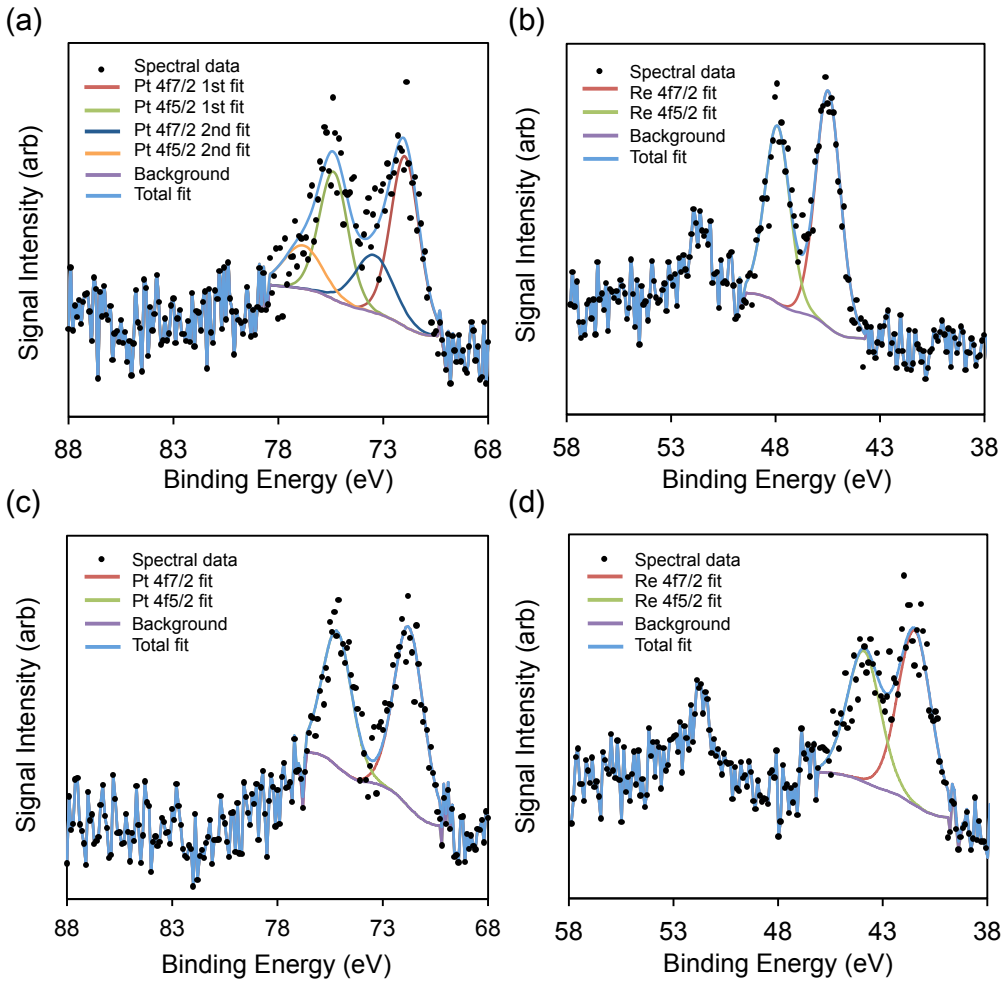

Figure 2.9 Influence of an initial inert headspace (345 kPa N_2) on the oxidation state of Pt (a) and Re (b), as well as the influence of an initial reducing headspace (2.586 MPa H_2) with Pt (c) and Re (d) after exposure to hydrothermal media for 3 h at 300°C.

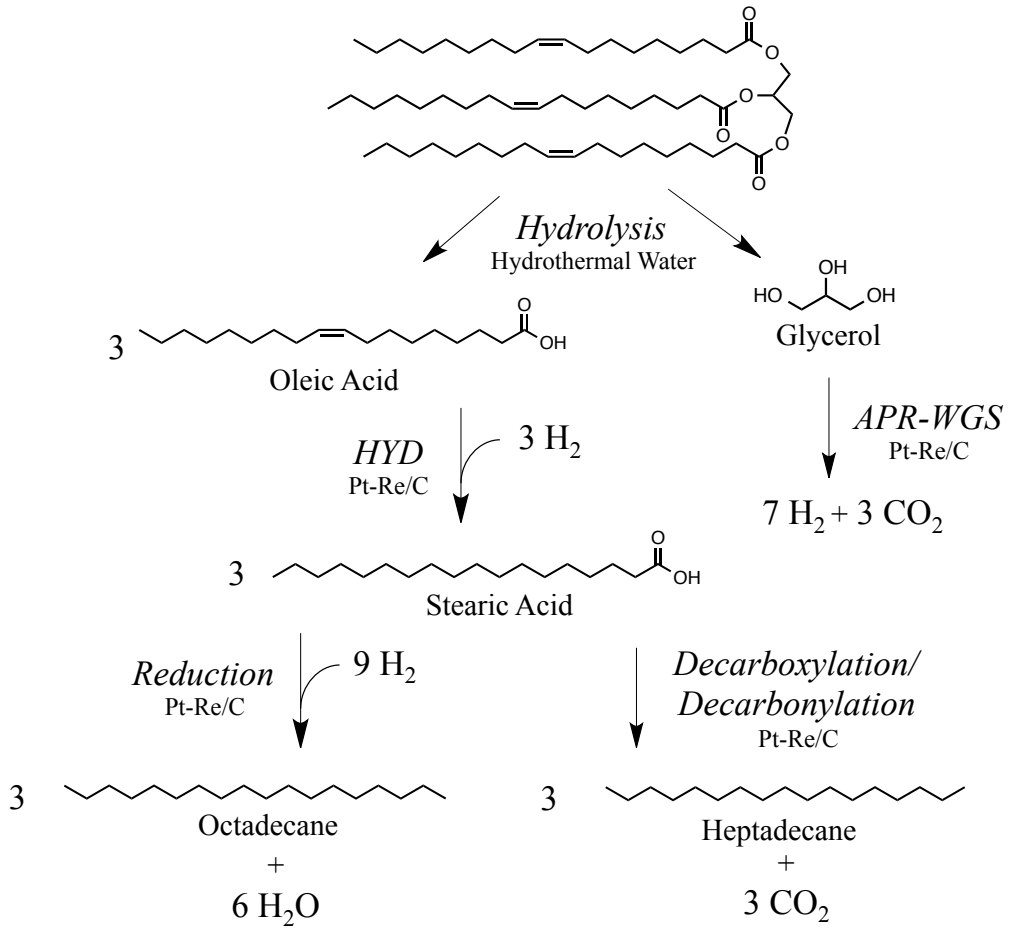

Figure 2.10 Proposed reaction scheme and product yields for hydrothermal processing of the triacylglyceride triolein into hydrocarbons and in situ H_2.

Table 2.1 Physisorption and chemisorption parameters for commercial Pt/C, Pt-Re/C as prepared, and Pt-Re/C following hydrothermal exposure.

Catalyst	S_{BET} (m^2/g)	Pore volume (cm^3/g)[a]	Avg. pore dia. (Å)[a]	CO uptake (μ mol/g)	H uptake (μ mol/g)	CO:H uptake ratio	Dispersion[c] (%)
Pt/C commercial	1075	0.715	10.23	130	102	1.3	51
Pt-Re/C as prepared	750	0.607	10.06	112	52	2.2	42
Pt-Re/C HT exposure[b]	675	0.507	10.04	84	30	2.8	32

[a] Pore volume and average pore diameter determined by BJH desorption
[b] Hydrothermal exposure at 300°C for 3 h
[c] Dispersion calculated based on CO chemisorption

Table 2.2 Glycerol addition to produce in situ H_2 production and promote oleic acid HYD-DOX using Pt/C and Pt-Re/C with an initial inert gas reactor headspace. [a]

Catalyst	Glycerol loading (g)	H_2 residual in headspace (mmol)	Oleic acid conversion (%)	Fatty acid and hydrocarbon molar yields	
				Stearic acid (%)	Heptadecane (%)
Pt/C	0	ND	31	31	ND
Pt/C	5	48	100	75	24
Pt-Re/C	5	50	92	53	37

[a] Reaction conditions: 300°C, initial head-gas = 345 kPa N_2, 20 g oleic acid, 0.5 g catalyst, 80 g water, time at temperature 9 h. (Note: ND = not detected).

CHAPTER 3

LIGNIN VALORIZATION THROUGH INTEGRATED BIOLOGICAL FUNNELING AND CHEMICAL CATALYSIS [1]

3.1 Abstract

Lignin is an energy-dense, heterogeneous polymer comprised of phenylpropanoid monomers used by plants for structure, water transport, and defense, and it is the second most abundant biopolymer on Earth after cellulose. In production of fuels and chemicals from biomass, lignin is typically underutilized as a feedstock and burned for process heat because its inherent heterogeneity and recalcitrance make it difficult to selectively valorize. In Nature, however, some organisms have evolved metabolic pathways that enable the utilization of lignin-derived aromatic molecules as carbon sources. Aromatic catabolism typically occurs via upper pathways that act as a "biological funnel" to convert heterogeneous substrates to central intermediates, such as protocatechuate or catechol. These intermediates undergo ring cleavage and are further converted via the b-ketoadipate pathway to central carbon metabolism. Here, we employ a natural aromatic-catabolizing organism, *Pseudomonas putida* KT2440, to demonstrate that these aromatic metabolic pathways can be employed to convert both aromatic model compounds and heterogeneous, lignin-enriched streams derived from pilot-scale biomass pretreatment into medium chain length polyhydroxyalkanoates (*mcl*-PHAs). *mcl*-PHAs were then isolated from the cells, and demonstrated to be similar in physico-chemical properties to

[1] A modified version of Chapter 3 was published in Proceedings of the National Academy of Sciences, 2014, 111, 33, 12013-12018. (D.R. Vardon co-lead author with co-lead authors J.G. Linger, M.T. Guarnieri, and E.M Karp, as well as co-authors G.B. Hunsinger, M.A. Franden, C.W. Johnson, G. Chupka, T.J. Strathmann, P.T. Pienkos, and G.T. Beckham).

conventional carbohydrate-derived *mcl*-PHAs, which have applications as bioplastics. In a further demonstration of their utility, *mcl*-PHAs were catalytically converted to both chemical precursors and fuel-range hydrocarbons. Overall, this work demonstrates that the use of aromatic catabolic pathways enables an approach to valorize lignin by overcoming its inherent heterogeneity to produce fuels, chemicals, and materials.

3.2 Introduction

Lignocellulosic biomass represents a vast resource for the production of renewable fuels and chemicals to offset global fossil fuel usage. For decades, research has been undertaken to develop processes for valorizing plant polysaccharides, cellulose and hemicellulose.[1–8] Lignin, an alkyl-aromatic polymer comprising 15-30% of biomass, is typically underutilized in selective conversion processes, and is instead relegated for heat and power.[1,6–8] The need for lignin utilization is a problem of growing urgency because production of waste lignin will soar with the commercialization of lignocellulosic biofuels. The inability to valorize lignin, despite being the most energy dense polymer in plant cell walls due to its higher C-to-O ratio relative to carbohydrates, is due to its inherent heterogeneity and recalcitrance. Lignin is composed of 3 monomeric phenylpropanoid units connected by C-C and C-O bonds.[9] Although lignin depolymerization has been studied across a broad range of catalytic, thermal, and biological routes,[10,11] the product slate obtained from depolymerization is almost invariably heterogeneous, making lignin valorization a daunting challenge.

In Nature, some fungi and bacteria depolymerize lignin using powerful oxidative enzymes.[10,12–14] This pool of aromatic compounds present during biomass decomposition likely triggered evolution of microbial pathways for utilizing aromatic molecules as carbon sources.

Many aromatic-catabolizing organisms employ "upper pathways", wherein a diverse battery of enzymes "funnels" aromatic molecules to central intermediates, such as catechol and protocatechuate (**Figure 3.1**). From these intermediates, dioxygenase enzymes cleave carbon-carbon bonds in the aromatic rings to produce ring-opened species[15–18] that are metabolized via the β-ketoadipate pathway to central carbon metabolism,[19,20] thus enabling microorganisms to metabolize a broad range of aromatic species. These pathways have long been studied for their catalytic novelty in C-C bond cleavage in aromatic rings[15–17] and highlight the ability for microbes to evolve mechanisms for xenobiotic catabolism, often driven by man-made pollution.[18] From a biomass conversion standpoint, these upper pathways offer a direct, versatile approach to funnel the heterogeneous portfolio of molecules produced from lignin depolymerization to targeted intermediates for upgrading to fuels, chemicals, and materials.

As a demonstration of the potential of the aromatic catabolic pathways for lignin valorization, here we employ an aromatic-catabolizing bacterium with a diverse metabolic repertoire,[21] *Pseudomonas putida* KT2440 (hereafter *P. putida*), to produce medium-chain-length (C6-C14) polyhydroxyalkanoates (*mcl*-PHAs) from lignin in an integrated process (**Figure 3.1**). *mcl*-PHAs are high-value polymers that can serve as plastics or adhesives,[22] or can be depolymerized and converted to chemical precursors[23] or methyl-ester-based fuels (e.g., biodiesel).[24] In *P. putida*, *mcl*-PHAs can be generated through fatty acid synthesis via the central metabolite, acetyl-CoA.[25] To produce lignin-enriched streams for *mcl*-PHA production via biological funneling, pilot-scale alkaline pretreatment was used to depolymerize lignin from biomass to the aqueous phase (**Figure 3.1**). The pretreated solids, which mainly consist of polysaccharides, can be valorized through known routes such as enzymatic hydrolysis and fermentation or via catalytic routes.[3–6] The resulting alkaline pretreated liquor (APL) was fed to

P. putida, which under nitrogen depletion induces *mcl*-PHA production. After biological conversion of APL, the cells were harvested and the *mcl*-PHAs were extracted and characterized. We further demonstrate depolymerization of *mcl*-PHAs to alkenoic acids, which are precursors for diverse chemical applications. Subsequently, a bimetallic catalyst was used to convert alkenoic acids to alkanes. Overall, this study illustrates the concept of coupling upstream lignin depolymerization and downstream catalysis to a biological funneling utilizing bacterial aromatic catabolic pathways to overcome the intrinsic heterogeneity of lignin.

3.3 Results

To obtain a process stream enriched in lignin-derived compounds, alkaline pretreatment was first employed to produce APL using corn stover in a 1900-L pretreatment vessel with 70 mg NaOH/g dry biomass. Anthraquinone was also co-charged to the reactor at a loading of 0.2% (w/w), which serves to maximize polysaccharide retention in the solids via minimization of polysaccharide "peeling" reactions.[26] From pretreatment, 56% of the lignin is fractionated to the APL while 95% of the glucan and 81% of the xylan are retained in the solids. Based on mass closure, the aqueous fraction of APL consists mostly of lignin, extractives, inorganic components, and acetate, at 32%, 23%, 11% and 8% w/w, respectively (**Figure 3.2**). The APL molecular weight distribution consists of major peaks at 200, 250, and 350 Da, suggesting that most APL components are monomers, dimers, and trimers (**Figure 3.3**). Primary components include *p*-coumaric acid, vanillic acid, ferulic acid, and acetate among others (**Table 3.1, Figure 3.4**). Glucose, which is the only biomass-derived sugar in APL utilizable by *P. putida* KT2440, is present at only 0.13 g/L. The residual solids are enriched in polysaccharides, and are readily digestible by an industrial cellulase cocktail. In particular, approximately 90% glucan conversion

and greater than 50% xylan conversion are reached within 48 hours using the Novozymes CTec2 cocktail, providing a stream for parallel carbohydrate upgrading through established routes (**Figure. 3.1**).[2–8]

We subsequently evaluated the ability of *P. putida* to utilize several individual molecules derived from both lignin and polysaccharides present in APL for cell growth and *mcl*-PHA production. Based on identification of the most prevalent species in APL relative to previous genomics analyses of *P. putida*,[21,27] we predict that most of the aromatic molecules present in APL (**Table 3.1**) will be catabolized via the b-ketoadipate pathway, as illustrated in **Figure 3.5**. To test this prediction, we then grew *P. putida* in 250-mL shake flasks with both single and mixed model carbon sources representative of APL components (**Figure 3.6**). Flow cytometry was used in all cases to monitor the accumulation of *mcl*-PHAs (**Figure 3.7**). As shown in **Figure 3.6A**, *p*-coumaric acid, ferulic acid, and glucose all led to *mcl*-PHA accumulation in *P. putida* at comparable levels, namely 34-39%-cell dry weight (cdw). Acetate, which is quite prevalent in APL due to deacetylation of hemicellulose side chains in caustic conditions,[28] is the exception, with only 20%-cdw production of *mcl*-PHAs (**Figure 3.6A**). The corresponding volumetric productivity ranges from 0.15-0.17 g/L *mcl*-PHAs, with acetate producing 0.10 g/L. *P. putida* was also grown in a mixture of the same four model compounds at equivalent starting concentrations, which reached 34%-cdw and 0.15 g/L, indicating that lignin and carbohydrate-derived species are co-converted to *mcl*-PHAs (**Figure 3.6B**). It is noted that *p*-coumaric acid, glucose, and acetate are all fully utilized by 24 hours, whereas ferulic acid is only approximately 70% utilized by 48 hours. As shown in **Figure 3.5**, ferulic acid goes through many of the same enzymatic steps in *P. putida* as *p*-coumaric acid. Assuming that it is not regulated differently than *p*-coumaric acid, ferulic acid may simply be a poor substrate relative to *p*-coumaric acid for

the overlapping enzymatic steps. Cultures grown with high acetate levels also exhibit co-utilization with similar *mcl*-PHA productivity (33%-cdw, 0.12 g/L), further suggesting that aromatic and carbohydrate-derived species will be used simultaneously in complex mixtures like APL (**Figure 3.8**).

Based on the ability of *P. putida* to convert individual compounds to *mcl*-PHAs, we examined *mcl*-PHA production in shake-flask conditions with APL as a sole carbon source (**Figure 3.6D**). Substrate conversion was not tracked, as conventional analytical methods are inadequate for quantitatively characterizing APL.[29] Interestingly, *P. putida* grows quite well in APL without appreciable dilution, beyond adding a small amount of modified minimal M9 salts and without removal of potential inhibitors. Intracellular *mcl*-PHAs accumulate over 48 hours with APL, with a fluorescence intensity distribution at 610 nm similar to *p*-coumaric acid alone (**Figure 3.6C**). The fluorescence data and yield of *mcl*-PHAs from APL (0.252 g/L at 32%-cdw) are comparable to the model compound experiments, demonstrating that an aromatic-catabolizing organism can convert lignin-enriched streams derived from industrially-relevant feedstocks to a value-added product (**Figure 3.6**). To confirm that lignin monomers were incorporated into *mcl*-PHAs in APL, shake-flask experiments were performed using APL supplemented with ^{13}C-labeled *p*-coumaric acid. Analysis of the $^{13}C/^{12}C$ ratio for major derivatized hydroxyacids methyl esters (HAMEs) confirmed significant ^{13}C-enrichment of the *mcl*-PHAs due to labeled *p*-coumarate incorporation (**Figure 3.9**), even with initial supplementation at trace levels (3.5 mg/L ^{13}C from labeled p-coumarate of the 11,300 mg/L total APL carbon). Going forward, there are known means to improve *mcl*-PHA production via fermentation optimization, substrate feed concentration, and organism engineering,[22] as outlined below.

To produce sufficient quantities of *mcl*-PHAs for material characterization and processing, a 14-L batch cultivation of *P. putida* was grown in APL as a sole carbon source in a laboratory fermenter (**Figure 3.6D**). Nile Red staining via fluorescence microscopy and quantitation per cell confirmed that the primary increase in fluorescence, reflective of *mcl*-PHA production, occurs within 24 hours of cultivation. Additionally, flow cytometry data in the 14-L batch cultivation are comparable to shake-flask results (**Figure 3.10**). Characterization of APL-derived *mcl*-PHAs indicated that their physicochemical properties are comparable to those derived from carbohydrates (**Figure 3.11B, 3.12, 3.13**).[22,30–32] Analysis of the hydroxyacid monomer distribution showed that the *mcl*-PHA polymer primarily comprises 3-hydroxydecanoic acid (HA-10; 55%), 3-hydroxyoctanoic acid (HA-8; 22%), 3-hydroxydodecanoic acid (HA-12; 16%), 3-hydroxytetradecancoic acid (HA-14; 4%), and 3-hydroxyhexanoic acid (HA-6; 3%) (**Figure 3.11C**).

Monomers derived from *mcl*-PHAs can also be utilized for products beyond bioplastics, such as for chemical precursors or fuels. To that end, APL-derived *mcl*-PHAs were thermally depolymerized at 250°C under inert atmosphere to produce alkenoic acids,[33] which can serve as a platform intermediate for a wide array of chemicals, similar to other biologically-derived acids.[34–36] This thermal process results in dehydration and monomer products reflective of the parent polymer (**Figure 3.14**, **Table 3.2**). Additionally, tandem thermal depolymerization of APL-derived *mcl*-PHAs and catalytic deoxygenation of the resulting alkenoic acids was employed to produce fuel-range hydrocarbons (**Figure 3.11C**). Catalytic deoxygenation was performed with a Pt-Re/C catalyst via hydrogenation and decarboxylation-decarbonylation (denoted as "HYD/DOX" in **Figure 3.11**) at 300°C in water under mild hydrogen pressure (2.5 MPa initial H_2 loading at 25°C) (**Figure 3.11A,C**).[37] The use of water facilitates reforming of

renewable H_2-donors *in situ*,[38] while CO produced from decarbonylation can react with water to produce H_2 via the water-gas-shift reaction, minimizing external H_2 requirements. The product distribution is reflective of the *mcl*-PHA polymer, and demonstrates conversion of *mcl*-PHAs to fuel-range hydrocarbons (**Figure 3.15**, **Table 3.3**).

3.4 Discussion

The conversion of carbohydrates via fermentation has provided humanity with renewable transportation fuels and chemicals for well over a century. Conversely, the only market for lignin to date on a scale concomitant with fuels and chemicals derived from carbohydrates is heat and power. On a much smaller scale, the primary market to date for lignin beyond niche materials is in the production of vanillin and lignosulfonates, markets that would be swamped by orders of magnitude given the potential for lignin production in the growing, worldwide biofuels economy. Thus, lignin valorization strategies that incorporate new approaches are desperately needed.[7] From a biological conversion standpoint, previous studies have either focused on the modification of upper pathways to produce value-added aromatics, such as vanillin,[39] or have shown that single aromatic model compounds can be converted to intermediates such as lipids.[40,41] Here, we show that the use of microbial, aromatic catabolic pathways on a mixture of biomass-derived lignin substrates can overcome the primary, inherent challenge in lignin valorization, namely the heterogeneity of lignin. It is important to note that significant improvements to *mcl*-PHA production with productivities of 1-3 g/L/hr and volumetric concentrations near 100 g/L required to reach economic viability.[42] It has been shown that improvements of this magnitude are possible in *mcl*-PHA production in wild-type *P. putida* from different substrates (e.g., glucose or fatty acids) via fed-batch fermentation and concentrating the

substrate.[22] To this end, we note that a 5x concentration of APL produces an equivalent, per-cell PHA fluorescence intensity and culture density, thus demonstrating equivalent titers can be achieved in a concentrated APL stream (**Table 3.4**). These previous results and techno-economic analyses suggest that further development and optimization of this approach via modifications to fermentation conditions could eventually enable the scalable production of *mcl*-PHAs from lignin-enriched substrates such as APL or other lignin-derived process streams.[22,42]

Additionally, *mcl*-PHAs have a broad range of potential markets, both for small- and large volume applications. There are ongoing research efforts to tailor *mcl*-PHAs as neat or blended bioplastics for films, coatings, biocompatible drug-delivery and biomedical materials, and organic/inorganic composites.[43] The extended carbon side chain of *mcl*-PHAs imparts unique properties by disrupting the regularity of the polymer backbone compared to short-chain PHAs, allowing for greatly reduced melting and glass transition temperature, as well as crystallinity.[44] PHAs can be depolymerized by several routes, including thermal degradation,[33] aqueous hydrolysis,[45] and extracellular enzyme depolymerases.[23] Alternatively, hydroxyacid monomers can be directly produced during fermentation by genetic knockout of PHA synthases.[46] The resulting monomeric acids can potentially serve as a platform for producing a wide array of value-added chemicals including diols, ketones, amides, and nitriles, similar to other biologically derived carboxylic acids (e.g., lactic acid, levulinic acid, succinic acid).[34–36] Additionally, these monomers can be converted to fuel substitutes,[5] as previously demonstrated with methyl esters (i.e., biodiesel) derived from *mcl*-PHAs,[24] and fully deoxygenated hydrocarbon fuels, as described in this study. These carbon chain lengths fall primarily within the range of jet (C8-C16) and diesel grade (C8-C21) fuels, which is particularly promising as heavy-duty vehicle and airline fuel consumption is anticipated to grow substantially in the near

future.[47] These forms of transportation require power sources that are not readily substituted with other renewables (e.g., short-chain alcohols, electric, fuel cell, etc.), thus a market for *mcl*-PHAs derived from lignin and carbohydrates may also be eventually possible at a scale of renewable fuels.

Lastly, the approach developed here is merely an example of an integrated process for lignin valorization wherein a "biological funneling" step can be utilized with a lignin depolymerization step and biological or catalytic upgrading. There is significant versatility and modularity in each step, enabling adaptation to different biomass feedstocks and desired fuel and chemical portfolios, thus holding promise towards industrial application. Namely, lignin depolymerization is possible through many established routes, and thus many depolymerization processes can likely be employed. For example, biological lignin depolymerization is possible with oxidative fungal and bacterial enzymes,[10,12–14] transition metal catalysts,[11,48–51] homogeneous and heterogeneous alkaline catalysts,[52–55] oxidation catalysts,[11] and thermal routes. The selectivity of each of these depolymerization strategies will dictate the aromatic-derived substrates for biological conversion. This in turn will guide the selection of genes present needed in the upper pathways, not all of which may exist in a single organism, thus requiring pathway engineering. From a biological conversion standpoint, aromatic catabolic pathways can be engineered to funnel the products to different biological intermediates (i.e. not just *mcl*-PHAs), thus opening up a new field of metabolic engineering for lignin utilization. Additionally, process streams from industrial-scale biomass depolymerization may likely contain additional non-lignin derived molecules, such as acetate or hemicellulose-derived sugars, which can be potentially be simultaneously funneled to desired products, thus maximizing carbon utilization from biomass. Moreover, the production of biofuel intermediates similar to those currently produced from

sugars, such as isoprenoids, fatty acids, or higher-chain alcohols, is plausible given the coupling of aromatic upper pathways with the proper downstream genetic modifications.[4] Generally, the approach we demonstrate here can be combined with many lignin isolation and biocatalytic upgrading strategies to facilitate the development of an immense range of molecules derived from lignin.

3.5 Conclusion

The conversion of biomass-derived polysaccharides has provided mankind with renewable fuels and chemicals for well over a century. Conversely, the only use for lignin to date on a scale concomitant with polysaccharide-derived fuels and chemicals is heat and power. Here, we demonstrate a flexible, integrated process that overcomes the inherent challenges in lignin valorization, namely lignin heterogeneity, thus enabling comprehensive utilization of biomass polymers to produce renewable fuels, chemicals, and materials for a sustainable energy economy.

3.6 Methods

3.6.1 Corn stover alkaline pretreatment

To obtain a lignin-rich stream for upgrading, corn stover from Idaho National Laboratory (100 kg, ¼" hammer milled, Lot #4) was pretreated with 70 mg NaOH/g dry stover and anthraquinone (0.2% charge w/w dry stover) at 7 wt% solids in a 1,900 L, jacketed paddle mixer (American Process Systems, Gurnee, IL). The slurry was indirectly heated to 100°C with 30-40 psig of saturated steam on the vessel jackets, with a heat ramp of ~ 2 h. After 30 min at temperature, the slurry was cooled to 60°C with jacketed cooling water. APL at a pH of ~12 was

gravity drained. A continuous screw press (Vincent Corp. Model CP10, Tampa, FL) dewatered the residual pretreated stover to ~20 wt% solids, and screw press-recovered APL was added to the gravity-drained APL. Biomass and pretreated solids were characterized by compositional analysis (***Supplemental Information***). Pretreated solids were subjected to enzymatic hydrolysis (***Supplemental Information***). APL was characterized by compositional analysis, gel permeation chromatography (GPC), liquid chromatography, and YSI analysis (***Supplemental Information***).

3.6.2 *P. putida* cultivation.

mcl-PHA production with *P. putida* was initially examined in shake flask cultures. To support growth, APL was adjusted to pH 7.0 using 10 N H_2SO_4 and supplemented with 10X modified M9 salts (per liter of 10X-M9: 6.78 g Na_2PO_4, 3 g KH_2PO_4, 0.5 g NaCl, 10 N NaOH to pH 7.0) at 10% volume. Subsequently, 2 mL of 1 M $MgSO_4$, and 100 µL of 1 M $CaCl_2$ were added to make 0.9X APL; 1X M9 medium, referred to as "M9-APL". A 500-mL seed culture of *P. putida* KT2440 was grown overnight in LB at 30°C, then diluted 5-fold in LB with continued growth for 2 h to achieve a logarithmic growth phase. The culture was pelleted via centrifugation, washed once in PBS, and used to inoculate 1-L flasks containing different media to a total volume of 250 mL at 0.05 OD. Seven conditions were set up in duplicate. Each contained 1xM9 salts with varied carbon sources: (1) 2 g/L glucose, (2) 2 g/L acetate (sodium acetate), (3) 2 g/L p-coumaric acid, (4) 2 g/L trans-ferulic acid, (5) mixed carbon medium at equal concentrations (0.5 g/L glucose, 0.5 g/L p-coumaric acid, 0.5 g/L trans-ferulic acid, and 0.5 g/L acetate), (6) mixed carbon medium at high acetate concentration (1.0 g/L acetate, 0.3 g/L glucose, 0.3 g/L p-coumaric acid, 0.3 g/L trans-ferulic acid), (7) and APL (90% volume, 3 µm filtered). Cultures were grown at 30°C for 48 h at 225 rpm and periodically sampled for analysis.

Carbon utilization was monitored by HPLC for defined media.[56] *mcl*-PHA production was monitored by flow cytometry via Nile Red staining (***Supplemental Information***). To determine cell dry weight at 48 h, 200 mL of culture was centrifuged, washed in 10% PBS, re-centrifuged, and lyophilized. *mcl*-PHAs were recovered by accelerated solvent extraction and ethanol precipitation (***Supplemental Information***). ^{13}C-enrichment of *mcl*-PHAs derived from APL supplemented with ^{13}C-labeled monomers was performed in shake flask cultures, with *mcl*-PHAs derivatized and analyzed by gas chromatography isotope ratio mass spectroscopy (***Supplemental Information***).

mcl-PHAs were produced in larger quantities for upgrading using *P. putida* grown in a 14-L BioFlo 3000 batch reactor (New Brunswick Scientific) with M9-APL . Seed cultures were grown overnight in LB medium to an optical density at 600 nm (OD_{600}) of 3.5-4.0, centrifuged, washed once in 1X M9 medium, and used to inoculate cultures to a starting OD_{600} of 0.05 in M9-APL. Supplemental nitrogen $(NH_4)_2SO_4$ was either withheld, or added at 1 mM. Excess nitrogen (10 mM $(NH_4)_2SO_4$) was utilized as a negative control for flow cytometry analysis and to demonstrate the dependence of *mcl*-PHA production on nitrogen content in APL. The temperature was maintained at 30°C, and mixing was achieved using a bottom marine impeller and mid-height Rushton impeller at 200 rpm. Aeration was set at 0.35 VVM using 100% air and pH at 7.0 was controlled using KOH/HCl. *mcl*-PHA accumulation was monitored by fluorescence microscopy and flow cytometry (***Supplemental Information***). Cultivations ran for 72 hours, followed by centrifugation and lyophilization to harvest cells. *mcl*-PHAs were recovered by accelerated solvent extraction and characterized by GPC and thermal analysis (***Supplemental Information***). *mcl*-PHA monomer distribution was determined by methylation and gas chromatography (***Supplemental Information***).

3.6.3 *mcl*-PHA depolymerization and upgrading

mcl-PHAs were thermally depolymerized to produce free alkenoic acids for catalytic upgrading. Thermal depolymerization was performed using a Parr 5000 Multireactor (Parr Instruments), outfitted with 75-mL reactor vessels. The reactor vessel was loaded with 445 mg of recovered *mcl*-PHAs and purged with Ar for three cycles. The gas purge line was then closed, and the reactor was heated to 250°C for 30 min at temperature. The depolymerization products were recovered in dichloromethane, filtered (0.2-µm PTFE), and identified by gas chromatography, as described in ***Supplemental Information***.

Depolymerized alkenoic acids derived from *mcl*-PHAs were catalytically converted to hydrocarbons over a platinum-rhenium (Pt-Re) catalyst supported on activated carbon using water as a solvent. Pt-Re/C (5 wt% Pt, 4 wt% Re) was prepared by aqueous adsorption of Re, using ammonium perrhenate (Sigma Aldrich) as a precursor, onto commercial Pt/C (Sigma Aldrich), followed by *in situ* reduction at 200°C using 1.4 MPa of H_2 loaded into the reactor at ambient temperature. Catalyst material properties were previously characterized. Catalytic deoxygenation and reduction of thermally depolymerized *mcl*-PHAs was conducted using the Parr 5000 Multireactor described above. The 75-mL reactor vessel was loaded with 270 mg of depolymerized *mcl*-PHA, 50 mg of Pt-Re/C, and 9.8 mL of deionized water. Prior to conversion, the vessel was purged with Ar for three cycles, and pressurized to 2.75 MPa with H_2 at room temperature. The reactors were heated to 300°C under rapid stirring for 180 min at temperature. Catalysis products were recovered in CH_2Cl_2, filtered (0.2-µm PTFE), and the product distribution determined by gas chromatography, as described in ***Supplemental Information***.

3.7 Supplemental Information

3.7.1 Compositional analysis of corn stover pretreated solids

Compositional analysis was conducted on the pretreated residual solids to quantify the carbohydrate retention and lignin removal. The mass of the recovered dry solids was measured by drying a subsample of solid fraction for several days in a 40°C vacuum oven until the mass stabilized to a constant value. Compositional analysis of the recovered solids was subsequently performed in accordance with standard NREL Laboratory Analytical Procedures (LAPs).[57,58] The APL is a heterogeneous mixture of acids, polysaccharides, monosaccharides, aromatic monomers (derived from lignin), high molecular weight lignin, and acetate.[29] The complexity of black liquor and its sensitivity to pH changes significantly complicates direct, detailed compositional analysis. Therefore, for the purposes of this work, we report the composition of the APL by difference from the known mass and composition of the dry biomass loaded into the pretreatment vessel and the resulting mass and composition of the retained solids, as shown in **Figure 3.2**.

3.7.2 Gel permeation chromatography (GPC) analysis of APL

To determine the molecular weight distribution of the APL, 20 mg of APL obtained from the alkaline pretreatment of corn stover was acetylated in a mixture of pyridine (0.5 mL) and acetic anhydride (0.5 mL) at 40°C for 24 h with stirring. The reaction was terminated by addition of methanol (0.2 mL) to neutralize the acetic anhydride. The acetylation solvents were then evaporated from the samples at 40°C under a stream of nitrogen gas. The samples were further dried in a vacuum oven at 40°C overnight. A final drying was performed under vacuum (1 torr) at room temperature for 1 h. The dried acetylated samples were dissolved in tetrahydrofuran

(THF, Baker HPLC grade) and then filtered (0.45-μm nylon membrane syringe filters) before GPC analysis. The acetylated samples appeared to be completely soluble in THF.

GPC analysis was performed using an Agilent HPLC with 3 GPC columns (Polymer Laboratories, 300 x 7.5 mm) packed with polystyrene-divinyl benzene copolymer gel (10-μm beads) having nominal pore diameters of 10^4, 10^3, and 10^2Å. The eluent was THF and the flow rate was 1.0 mL/min. An injection volume of 25 μL was used. The HPLC was attached to a diode array detector measuring absorbance at 260 nm (band width 40 nm). Retention time was converted into molecular weight (MW) by applying a calibration curve established using polystyrene standards.

3.7.3 Liquid chromatography component identification of APL

Liquid chromatography was employed to identify the primary components in APL. Individual chemical standards representing the compounds listed in Table S1 without asterisks were purchased from Sigma-Aldrich, with the exception of acetic acid (Fisher Scientific). HPLC solvents and modifiers consisted of deionized water (DI) (Barnstead Easy Pure^{II}), acetonitrile (Fisher HPLC grade), and formic acid (Sigma-Aldrich).

Analysis of samples was performed on an Agilent 1100 LC equipped with a G1315B Diode Array Detector (DAD) and in-line Electrospray Ionization (ESI) 2440A Mass Selective Detector (MSD) Ion Trap SL (Agilent Technologies). Each sample was placed in a cooled auto-sampler (10°C) and injected at a volume of 50 μL into the LC/MS system. Sample compounds were separated using reverse-phase chromatography on an YMC C30 Carotenoid 0.3 μm, 4.6 x 150 mm column (YMC America). The LC/MS method consisted of eluent gradients, flow rates, temperatures, and configurations according to prior methods. The degassed solvent regime

consisted of eluent A) DI modified with 0.03% formic acid, and eluent B) 9:1 acetonitrile and DI water also modified with 0.03% formic acid, which was prepared fresh at least 4 hours prior to analyses.

Flow from the HPLC-DAD was directly routed to the ESI-MSD Ion Trap. Tandem MS of major contributing ions was carried out via direct infusion on an Agilent 2440A MSD Ion Trap SL equipped with ESI source operating in negative mode. Source and ion trap conditions were calibrated and optimized with Agilent ESI-T tuning mix (P/N:G2431A) and using smart parameter setting (SPS) tuning with target m/z set to 165, compound stability 70%, trap drive 50%, capillary at 3500 V, fragmentation amplitude of 0.8 V with a 30 to 200% ramped voltage implemented for 50 ms, and an isolation width of 2 m/z (He collision gas). The ESI nebulizer gas was set to 60 psi, with dry gas flow of 11 L/min held at 350°C. A MS scan and precursor isolation-fragmentation scans were performed across the range m/z: 40-350.

An internal spectral database consisting of compounds previously identified as degradation products[59–62] was developed based on ESI-MS-MS scans for the precursor $(M-H)^-$ ion and product ion of each compound (**Table 3.1**, compounds not marked with an asterisk) through direct infusion experiments, as previously described.[62] Both the retention time and database search results for total and extracted ion chromatography for the precursor $(M-H)^-$ ion and at least one product ion were used to confirm the identity of compounds, while deconvolution of mass/charge ion fragmentation patterns was utilized to predict the identity of unknown compounds observed within the samples.

3.7.4 Glucose YSI measurement of APL

The glucose concentration in neutralized APL was measured using a YSI 7100 MBS (YSI Life Sciences, Yellow Springs, Ohio) instrument. To confirm the accuracy of this method, a

calibration curve was produced by adding known amounts of glucose into six samples of neutralized APL. Glucose concentrations of these six samples were measured using the YSI instrument and the results confirmed the known concentration of glucose added into these samples.

3.7.5 Enzymatic hydrolysis of residual solids

Enzymatic hydrolysis of the residual solids was conducted to determine the digestibility. Alkaline pretreated corn stover solids were washed five times with deionized water and stored in 30 mM NaAc pH 5.0 and at 4°C prior to enzymatic hydrolysis. Fungal cellulase enzymes (CTec2, Novozymes) were loaded at 10 or 20 mg of protein per g of glucan in a 1% biomass solids slurry and incubated at 50°C in 20 mM NaAc, pH 5.0 for 120 hours. Digestions were conducted in sealed 1.5-mL vials with continuous mixing by inversion at 10-12/min. Substrates were loaded at 10 mg dry biomass per mL in 1.4-mL reaction volumes. Representative (with respect to both solid and liquid phases of the digestion slurry) 0.1-mL samples were withdrawn from well-mixed digestion slurries at selected time-points during the digestions. The aliquots were then diluted 10-fold with deionized water and immersed in a boiling-water bath for 10 min to inactivate the enzymes and terminate the reaction. The diluted and terminated digestion aliquots were then filtered through 0.2-μm nominal-pore-size nylon syringe-filters (Pall/Gelman Acrodisc-13) to remove residual substrate and, presumably, most of the denatured enzyme. Released cellobiose and glucose and xylose in the diluted samples were then determined by HPLC analysis on an Aminex HPX-87H column (Bio-Rad Laboratories, Inc.) operated at 55°C with 0.01 N H_2SO_4 as mobile phase at 0.6 mL/min in an Agilent 1100 HPLC system with refractive-index detection. The resulting glucose, cellobiose, and xylose concentrations

calculated (in mg/mL) for each digestion mixture was converted to *anhydro*-glucose and *anhydro*-cellobiose concentrations, respectively, by subtracting out the proportional weight added to each molecule by the water of hydrolysis. The sum of the concentrations of *anhydro*-glucose and *anhydro*-cellobiose, which sum is equivalent to the weight-concentration of the glucan chain that was hydrolyzed to produce the soluble sugars, was then divided by the initial weight-concentration of glucan and xylan in the digestion mixture and multiplied by 100% to yield activity results as percent conversion.

3.7.6 Fluorescent microscopy of *P. putida*

mcl-PHA accumulation was visually assayed using epifluorescence microscopy. To prepare cells for imaging, 1 mL of culture grown in APL was harvested at t=0, 6, 12, 24, and 48 hours post-inoculation via centrifugation at 5,000 × *g* at room temperature for 5 min. The culture supernatant was removed, and cells were washed twice in PBS, fixed in 3:1 ethanol:acetic acid for 10 min, and washed twice in 1X PBS, followed by resuspension in 1 mL PBS, as described previously.[63] Cells were stained with 10 μg/mL Nile Red (Molecular Probes, Invitrogen Corporation) for 5 min, and immobilized on microscope coverslips by mixing with 1% low-melting-temperature agarose (heated to 65°C to solubilize) in a 1:1 ratio. Images were acquired using a Nikon Eclipse 80i microscope. Nile Red fluorescence was detected between 560 and 590 nm using band-pass filtering.

3.7.7 Fluorescence quantitation of *P. putida*

Fluorescence emission of Nile Red was obtained using a FLUOstar Omega microplate reader (BMG Labtech), equipped with emission and excitation filters of 485/12 and 590/10 nm,

respectively. Cells were harvested, diluted to OD_{600} = 0.1 in M9 media, washed in PBS, and stained with Nile Red, as described above. Top optic positioning was utilized with 0.2 s positioning delay, a gain setting of 500, and 10 flashes per well. All measurements were obtained in 96-well, black, round-bottom plates (Corning Costar) at room temperature, in 200-µL reaction volumes.

3.7.8 Flow cytometry of *P. putida*

To assay PHA accumulation, we used Nile Red staining and detection using a FACS aria (BD Biosciences, San Jose CA). One milliliter of cell culture was centrifuged and washed in phosphate buffered saline (PBS). Cells were then stained using 0.5mg/ml Nile Red dissolved in DMSO for 15 minutes, then washed twice in PBS. Samples were loaded into the FACS aria and screened for Nile Red Fluorescence using a 488 nm wavelength laser coupled with 610/20 nm detection. For each sample 20,000 events were recorded to generate the histograms. For time-course experiments, cells were frozen at -20° C following the suspension in Nile Red/DMSO. Following the conclusion of the time course, all samples were analyzed by flow cytometry in parallel.

3.7.9 Accelerated solvent extraction of *P. putida*

mcl-PHAs were extracted from *P. putida* with dichloromethane using a Dionex 200 and Dionex 350 Accelerated Solvent Extractor (ASE) (Dionex Instruments). Extractions were performed at 50°C and 10 MPa over 4 cycles with a 100% flush volume. The extract was concentrated to 10% of the initial volume using a rotary evaporator, and the *mcl*-PHAs were precipitated from the crude extract using ice-cold ethanol. Residual solvent was removed under

flowing N_2 at 40°C, prior to drying under vacuum at 40°C overnight to recover purified *mcl*-PHAs.

3.7.10 Gas chromatography (GC) analysis of *mcl*-PHA monomer distribution

The *mcl*-PHA monomer hydroxyacid profile was determined by methanolysis of the purified PHA extract with BF_3.[64] Hydroxyacid methyl esters were identified and the distribution quantified by gas chromatography mass spectroscopy (GC-MS) using an Agilent 7890A GC equipped with a 5975C MSD (Agilent Technologies). The GC was outfitted with an Agilent DB-FFAP column (30 m × 0.25-mm id, 0.25-µm film), and helium (0.8 mL/min column flow) was used as the carrier gas. The injector volume was set to 1 µL using an Agilent auto-sampler. The GC/MS method consisted of a front inlet temperature of 250°C, MS transfer line temperature of 250°C, and scan range from 35 m/z to 550 m/z. A starting temperature of 40°C was held for 5 minutes and then ramped at 5°C/min to a temperature of 250°C and held for 20 minutes. HP MSD Chemstation software (Agilent) equipped with NIST11 database Rev. 2.0G (May 19, 2011 build) was used to identity unknown compounds found within the samples. The mass spectrometer signal response for C_8 and C_{10} hydroxyacid methyl esters (HAME) was determined with HAME standards prepared from known quantities of 3-hydroxyoctanoic and 3-hydroxydecanoic acid obtained from Sigma Aldrich. The remaining HAME response factors were normalized to the nearest HAME standard.

3.7.11 Conversion of ^{13}C-labeled *p*-coumarate and xylose to *mcl*-PHAs by *P. putida*

To definitively conclude that lignin-derived molecules are being metabolized to *mcl*-PHAs in the APL, we supplemented APL with labeled p-coumaric acid-1,2,3-$^{13}C_3$ (Sigma-

Aldrich), and monitored for the inclusion of ^{13}C in extracted and derivatized *mcl*-PHAs via Gas Chromatography-Isotope-Ratio Mass Spectrometry (GC-IRMS). As a negative control, we also separately used labeled D-xylose-$^{13}C_5$ (Omicron), a compound present in APL that is unable to be metabolized by *P. putida* KT2440. To ensure sterility, APL was centrifuged (30', 22,000 x g) and the supernatant was sequentially filtered via vacuum filtration using reduced pore sizes (11 µm, 6 µm, 2 µm, to minimize filter clogging) followed by sterile 0.2-µm filtration. As described in the main text, this APL was mixed with 10X M9 salts to make 0.9X APL; 1X M9 (supplemented with 1mM $(NH_4)_2SO_4$). *P. putida* was grown overnight in LB medium, and then diluted 20-fold in LB and allowed to outgrow for 2 h. Cells were centrifuged and washed in 0.9X APL; 1X M9 and then inoculated to an OD_{600} of 0.1 in two separate 500-mL baffled flasks in a total volume of 200 mL. These twin cultures were grown for 4 h in the absence of labeled compounds. *mcl*-PHAs accumulation typically is not detectable prior to 6 h in our experiments, and given the small amount of ^{13}C-labeled compounds we were adding to the APL, we wanted to maximize flux to PHAs to ensure detection. Following this 4 h growth, 3 mg of either ^{13}C-labeled p-coumarate or xylose was added (pre-dissolved in 3 mL of M9-medium) to the growing cultures. Cultures were allowed to grow for an additional 44 h (48 h total), then harvested and lyophilized for analysis.

3.7.12 GC isotope ratio mass spectroscopy (IRMS) analysis of *mcl*-PHAs

For ^{13}C-analysis by GC-IRMS, lyophilized cell pellets grown on APL supplemented with labeled p-coumaric acid and D-xylose were derivatized directly by methanolysis with BF_3 to produce HAMEs.[64] The $^{13}C/^{12}C$ ratios of major derivatized hydroxyacids (3-hydroxyoctanoic acid, 3-hydroxydecanoic acid, 3-hydroxydodecanoic acid) were compared for (1) APL

supplemented with ^{13}C-labeled *p*-coumaric acid, (2) APL supplemented with ^{13}C-labeled D-xylose, and (3) APL without ^{13}C-labeled supplement. HAME $^{13}C/^{12}C$ ratios were identified using a Thermo Trace GC Ultra coupled to a Delta V Advantage IRMS via a GC Isolink Device (Thermo Scientific, Bremen Germany). The temperature in the isolink was set to 100°C. The GC was outfitted with a SGE BPX5 column (60m × 0.25-mm id, 0.25-µm film). Splitless injections were performed with an injection volume of 1 µL or 0.1 µL. All other conditions (e.g., gas carrier, flow rate, injector temperature, oven settings) were identical to those described above for HAME profile analysis by GC-MS. To compare levels of ^{13}C-enrichment, $\delta^{13}C$ values were calculated (**Eqn. 3.1)** by comparing the HAME $^{13}C/^{12}C$ ratio to Vienna Pee Dee Belemnite (PDB).

Positive $\delta^{13}C$ values are indicative of significant ^{13}C-enrichment due to labeled substrate incorporation into the *mcl*-PHA polymer. The GC-IRMS mass 45 signal intensities, corresponding primarily to $^{13}C^{16}O_2$, were plotted as shown in **Figure 3.15** to compare relative sample HAME monomer distribution ratios.

Eqn 3.1 $$\delta^{13}C = 1000\left[\frac{\left(\delta^{13}C/\delta^{12}C\right)_{HAME} - \left(\delta^{13}C/\delta^{12}C\right)_{PDB}}{\left(\delta^{13}C/\delta^{12}C\right)_{PDB}}\right]$$

3.7.13 GPC and thermal analysis of *mcl*-PHAs

The *mcl*-PHA molecular weight distribution was analyzed by GPC with a refractive index detector, as described above, with the exception of a 100-µL injection volume and refractive index detector. The GPC chromatogram and corresponding MW-distribution parameters are shown in **Figure 3.12**. Thermal properties of *mcl*-PHAs were analyzed by differential scanning

calorimetry (DSC) and thermal gravimetric analysis (TGA) (**Figure 3.13**). The glass transition temperature (T_g) was measured using a TA DSC 2000 (TA Instruments) by heating the sample to 100°C at a rate of 25°C/min under flowing N_2 (20 mL/min), followed by a isothermal hold for 1 min, and rapid cooling to -90°C. The melting temperature (T_m) was analyzed using a TA DSC 1000 by heating the sample from 0-100°C at a rate of 10°C/min. Lastly, the thermal decomposition temperature (T_d), indicative of 5 wt.% loss, was determined using a Setaram SETSYS Evolution TGA instrument (Setaram) by heating the sample from 50-400°C at a rate of 10°C/min.

3.7.14 GC analysis of thermally depolymerized *mcl*-PHAs

mcl-PHA thermal depolymerization products were recovered in dichloromethane, filtered (0.2-µm PTFE), and identified by GC-MS using the method described above for HAME analysis. The total ion chromatogram (TIC) and listing of major identified products with retention times is provided in **Figure 3.14** and **Table 3.2**.

3.7.15 GC Analysis of Catalysis Products.

Catalytic upgrading products were recovered in dichloromethane, filtered (0.2-µm PTFE), and the distribution quantified by GC-MS using an Agilent 6890N gas chromatograph and 5973N MSD. The GC was outfitted with an Agilent HP-5MS column (30 m × 0.25-mm id, 0.25-µm film), and helium (0.8 mL/min column flow) was used as the carrier gas. The injector volume was set to 1 µL using an Agilent auto-sampler. The GC/MS method consisted of a front inlet temperature of 270°C, MS transfer line temperature of 280°C, and scan range from 35 m/z to 550 m/z. A starting temperature of 35°C was held for 3 minutes and then ramped at 15°C/min

to a temperature of 225°C with a final hold time of 1 minute. HP MSD Chemstation software (Agilent) equipped with NIST11 database Rev. 2.0G (May 19, 2011 build) was used to identity unknown compounds found within the samples. Mixed alkane standards (Sigma Aldrich) were used to determine mass spectrometer instrument response factors, and cyclic hydrocarbon response factors were estimated based on the nearest linear hydrocarbon. The total ion chromatogram (TIC) and listing of major identified products with retention times is provided in **Figure 3.15** and **Table 3.3**.

3.8 References Cited

1. Ragauskas, A. J. *et al.* Lignin Valorization: Improving Lignin Processing in the Biorefinery. *Science* **344,** 1246843 (2014).
2. Ragauskas, A. J. *et al.* The Path Forward for Biofuels and Biomaterials. *Science* **311,** 484–489 (2006).
3. Stephanopoulos, G. Challenges in Engineering Microbes for Biofuels Production. *Science* **315,** 801–804 (2007).
4. Peralta-Yahya, P. P., Zhang, F., del Cardayre, S. B. & Keasling, J. D. Microbial engineering for the production of advanced biofuels. *Nature* **488,** 320–328 (2012).
5. Alonso, D. M., Bond, J. Q. & Dumesic, J. A. Catalytic conversion of biomass to biofuels. *Green Chem* **12,** 1493–1513 (2010).
6. Himmel, M. E. *et al.* Biomass Recalcitrance: Engineering Plants and Enzymes for Biofuels Production. *Science* **315,** 804–807 (2007).
7. Tuck, C. O., Pérez, E., Horváth, I. T., Sheldon, R. A. & Poliakoff, M. Valorization of Biomass: Deriving More Value from Waste. *Science* **337,** 695–699 (2012).
8. Chundawat, S. P. S., Beckham, G. T., Himmel, M. E. & Dale, B. E. Deconstruction of Lignocellulosic Biomass to Fuels and Chemicals. *Annu. Rev. Chem. Biomol. Eng.* **2,** 121–145 (2011).
9. Boerjan, W., Ralph, J. & Baucher, M. Lignin Biosynthesis. *Annu. Rev. Plant Biol.* **54,** 519–546 (2003).
10. Kirk, T. K. & Farrell, R. L. Enzymatic combustion: the microbial degradation of lignin. *Annu. Rev. Microbiol.* **41,** 465–505 (1987).

11. Zakzeski, J., Bruijnincx, P. C., Jongerius, A. L. & Weckhuysen, B. M. The catalytic valorization of lignin for the production of renewable chemicals. *Chem. Rev.* **110,** 3552–3599 (2010).
12. Floudas, D. *et al.* The Paleozoic Origin of Enzymatic Lignin Decomposition Reconstructed from 31 Fungal Genomes. *Science* **336,** 1715–1719 (2012).
13. Bugg, T. D., Ahmad, M., Hardiman, E. M. & Singh, R. The emerging role for bacteria in lignin degradation and bio-product formation. *Curr. Opin. Biotechnol.* **22,** 394–400 (2011).
14. Bugg, T. D. H., Ahmad, M., Hardiman, E. M. & Rahmanpour, R. Pathways for degradation of lignin in bacteria and fungi. *Nat. Prod. Rep.* **28,** 1883–1896 (2011).
15. Harayama, S., Kok, M. & Neidle, E. L. Functional and Evolutionary Relationships Among Diverse Oxygenases. *Annu. Rev. Microbiol.* **46,** 565–601 (1992).
16. Bugg, T. D. H. Dioxygenase enzymes: catalytic mechanisms and chemical models. *Tetrahedron* **59,** 7075–7101 (2003).
17. Vaillancourt, F. H., Bolin, J. T. & Eltis, L. D. The Ins and Outs of Ring-Cleaving Dioxygenases. *Crit. Rev. Biochem. Mol. Biol.* **41,** 241–267 (2006).
18. Fuchs, G., Boll, M. & Heider, J. Microbial degradation of aromatic compounds — from one strategy to four. *Nat. Rev. Microbiol.* **9,** 803–816 (2011).
19. Harwood, C. S. & Parales, R. E. The β-ketoadipate pathway and the biology of self-identity. *Annu. Rev. Microbiol.* **50,** 553–590 (1996).
20. Ornston, L. N. & Stanier, R. Y. The Conversion of Catechol and Protocatechuate to β-Ketoadipate by Pseudomonas putida I. Biochemistry. *J. Biol. Chem.* **241,** 3776–3786 (1966).

21. Jiménez, J. I., Miñambres, B., García, J. L. & Díaz, E. Genomic analysis of the aromatic catabolic pathways from Pseudomonas putida KT2440. *Environ. Microbiol.* **4,** 824–841 (2002).

22. Chen, G.-Q. A microbial polyhydroxyalkanoates (PHA) based bio- and materials industry. *Chem. Soc. Rev.* **38,** 2434–2446 (2009).

23. Gangoiti, J., Santos, M., Llama, M. J. & Serra, J. L. Production of Chiral (R)-3-Hydroxyoctanoic Acid Monomers, Catalyzed by *Pseudomonas fluorescens* GK13 Poly(3-Hydroxyoctanoic Acid) Depolymerase. *Appl. Environ. Microbiol.* **76,** 3554–3560 (2010).

24. Zhang, X., Luo, R., Wang, Z., Deng, Y. & Chen, G.-Q. Application of (R)-3-Hydroxyalkanoate Methyl Esters Derived from Microbial Polyhydroxyalkanoates as Novel Biofuels. *Biomacromolecules* **10,** 707–711 (2009).

25. Rehm, B. H. A., Mitsky, T. A. & Steinbüchel, A. Role of Fatty Acid De Novo Biosynthesis in Polyhydroxyalkanoic Acid (PHA) and Rhamnolipid Synthesis by Pseudomonads: Establishment of the Transacylase (PhaG)-Mediated Pathway for PHA Biosynthesis inEscherichia coli. *Appl. Environ. Microbiol.* **67,** 3102–3109 (2001).

26. Heitner, C., Dimmel, D. & Schmidt, J. *Lignin and Lignans: Advances in Chemistry*. (CRC Press, 2011).

27. Nelson, K. E. *et al.* Complete genome sequence and comparative analysis of the metabolically versatile Pseudomonas putida KT2440. *Environ. Microbiol.* **4,** 799–808 (2002).

28. Chen, X. *et al.* Improved ethanol yield and reduced Minimum Ethanol Selling Price (MESP) by modifying low severity dilute acid pretreatment with deacetylation and mechanical refining: 1) Experimental. *Biotechnol. Biofuels* **5,** 60 (2012).

29. Sjöström, E. & Alen, R. *Analytical Methods in Wood Chemistry, Pulping, and Papermaking*. (Springer Science & Business Media, 2013).

30. Abe, H., Ishii, N., Sato, S. & Tsuge, T. Thermal properties and crystallization behaviors of medium-chain-length poly(3-hydroxyalkanoate)s. *Polymer* **53,** 3026–3034 (2012).

31. Poirier, Y., Nawrath, C. & Somerville, C. Production of Polyhydroxyalkanoates, a Family of Biodegradable Plastics and Elastomers, in Bacteria and Plants. *Nat. Biotechnol.* **13,** 142–150 (1995).

32. El-Hadi, A., Schnabel, R., Straube, E., Müller, G. & Henning, S. Correlation between degree of crystallinity, morphology, glass temperature, mechanical properties and biodegradation of poly (3-hydroxyalkanoate) PHAs and their blends. *Polym. Test.* **21,** 665–674 (2002).

33. Sato, S., Ishii, N., Hamada, Y., Abe, H. & Tsuge, T. Utilization of 2-alkenoic acids for biosynthesis of medium-chain-length polyhydroxyalkanoates in metabolically engineered Escherichia coli to construct a novel chemical recycling system. *Polym. Degrad. Stab.* **97,** 329–336 (2012).

34. Dusselier, M., Wouwe, P. V., Dewaele, A., Makshina, E. & Sels, B. F. Lactic acid as a platform chemical in the biobased economy: the role of chemocatalysis. *Energy Environ. Sci.* **6,** 1415–1442 (2013).

35. Cukalovic, A. & Stevens, C. V. Feasibility of production methods for succinic acid derivatives: a marriage of renewable resources and chemical technology. *Biofuels Bioprod. Biorefining* **2,** 505–529 (2008).

36. Rackemann, D. W. & Doherty, W. O. The conversion of lignocellulosics to levulinic acid. *Biofuels Bioprod. Biorefining* **5,** 198–214 (2011).

37. Vardon, D. R. *et al.* Hydrothermal catalytic processing of saturated and unsaturated fatty acids to hydrocarbons with glycerol for in situ hydrogen production. *Green Chem.* 1507–1520 (2014).

38. Cortright, R. D., Davda, R. R. & Dumesic, J. A. Hydrogen from catalytic reforming of biomass-derived hydrocarbons in liquid water. *Nature* **418,** 964–967 (2002).

39. Sainsbury, P. D. *et al.* Breaking Down Lignin to High-Value Chemicals: The Conversion of Lignocellulose to Vanillin in a Gene Deletion Mutant of Rhodococcus jostii RHA1. *ACS Chem. Biol.* **8,** 2151–2156 (2013).

40. Kosa, M. & Ragauskas, A. J. Bioconversion of lignin model compounds with oleaginous Rhodococci. *Appl. Microbiol. Biotechnol.* **93,** 891–900 (2011).

41. Kosa, M. & Ragauskas, A. J. Lignin to lipid bioconversion by oleaginous *Rhodococci*. *Green Chem.* **15,** 2070–2074 (2013).

42. Hermann, B. G. & Patel, M. Today's and tomorrow's bio-based bulk chemicals from white biotechnology. *Appl. Biochem. Biotechnol.* **136,** 361–388 (2007).

43. Chen, G. G.-Q. *Plastics from Bacteria: Natural Functions and Applications*. (Springer Science & Business Media, 2009).

44. Rai, R., Keshavarz, T., Roether, J. A., Boccaccini, A. R. & Roy, I. Medium chain length polyhydroxyalkanoates, promising new biomedical materials for the future. *Mater. Sci. Eng. R Rep.* **72,** 29–47 (2011).

45. Saeki, T., Tsukegi, T., Tsuji, H., Daimon, H. & Fujie, K. Hydrolytic degradation of poly[(R)-3-hydroxybutyric acid] in the melt. *Polymer* **46,** 2157–2162 (2005).

46. Chung, A., Liu, Q., Ouyang, S.-P., Wu, Q. & Chen, G.-Q. Microbial production of 3-hydroxydodecanoic acid by pha operon and fadBA knockout mutant of Pseudomonas putida KT2442 harboring tesB gene. *Appl. Microbiol. Biotechnol.* **83,** 513–519 (2009).
47. Milbrandt, A., Kinchin, C. & McCormick, R. L. The Feasibility of Producing and Using Biomass-Based Diesel and Jet Fuel in the United States. *NREL Tech. Rep.* (2013).
48. Pepper, J. M. & Hibbert, H. Studies on Lignin and Related Compounds. LXXXVII. High Pressure Hydrogenation of Maple Wood1. *J. Am. Chem. Soc.* **70,** 67–71 (1948).
49. Pepper, J. M. & Lee, Y. W. Lignin and related compounds. I. A comparative study of catalysts for lignin hydrogenolysis. *Can. J. Chem.* **47,** 723–727 (1969).
50. Rinaldi, R. & Schüth, F. Design of solid catalysts for the conversion of biomass. *Energy Environ. Sci.* **2,** 610–626 (2009).
51. Parsell, T. H. *et al.* Cleavage and hydrodeoxygenation (HDO) of C–O bonds relevant to lignin conversion using Pd/Zn synergistic catalysis. *Chem. Sci.* **4,** 806–813 (2013).
52. Miller, J. E., Evans, L., Littlewolf, A. & Trudell, D. E. Batch microreactor studies of lignin and lignin model compound depolymerization by bases in alcohol solvents. *Fuel* **78,** 1363–1366 (1999).
53. Deng, H. *et al.* Perovskite-type Oxide LaMnO3: An Efficient and Recyclable Heterogeneous Catalyst for the Wet Aerobic Oxidation of Lignin to Aromatic Aldehydes. *Catal. Lett.* **126,** 106–111 (2008).
54. Roberts, V. M. *et al.* Towards Quantitative Catalytic Lignin Depolymerization. *Chem. – Eur. J.* **17,** 5939–5948 (2011).
55. Sturgeon, M. R. *et al.* Lignin depolymerisation by nickel supported layered-double hydroxide catalysts. *Green Chem.* **16,** 824–835 (2014).

56. Franden, M. A., Pienkos, P. T. & Zhang, M. Development of a high-throughput method to evaluate the impact of inhibitory compounds from lignocellulosic hydrolysates on the growth of Zymomonas mobilis. *J. Biotechnol.* **144,** 259–267 (2009).

57. Sluiter, J. B., Ruiz, R. O., Scarlata, C. J., Sluiter, A. D. & Templeton, D. W. Compositional Analysis of Lignocellulosic Feedstocks. 1. Review and Description of Methods. *J. Agric. Food Chem.* **58,** 9043–9053 (2010).

58. Templeton, D. W., Scarlata, C. J., Sluiter, J. B. & Wolfrum, E. J. Compositional Analysis of Lignocellulosic Feedstocks. 2. Method Uncertainties. *J. Agric. Food Chem.* **58,** 9054–9062 (2010).

59. Balan, V. *et al.* Enzymatic digestibility and pretreatment degradation products of AFEX-treated hardwoods (Populus nigra). *Biotechnol. Prog.* **25,** 365–375 (2009).

60. Chen, S.-F., Mowery, R. A., Castleberry, V. A., Walsum, G. P. van & Chambliss, C. K. High-performance liquid chromatography method for simultaneous determination of aliphatic acid, aromatic acid and neutral degradation products in biomass pretreatment hydrolysates. *J. Chromatogr. A* **1104,** 54–61 (2006).

61. Chen, S.-F., Mowery, R. A., Chambliss, C. K. & van Walsum, G. P. Pseudo reaction kinetics of organic degradation products in dilute-acid-catalyzed corn stover pretreatment hydrolysates. *Biotechnol. Bioeng.* **98,** 1135–1145 (2007).

62. in (ed. Mielenz, J. R.) (Humana Press, 2009). at <http://link.springer.com/protocol/10.1007/978-1-60761-214-8_10#page-1>

63. Chao, Y. & Zhang, T. Optimization of fixation methods for observation of bacterial cell morphology and surface ultrastructures by atomic force microscopy. *Appl. Microbiol. Biotechnol.* **92,** 381–392 (2011).

64. Furrer, P. *et al.* Quantitative analysis of bacterial medium-chain-length poly([R]-3-hydroxyalkanoates) by gas chromatography. *J. Chromatogr. A* **1143,** 199–206 (2007).

65. Alen, R. & Vikkula, A. Formation of lignin monomers during alkaline delignification of softwood. *Holzforschung* **43,** 397–400 (1989).

66. Alén, R., Niemelä, K. & Sjöström, E. Gas-liquid chromatographic separation of hydroxy monocarboxylic acids and dicarboxylic acids on a fused-silica capillary column. *J. Chromatogr. A* **301,** 273–276 (1984).

67. Niemelä, K. & Sjöström, E. Simultaneous identification of aromatic and aliphatic low molecular weight compounds from alkaline pulping liquor by capillary gas-liquid chromatography-mass spectrometry. *Holzforschung* **40,** 361–368 (1986).

68. Niemela, K. GLC-MS studies on pine kraft black liquors. I: Identification of monomeric compounds. *Holzforschung* **42,** 169–173 (1988).

69. Niemela, K. GLC-MS studies on pine kraft black liquors. II: Identification of hydroxy acids with a stilbene structure. *Holzforschung* **42,** 175–176 (1988).

70. Niemelä, K. GLC-MS studies on pine kraft black liquors. V: Identification of catechol compounds. *Holzforschung* **43,** 99–103 (1989).

71. Niemela, K. The formation of 2-hydroxy-2-cyclopenten-1-ones from polysaccharides during kraft pulping of pine wood. *Carbohydr. Res.* **184,** 131–137 (1988).

72. Niemelä, K. GLC-MS studies on pine kraft black liquors. VI. Identification of thiophenecarboxylic acids. *Holzforsch.-Int. J. Biol. Chem. Phys. Technol. Wood* **43,** 169–171 (1989).

73. Niemelä, K. Identification of O-α-d-galactopyranosylsaccharinic acids as their trimethylsilyl derivatives by mass spectrometry. *Carbohydr. Res.* **194,** 37–47 (1989).

74. Venica, A. D., Chen, C.-L. & Gratzl, J. S. Soda-AQ delignification of poplar wood. Part 2: Further degradation of initially dissolved lignins. *Holzforschung* **62,** 637–644 (2008).

75. Venica, A. D., Chen, C.-L. & Gratzl, J. S. Soda–AQ delignification of poplar wood. Part 1: Reaction mechanism and pulp properties. *Holzforschung* **62,** 627–636 (2008).

3.9 Figures and Tables

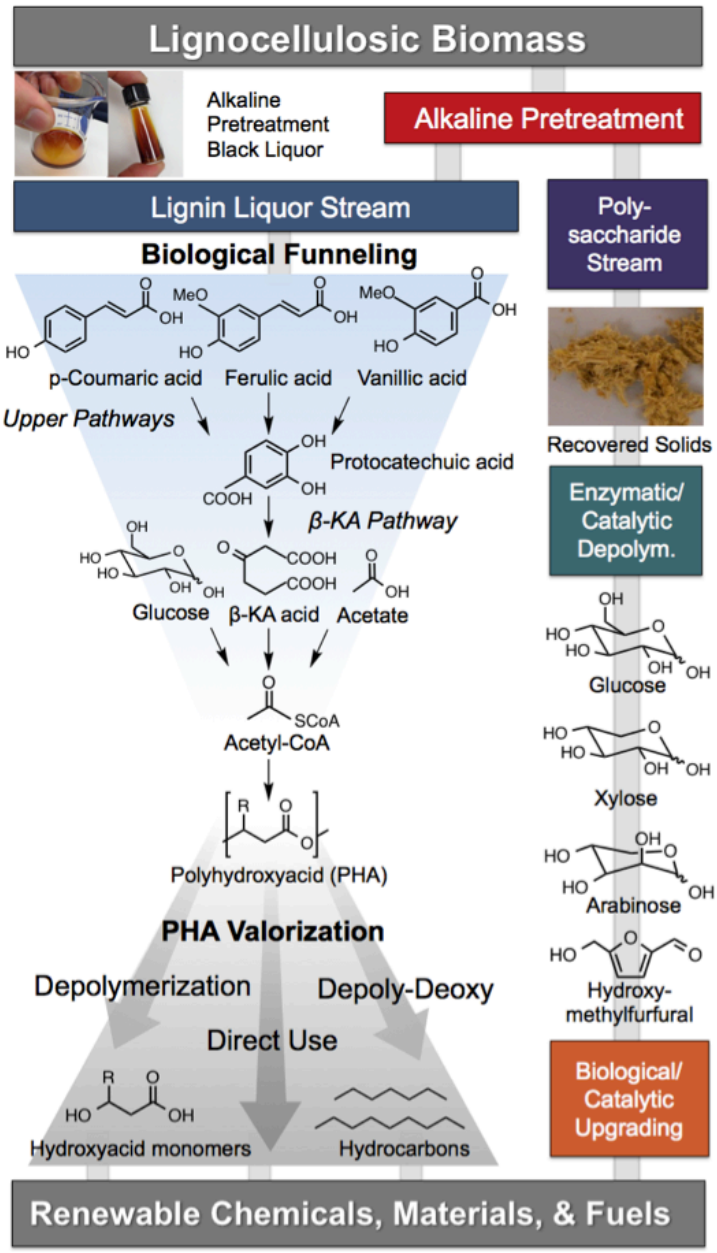

Figure 3.1 Integrated production of fuels, chemicals, and materials from biomass-derived lignin via natural aromatic catabolic pathways and chemical catalysis. Biomass fractionation can yield streams enriched in lignin and polysaccharides, which can be converted along parallel processes.

The challenges associated with lignin's heterogeneity are overcome in a "biological funneling" process through upper pathways that produce central intermediates (e.g., protocatechuic acid). Dioxygenases cleave the aromatic rings of these intermediates, which are metabolized through the b-ketoadipate (b-KA) pathway to acetyl-CoA. As shown, residual glucose and acetate present will also be metabolized to acetyl-CoA, the primary entry point to *mcl*-PHA production via fatty acid synthesis. We demonstrate *mcl*-PHA production, which are biodegradable polymers. *mcl*-PHAs are converted to alkenoic acids, and further depolymerized and deoxygenated ("depoly-deoxy") into hydrocarbons, thus demonstrating the production of fuels, chemicals, and materials from lignin and other biomass-derived substrates.

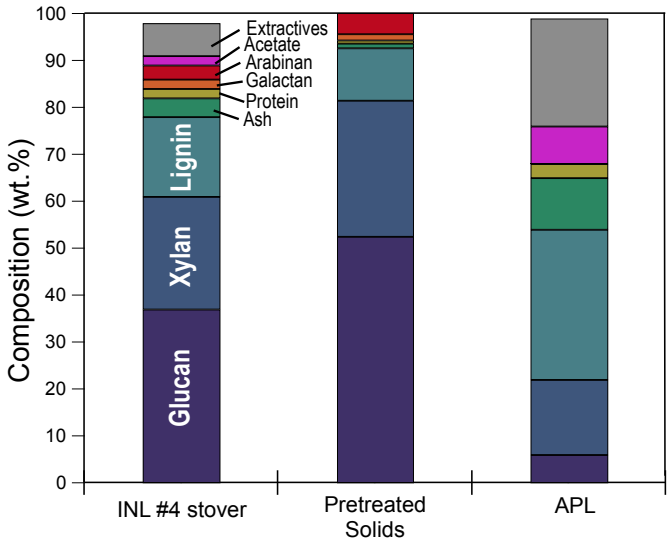

Figure 3.2 Biomass compositional analysis for the alkaline pretreatment step. The composition of the starting corn stover, resulting pretreated solids, and the composition of the material solubilized into the APL are shown on a w/w basis. The pretreatment conditions for the material shown here are 100°C for 30 minutes with an NaOH loading of 70 mg NaOH/g dry stover at 7 wt% solids and 0.2% AQ charge (w/w on dry corn stover). The initial corn stover (Idaho National Laboratories Lot #4) is shown in the left most bar and has a w/w composition of: 37% glucan, 24% xylan, 17% lignin, 4% ash, 2% protein, 2% galactan, 3% arabinan, 2% acetate, and 7% extractives. The recovered solids are enriched in carbohydrates and retain 67% of the mass of the dry corn stover loaded into the reactor. The measured w/w composition of the pretreated solid, shown in the middle bar, is: 53% glucan, 29% xylan, 11% lignin, 1% ash, 1% protein, 1% galactan, 5 % arabinan, 0% acetate, and 0% extractives. The composition of the material solubilized into the APL is presented in the right most bin labeled "APL" and its w/w composition is: 6% glucan, 16% xylan, 32% lignin, 11% ash, 3% protein, 0% galactan, 0% arabinan, 8% acetate, and 23 % extractives.

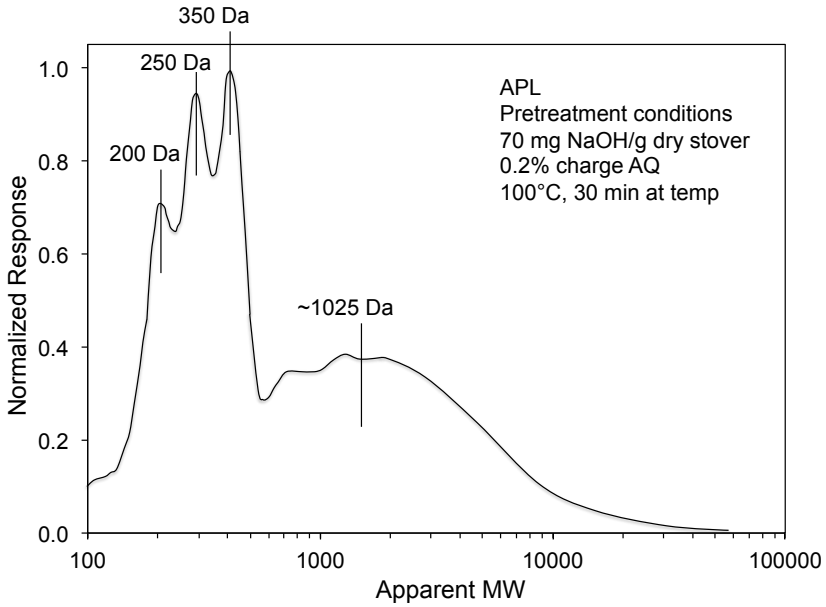

Figure 3.3 GPC chromatogram of APL. The APL chromatogram shows three large peaks of low molecular weight components at apparent molecular weights of ~200, ~250, and ~350 Da, suggesting the majority of the components in the APL are in the monomer, dimer, and trimer range. A broad peak centered at an apparent molecular weight of ~1,025 Da likely represents lignin fragments that are not fully depolymerized. The overall apparent molecular weight average of the APL is estimated to be 1,100 Da. Here, the larger intensity of the low molecular weight components points to the effectiveness of the anthraquinone additive, which increases the fragmentation of the lignin polymer during pretreatment.

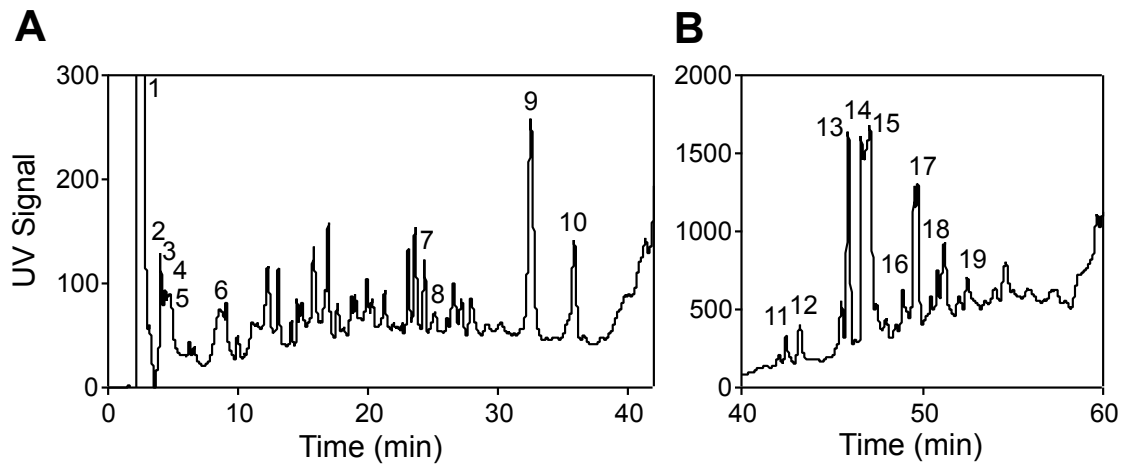

Figure 3.4 LC chromatogram of APL. (A) Chromatogram obtained from APL using the liquid chromatography method described above, for retention times between 0 and 42 min. (B) Chromatogram from APL for retention times between 40 and 60 min; the y axis scale for these retention times has been expanded from that presented in (A) to capture the full peak heights in this region. Major identified compounds are listed in **Table 3.1**.

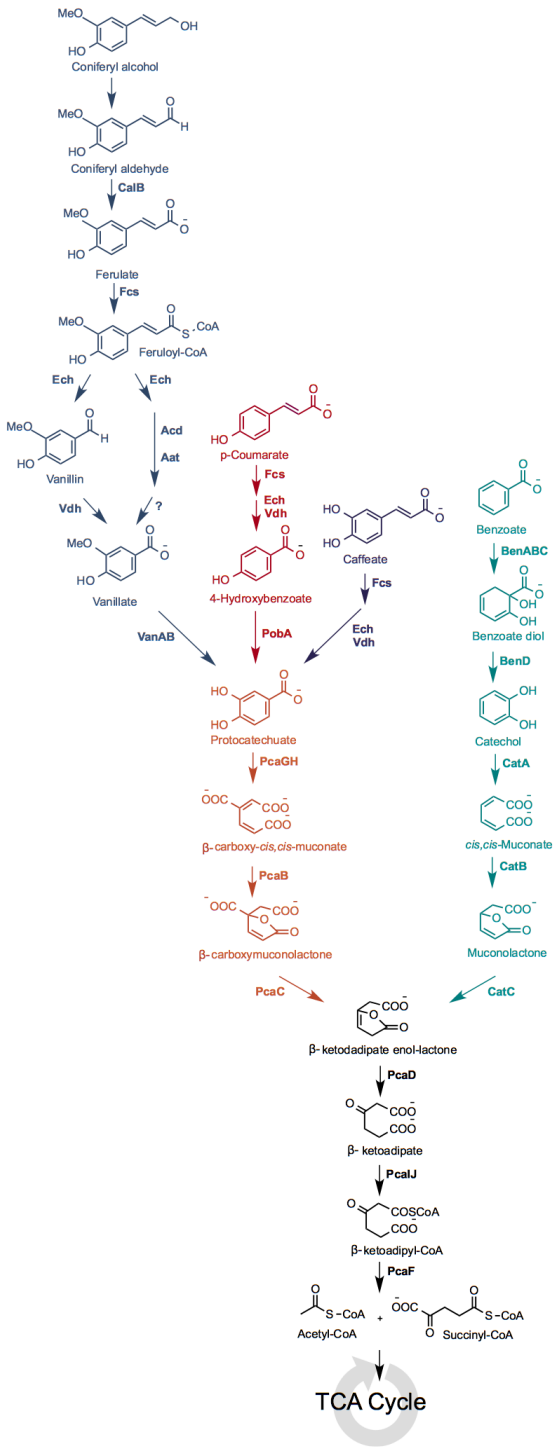

Figure 3.5 Catabolic pathways. Biological funneling of aromatic molecules to central metabolism (TCA cycle) in *P. putida* strain KT2440.

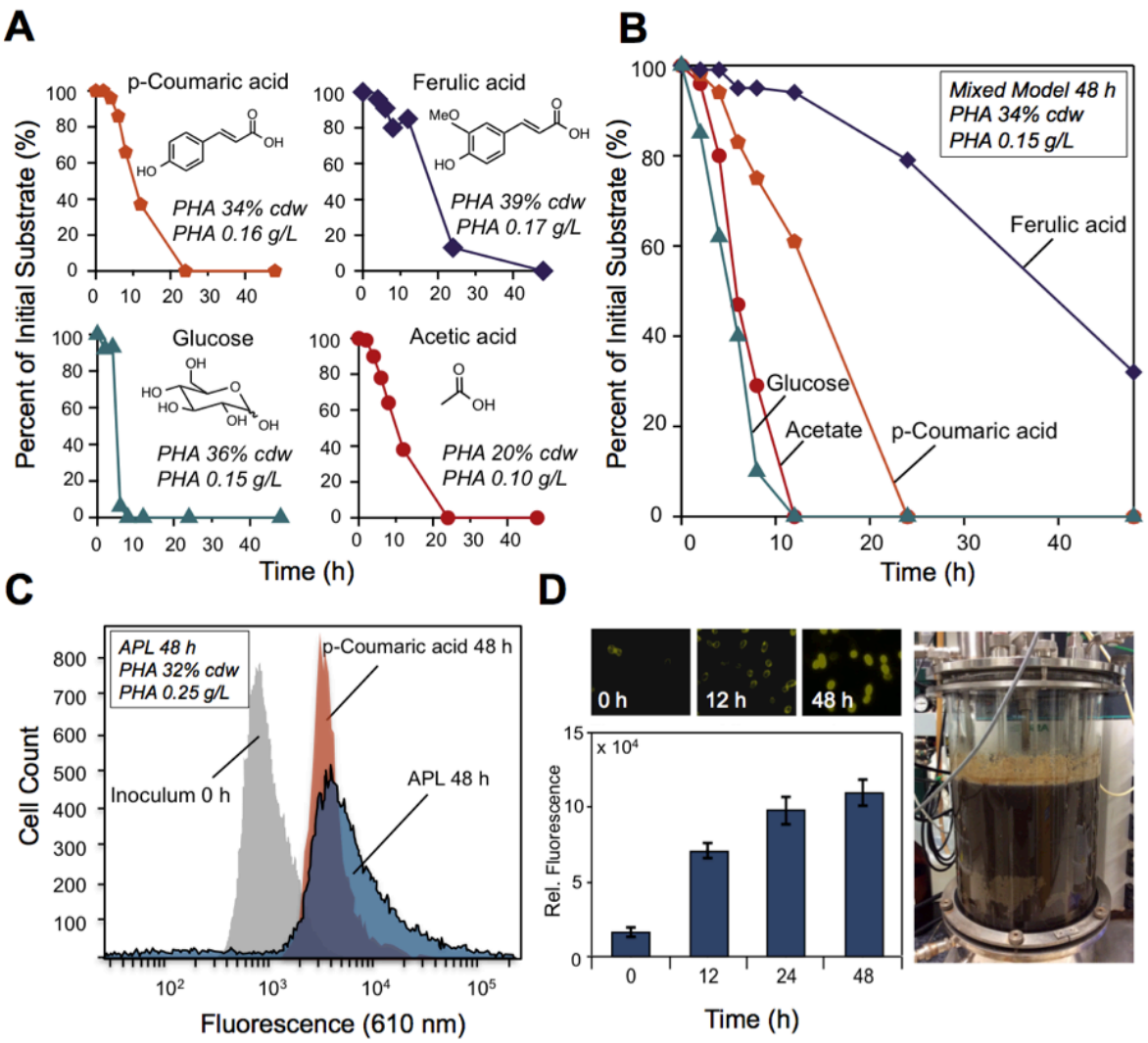

Figure 3.6 Biological conversion of lignin-derived aromatic molecules and carbohydrate-derived products in APL to *mcl*-PHAs in *P. putida*. (A) Conversion and *mcl*-PHA production from representative model compounds present in APL, each at 2 g/L. (B) Conversion and *mcl*-PHA production of a mixture of four representative model compounds from APL, each loaded at 0.5 g/L. (C) Flow cytometry of Nile Red stained cells for *mcl*-PHA accumulation. Cell counts are plotted as a function of fluorescence intensity in the initial inoculum (t=0) and cultures at t=48 hours for a model substrate, p-coumaric acid, and APL grown in 250-mL shake flasks, with the corresponding total *mcl*-PHA production from APL shown in the inset. (D) Fluorescence

imaging of cells at 0, 12, and 48 h stained with Nile Red demonstrates *mcl*-PHA production from APL (*top*). Fluorescence quantitation of *P. putida* cells from the APL conversion as a function of time adjusted to an equivalent cell density (*bottom*). Biological APL conversion by *P. putida* in a 14-L fermenter (*right*).

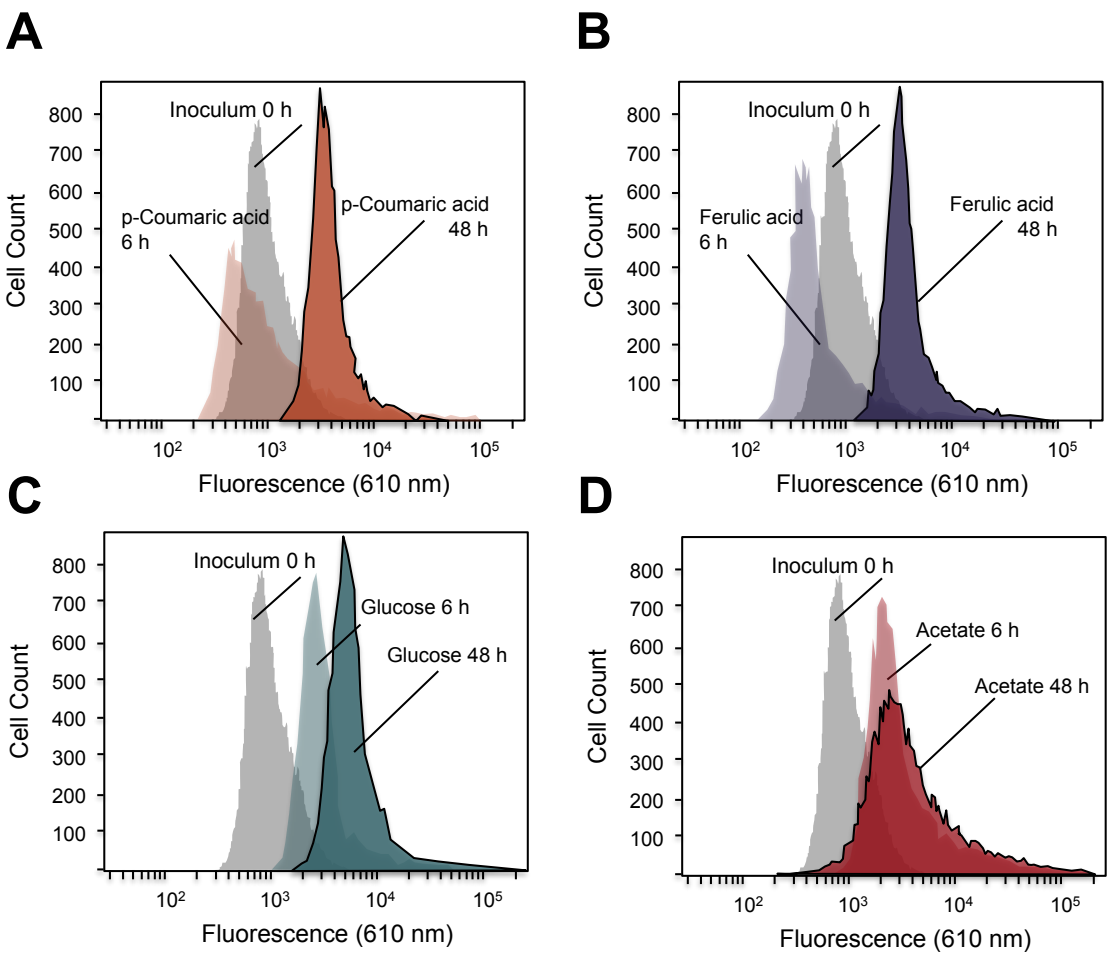

Figure 3.7 Flow cytometry of model compounds. Shake flask cultures of *P. putida* were grown with single model compounds including (A) p-coumaric acid, (B) ferulic acid, (C) glucose, and (D) acetate, each at a concentration of 2 g/L. Flow cytometry analysis of the relative cell fluorescence (610 nm), indicative of *mcl*-PHA production, was performed on the initial inoculum, 6 h, and 48 h cultivation time points.

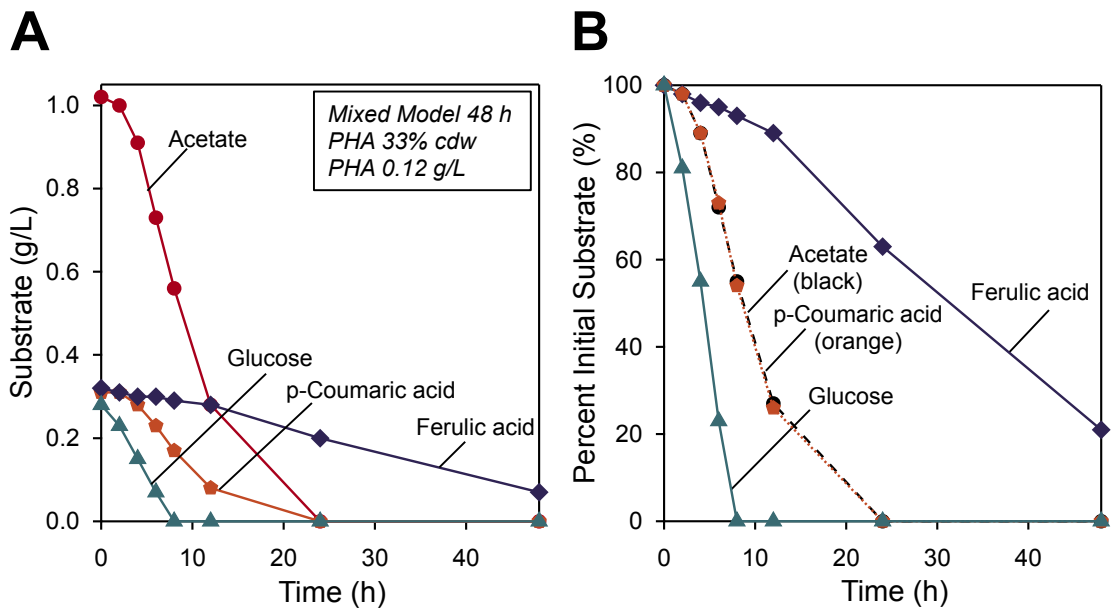

Figure 3.8 Mixed model compound substrate utilization. Shake flask cultures of *P. putida* were grown with mixed model compounds including *p*-coumaric acid, ferulic acid, glucose, and acetate, each at a concentration of 0.3 g/L with the exception of acetate at 1.0 g/L. Data are provided in (A) g/L of substrate, and (B) percent substrate concentration normalized to the initial loading, with the corresponding total *mcl*-PHA production shown in the inset.

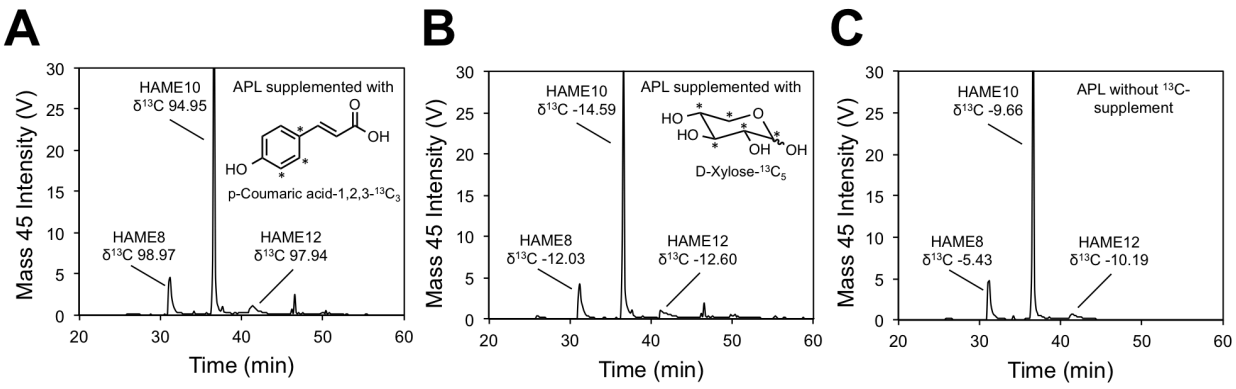

Figure 3.9 ^{13}C-enrichment levels in *mcl*-PHAs derived from APL. Mass 45 signal intensities and δ^{13}C values for derivatized methyl esters of major hydroxyacids, 3-hydroxyoctanoic acid (HAME8), 3-hydroxydecanoic acid (HAME10), and 3-hydroxydodecanoic acid (HAME12) recovered from cultures grown on complex APL with (A) supplemented ^{13}C-labeled p-coumaric acid, (B) supplemented ^{13}C-labeled D-xylose, and (C) no ^{13}C-labeled supplement. Comparable mass 45 signal profiles indicate similar HAME monomer distribution ratios, while positive δ^{13}C values indicate significant ^{13}C-enrichment due to labeled substrate incorporation into the *mcl*-PHA polymer. The lack of enrichment with ^{13}C-labeled xylose demonstrates that ^{13}C transfer from supplemented carbon sources to *mcl*-PHAs is specific and dependent upon the presence of functional metabolic pathways, as *P. putida* KT2440 is unable to utilize xylose.

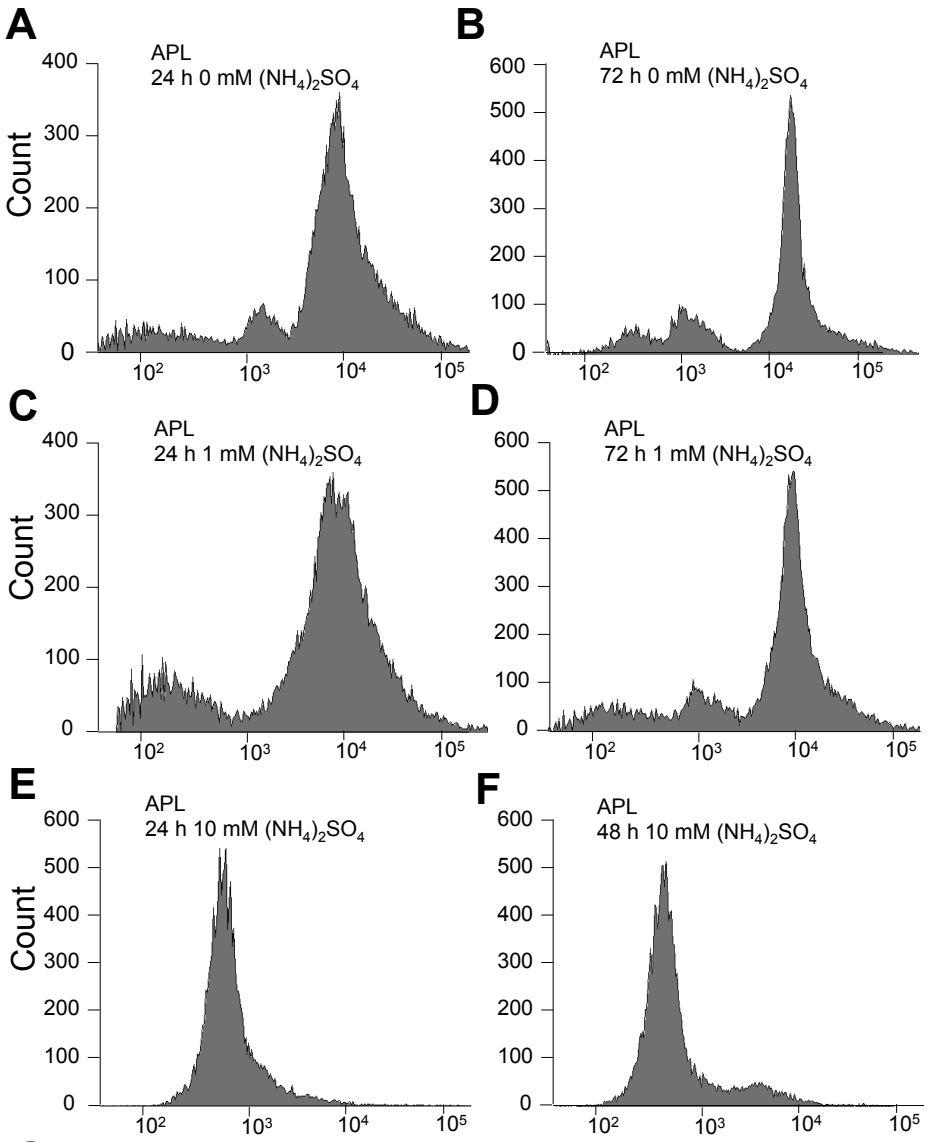

Figure 3.10 Flow cytometry of APL-derived Nile Red stained cells. *mcl*-PHA production in *P. putida* grown in (A, B) APL or (C, D) APL supplemented with 1 mM $(NH_4)_2SO_4$ during 14-L cultivations. Additionally, a culture grown in APL supplemented with 10 mM $(NH_4)_2SO_4$ (50-mL culture volume in 250-mL baffled flasks) is shown to highlight the nitrogen dependence of *mcl*-PHA production in APL over 48 h (E, F).

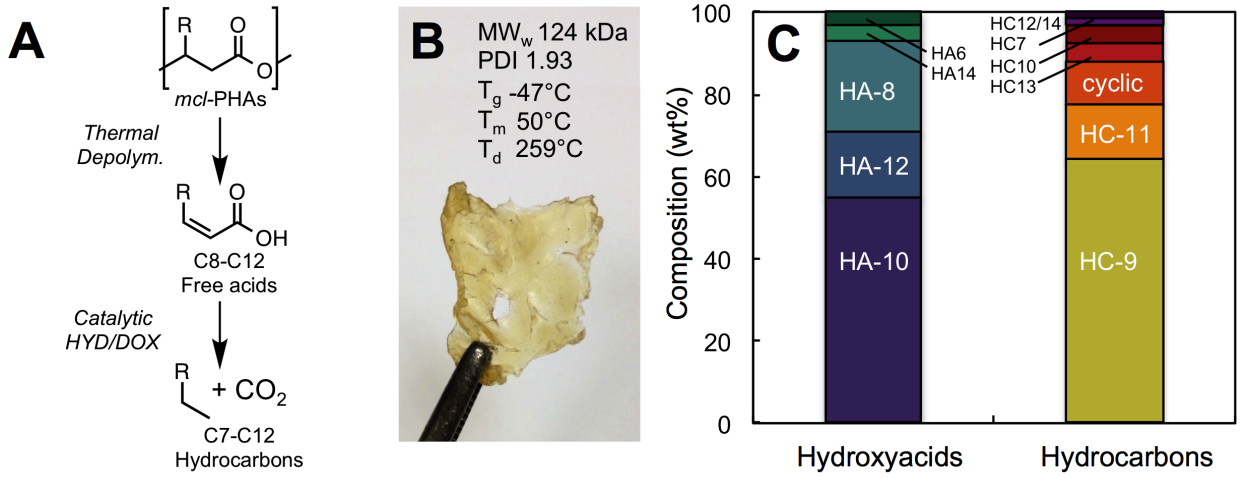

Figure 3.11 APL-derived *mcl*-PHA physicochemical properties and catalytic upgrading to chemical precursors and fuels. (A) Example of thermal-catalytic upgrading pathway for *mcl*-PHAs to chemical precursors and hydrocarbon fuels. (B) APL-derived *mcl*-PHAs and physicochemical properties including weight-average molecular weight (MW_w), polydispersity index (PDI), glass transition temperature (T_g), melting point (T_m), and 5%-decomposition temperature (T_d). (C) Initial *mcl*-PHA hydroxyacid composition (*left*) and alkane distribution (*right*) after thermal depolymerization and catalytic deoxygenation.

.

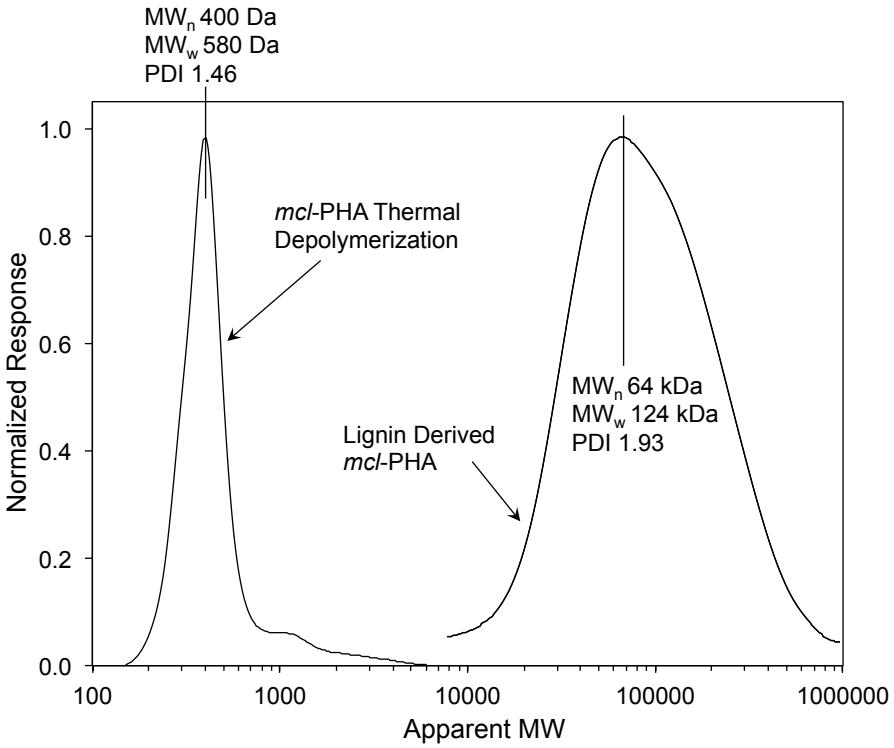

Figure 3.12. GPC chromatogram of *mcl*-PHAs before (right) and after (left) thermal depolymerization. The molecular weight distribution number average (MW_n), weight average (MW_w), and polydispersity index (PDI) are provided for each sample. Thermal depolymerization of *mcl*-PHAs was performed at 250°C for 30 min at temperature under an inert Ar atmosphere.

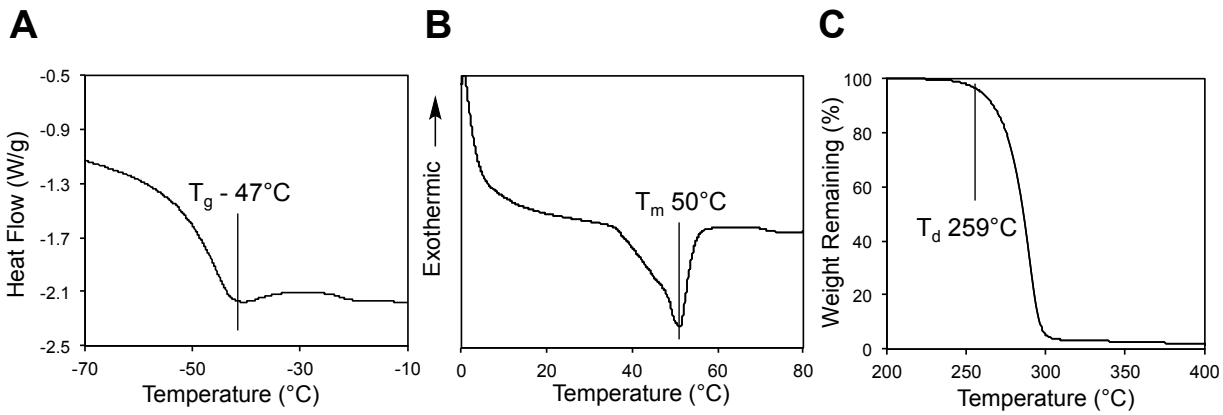

Figure 3.13. Thermal properties of *mcl*-PHAs determined by DSC and TGA. (A) Glass transition temperature (T_g), and (B) melting temperature (T_m) of *mcl*-PHAs, as measured by DSC. (C) Thermal decomposition temperature of *mcl*-PHAs, indicated by 5 wt% sample loss, as measured by TGA.

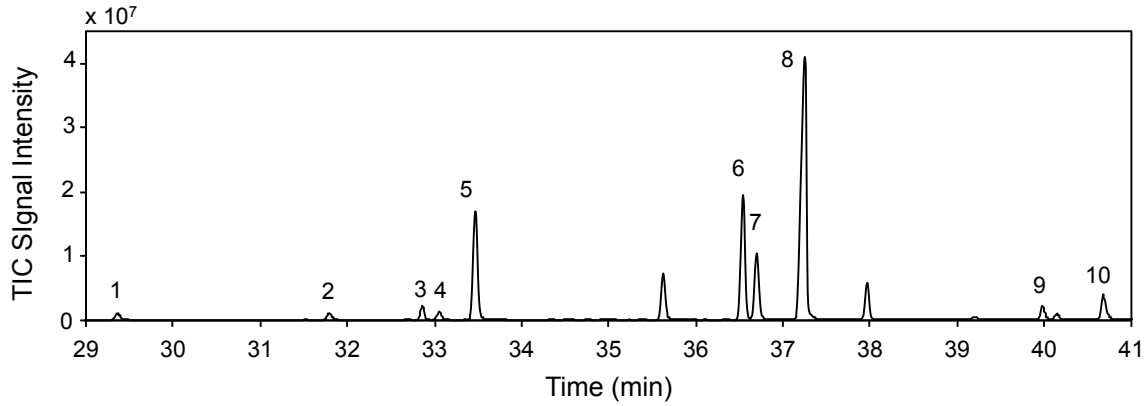

Figure 3.14 GC-MS TIC of alkenoic acids produced by thermal depolymerization of *mcl*-PHAs. Thermal depolymerization of *mcl*-PHAs was performed at 250°C for 30 min at temperature under an inert Ar atmosphere. Major identified compounds are listed in **Table 3.2**.

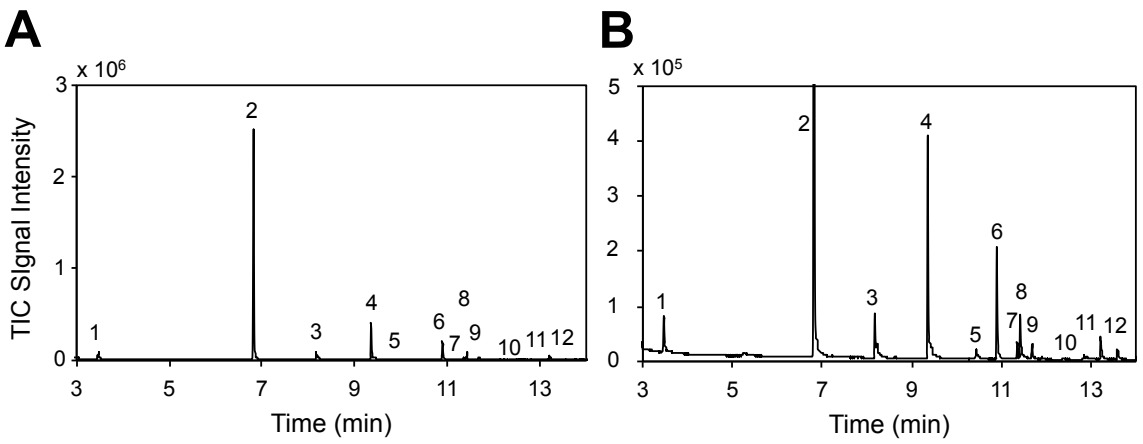

Figure 3.15 GC-MS TIC of hydrocarbons derived from the thermal depolymerization and catalytic deoxygenation of *mc*l-PHAs. Catalytic deoxygenation of *mcl*-PHAs was performed using with a Pt-Re/C catalyst using water as a solvent at 300°C for 180 min, with an initial reactor headspace pressurized to 2.75 MPa with H_2 at ambient temperature. (A) GC-MS chromatogram and major identified product peaks for retention times between 3 and 14 minutes. (B) Chromatogram y-axis scale has been expanded from that presented in (A) to capture the full peak heights in this region. Major identified compounds are listed in **Table 3.3**.

Table 3.1 Low molecular weight compounds identified or reported (*) in APL by LC-MS-MS.

Peak No.	RT (min)	Identified or reported compounds in APL
1	2.3	Malonic acid
2	2.7	Malic acid
3	2.8	Acetic acid
4	2.9	Lactic acid
5	4.9	Citric acid
6	9.4	Levulinic acid
7	25.2	Salicylic acid
8	25.3	Vanillyl alcohol*
9	32.5	4-Hydroxybenzaldehyde
10	35.6	Vanillic acid
11	42.5	Syringic acid
12	43.3	Vanillin
13	46.4	Syringaldehyde
14	46.6	Coniferyl alcohol*
15	46.6	p-Coumaric acid
16	47.7	Sinapyl alcohol*
17	49.0	Ferulic acid
18	49.9	Sinapic acid
19	53.4	Coniferyl aldehyde*
ND	-	Eugenol*
ND	-	Guaiacol*
ND	-	Syringol*

* Known from previous literature[65–75]

Table 3.2. Volatile components identified by GC-MS for the thermal depolymerization of *mcl*-PHAs. Repeated entries are indicative of isomeric forms, which are chromatographically separated.

Peak No.	RT (min)	Catalytic Deoxygenation Species
1	29.4	2-Hexenoic acid
2	32.9	3-Octenoic acid
3	33.1	2-Octenoic acid
4	33.5	2-Octenoic acid
5	36.5	3-Decenoic acid
6	36.7	3-Decenoic acid
7	37.3	2-Decenoic acid
8	40.0	1-Tetradecene
9	40.2	5-Dodecenoic acid
10	40.7	2-Dodecenoic acid

Table 3.3. Volatile hydrocarbons identified by GC-MS derived from the thermal depolymerization and catalytic deoxygenation of *mcl*-PHAs. Linear hydrocarbons were matched with known standards and cyclic hydrocarbons were identified using GC-MS NIST library matches.

Peak No.	RT (min)	Compound Name
1	3.4	Heptane
2	6.8	Nonane
3	8.2	Decane
4	9.4	Undecane
5	10.4	Dodecane
6	10.9	Cyclic hydrocarbon
7	11.3	Cyclic hydrocarbon
8	11.4	Tridecane
9	11.7	Cyclic hydrocarbon
10	12.3	Tetradecane
11	12.9	Cyclic hydrocarbon
12	13.6	Branched hydrocarbon

Table 3.4. Fluorescence intensity as a function of APL concentration. The fluorescence intensity was normalized at an equivalent optical density.

APL Concentration	Fluorescence Intensity (t=24 hours)
1x	99,600 ± 6,040
5x	105,400 ± 10,842

CHAPTER 4

ADIPIC ACID PRODUCTION FROM LIGNIN [1]

4.1 Abstract

Lignin is an alkyl-aromatic polymer present in plant cell walls for defense, structure, and water transport. Despite exhibiting a high-energy content, lignin is typically slated for combustion in modern biorefineries due to its inherent heterogeneity and recalcitrance, whereas cellulose and hemicellulose are converted to renewable fuels and chemicals. However, it is critical for the viability of third-generation biorefineries to valorize lignin alongside polysaccharides. To that end, we employ metabolic engineering, separations, and catalysis to convert lignin-derived species into *cis,cis*-muconic acid, for subsequent hydrogenation to adipic acid, the latter being the most widely produced dicarboxylic acid. First, *Pseudomonas putida* KT2440 was metabolically engineered to funnel lignin-derived aromatics to *cis,cis*-muconate, which is an atom-efficient biochemical transformation. This engineered strain was employed in fed-batch biological cultivation to demonstrate a *cis,cis*-muconate titer of 13.5 g/L in 78.5 h from a model lignin-derived compound. *cis,cis*-Muconic acid was recovered in high purity (>97%) and yield (74%) by activated carbon treatment and crystallization (5°C, pH 2). Pd/C was identified as a highly active catalyst for *cis,cis*-muconic acid hydrogenation to adipic acid with high conversion (>97%) and selectivity (>97%). Under surface reaction controlling conditions (24°C, 24 bar, ethanol solvent), purified *cis,cis*-muconic acid exhibits a turnover frequency of 23-30 sec^{-1} over Pd/C, with an apparent activation energy of 70 kJ/mol. Lastly, *cis,cis*-muconate

[1] A modified version of Chapter 4 was published in Energy & Environmental Science, 2015, 8,617-628. (D.R. Vardon co-lead author with co-lead authors M.A. Franden, C.W. Johnson, and E.M Karpk, as well as co-authors M.T. Guarnieri, J.G. Linger, M.J. Salm, T.J. Strathmann, P.T. Pienkos, and G.T. Beckham).

was produced with engineered *P. putida* grown on a biomass-derived, lignin-enriched stream, demonstrating an integrated strategy towards lignin valorization to an important commodity chemical.

4.2 Introduction

Lignocellulosic biomass offers a vast, renewable resource for the sustainable production of fuels, chemicals, and materials. To date, polysaccharides have been the primary biomass fraction of interest in selective conversion processes, leaving significant opportunities for valorizing underutilized components such as lignin.[1–3] Lignin, a heterogeneous aromatic polymer, is the second most abundant biopolymer after cellulose, representing 15 to 40% dry weight of plants; despite its abundance, the inherent heterogeneity and recalcitrance of lignin typically limits its use to heat and power in biochemical conversion processes.[2,4] However, as next generation biorefineries come online to produce carbohydrate-derived fuels at commodity scale, large quantities of lignin will be generated, with recent analysis pointing that lignin valorization can play a key role for their economic viability and environmental sustainability.[1,3,5]

In nature, lignin depolymerization is accomplished primarily by powerful oxidative enzymes secreted by rot fungi and some bacteria.[6] This process releases aromatic monomers during plant cell wall deconstruction, and multiple strategies have evolved for metabolism of these aromatic species. The most studied aromatic catabolic approach employs upper pathways to channel aromatic molecules into the b-ketoadipate pathway via central intermediates, such as catechol and protocatechuate.[7,8] This strategy offers a direct means to upgrade a heterogeneous slate of lignin-derived aromatic species via a “biological funneling” approach.[9]

Catechol is a primary central intermediate from the upper pathways into the b-ketoadipate pathway. Many aromatic-catabolizing organisms employ a catechol-1,2-dioxygenase enzyme to ring open catechol to *cis,cis*-muconate (hereafter referred to as muconic acid or muconate), which is a promising intermediate for commodity chemicals. Muconate is situated well before aromatic-derived species enter central carbon metabolism (i.e., the tricarboxylic acid (TCA) cycle), allowing for much greater atom efficiencies compared to products derived from acetyl-CoA (e.g., lipids, polyhydroxyalkanoates), the latter which require additional metabolic steps that divert carbon to microbial biomass production and CO_2. Previous demonstrations for biological production of muconate via catechol ring-opening have focused on food-grade or single feedstocks, such as glucose,[10,11] benzoate,[12] catechol,[13] and styrene.[14]

Muconic acid can be converted into myriad downstream products, including adipic acid, which is the most commercially important dicarboxylic acid.[15] Adipic acid has a market volume of 2.6 million tons per year with an annual demand growth forecast of 3-3.5% globally.[16] It has uses as a polymer precursor for nylon, plasticizers, lubricants, and polyester polyols.[15,17] Conventional adipic acid production involving nitric acid oxidation of benzene is highly damaging to the environment.[15] However, a recent analysis of biorefinery lignin utilization for adipic acid production points to major economic and greenhouse gas offsets using an integrated biological and chemical catalysis approach.[5]

To effectively convert lignin to adipic acid, the development of integrated downstream separations and catalysis, alongside metabolic engineering, will be critical for commercially viable technologies, as illustrated in **Figure 4.1.** Separation processes alone have been estimated to account for up to 60% of the final product cost for sugar-derived fermentation acids, such as lactic acid and succinic acid, a scenario likely to be encountered with muconic acid as well.[18]

Likewise, the impact of trace fermentation impurities unique to lignin in downstream separations and catalysis has yet to be explored. To date, only demonstration reactions have been performed for the catalytic reduction of glucose-derived muconic acid to adipic acid,[10,11] and questions remain regarding catalyst activity screening, the impact of upstream separations, and the intrinsic activity parameters under surface reaction controlling conditions.

Here, we demonstrate an integrated scheme for the conversion of lignin to adipic acid via biologically derived muconic acid. Specifically, we engineered *P. putida* KT2440 to funnel lignin-derived aromatics to muconate as the organism is amenable to genetic manipulation, tolerant to a wide variety of physical and chemical stresses, and capable of utilizing numerous lignin-derived aromatic molecules.[19] To purify muconic acid from culture media, we leveraged the ring-opened aliphatic structure of muconic acid relative to aromatic feedstocks and metabolic intermediates via preferential adsorption of the latter, followed by low temperature and pH crystallization.[20] Noble metal catalysts were screened for muconic acid hydrogenation, and the most active formulation was evaluated under surface reaction controlling conditions to estimate the turnover frequency and apparent activation energy. Lastly, muconate was produced biologically from a corn-stover derived, lignin-enriched stream, serving as proof-of-concept for an integrated biological and chemical lignin valorization process.

4.3 Results

4.3.1 Metabolic engineering for muconate production

Muconate is produced natively in *P. putida* by the action of a catechol-1,2-dioxygenase enzyme as an intermediate in the catechol branch of the b-ketoadipate pathway.[19] Protocatechuate is metabolized via another branch of the b-ketoadipate pathway that does not

include muconate as an intermediate. Given that many lignin-derived species will be funneled through one of these two central aromatic intermediates, our metabolic engineering strategy aimed to convert aromatics from both the catechol and protocatechuate branches of the b-ketoadipate pathway to muconate, as shown in **Figure 4.2**. To capture aromatic species that are metabolized through protocatechuate, *pcaHG*, which encodes a protocatechuate 3,4 dioxygenase, was replaced with *aroY*, encoding a protocatechuate decarboxylase from *Enterobacter cloacae*[21] (**Figure 4.3**) using a marker-free homologous recombination system.[22,23] This enabled the conversion of protocatechuate and upstream metabolites to catechol, while simultaneously eliminating further catabolism of protocatechuate to b-ketoadipate.

P. putida was then engineered to expand substrate utilization and to eliminate further metabolism of muconate. Intradiol ring opening of catechol to muconate is accomplished by two redundant dioxygenases, CatA and CatA2. CatA is encoded along with CatB and CatC, the next two enzymes in the catechol branch of b-ketoadipate pathway, in an operon regulated by CatR, a LysR family transcriptional regulator.[24] In order to eliminate further metabolism of muconate and enable strong, constitutive expression of CatA, a genomic section containing *catR*, *catBC*, and the promoter for *catBCA* was replaced with the tac promoter.[25] Lastly, as phenol is a commonly-derived lignin intermediate, we integrated the genes encoding the phenol monooxygenase from *Pseudomonas sp.* CF600,[26] *dmpKLMNOP,* downstream of *catA* to form an operon driven by the tac promoter (**Figure 4.3**).

The metabolic performance of the engineered *P. putida* strain, KT2440-CJ103, was evaluated in shake-flask experiments to demonstrate substrate utilization and production of muconate from model lignin-derived monomers, using acetate as a carbon and energy source (**Figure 4.4**, further details provided in **Figure 4.5**). KT2440-CJ103 successfully produces

muconate from catechol, phenol, and benzoate via the catechol branch, as well as from protocatechuate, coniferyl alcohol, ferulate, vanillin, caffeate, *p*-coumarate, and 4-hydroxybenzoate via the protocatechuate branch. We observed muconate yields ranging from 14% with coniferyl alcohol to 93% with benzoate. For compounds metabolized through vanillate (coniferyl alcohol, ferulate, and vanillin), yields were quite low with substantial accumulation of the intermediate vanillate, likely due to regulation as discussed below. In contrast, for compounds metabolized through the catechol branch (phenol, catechol, benzoate), as well as *p*-coumarate and 4-hydroxybenzoate, yields were significantly higher. Lastly, substrate loss from abiotic oxidation (data not shown) contributed to reduced yields from caffeate, and to a lesser extent, catechol. Additional experiments to test the influence of glucose or acetate as a co-fed carbon source for energy and cell growth showed higher muconate yields from cultures grown on glucose, likely due to the additional reducing equivalents and ATP generated by glucose metabolism (**Table 4.1**).

4.3.2 Fed-batch biological conversion with *p*-coumarate

We next sought to demonstrate the performance of the engineered strain in a fed-batch bioreactor experiment, expecting that greater production of muconate could be achieved with increased aeration, pH control, and a metered dosing of substrates for growth and conversion. Dissolved oxygen static (DO-stat) fed-batch biological conversion by KT2440-CJ103 yielded a muconate titer of 13.5 g/L after 78.5 h using *p*-coumarate as a model lignin monomer substrate, over 15 times greater than shake flask results (**Figure 4.4B**). Preliminary experiments indicated that muconate production from *p*-coumarate was significantly inhibited in the presence of excess glucose or acetate, potentially due to catabolite repression control or other regulatory

inhibition.[27–29] Therefore, DO-stat was used to maintain glucose levels below 1 mM[30] and co-feed *p*-coumarate and ammonium sulfate (**Figure 4.6**). During the course of cultivation, protocatechuate buildup occurred. Moreover, as the cultivation progressed past 60 h, muconate levels plateaued and 4-hydroxybenzoate, a metabolite upstream of protocatechuate, accumulated. The color of the culture medium darkened over time, as shown in **Figure 4.4**, first panel. It may be possible to achieve higher yields with less by-product formation via strain development and process optimization, as discussed below.

4.3.3 Separation and recovery of muconic acid

To ultimately produce high-purity adipic acid as a final product from lignin, our next goal was to recover muconate selectively from cell-free culture media as impurities resulting from biological conversion media and aromatic intermediates will undoubtedly affect the quality and performance of adipic acid during polymerization or subsequent chemical transformations. The biological ring opening of muconate allowed for facile purification from culture media containing non-target aromatic metabolites (e.g., protocatechuate and 4-hydroxybenzoate) using activated carbon due to the high adsorption affinity of oxygenated aromatics in comparison to aliphatic acids.[31,32] After adding activated carbon to the culture media at 12.5% (wt/vol) with stirring for 1 h,[33] nearly complete removal (below detectable limit by HPLC) of protocatechuate and 4-hydroxybenzoate was achieved, while the majority of muconate (89% of initial culture media concentration, mass/vol) remained in solution (**Figure 4.7**). Muconic acid was then crystallized by reducing the pH and temperature, following from the strong pH and temperature dependence of dicarboxylic acids.[33,34] At pH 2 and 5°C, muconic acid readily precipitated from

solution and crystals were recovered by vacuum filtration. This method recovered 74% of the muconic acid in the purified broth with a high degree of purity (>97%), as shown in Fig. 3.

4.3.4 Catalytic hydrogenation of muconic acid to adipic acid

Catalyst screening experiments were then conducted to identify highly active materials for muconic acid hydrogenation at low temperature and pressure. Commercial noble metal catalysts supported on carbon were initially tested at 5 wt% loading, including Pd, Pt, and Ru. Characterization of the virgin catalyst materials (**Figure 4.8**, **Table 4.2**) revealed the metals were dispersed as small crystallites, with comparable support surface areas (705-1075 m^2/g), pore volumes (0.51-0.71 mL/g), and a wider range of exposed active metal areas (22-51% dispersion). Screening experiments found that Pd/C was by far the most active catalyst, with consistent activity trends when using M9 culture media (aqueous solution containing salts to support biological growth) or ethanol, as a representative protic polar organic solvent (**Figure 4.9**). During the course of the reaction, 2-hexenedioc acid was observed as the primary intermediate, likely due to the low temperature conditions that minimized competing nonselective reaction pathways (**Figure 4.10**). For reactions that went to completion with Pd, selectivity to adipic acid was >97% (mol/mol) (**Figure 4.8**).

Additional hydrogenation conditions were examined with Pd/C to (i) determine its activity under surface reaction controlling conditions, (ii) evaluate the apparent activation energy for muconic acid reduction, and (iii) demonstrate its utility with muconic acid recovered from fed-batch biological conversion. Experiments conducted at two different Pd loadings (1 wt% and 2 wt% Pd/C) exhibited comparable turn over frequencies (TOF; 23 ± 6 sec^{-1} and 30 ± 6 sec^{-1}, respectively, at 24 bar of hydrogen and 24°C in ethanol), supportive of surface reaction

controlling conditions by the Koros-Nowak criterion (ESI Fig. S6†).[35] Experiments to measure the hydrogenation rate of muconic acid at varying temperatures estimated an apparent activation energy of ~70 kJ/mol (**Figure 4.8C**, **Figure 4.12**), significantly above values indicative of mass transfer limitation (<20 kJ/mol).[36] Hydrogenation with Pd/C was then demonstrated with muconic acid obtained from fed-batch biological conversion of *p*-coumarate after activated carbon purification and crystallization. Hydrogenation at room temperature progressed rapidly in a series reaction (**Figure 4.8D**, muconic acid TOF 25 ± 3 sec^{-1}), resulting in high purity adipic acid as the final product (>97% mass/mass. Variability in sample mass closure was attributed to error introduced during sampling and filtration of reactor contents prior to analysis, as well as potential adsorption of organics to the catalyst carbon support, with individual species concentrations and molar closure provided in **Table 4.3**. After the reaction, analysis of the ethanol solvent indicated that leaching of Pd occurred to a minor extent (7 μg/L, 0.8% of the loaded metal), which can occur due to the acidic liquid phase conditions employed.[37]

4.3.5 Biological conversion of depolymerized lignin

Lastly, as an initial proof of concept for this process scheme, muconate was produced from biomass-derived lignin in shake flask conditions. Namely, alkaline pretreatment with NaOH and anthraquinone (AQ) was applied to corn stover at 70 mg NaOH/g dry biomass with an AQ concentration of 0.2 wt% of dry stover, in a manner similar to our previous work.[9,38] The resulting alkaline pretreated liquor (APL) stream contains a substantial amount of lignin-derived aromatics, acetate, biomass extractives, and very minor concentrations of sugars (<0.5 g/L of any monomeric sugar).[9,38] The pH of APL was reduced to 7 with the addition of H_2SO_4. The liquor was then filtered through a 0.2 μm filter for sterilization and to remove residual solids. Flasks

containing 25 mL M9 minimal medium supplemented with 0.9X APL were then inoculated with *P. putida* KT2440 or KT2440-CJ103 and cultured for three days. Following biological conversion, cells were removed by centrifugation and activated carbon (12.5 wt/vol%) was added to the remaining culture media to remove non-target aromatics and facilitate analysis by HPLC. The complexity and pH sensitivity of APL impedes direct quantitative compositional analysis by conventional methods;[39] however, analysis by HPLC detected significant levels of muconic acid in cultures grown with *P. putida* KT2440-CJ103, while no significant quantities were detected in the blank APL control sample or with the native *P. putida* KT2440 (**Figure 4.13A**). Likewise, analysis of derivatized acids in unpurified culture samples by GC×GC-TOFMS (time-of-flight mass spectrometry) confirmed the identity of muconic acid and displayed comparable trends in concentration, as shown in of **Figure 4.13B**.

To track the conversion of primary aromatic and nonaromatic components in APL during shake flask cultivation, GC×GC-TOFMS was also employed. Analysis of APL determined that *p*-coumarate and ferulate were initially present at significant levels (0.92 g/L and 0.34 g/L, respectively), in addition to the short chain acids glycolate and acetate (0.46 g/L and 0.10 g/L, respectively), as shown in **Figure 4.13C**. Other aromatic acids, including benzoate, caffeate, vanillate, and 4-hydroxybenzoate, were not detected in significant levels (> 0.01 g/L). During shake flask cultivations, *P. putida* KT2440-CJ103 rapidly consumed glycolate and acetate, which can be used as sources of carbon and energy for growth. The primary aromatic components, *p*-coumarate and ferulate, were converted to 0.70 g/L of muconate after 24 h (**Figure 4.13C**). Based on the consumption of these two major aromatic acids, the molar yield to muconate was 67%.

4.4 Discussion

Techno-economic analysis has suggested that lignin valorization will become essential for the production of advanced biofuels.[5] As recently reviewed,[1] lignin valorization will be enabled by many different technological advances including genetic modifications of plants,[40–43], new biomass pretreatment and depolymerization technologies[3,38,44–47], tailored separation processes,[48] and catalytic product-slate diversification. Leveraging these developments for lignin valorization holds potential to capitalize on the unique aromatic functionality that greatly differentiates lignin from polysaccharides. Almost invariably, lignin depolymerization strategies result in a multitude of aromatic compounds.[1,3,49] Tasking microorganisms to funnel these heterogeneous organic molecules to simplified product streams can potentially overcome this limitation,[9] but significant considerations remain to realize this general approach.

Efficient conversion of substrate to product and high product yields are of crucial importance for economically viable biomass upgrading strategies. Unlike molecules targeted as products for biomass upgrading that are derived from pyruvate (ethanol, lactic acid), acetyl-CoA (fatty acids, wax esters, PHAs), or the TCA cycle (succinic acid), production of muconate occurs upstream of central carbon metabolism and thus is not subject to the competing interests of a growing cell and losses in carbon due to CO_2 and biomass production. Namely, conversion of aromatic molecules to muconate at high yields can occur concomitant with growth on non-aromatic substrates, such as acetate or glucose as demonstrated here. Indeed, yields from benzoate in our shake flask studies were 93% of the theoretical maximum.

Some other aromatic substrates, however, were not converted as efficiently, resulting in lower yields and the accumulation of intermediates such as protocatechuate, 4-hydroxybenzoate, and vanillate. It is likely that some of this accumulation is the result of transcriptional or

translational regulation of enzymes in these pathways. It is well known that many the aromatic degradation pathways involved in the production of muconate are controlled by transcriptional regulators.[8,50] While *catR* has been deleted in the production strain reported in this study, other transcriptional regulators such as BenR and VanR are likely to have contributed to accumulation of intermediates. It is also likely that transcription or translation of some of the enzymes involved are regulated, either directly or indirectly, by the Crc (catabolite repression control) protein. Crc is a global translational regulator that binds to specific RNA sequences to inhibit translation of targeted mRNAs and has been shown to regulate induction and repression of the catabolic pathways of amino acids, sugars, hydrocarbons, or aromatic compounds.[27–29] If transcriptional and/or translational regulation is a contributing factor in the accumulation of intermediates observed here, further engineering could be employed to affect expression of regulatory proteins or alter the binding targets of such proteins.

In addition to transcriptional and translational regulation, the enzymes involved could also be limited by kinetics or the thermodynamics of the reactions they catalyze. The protocatechuate decarboxylase, being an exogenous enzyme that is constitutively expressed in *P. putida* KT2440-CJ103, should not be regulated in transcription or translation. Nonetheless, an accumulation of protocatechuate was observed when producing muconate. This accumulation occurs in absence of an accumulation of the product, catechol, suggesting that equilibrium limitations are not present. Based on these observations, we hypothesize that either the specific activity of this protocatechuate decarboxylase is insufficient and/or that this enzyme is inhibited by muconic acid. Increasing the gene dosage of *aroY* or increasing the specific activity of the enzyme using protein engineering could be useful strategies for overcoming the accumulation of protocatechuate.

Finally, abiotic factors could also affect the conversion of these aromatic molecules to muconic acid. As mentioned previously, many of the cultures become darker with time. Indeed, in the absence of cells, the concentrations of some of the aromatic molecules decrease substantially in M9 minimal medium on similar time scales to the cultivation experiments and these solutions darken (data not shown). Oxidation products were not detected using the analytical methods described here, but the dark color of the spent media and the inability in some cases to account for all of the carbon metabolized by adding the muconic acid product with the intermediates accumulated suggests abiotic oxidation likely contributed to the lower yields observed in some cases. Further optimization of growth conditions might be useful in minimizing this oxidation, while increasing the activity of the individual enzymes may reduce the accumulation of intermediates that are likely to oxidize.

Regarding muconate production from biomass-derived lignin, further optimization of lignin depolymerization and bioprocess engineering, in addition to the metabolic engineering strategies discussed above, can provide a direct path forward for industrially relevant productivities and yields. In the current study, a biomass-derived, lignin-enriched substrate, APL, was used.[38] Alkaline treatment of biomass is typically used either in pulping to delignify biomass (at high severity), or as a pretreatment strategy to remove acetate and partially delignify biomass (at low severity).[38,51] However, in both cases, the resulting black liquor is not traditionally slated for subsequent upgrading. Thus, optimization of the alkaline pretreatment step has not been thoroughly conducted to our knowledge to yield a substrate with sufficiently high monomer concentrations required for industrially relevant biological conversion to muconate. With regards to bioprocess engineering, previous studies on non-lignin substrates have demonstrated that substantial process improvements can be achieved through control of substrate, growth media,

and oxygen delivery.[11,30,52] As such, coupled optimization of all aspects will be required to achieve industrially relevant muconate titer, productivity, and yield from lignin derived substrates.

In addition to improving yields during biological conversion, cost-effective separation strategies will be essential for valorizing lignin due to the necessary high carbon-to-product yield and purity requirements for renewable commodity chemicals. As noted previously, separation of biologically produced acids has been estimated to account for over 60% of production costs.[18] Selection of metabolic pathways that dramatically alter the chemical functionality of the parent lignin monomer (e.g., oxidative ring-opening to dicarboxylic acids) and its physicochemical properties (e.g., solubility, pK_a)[48] can greatly reduce the process intensity for separations. As demonstrated with the fed-batch conversion of *p*-coumaric acid, selective adsorption of non-target aromatic metabolites with activated carbon provides a facile mechanism for purifying muconic acid. Development of novel adsorbents that allow for non-target metabolite release and recycle can also maximize carbon utilization efficiency, similar to strategies being examined for oil spill remediation.[53] After purification, crystallization of muconic acid retains highly soluble salts and low molecular weight acids in the aqueous phase, minimizing the impact of impurities on downstream catalysis and end product purity. Although a fraction of muconic acid remained soluble in the culture media (~3.4 g/L) at low temperature and pH, higher titers in the culture media can greatly improve the fractional recovery by crystallization, which will be pursued in future studies.

As illustrated in this work, biological funneling can greatly simplify downstream catalytic processing for valorizing lignin as it can yield single intermediates.[9] Target compounds from biological conversion can be judiciously selected to ensure catalytic pathways are atom efficient,

while maintaining the high degree of chemical functionality inherent to biomass.[54] This is exemplified with muconic acid, in which the dicarboxylic functionality is retained for purposeful end-use as a polymer precursor, in lieu of full deoxygenation to hydrocarbon fuels. As demonstrated in this and previous efforts,[10,11] hydrogenation of muconic acid to adipic acid is nearly quantitative at mild temperatures, greatly reducing catalytic process intensity.

Within the framework of integrated bio-catalytic processing, advancements in catalyst design and engineering can also accelerate the use of lignin as feedstock for renewable chemical production. Knowledge regarding the activity and stability of conventional noble metals for muconic acid hydrogenation can provide a baseline for improved catalyst design. In worldwide catalysis efforts, material substitutes are currently being developed for platinum group metals to achieve comparable activity for chemistries critical to biomass valorization. Strategies include alloying primary metals with low-cost secondary metals,[55,56] utilizing earth abundant metal oxides and carbides,[57,58] and enhancing activity and selectivity through tailored synthesis of metal crystallite size, shape, and facets.[59,60] In addition to material design, knowledge regarding the activity of these catalysts in solvent systems compatible with separation processes and their sustained performance in the presence of residual impurities from biological conversion will be key to their development and implementation at scale.

4.5 Conclusion

Lignin has typically been viewed as a small volume or niche feedstock, such as for the production of vanillin or lignosulfonates, given its intrinsic heterogeneity and recalcitrance. In the context of biofuels production, lignin is currently seen through a similar lens, with initial biorefinery designs slating lignin for heat and power despite having a higher energy density and

C:O ratio than polysaccharides. However, recent economic and environmental analysis has shown that lignin valorization will be an essential component of next generation lignocellulosic biorefining.[5] To that end, here we have demonstrated an integrated strategy to combine biological funneling, separations, and chemical catalysis to produce adipic acid from lignin-derived aromatic molecules. More broadly, the ability to funnel a heterogeneous mixture of lignin-derived species coupled to the use of a tunable biocatalyst, tailored separations, and catalytic upgrading will enable the production of targeted, single intermediates with high atom efficiency, thus overcoming the intrinsic heterogeneity of lignin – the primary technical hurdle in lignin valorization. This overall co-design concept for lignin valorization offers a versatile path forward for the production of fuels, chemicals, and materials from lignin.

4.6 Methods

4.6.1 Strains, media, and growth conditions

Cells and media used for plasmid construction and gene replacements are described in ***Supplemental Information,*** **Figure 4.3**, **Table 4.4**, and **Table 4.5**. *P. putida* KT2440 (ATCC 47054) and its derivatives were grown shaking at 225 rpm, 30°C, in LB Broth or LB plates. During gene replacement, sucrose selection was performed on YT+25% sucrose plates (10 g/L yeast extract, 20 g/L tryptone, 250 g/L sucrose, 18 g/L agar). Shake flask and bioreactor experiments were performed using modified M9 minimal media containing 13.56 g/L disodium phosphate, 6 g/L monopotassium phosphate, 1 g/L NaCl, 2 g/L NH_4Cl, 2 mM $MgSO_4$, 100 μM $CaCl_2$, and 18 μM $FeSO_4$ (MM). Details regarding plasmid construction and gene replacement are described in ***Supplemental Information***.

4.6.2 Shake flask experiments with model monomers and APL

Fed batch and shake flask experiments were performed using 125 mL baffled flasks containing 25 mL modified M9 media supplemented with 10 mM sodium benzoate, coniferyl alcohol, ferulate, vanillin, caffeate, *p*-coumarate, 4-hydroxybenzoate or 5 mM phenol and 20 mM sodium acetate or 10 mM glucose. For shake flask experiments in which cells were grown on alkaline pretreated liquor (APL), M9 was supplemented with APL at a concentration of 0.9X.[9] Cultures inoculated with cells washed in modified M9 medium to OD_{600} 0.05, then incubated shaking at 30°C, 225 rpm. Every 12 hours, cultures were sampled for HPLC, OD_{600}, and pH measurement, pH adjusted, and fed sodium acetate or glucose. For cultures at pH > 7.4 or < 6.6, the pH was adjusted to 7.0 by adding 1N HCl or 1N NaOH. 20 mM or 10 mM glucose was added before returning the cultures to the incubator. Substrates and products were analyzed as described in ***Supplemental Information***.

4.6.3 Fed-batch fermentation

A seed batch culture of *P. putida* KT2440-CJ103 was started in a shake flask and grown overnight in LB, 30°C, 225 rpm. The next morning, cells were centrifuged 3,800×g, 10' and washed once with MM containing 10 mM glucose. Cultures were transferred to 700 mLs of the same medium in a 2L Applikon (Applikon Biotechnology, Inc.) EZ Control 2L bioreactor, starting at an initial OD_{600} of 0.2. Base pH was controlled by 2N NaOH to pH 7. The temperature was maintained at 30°C. Mixed air was used to deliver oxygen at a flow rate of 2 L/min. DO saturation was manually adjusted to ~ 50% by varying stirrer speed, from 250 to 650 rpm, and then maintained at 650 rpm for the duration of the experiment. At 5 h, 2 mM *p*-coumarate was added. When glucose was consumed at ~ 11.5 h, a large spike in DO was

observed, indicating that glucose was depleted and confirmed by YSI analysis. A separate pump was computer programmed to deliver for 30 seconds (~2.4 mL) a glucose: *p*-coumarate: ammonium sulfate (68.4:36.5:9 g/L) feed when DOT (dissolved oxygen tension) levels reached ≥75%. The feed caused a temporary drop in DOT to ~50%, until glucose concentrations fell again. As expected, DOT oscillations proceeded at similar frequencies (**Figure 4.6**), until the glucose:*p*-coumarate:ammonium sulfate feed was terminated at 75.5 h and the bioreactor was shut down at 78.5 h.

4.6.4 Purification and crystallization

Fed-batch fermentation broth was initially purified to remove non-target aromatic metabolites. The broth was purified by the addition of 12.5 w/v% activated carbon (Sigma Aldrich, Darco 100 mesh) with stirring at 350 rpm for 1 h.[33] Activated carbon was removed via vacuum filtration (0.2-µm PES filter assembly, Nalgene).

Muconic acid crystallization was initiated by adjusting the filtrate pH to 2 by HCl addition. The broth was chilled to 5°C and precipitated crystals were recovered by vacuum filtration (Nalgene). Crystals were dried for 24 h in a vacuum oven and weighed, prior to analysis by HPLC. Muconic acid purity post activated carbon, recovery following crystallization, and crystal purity were calculated based on **Eqn. 4.1-4.3**, respectively.

Eqn 4.1 $$\text{Post activated carbon purity (\%)} = \frac{\text{Muconic acid (g L}^{-1})}{\text{Total organic acids (g L}^{-1})} \times 100\%$$

Eqn 4.2 $$\text{Crystaillization recovery (\%)} = \frac{\text{Crystallized muconic acid (g)}}{\text{Muconci acid purified broth (g L}^{-1}) \times \text{Volume (L)}} \times 100\%$$

Eqn 4.3 $$\text{Crystallization purity (\%)} = \frac{\text{Crystallized muconic acid (g)}}{\text{Crystallized solids (g)}} \times 100\%$$

4.6.5 Catalysis

Commercial monometallic noble metal catalysts were screened for their hydrogenation activity with muconic acid. Catalysts at 5 wt% loading on activated carbon were obtained from Sigma Aldrich (Pt Pd, and Ru) and 1 wt% Pd/C was obtained from Alfa Aesar. Virgin catalyst materials were initially characterized to determine their average crystallite size and long-range order by x-ray diffraction, support surface area and pore volume by nitrogen physisorption, and active metal surface area by hydrogen chemisorption, with details described elsewhere.[61] Due to the high sensitivity of Pd dispersion with temperature,[62] Pd samples were reduced under flowing hydrogen (50 mL min^{-1}, 10% H_2 in Ar) at moderate temperature (125°C, 3°C min^{-1}) and held for 1 h. Following reduction, Pd samples were purged for 1 h under Ar and cooled to 45°C prior to H_2/O_2 titration. For calculations of Pd dispersion, the amount of hydrogen uptake that followed the second oxygen titration was used. A stoichiometry of 0.667 Pd sites per H_2 molecule was assumed to remove oxidized Pd-O species in the form of water and form the reduced Pd-H species.

Hydrogenation screening experiments with 5 wt% catalysts were performed in 200 proof ethanol using a Parr 5000 Multireactor system (Parr Instruments). For model compound studies, commercial *cis,cis*-muconic acid (Sigma Aldrich) was initially purified using activated carbon

and crystallized at low pH and temperature, as described above. Screening solvents included ethanol, as well as simulated culture media prepared with mock M9 culture media (Sigma Aldrich) adjusted to pH 7 with NaOH. Reactions were performed in triplicate using 75 mL vessels operating at 1600 rpm stirring, with hydrogen supplied at constant pressure by a distributed gas manifold operating in dead end mode. Samples were collected with an *in situ* sampling valve and syringe filtered (0.2-μm Nylon, VWR) prior to analysis by HPLC. After the reaction, leaching of Pd/C was determined by ICP-OES. The ethanol solution was vacuum filtered (0.2-μm PES filter assembly, Nalgene) and dried under nitrogen to remove solvent prior to analysis.

Conversion of muconic acid was calculated by dividing the moles of muconic acid measured in each sample by the moles of muconic acid at time zero. Selectivity to adipic acid was calculated by dividing the moles of adipic acid measured by the moles of muconic acid converted in each sample. The reduction of muconic acid was modeled as pseudo-first order to estimate the rate constant using non-linear regression with GraphPad Prism version 6.00 (Graphpad Software). Catalyst TOF was calculated by dividing the rate of muconic acid conversion (moles of muconic acid per second, estimated using the modeled pseudo-first order rate constant at 10% muconic acid conversion) by the moles of surface exposed active metal determined by chemisorption.

To evaluate the influence of mass transfer on the observed rate of muconic acid hydrogenation, the TOF of Pd was compared at two different catalyst metal contents and at varying temperature. Pd/C catalysts were prepared in house at 1 wt% and 2 wt% metal loading by incipient wetness to evaluate their TOF by the Koros-Nowak criterion.[35]. Pd-acetate (Sigma Aldrich) was dissolved in acetone and loaded onto sieved activated carbon (<270 mesh).

Catalysts were dried overnight and reduced in flowing hydrogen at 125°C for 2 h. Experiments were performed in triplicate at elevated pressure (24 bar) to facilitate hydrogen mass transfer. The activation energy for muconic acid hydrogenation was then estimated with the Arrhenius equation by varying the temperature from 12-40°C and measuring the influence on the observed TOF with commercial 1% Pd/C obtained from Alfa Aesar. The 95% confidence intervals for the observed TOF were calculated using non-linear regression with GraphPad Prism version 6.00 (Graphpad Software).

4.6.6 Analysis of APL-derived muconate

Activated carbon (12.5% w/v) was added to the samples taken from shake flasks with stirring for 1 h, prior to vacuum filtration (2 μm) and analysis by HPLC. To confirm the identity of muconic acid in APL, GCxGC-TOFMS analysis was performed. Acids present in the APL culture broth were converted to their ammonia salt form, reconstituted in pyridine and derivatized with the addition of *N*,*O*-Bis(trimethylsilyl)trifluoroacetamide (BSTFA), following a method similar to the one described by Alen et al.[63] The derivatized acids were analyzed on a LECO Pegasus GCxGC-TOFMS system with a Gerstel autosampler. Samples were run at a 30:1 split ratio using helium as a carrier gas and an injection volume of 1 μL. The first dimension utilized a 10-m Restek RTX-5 column and the second column dimension utilized a 0.75-m Agilent DB-1701 column. The mass spectrum and retention time of derivatized *cis,cis*-muconic acid was identified using a reference standard of *cis,cis*-muconic acid purchased from Sigma Aldrich that was converted to its ammonium salt form, dissolved in pyridine containing an internal standard of ammonium cylcohexane carboxylate and derivatized with BSTFA. For

quantification purposes, *p*-coumaric acid, ferulic acid, acetic acid and glycolic acid were also converted to their ammonium salts, reconstituted in pyridine, and derivatized with BSTFA.

4.7 Supplemental Information

4.7.1. Strains, plasmid construction, and gene replacement

Competent NEB (New England Biolabs, Inc., Ipswich, MA) C2925 and Life Technologies (Grand Island, NY) TOP10 was used for plasmid construction of *cis,cis*-muconate producing and phenol utilizing strains, respectively. NEB 5-alpha F'I^q *E. coli* was used for all remaining plasmid constructions and were grown shaking at 225 rpm, 37°C, in LB Broth (Lennox) containing 10 g/L tryptone, 5 g/L yeast extract, 5 g/L NaCl or on LB plates containing 15 g/L agar, with either 10 μg/mL tetracycline or 50 μg/mL kanamycin. *E. coli* was transformed according to the manufacturer's instructions.

Q5® Hot Start High-Fidelity 2X Master Mix (NEB) and primers synthesized by IDT (Integrated DNA Technologies, Inc., Iowa) were used in all PCR amplification for plasmid construction. Primer sequences are shown in **Table 4.4**. Plasmids were assembled using Gibson Assembly® Master Mix (NEB) according to the manufacturer's instructions. The sequences of all plasmid inserts were confirmed using Sanger sequencing (GENEWIZ, Inc., South Plainfield, NJ).

Plasmids for gene replacement were constructed in pCM433 (Addgene Inc., Cambridge, MA)[22] or pK18mobsacB from ATCC (American Type Culture Collection, Manassas, VA)[23], both of which are unable to replicate in *P. putida* and contain antibiotics to select for integration of the plasmid into the genome by homologous recombination and *sacB* to counter-select for recombination of the plasmid out of the genome.

The pCM433-based integration vector used to replace *catRBCA* with Ptac:*catA* (pMFL22) was constructed by Gibson assembly of 3 PCR products: LP29 and LP33 were used to amplify the homology region upstream from *catA*, LP30 and LP31 were used to amplify the tac promoter from Sigma pFLAG-CTC, LP32 and LP34 were used to amplify the entire coding region of *catA* including its native RBS. After assembly, the 2.2 kb fragment was amplified by PCR using primers LP29 and LP34, and cloned into the pCM433 vector using NotI sites.

The pK18mobsacB-based plasmid for integration of the phenol monooxygenase genes (pMFL56) was constructed by Gibson assembly of 3 PCR fragments using primers LP53 and LP48 to amplify the *catA* homology region, LP49 and LP50 for amplification of six phenol monooxygenase genes, *dmpKLMNOP* using pVI1261 as the template (provided by Dr. Victoria Shingler from the Department of Molecular Biology at Umeå University)[26], and primers LP51 and LP54 for amplification of the homology region downstream from *catA*. Fragments were then cloned into pK18-mob vector using NotI sites. (**Figure 4.3**)

In the plasmid for replacement of *pcaHG* with Ptac:*aroY* (pCJ023), the *aroY* gene (ADF69416) from *Enterobacter cloacae* ATCC13047 was optimized for expression in *P. putida* KT2440 using DNA 2.0's Gene Designer software and synthesized in two overlapping gBlock fragments by IDT (**Table 4.5**). The first fragment also contained the tac promoter, which was separated from the initiating ATG by a ribosome binding site with the sequence AGAGGAGGGAGA, designed using the Salis Lab RBS Calculator v1.1[64] at https://salis.psu.edu/software/. These fragments were then assembled by Gibson assembly and Ptac:*aroY* was amplified from this assembly with primers oCJ165 and oCJ166. Approximately 1 kb regions upstream and downstream of *pcaHG* were amplified using oCJ100/oCJ101, and oCJ102/oCJ103, respectively. The upstream region of homology, Ptac:*aroY*, and the downstream

region of homology were then assembled into pCM433 linearized with restriction enzymes AatII and SacI (NEB) (**Figure 4.3**).

Gene replacement plasmids were transformed into *P. putida* strains by electroporation. LB broth was inoculated to an OD_{600} of about 0.02 and incubated shaking at 225 rpm, 30°C, until an OD_{600} of 0.5 – 0.7 was reached. Cells were then centrifuged at 4°C, washed twice in ice-cold water and once in ice-cold 10% glycerol or 3 mM potassium phosphate (KPi), pH 7.0, before being resuspended in 1/100 of the culture's original volume of 10% glycerol (or 3mM KPi). Cells were then stored at -80°C or transformed by electroporation immediately. For transformation, 5 µL (200 ng – 2 µg) of plasmid DNA was added to 50 µL of the electrocompetent cells, transferred to a chilled 0.1-cm electroporation cuvette, and electroporated at 1.6 kV, 25 uF, 200 ohms. 450 µL SOC outgrowth medium (NEB) was added to the cells immediately after electroporation and the resuspended cells were incubated shaking at 225 rpm, 30°C, for one hour. The entire transformation was plated on LB agar plates containing appropriate antibiotics (30 µg/mL tetracycline for pCM433-based plasmids, 50 µg/mL kanamycin for pK18mobsacB-based plasmids) and incubated at 30°C overnight. Transformants were restreaked for single colonies on LB agar and incubated at 30°C overnight to reduce the possibility of untransformed cells being transferred. For sucrose counter-selection, restreaked transformants were streaked for single colonies on YT+20 or 25% sucrose plates (10 g/L yeast extract, 20 g/L tryptone, 250 g/L sucrose, 18 g/L agar) and incubated at 30°C overnight. *P. putida* KT2440 containing the *sacB* gene can grow, although very slowly, on YT+20% or 25% sucrose media. Therefore, colonies presumed to have recombined the *sacB* gene out of the genome – those colonies that were larger than most – were restreaked on YT+25% sucrose plates and incubated at 30°C overnight to reduce the possibility that cells that had not recombined

would be carried along with sucrose resistant isolates. Colonies from the second YT+25% sucrose plates were subjected to colony PCR to check for gene replacement at both junctions. These isolates were also plated on LB plates containing appropriate antibiotics to ensure that they had lost antibiotic resistance and, thus, represented pure gene replacements. The following designations of strains constructed for this publication are as follows: *P putida* KT2440-MLF30 (Δ*catRBCA*::Ptac:*catA*), *P putida* KT2440-MFL59 (Δ*catRBCA*::Ptac:*catA*:*dmpKLMNOP*) *P. putida* KT2440-CJ103 (Δ*catRBCA*::Ptac:*catA*:*dmpKLMNOP* Δ*pcaHG*::*Ptac*:*aroY*).

4.7.2. Analysis of organic substrates and products

Concentrations of glucose, acetate, *cis,cis*-muconate, and remaining aromatic substrates and products were determined from filtered sample supernatants by high performance liquid chromatography (HPLC) on an Agilent1100 series system (Agilent USA, Santa Clara, CA) utilizing a Phenomenex Rezex RFQ-Fast Fruit H+ column (Phenomenex, Torrance, CA) and cation H+ guard cartridge (Bio-Rad Laboratories, Hercules, CA) operating at 85°C. Dilute sulfuric acid (0.01 N) was used as the isocratic mobile phase at a flow rate of 1.0 mL/min. Refractive index and diode array detectors were used for compound detection. By-products were identified by co-elution at the same retention time with pure compounds as well as having matching spectral profiles as that of pure compounds.

Glucose and nitrogen (as the ammonium ion) was monitored using a YSI MBS 7100 Analyzer (YSI Incorporated Life Sciences, Yellow Springs, Ohio).

The cell density of the cultures was determined by measuring the optical density at 600 nm (OD_{600}) of the culture against an LB or M9 blank on a Beckman DU640 spectrophotometer (Beckman Coulter, Brea CA). In cultures that had turned dark during growth, the OD was

calculated by measuring the OD_{600} of the culture and subtracting the OD_{600} of the media following centrifugation to pellet cells.

4.8 References Cited

1. Ragauskas, A. J. *et al.* Lignin Valorization: Improving Lignin Processing in the Biorefinery. *Science* **344,** 1246843 (2014).
2. Chundawat, S. P. S., Beckham, G. T., Himmel, M. E. & Dale, B. E. Deconstruction of Lignocellulosic Biomass to Fuels and Chemicals. *Annu. Rev. Chem. Biomol. Eng.* **2,** 121–145 (2011).
3. Zakzeski, J., Bruijnincx, P. C., Jongerius, A. L. & Weckhuysen, B. M. The catalytic valorization of lignin for the production of renewable chemicals. *Chem. Rev.* **110,** 3552–3599 (2010).
4. Himmel, M. E. *et al.* Biomass Recalcitrance: Engineering Plants and Enzymes for Biofuels Production. *Science* **315,** 804–807 (2007).
5. Davis, R. *et al.* Process design and economics for the conversion of lignocellulosic biomass to hydrocarbons: Dilute-acid and enzymatic deconstruction of biomass to sugars and biological conversion of sugars to hydrocarbons. *NREL Tech. Rep.* 88–101 (2013).
6. Martínez, Á. T. *et al.* Biodegradation of lignocellulosics: microbial, chemical, and enzymatic aspects of the fungal attack of lignin. *Int. Microbiol.* **8,** 195–204 (2010).
7. Fuchs, G., Boll, M. & Heider, J. Microbial degradation of aromatic compounds — from one strategy to four. *Nat. Rev. Microbiol.* **9,** 803–816 (2011).
8. Harwood, C. S. & Parales, R. E. The β-ketoadipate pathway and the biology of self-identity. *Annu. Rev. Microbiol.* **50,** 553–590 (1996).
9. Linger, J. G. *et al.* Lignin valorization through integrated biological funneling and chemical catalysis. *Proc. Natl. Acad. Sci.* **111,** 12013–12018 (2014).

10. Draths, K. M. & Frost, J. W. Environmentally compatible synthesis of adipic acid from D-glucose. *J. Am. Chem. Soc.* **116,** 399–400 (1994).
11. Niu, W., Draths, K. M. & Frost, J. W. Benzene-Free Synthesis of Adipic Acid. *Biotechnol. Prog.* **18,** 201–211 (2002).
12. Wu, C.-M. *et al.* Microbial synthesis of *cis,cis*-muconic acid from benzoate by *Sphingobacterium* sp. mutants. *Biochem. Eng. J.* **29,** 35–40 (2006).
13. Gomi, K. & Horiguchi, S. Purification and Characterization of Pyrocatechase from the Catechol-assimilating Yeast *Candida maltosa*. *Agric. Biol. Chem.* **52,** 585–587 (1988).
14. Wu, C.-M., Lee, T.-H., Lee, S.-N., Lee, Y.-A. & Wu, J.-Y. Microbial synthesis of cis,cis-muconic acid by *Sphingobacterium* sp. GCG generated from effluent of a styrene monomer (SM) production plant. *Enzyme Microb. Technol.* **35,** 598–604 (2004).
15. Vyver, S. V. de & Román-Leshkov, Y. Emerging catalytic processes for the production of adipic acid. *Catal. Sci. Technol.* **3,** 1465–1479 (2013).
16. Polen, T., Spelberg, M. & Bott, M. Toward biotechnological production of adipic acid and precursors from biorenewables. *J. Biotechnol.* (2012). doi:10.1016/j.jbiotec.2012.07.008
17. Musser, M. T. in *Ullmann's Encyclopedia of Industrial Chemistry* (Wiley-VCH Verlag GmbH & Co. KGaA, 2000). at <http://onlinelibrary.wiley.com/doi/10.1002/14356007.a01_269/abstract>
18. Bechthold, I., Bretz, K., Kabasci, S., Kopitzky, R. & Springer, A. Succinic Acid: A New Platform Chemical for Biobased Polymers from Renewable Resources. *Chem. Eng. Technol.* **31,** 647–654 (2008).

19. Jiménez, J. I., Miñambres, B., García, J. L. & Díaz, E. Genomic analysis of the aromatic catabolic pathways from *Pseudomonas putida* KT2440. *Environ. Microbiol.* **4,** 824–841 (2002).

20. Li, Q. *et al.* One step recovery of succinic acid from fermentation broths by crystallization. *Sep. Purif. Technol.* **72,** 294–300 (2010).

21. Yoshida, T., Inami, Y., Matsui, T. & Nagasawa, T. Regioselective carboxylation of catechol by 3,4-dihydroxybenzoate decarboxylase of Enterobacter cloacae P. *Biotechnol. Lett.* **32,** 701–705 (2010).

22. Marx, C. J. Development of a broad-host-range *sacB*-based vector for unmarked allelic exchange. *BMC Res. Notes* **1,** 1 (2008).

23. Schäfer, A. *et al.* Small mobilizable multi-purpose cloning vectors derived from the *Escherichia coli* plasmids pK18 and pK19: selection of defined deletions in the chromosome of Corynebacterium glutamicum. *Gene* **145,** 69–73 (1994).

24. Van Duuren, J. B. J. H. *et al.* Generation of a catR deficient mutant of *P. putida* KT2440 that produces *cis, cis*-muconate from benzoate at high rate and yield. *J. Biotechnol.* **156,** 163–172 (2011).

25. Boer, H. A. de, Comstock, L. J. & Vasser, M. The tac promoter: a functional hybrid derived from the trp and lac promoters. *Proc. Natl. Acad. Sci.* **80,** 21–25 (1983).

26. Nordlund, I., Powlowski, J. & Shingler, V. Complete nucleotide sequence and polypeptide analysis of multicomponent phenol hydroxylase from Pseudomonas sp. strain CF600. *J. Bacteriol.* **172,** 6826–6833 (1990).

27. Moreno, R., Martínez-Gomariz, M., Yuste, L., Gil, C. & Rojo, F. The *Pseudomonas putida* Crc global regulator controls the hierarchical assimilation of amino acids in a complete medium: Evidence from proteomic and genomic analyses. *Proteomics* **9,** 2910–2928 (2009).
28. Morales, G. *et al.* The *Pseudomonas putida* Crc Global Regulator Controls the Expression of Genes from Several Chromosomal Catabolic Pathways for Aromatic Compounds. *J. Bacteriol.* **186,** 1337–1344 (2004).
29. Hernández-Arranz, S., Moreno, R. & Rojo, F. The translational repressor Crc controls the Pseudomonas putida benzoate and alkane catabolic pathways using a multi-tier regulation strategy. *Environ. Microbiol.* **15,** 227–241 (2013).
30. Bang, S.-G. & Choi, C. Y. DO-stat fed-batch production of *cis, cis*-muconic acid from benzoic acid by *Pseudomonas putida* BM014. *J. Ferment. Bioeng.* **79,** 381–383 (1995).
31. Franz, M., Arafat, H. A. & Pinto, N. G. Effect of chemical surface heterogeneity on the adsorption mechanism of dissolved aromatics on activated carbon. *Carbon* **38,** 1807–1819 (2000).
32. Dąbrowski, A., Podkościelny, P., Hubicki, Z. & Barczak, M. Adsorption of phenolic compounds by activated carbon—a critical review. *Chemosphere* **58,** 1049–1070 (2005).
33. Luque, R. *et al.* Chemical transformations of succinic acid recovered from fermentation broths by a novel direct vacuum distillation-crystallisation method. *Green Chem.* **11,** 193–200 (2009).
34. Urbanus, J., Roelands, C. P. M., Verdoes, D. & ter Horst, J. H. Intensified crystallization in complex media: Heuristics for crystallization of platform chemicals. *Chem. Eng. Sci.* **77,** 18–25 (2012).

35. Madon, R. J. & Boudart, M. Experimental criterion for the absence of artifacts in the measurement of rates of heterogeneous catalytic reactions. *Ind. Eng. Chem. Fundam.* **21,** 438–447 (1982).
36. Fogler, H. S. *Elements of Chemical Reaction Engineering*. (Prentice Hall, 2005).
37. Besson, M. & Gallezot, P. Deactivation of metal catalysts in liquid phase organic reactions. *Catal. Today* **81,** 547–559 (2003).
38. Karp, E. M. *et al.* Alkaline Pretreatment of Corn Stover: Bench-Scale Fractionation and Stream Characterization. *ACS Sustain. Chem. Eng.* **2,** 1481–1491 (2014).
39. Sjöström, E. & Alen, R. *Analytical Methods in Wood Chemistry, Pulping, and Papermaking*. (Springer Science & Business Media, 1998).
40. Bonawitz, N. D. *et al.* Disruption of Mediator rescues the stunted growth of a lignin-deficient *Arabidopsis* mutant. *Nature* **509,** 376–380 (2014).
41. Chen, F. & Dixon, R. A. Lignin modification improves fermentable sugar yields for biofuel production. *Nat. Biotechnol.* **25,** 759–761 (2007).
42. Ciesielski, P. N. *et al.* Engineering plant cell walls: tuning lignin monomer composition for deconstructable biofuel feedstocks or resilient biomaterials. *Green Chem.* **16,** 2627–2635 (2014).
43. Simmons, B. A., Loqué, D. & Ralph, J. Advances in modifying lignin for enhanced biofuel production. *Curr. Opin. Plant Biol.* **13,** 312–319 (2010).
44. Bozell, J. J. *et al.* Solvent fractionation of renewable woody feedstocks: Organosolv generation of biorefinery process streams for the production of biobased chemicals. *Biomass Bioenergy* **35,** 4197–4208 (2011).

45. Fort, D. A. *et al.* Can ionic liquids dissolve wood? Processing and analysis of lignocellulosic materials with 1-n-butyl-3-methylimidazolium chloride. *Green Chem.* **9,** 63 (2007).

46. Parsell, T. H. *et al.* Cleavage and hydrodeoxygenation (HDO) of C–O bonds relevant to lignin conversion using Pd/Zn synergistic catalysis. *Chem. Sci.* **4,** 806–813 (2013).

47. Sturgeon, M. R. *et al.* A Mechanistic Investigation of Acid-Catalyzed Cleavage of Aryl-Ether Linkages: Implications for Lignin Depolymerization in Acidic Environments. *ACS Sustain. Chem. Eng.* **2,** 472–485 (2014).

48. Ramaswamy, S., Huang, H.-J. & Ramarao, B. *Separation and Purification Technologies in Biorefineries*. (John Wiley and Sons Ltd, 2012).

49. Mu, W., Ben, H., Ragauskas, A. & Deng, Y. Lignin Pyrolysis Components and Upgrading—Technology Review. *BioEnergy Res.* **6,** 1183–1204 (2013).

50. Ornston, L. N. & Parke, D. Properties of an inducible uptake system for beta-ketoadipate in *Pseudomonas putida*. *J. Bacteriol.* **125,** 475–488 (1976).

51. Chen, X. *et al.* The impacts of deacetylation prior to dilute acid pretreatment on the bioethanol process. *Biotechnol. Biofuels* **5,** 8 (2012).

52. Van Duuren, J. B. J. H. *et al.* pH-stat fed-batch process to enhance the production of *cis,cis*-muconate from benzoate by *Pseudomonas putida* KT2440-JD1. *Biotechnol. Prog.* **28,** 85–92 (2012).

53. Korhonen, J. T., Kettunen, M., Ras, R. H. A. & Ikkala, O. Hydrophobic Nanocellulose Aerogels as Floating, Sustainable, Reusable, and Recyclable Oil Absorbents. *ACS Appl. Mater. Interfaces* **3,** 1813–1816 (2011).

54. Dusselier, M., Mascal, M. & Sels, B. F. in 1–40 (Springer Berlin Heidelberg, 2014). at <http://link.springer.com/chapter/10.1007/128_2014_544>

55. Yu, W., Porosoff, M. D. & Chen, J. G. Review of Pt-Based Bimetallic Catalysis: From Model Surfaces to Supported Catalysts. *Chem. Rev.* **112,** 5780–5817 (2012).

56. Alonso, D. M., Wettstein, S. G. & Dumesic, J. A. Bimetallic catalysts for upgrading of biomass to fuels and chemicals. *Chem. Soc. Rev.* **41,** 8075–8098 (2012).

57. Ji, N. *et al.* Direct Catalytic Conversion of Cellulose into Ethylene Glycol Using Nickel-Promoted Tungsten Carbide Catalysts. *Angew. Chem.* **120,** 8638–8641 (2008).

58. Prasomsri, T., Nimmanwudipong, T. & Román-Leshkov, Y. Effective hydrodeoxygenation of biomass-derived oxygenates into unsaturated hydrocarbons by MoO3 using low H2 pressures. *Energy Environ. Sci.* **6,** 1732–1738 (2013).

59. Somorjai, G. A., Frei, H. & Park, J. Y. Advancing the Frontiers in Nanocatalysis, Biointerfaces, and Renewable Energy Conversion by Innovations of Surface Techniques. *J. Am. Chem. Soc.* **131,** 16589–16605 (2009).

60. Galvis, H. M. T. *et al.* Supported Iron Nanoparticles as Catalysts for Sustainable Production of Lower Olefins. *Science* **335,** 835–838 (2012).

61. Vardon, D. R. *et al.* Hydrothermal catalytic processing of saturated and unsaturated fatty acids to hydrocarbons with glycerol for in situ hydrogen production. *Green Chem.* 1507–1520 (2014).

62. Gurrath, M. *et al.* Palladium catalysts on activated carbon supports: Influence of reduction temperature, origin of the support and pretreatments of the carbon surface. *Carbon* **38,** 1241–1255 (2000).

63. Alén, R., Niemelä, K. & Sjöström, E. Gas-liquid chromatographic separation of hydroxy monocarboxylic acids and dicarboxylic acids on a fused-silica capillary column. *J. Chromatogr. A* **301,** 273–276 (1984).

64. Salis, H. M., Mirsky, E. A. & Voigt, C. A. Automated design of synthetic ribosome binding sites to control protein expression. *Nat. Biotechnol.* **27,** 946–950 (2009).

4.9 Figures and Tables

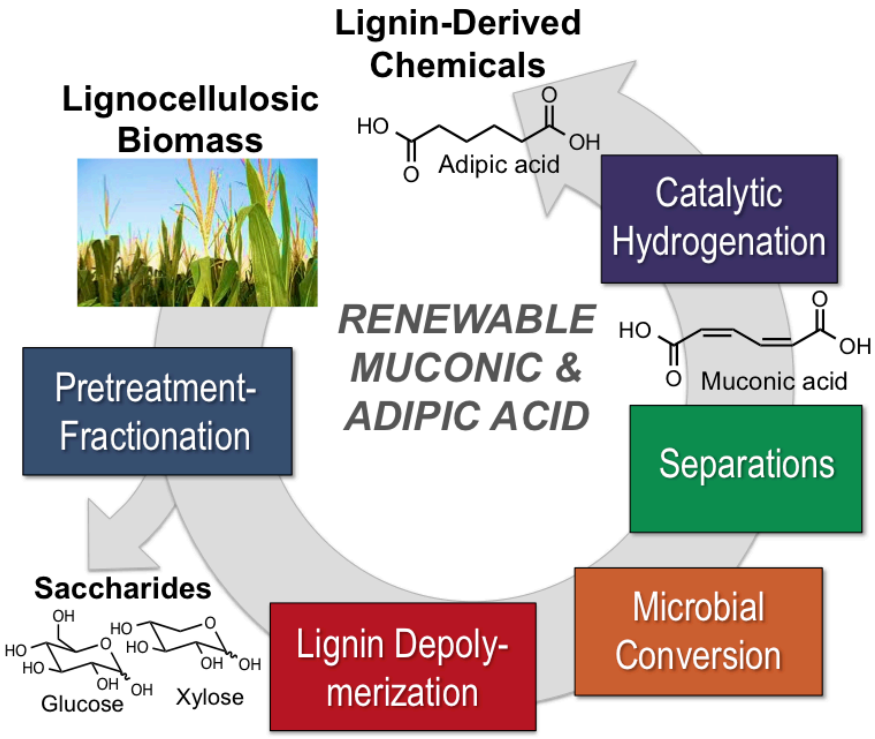

Figure 4.1. Integrated biorefinery process scheme to produce muconic and adipic acid from lignin. Alkaline pretreatment fractionates biomass and depolymerizes lignin to produce an aromatic-rich aqueous stream. Engineered *P. putida* then biologically funnels lignin-derived aromatics to muconate, which is purified and separated. Lastly, catalytic hydrogenation converts muconic acid to adipic acid, demonstrating a new class of lignin-derived commodity chemicals.

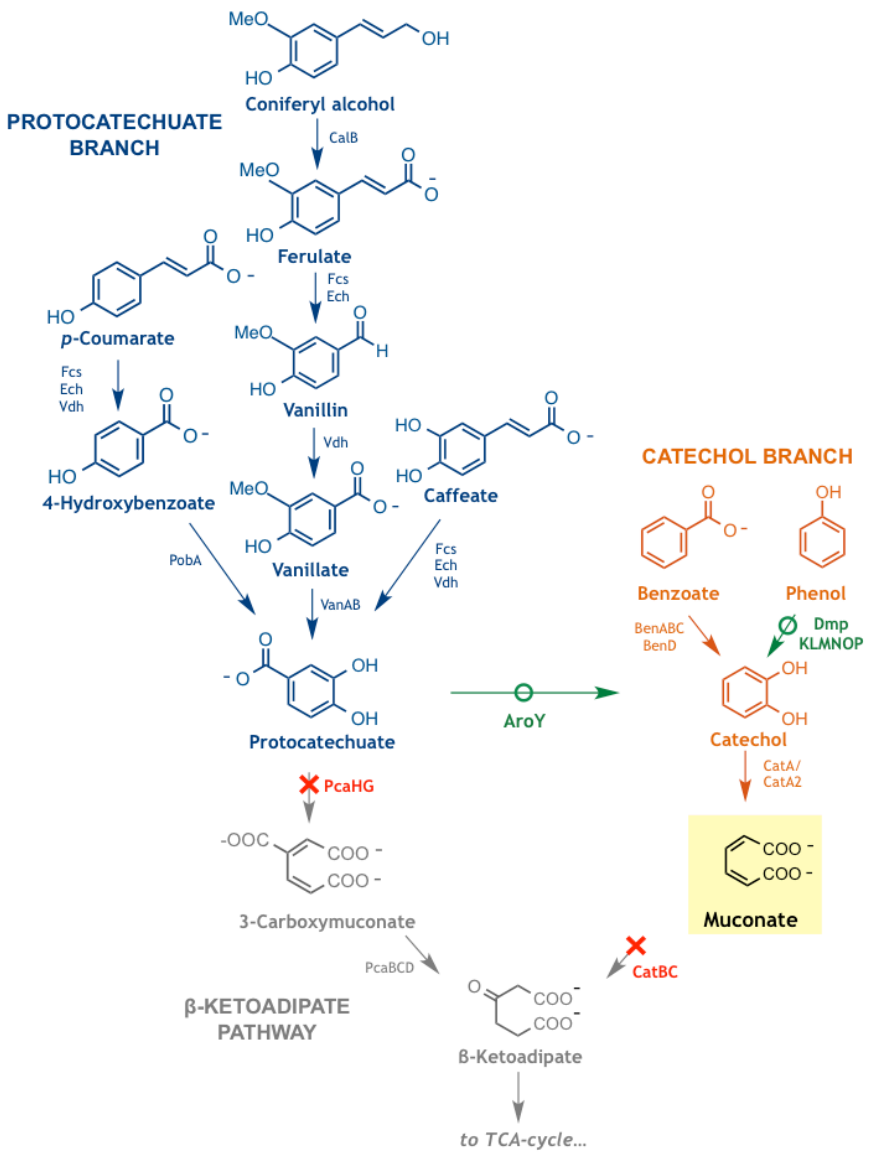

Figure 4.2. Biological funneling of lignin aromatics to muconate. *P. putida* KT2440 was engineered to delete genes encoding PcaHG and CatBC (red crossed arrow) and insert genes encoding AroY and DmpKLMNOP (green circled arrow), enabling biological funneling of diverse lignin-derived monomers to muconate.

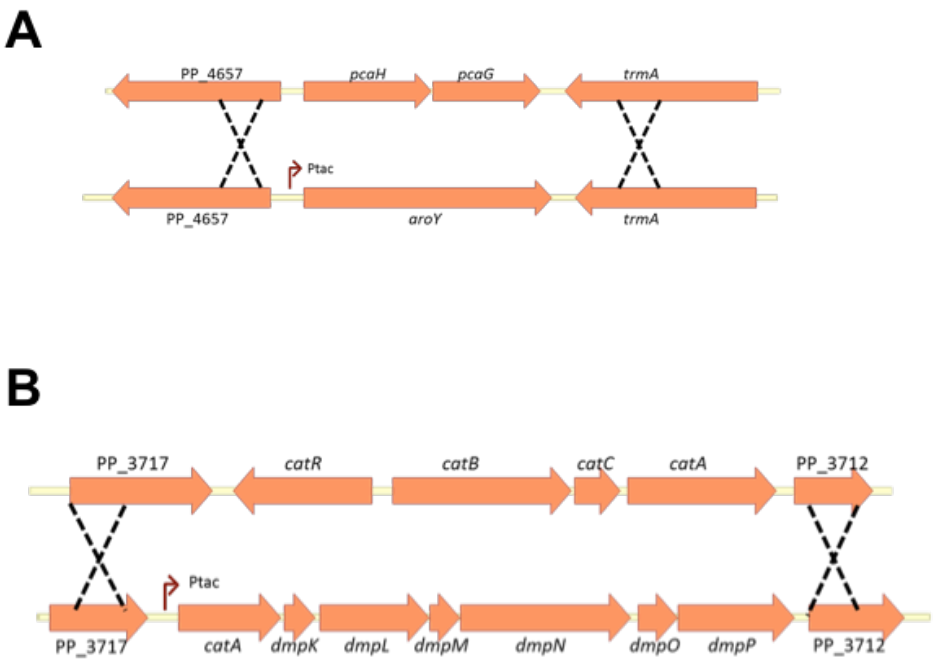

Figure 4.3. Gene replacement of 3,4 protocatechuate decarboxylase genes (*pcaHG*) with *aroY* from *Enterobacter cloacae* (A) and substitution of *catR* and *catBCA* with *catA* and *dmpKLMNOP* on one operon (B).

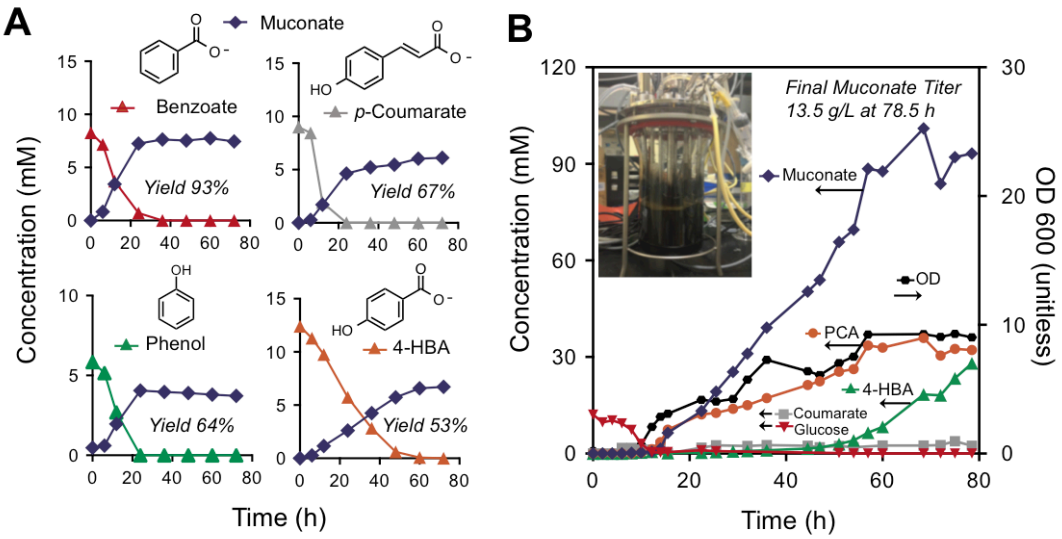

Figure 4.4. Biological conversion of lignin-derived aromatics to muconate. (A) Shake flask experiments using *P. putida* KT2440-CJ103 to convert benzoate, *p*-coumarate, phenol, and 4-hydroxybenzoate (4-HBA) to muconate. (B) DO-stat fed-batch cultivation of *P. putida* KT2440-CJ103 using glucose as a carbon source to convert *p*-coumarate to muconate. Horizontal arrows indicate corresponding axis for tracked compounds and optical density at 600 nm (OD 600).

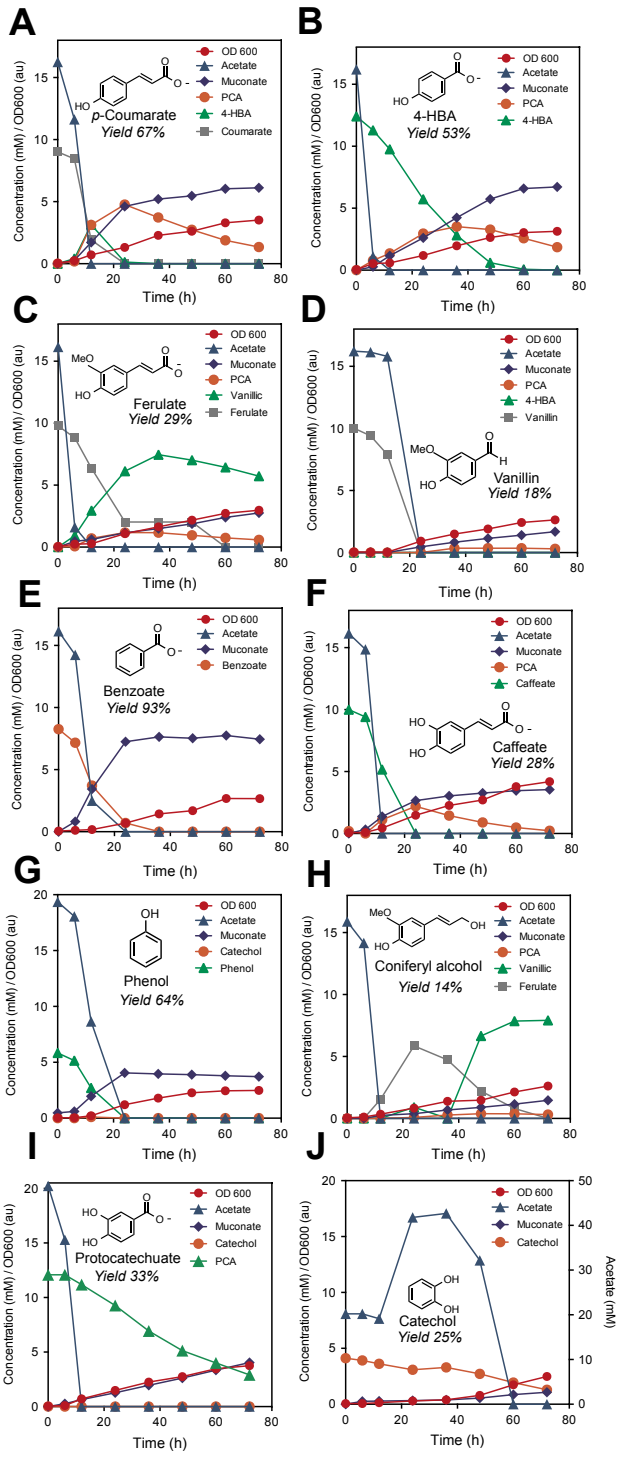

Figure 4.5. Shake flask experiments with *P. putida* KT2440-CJ103 with model lignin monomers. Experiments were conducted in 125-mL baffled flasks containing 25 mL of M9 media supplemented with 20 mM sodium acetate and 10 mM substrate, with the exception of

phenol and catechol, which were added at 5 mM due to growth inhibition at higher concentrations. Additional sodium acetate (20 mM) was added after 12 hours of growth and every 12 hours thereafter. Representative examples of duplicate experiments are shown. Note: Coniferyl alcohol was not monitored by HPLC (panel H).

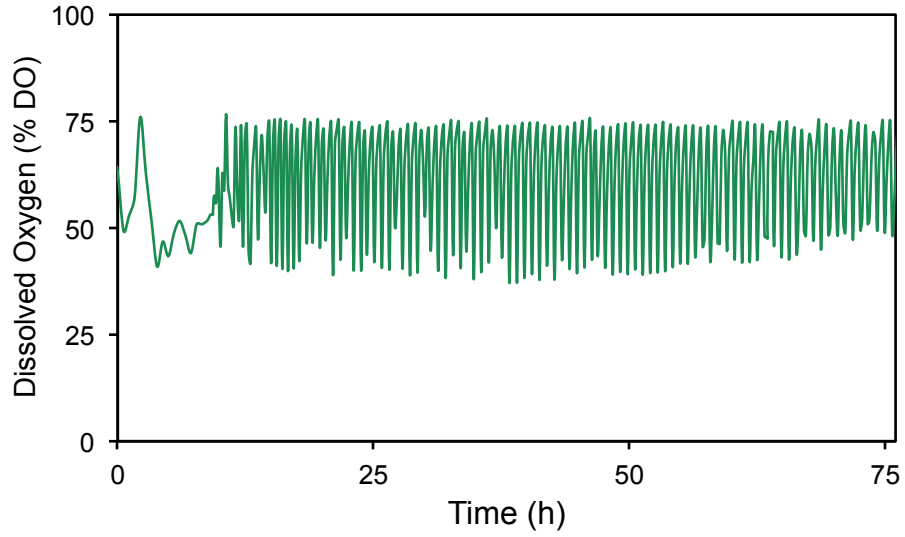

Figure 4.6. Dissolved oxygen (DO) during course of DO-stat fed-batch cultivation of P. putida KT2440-CJ103. DO oscillation occurred simultaneously with the addition of the glucose:*p*-coumarate:ammonium sulfate feed until process was terminated at 75.5 h and the bioreactor was shut down at 78.5 h.

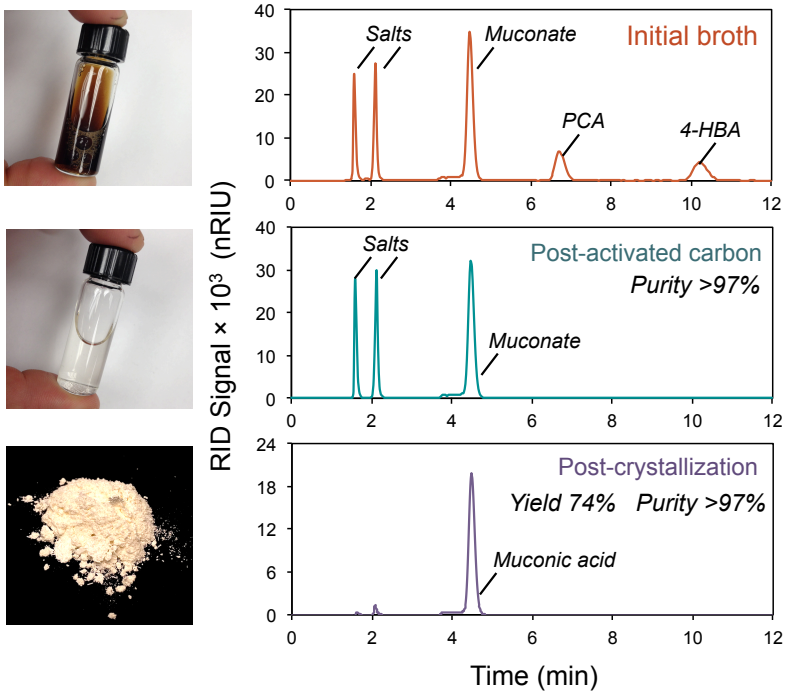

Figure 4.7. Separation of muconic acid following fed-batch biological conversion of *p*-coumarate. Fed-batch culture broth containing muconate derived from *p*-coumarate was purified using activated carbon to remove aromatic metabolic intermediates, which consisted primarily of protocatechuate (PCA) and 4-hydroxybenzoate (4-HBA). Following purification, muconic acid was recovered in high yield (74%) and purity (97%) by crystallization at reduced pH and temperature (pH 2, 5°C).

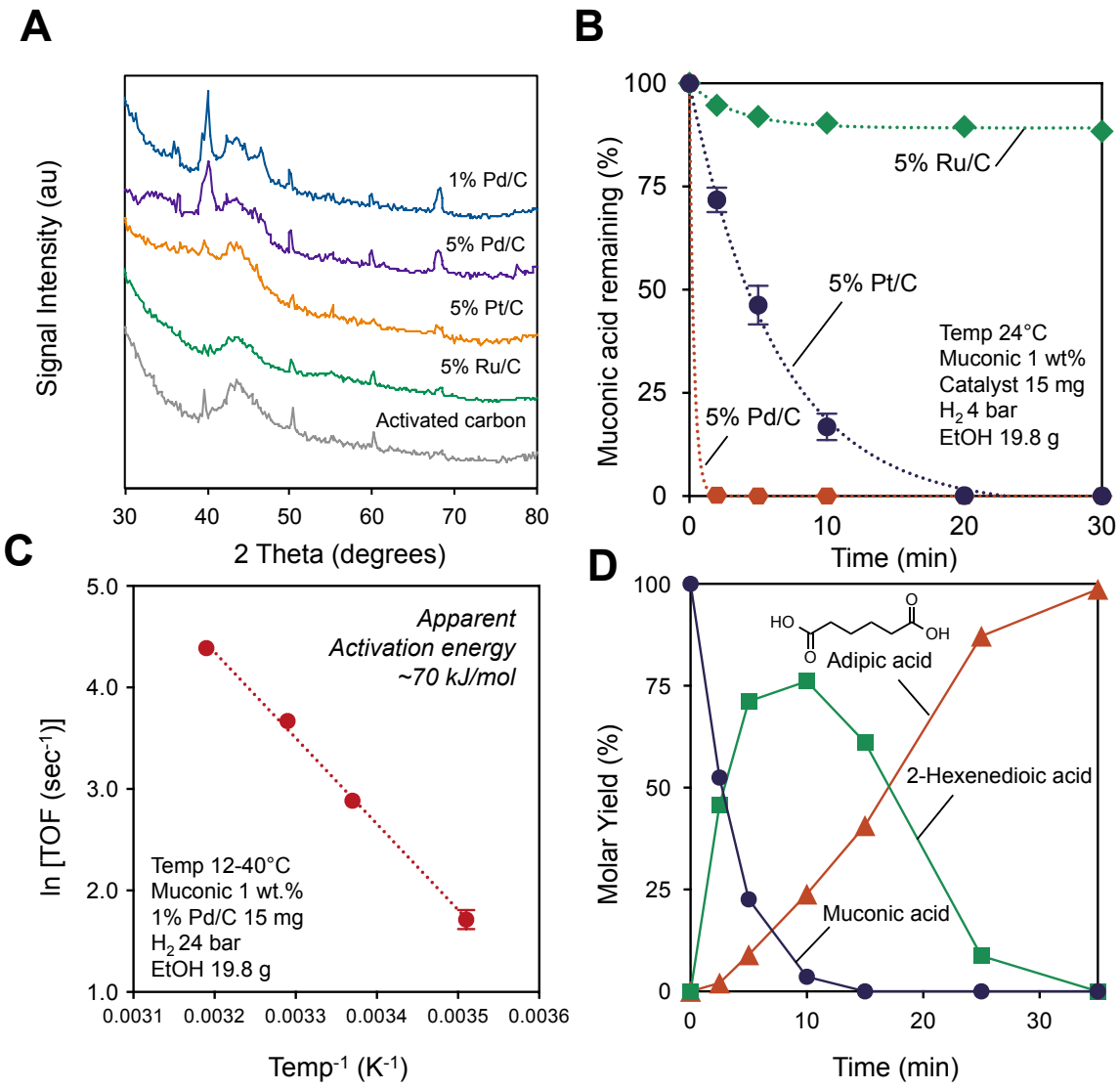

Figure 4.8. Catalytic hydrogenation of muconic acid to adipic acid. (A) X-ray diffraction analysis of commercial catalysts confirmed metals were highly dispersed as small crystallites, with additional material properties described in the ***Supplemental Information***. Variations in XRD spectra with the carbon support were attributed to materials obtained from differing vendors. (B) Noble metal catalysts were first screened with purified muconic acid obtained commercially for hydrogenation to adipic acid under mild conditions, with pseudo-first order kinetic parameter fits indicated by dashed lines. Reactions were performed in triplicate, with

error bars indicating the conversion standard deviation. (C) The activity of commercial 1% Pd/C was evaluated under surface reaction controlling conditions to estimate the apparent activation energy for muconic acid hydrogenation in ethanol (EtOH) using the Arrhenius equation. (D) Catalytic conversion of muconic acid derived from fed-batch biological conversion of *p*-coumaric acid following activated carbon purification and crystallization. Reaction conditions were as follows: temperature 24°C, muconic acid 200 mg, commercial 1% Pd/C 15 mg, H_2 pressure 24 bar, EtOH solvent 19.8 g. Typical mass closure was >97%, with species concentrations shown in **Table 4.3**.

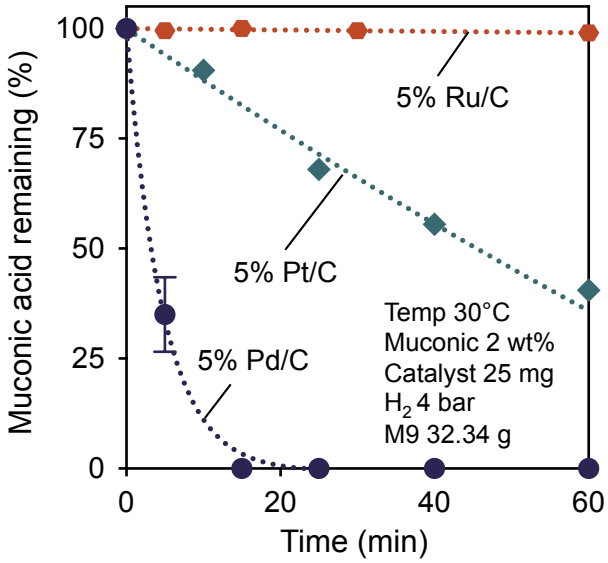

Figure 4.9. Catalytic screening of muconic acid hydrogenation with noble metal catalysts in M9 media. Hydrogenation reactions were performed using commercial Pd, Pt, and Ru on carbon catalysts (5 wt% metal loading) using in M9 media at 30°C. Reaction conditions were as follows: muconic acid 0.66 g, solvent 32.34 g, H_2 pressure 4 bar, catalyst loading 25 mg, stirring 1600 rpm. Reactions were performed in duplicate with error bars indicating conversion standard deviation. Dashed lines indicate pseudo-first order kinetic parameter fits.

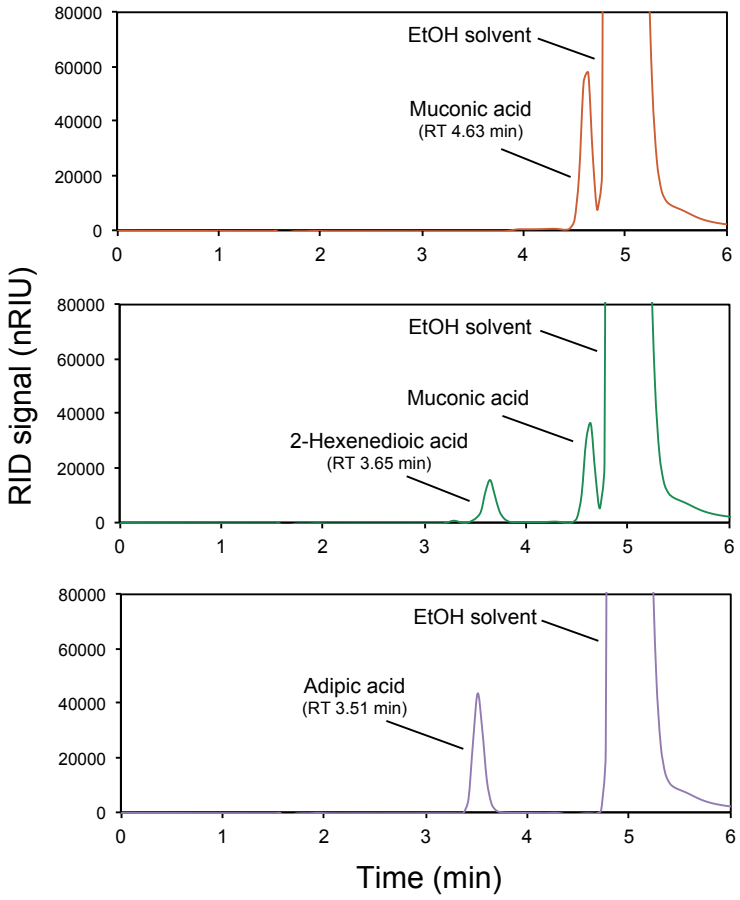

Figure 4.10. Catalytic conversion of muconic acid to adipic acid, with 2-hexenedioic acid as the primary intermediate. Reaction conditions were as follows: muconic acid 200 mg, ethanol (EtOH) solvent 19.8 g, H_2 pressure 24 bar, catalyst loading 15 mg, stirring 1600 rpm. Product identities were confirmed by GCxGC-TOFMS.

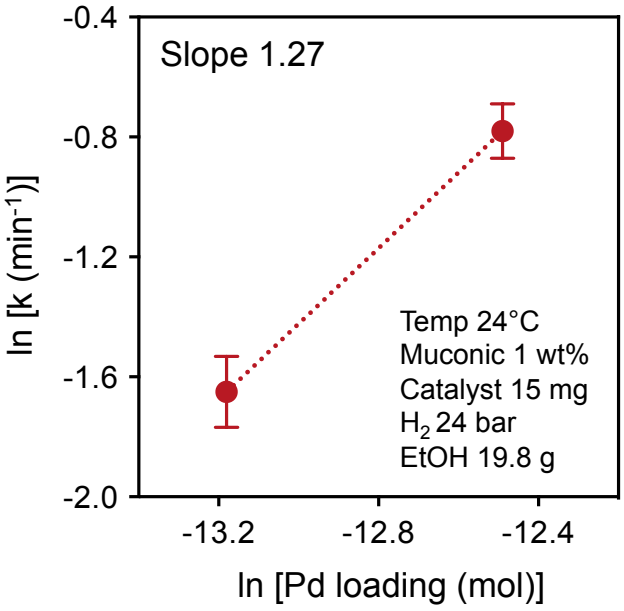

Figure 4.11. Koros-Nowak criterion to evaluate the influence of mass transfer on muconic acid hydrogenation with Pd/C.[35] A slope of unity supports surface reaction-controlling conditions. Reductions were performed using 1 wt% and 2 wt% Pd/C catalyst synthesized in house. Reaction conditions were as follows: muconic acid 200 mg, ethanol (EtOH) solvent 19.8 g, H_2 pressure 24 bar, catalyst loading 15 mg, stirring 1600 rpm. Rates constants were estimated using pseudo-first order kinetic parameters. Reactions were performed in triplicate, with error bars representing the 95% confidence intervals for the estimated rate constant.

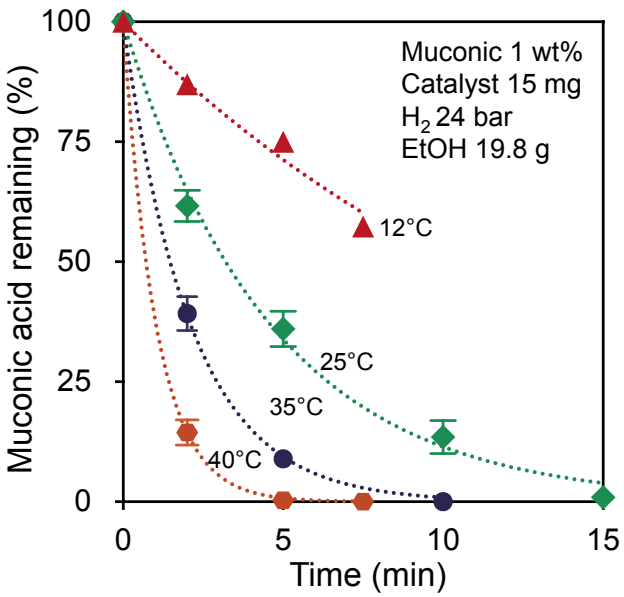

Figure 4.12. Influence of temperature on the activity of muconic acid hydrogenation with Pd/C. Reductions were performed using a commercial 1 wt% Pd/C catalyst from Alfa Aesar. Reaction conditions were as follows: muconic acid 200 mg, ethanol (EtOH) solvent 19.8 g, H_2 pressure 24 bar, catalyst loading 15 mg, stirring 1600 rpm. Reactions were performed in triplicate with error bars representing conversion standard deviations. Rates constants were estimated using pseudo-first order kinetic parameters, with dashed lines indicating parameter fits.

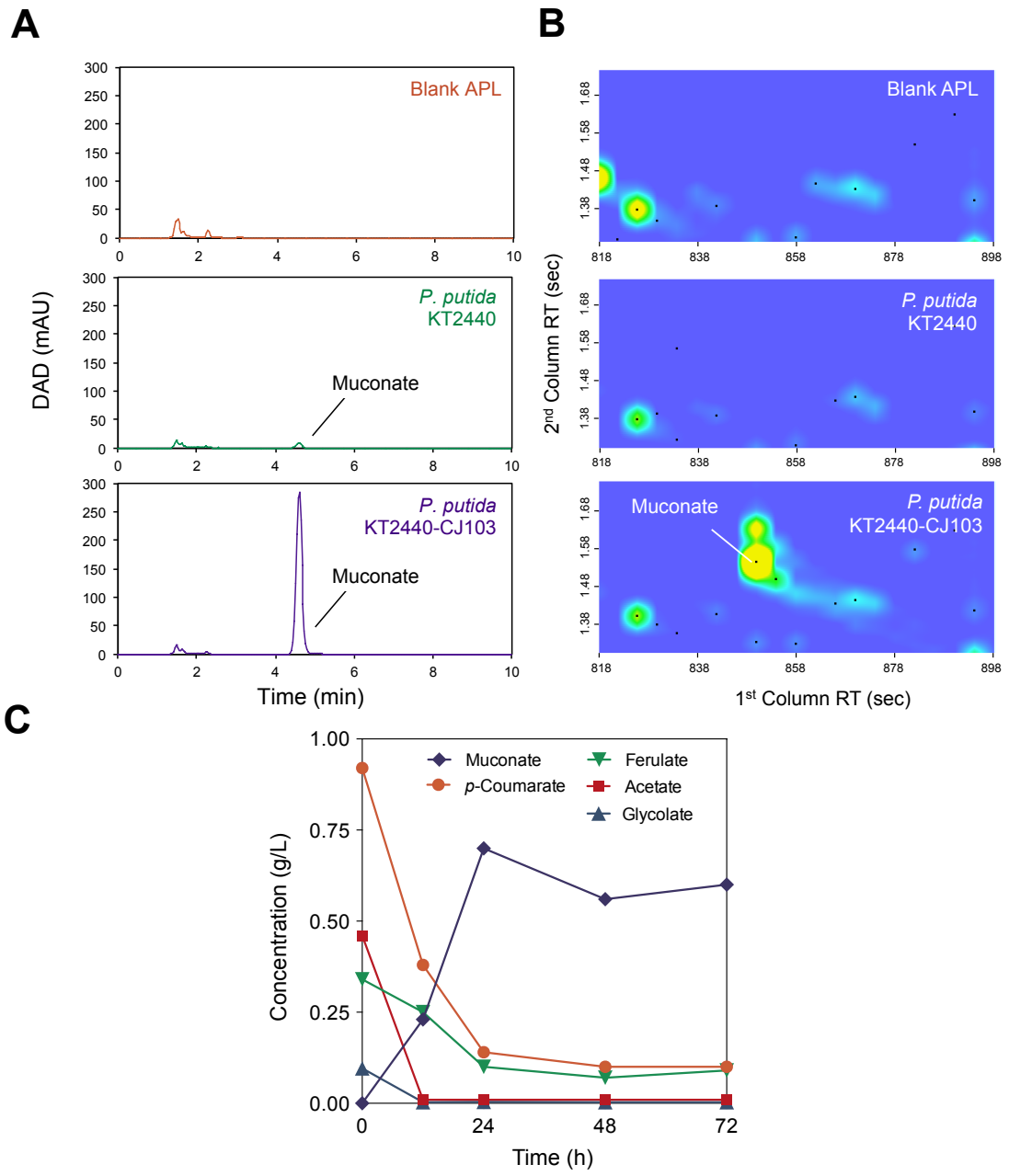

Figure 4.13. Biological production of muconate from a depolymerized lignin stream. (A) HPLC analysis of culture media purified by activated carbon confirmed that alkaline pretreated liquor (APL) was converted to muconic acid after 72 h by the engineered strain *P. putida* KT2440-CJ103, while no significant quantities were detected using the native organism *P. putida* KT2440

or in blank APL. (B) GCxGC-TOF-MS analysis of derivatized acids in the unpurified culture samples confirmed the identity of muconic acid, with comparable trends in concentration. (C) Shake flask cultivation with *P. putida* KT2440-CJ103 in APL demonstrated that major aromatic acids and short chain acids were metabolized, producing a maximum muconate concentration of 0.70 g/L after 24 h.

Table 4.1. Shake flask experiments with *P. putida* KT2440-CJ103 using model lignin monomers and supplemental glucose or acetate. Experiments were conducted in 125-mL baffled flasks containing 25 mL of M9 media supplemented with 20 mM sodium acetate or 10 mM of glucose and 10 mM substrate. Muconate yields reported at 72 h.

Substrate	Muconate Molar Yield w/ Glucose (%)	Muconate Molar Yield w/ Acetate (%)
Benzoate	93.4	88.8
Coumarate	90.2	69.2
Ferulate	39.1	29.9

Table 4.2. Physisorption and chemisorption properties of catalysts evaluated for muconic acid hydrogenation.

Catalyst	Vendor	S_{BET} (m^2/g)	Pore Volume (cc/g)	Dispersion (%)
5% Pt	Sigma	1075	0.71	51
5% Pd	Sigma	750	0.51	22
5% Ru	Sigma	705	0.66	38
1% Pd	Alfa Aesar	825	0.66	19
1% Pd	In-house	781	0.33	13
2% Pd	In-house	760	0.33	12

Table 4.3 Individual compound molar concentrations and molar closure during catalytic hydrogenation of muconic acid derived from the fed-batch biological conversion.

Time (min)	Muconic (mmol)	2-HDA (mmol)	Adipic (mmol)	Molar Closure (%)
0	57.6	0.0	0.0	100.0
2.5	30.2	45.8	1.2	100.4
5.0	13.0	71.2	5.2	102.8
10.0	2.1	76.1	13.8	103.5
15.0	0.0	61.1	23.5	101.8
25.0	0.0	8.7	50.2	95.8
35.0	0.0	0.0	56.8	98.7

Reaction conditions were as follows: temperature 24°C, muconic acid 200 mg, commercial 1% Pd/C 15 mg, H_2 pressure 24 bar, EtOH solvent 19.8 g. Typical mass closure was >97%.

Table 4.4. Primers used in construction of gene replacement plasmids

Primer	Sequence (5'-3')
LP29	GCGACACGAAGCTGTATAGCCCTGCCCTATTG
LP30	GCTATACAGCTTCGTGTCGCTCAAGGCG
LP31	ACCTCGTATTGTGTGAAATTGTTATCCGCTCAC
LP32	AATTTCACACAATACGAGGTAAGCACGATG
LP33	CCGCGGCCGCCATCATTGAGACCGCGCG
LP34	CCGCGGCCGCGTGACATAACCTCGAACTCAG
LP48	CAGGACATCATCAGCCCTCCTGCAACGC
LP49	GGAGGGCTGATGATGTCCTGCGCAAGCC
LP50	AACCTCGAACTCAGATGCGCTTGAACAGG
LP51	GCGCATCTGAGTTCGAGGTTATGTCACTGTGATTTTG
LP53	ATCCCCGGGTACCGAGCTCGAATTCATGACCGTGAAAATTTCCCACACTG
LP54	CAGCTATGACCATGATTACGAATTCTTGAATGCCGGCAACCCG
oCJ100	CCGAAAAGTGCCACCTGACGTCGGCCTTGCTGCTGCAG
oCJ101	GCCGCAGCTCGAGATCTGGAATTGTGAGAACGCCTGG
oCJ102	AGATCTCGAGCTGCGGCCGCGGTGAAGCTTGGGGCC
oCJ103	GCTGGATCCTCTAGTGAGCTCACGATTTCCCCATTGCCAG
oCJ165	CCAGGCGTTCTCACAATTCCAGATCTG
oCJ166	GAGCGGCCCCAAGCTTCACCGCGGCCGCTCACTTCTTGTCGCTGAACAGCTCTGG

Table 4.5. Sequence of synthetic DNA fragments containing the tac promoter and the *E. cloacae aroY* gene optimized for expression in *P. putida* K2440. The start and stop codons of *aroY* are indicated by bold text.

Fragment 1:

CCAGGCGTTCTCACAATTCCAGATCTGAGCTGTTGACAATTAATCATCGGCTCGTAT
AATGTGTGGAATTGTGAGCGGATAACAATTTCACACAGAGGAGGGAGA**ATG**CAGAACCCGA
TCAACGACCTGCGCTCCGCGATCGCGCTGCTGCAACGCCATCCGGGTCACTACATCGAAACC
GACCACCCGGTCGACCCGAACGCCGAACTGGCCGGTGTGTACCGCCACATCGGTGCGGGTG
GCACCGTGAAACGTCCGACCCGCACCGGTCCAGCCATGATGTTCAACAGCGTGAAGGGCTAC
CCAGGCAGCCGCATCCTGGTGGGCATGCACGCCAGCCGTGAACGTGCCGCCCTGCTGCTGGG
CTGCGTGCCAAGCAAACTGGCGCAGCACGTGGGCCAGGCCGTGAAGAACCCGGTGGCCCCA
GTGGTGGTGCCAGCCAGCCAAGCCCCATGCCAAGAACAGGTGTTCTACGCCGACGACCCGG
ACTTCGACCTGCGCAAGCTGCTGCCAGCCCCAACCAACACCCCGATCGATGCCGGTCCGTTC
TTCTGCCTGGGCCTGGTGCTGGCGAGCGACCCGGAAGATACCAGCCTGACCGACGTGACCAT
CCACCGCCTGTGCGTGCAAGAGCGCGACGAGCTGAGCATGTTCCTGGCCGCCGGTCGCCACA
TCGAGGTGTTCCGCAAGAAGGCCGAAGCCGCCGGTAAGCCGCTGCCGGTGACCATCAACAT
GGGCCTGGACCCAGCCATCTACATCGGTGCCTGCTTCGAAGCGCCAACCACCCCGTTCGGCT
ACAACGAGCTGGGTGTGGCC

Fragment 2:

ACAACGAGCTGGGTGTGGCCGGTGCCCTGCGTCAGCAACCGGTGGAACTGGTGCAG
GGCGTGGCCGTGAAAGAGAAGGCGATCGCGCGTGCCGAGATCATCATCGAGGGCGAACTGC
TGCCAGGCGTGCGCGTGCGCGAAGATCAGCACACCAACACCGGTCACGCCATGCCGGAATT
CCCAGGCTACTGCGGTGAGGCCAACCCGAGCCTGCCGGTGATCAAGGTGAAGGCCGTGACC
ATGCGCAACCACGCCATCCTGCAGACCCTGGTGGGTCCGGGTGAGGAACACACCACCCTGGC
GGGTCTGCCGACCGAAGCCAGCATCCGCAACGCCGTGGAAGAGGCGATCCCAGGCTTCCTG
CAGAACGTGTACGCCCACACCGCCGGTGGCGGTAAGTTCCTGGGCATCCTGCAGGTCAAGAA
GCGCCAGCCGAGCGACGAAGGCCGTCAGGGCCAAGCCGCCCTGATCGCCCTGGCCACCTAC
AGCGAGCTGAAGAACATCATCCTGGTGGACGAGGACGTGGACATCTTCGACAGCGACGACA
TCCTGTGGGCCATGACCACCCGCATGCAGGGCGACGTGAGCATCACCACCCTGCCAGGCATC
CGTGGCCATCAGCTGGACCCGAGCCAGAGCCCAGACTACAGCACCAGCATCCGTGGCAACG
GCATCAGCTGCAAGACCATCTTCGACTGCACCGTGCCGTGGGCCCTGAAAGCCCGTTTCGAG
CGTGCCCCATTCATGGAAGTGGACCCGACCCCGTGGGCCCCAGAGCTGTTCAGCGACAAGAA
GTGAGCGGCCGCGGTGAAGCTTGGGGCCGCTC

CHAPTER 5

CIS,CIS-MUCONIC ACID: DOWNSTREAM SEPARATION AND CATALYSIS TO BIO-ADIPIC ACID FOR NYLON-6,6 POLYMERIZATION

5.1 Abstract

cis,cis-Muconic acid is a polyunsaturated dicarboxylic acid that can be produced renewably via the biological conversion of sugars and lignin-derived aromatic compounds. Subsequently, muconic acid can be catalytically converted to adipic acid – the most commercially abundant dicarboxylic acid manufactured from petroleum. Nylon-6,6 is the major industrial application for adipic acid, consuming 85% of market demand; however, high purity adipic acid (99.8%) is required for polymer synthesis. As such, process technologies are needed to effectively separate and catalytically transform biologically derived muconic acid to adipic acid in high purity over stable catalytic materials. To that end, this study (1) examines the staged recovery of muconic acid from culture media, (2) screens platinum group metals (e.g., Pd, Pt, Rh, Ru) for activity and stability against leaching on activated carbon (AC) and silica supports, (3) evaluates the time-on-stream stability of Rh/AC during the continuous hydrogenation of bio-muconic acid, and (4) demonstrates the polymerization of bio-adipic acid to nylon-6,6. Separation experiments confirmed AC effectively removed undesired organics and color compounds, but subsequent pH/temperature shift crystallization resulted in significant levels of Na, P, K, S and N. Ethanol dissolution of muconic acid precipitated bulk salts, achieving a purity of 99.8%. Batch catalysis screening reactions determined that Rh and Pd were both highly active compared to Pt and Ru, but Pd leached significantly (1-9%) on both supports.

Testing of Rh/C in a continuous trickle-bed reactor confirmed stable catalyst conversion for 100 h time-on-stream (<5% change from initial 48 h average). Lastly, polymerization of bio-adipic acid produced nylon-6,6 with comparable properties to its petrochemical counterpart, demonstrating a path towards bio-based nylon production via muconic acid.

5.2 Introduction

Lignocellulosic biomass offers significant potential for producing both fuels and chemicals from a renewable resource, towards the aim of displacing a fraction of global petroleum consumption.[1–5] Similar to a petroleum refinery, production of renewable fuels from biomass can provide economies of scale to meet critical energy needs in the transportation sector, while generating myriad value-added chemicals to improve net profitability. Lignocellulosic biomass can be deconstructed into carbohydrate and lignin fractions to support valorization to fuel, chemical, and material building block substitutes,[6–9] allowing for tailored upgrading processes that incorporate biological and chemo-catalytic technologies.[10–12] The high oxygen content of biomass (~35-45%) also makes it ideal for targeting oxygen-rich platform molecules with high atom efficiency, relative to petroleum where oxygen must be added to the feedstock.[13]

Muconic acid is one such promising oxygen-rich platform molecule that can be produced from both the carbohydrate[14,15] and lignin fraction[16] of lignocellulosic biomass. From sugars, muconic acid can be produced by rerouting aromatic amino acid synthesis pathways to produce catechol, which is then oxidatively ring opened to produce muconic acid as the terminal metabolite.[17–20] Alternatively, lignin-derived aromatic compounds can be catabolized in certain microorganisms that utilize native “upper pathways” to funnel aromatic compounds into central

intermediates such as catechol,[21] which is the direct intermediate prior to oxidative ring opening for muconic acid. Valorization of lignin to fuels and chemicals has significant economic and environmental potential, due to its unique aromatic polymer structure, relative abundance in biomass, and underutilization within the context of modern biorefineries. Following biological production from both sugar or lignin derived monomers, muconic acid can then be readily converted by chemo-catalysis to myriad high-value petrochemical substitutes, including adipic acid.[14–16]

Adipic acid is the most prevalent dicarboxylic acid produced from petroleum,[22,23] with a global market estimated at greater than 2.7 million tonnes per year and market price over $1700 per ton.[24] Adipic acid has multiple product applications, including use in the manufacture of plastics, textiles, lubricants, and additive in the food and cosmetic industry. Its largest application is as a monomer building block for nylon-6,6 production, which consumes ~85% of adipic acid market demand.[23] Due to the negative environmental impacts associated with conventional adipic acid production, significant research efforts are underway to identify alternative "green" production processes.[22,23,25,26] However, development of integrated biological and catalytic process configurations that produce adipic acid in high yield, *as well as purity*, will be a key consideration due to the stringent purity requirements for polymer precursors, as shown in **Table 5.1**.[27] Specifically, the impact of residual broth constituents on downstream unit operations must be addressed,[28] in addition to developing highly active, selective, and stable catalysts for bio-product upgrading.[29]

A wide variety of impurities can be introduced during the biological production of muconic acid, similar to the challenges faced with other target bio-derived molecules (e.g., ethanol, succinic acid, lactic acid). These impurities can include fermentation salts, nutrients and

media to support growth, unconverted substrate, extracellular proteins and lysed cell contents, as well as the buildup of non-target metabolites.[30–32] Accumulation of these constituents in culture broth can vary greatly depending on the microorganism, substrate used for conversion, biological growth conditions and bioreactor design, and broth pretreatment.[33–36] Likewise, utilization of monomers streams derived from complex lignocellulosic biomass can vary greatly depending on the biomass fraction of interest (e.g., cellulose, hemicellulose, lignin), choice of feedstock (e.g., herbaceous, hardwoods, softwoods), and depolymerization technology. Understanding the impact of biological broth impurities on subsequent separation and catalytic unit operations will be key for meeting the compositional and purity requirements for renewable chemical and polymer applications. [30–32,37]

As such, this manuscript examines the downstream separation and catalytic upgrading of biologically derived *cis,cis*-muconic acid to produce adipic acid for nylon-6,6 polymerization. Muconic acid was produced using an engineered strain of *Pseudomonas putida* KT2440 via fed-batch conversion of benzoate, a model oxygenated aromatic compound that is commonly used in the study of aromatic catabolism. Staged separation and purification of biological culture media was then performed to monitor the level of inorganic and organic impurities in recovered muconic acid with each treatment step. Batch reactor catalytic screening reactions assessed muconic acid hydrogenation activity and resistance against leaching for platinum group metals on both activated carbon and silica supports, while continuous time-on-stream testing was performed for 100 h in a trickle-bed reactor to evaluate changes in down-selected catalyst activity and stability. Lastly, nylon-6,6 was synthesized from biologically derived adipic acid to compare its polymer properties against nylon-6,6 produced from petroleum derived adipic acid.

5.3 Results

5.3.1 Biological production of muconic acid

To generate muconic acid for downstream processing, fed-batch biological conversion of benzoate was conducted with the engineered strain *Pseudomonas putida* KT2440-CJ103, described in previous work by our group.[16] The results of the fermentation are shown in **Figure 5.1**. For aromatics such as benzoate, muconic acid is produced by oxidative ring opening from catechol.[38] In this work, glucose was used as a carbon source to support biological growth and functioning, although other low-cost alternatives, such as acetic acid, can be used to support growth as well.[16] Benzoate feeding was based on DO stat control,[39] while pH was controlled with NaOH, resulting in sodium muconate as the predominant species at pH 7. Muconate was produced at a titer of 7.97 g/L after 32 h, while residual benzoic acid was present at 0.94 g/L. Historically, muconate titer from benzoate have been reported as high as 44.1 g/L;[40] however, optimization of biological productivity was beyond the scope of this study. After terminating the fed-batch run, cells were removed by centrifugation and filtration for subsequent broth processing.

5.3.2 Separation and purification of muconic acid

Muconic acid was then purified and recovered from cell-free culture media, with the purity of muconic acid monitored at each step, as shown in **Table 5.2**. The separation process initially consisted of activated carbon purification to remove soluble organic broth impurities and pH/temperature shift crystallization to precipitate muconic acid from purified broth solution and recover solid crystals for drying, as demonstrated in previous work.[16] As an additional step, ethanol dissolution and microfiltration was examined to remove bulk inorganic salts prior to

catalytic hydrogenation and polymerization, and generate a liquid phase for trickle bed catalytic processing.

Initially, the broth was treated with activated carbon due to its relatively low cost, origin from renewable resources, and effectiveness for removing impurities from aqueous media.[16,41–44] An activated of activated carbon loading of 2 wt/vol% was needed to remove residual benzoate from the culture broth to below detectable limits by high performance liquid chromatography diode array detection (HPLC-DAD). Color compounds in the broth were also removed to a significant extent, turning the broth from a coffee-colored appearance to semi-clear (see **Figure 5.2**); however, non-selective adsorption of resulted in a 16% reduction in muconate broth concentration (6.86 g/L).

Following activated carbon treatment, muconic acid was precipitated from the broth by the pH/temperature shift crystallization.[16] By adjusting the broth pH to 2 with sulfuric acid and reducing the temperature to 5°C, muconic acid readily crashed from solution. Precipitated muconic acid crystals were then vacuum filtered (0.2-μm PES) and dried in a vacuum oven for 48 h. Purity analysis by differential scanning calorimetry (DSC) melting point analysis[45] determined the muconic acid crystals were only 97.83 ± 0.05% pure at this stage (see **Figure 5.3**), below the 99.8% required for adipic acid polymer applications.[27] Since the rate of crystal nucleation was not controlled for this bench-scale demonstration, entrainment of culture broth within crystals may have resulted in significant inorganic impurity carry over.[46]

Combustion analysis of muconic acid crystals at 700°C measured a sample ash content of 1.44% (wt/wt), and elemental analysis by ICP-MS and nitrogen chemiluminescence confirmed major impurities as Na (4750 ppm), S (3540 ppm), P (2860 ppm), K (1030 ppm), and N (336 ppm), as shown in **Figure 5.4**, with a full listing of screened elements provided in **Table 5.3**.

Due to the large sample requirements for trace elemental analysis, only single batch samples were analyzed. Elemental impurities identified in biologically derived muconic acid differed greatly compared to impurities observed in chemically derived muconic acid obtained from Sigma Aldrich, with the latter being much lower in Na, S, P, K, and N, but higher in Fe and Cl. The major inorganic impurities identified in bio-derived muconic acid are known poisons to platinum group metals,[47–49] requiring removal strategies prior to catalysis. Likewise, polymer-grade adipic acid requires trace levels of Fe (< 0.2 ppm) and N (< 20 ppm N),[27] necessitating further treatment.

In order to reduce the level of inorganic impurities in muconic acid and generate a liquid media suitable for trickle-bed catalytic processing, muconic acid crystals were dissolved in ethanol and filtered through a 0.2-μm PES membrane. Upon EtOH dissolution, the muconic acid-ethanol solution was initially cloudy, likely due to insoluble salts, while after filtration the solution was strikingly clear (see **Figure 5.2**). Analysis of filtered and dried muconic acid after ethanol dissolution revealed an overall DSC-purity of 99.76 ± 0.04% (**Table 5.2**), with a dramatic reduction in elemental impurities. Analysis by ICP-MS determined that Na was reduced by 96%, S by 99%, P by 60%, K by 82%, and N by 62% (**Figure 5.4**), consistent with reductions in low-concentration elements (<100 ppm Al, Cl, Mg) (**Table 5.3**). Although a reduction in Fe to <0.2 ppm could not be definitively confirmed due to the large sample requirements, bio-muconic acid Fe levels were much lower (<1 ppm) compared to muconic acid of chemical origin (141 ppm). Unfortunately, N levels in bio-muconic acid were still above the polymer precursor specification of 20 ppm, likely due to residual fermentation proteins that were not removed during activated carbon treatment and microfiltration.

5.3.3 Batch reactor screening for catalyst activity and leaching

Batch reactor catalyst screening experiments were conducted with platinum group metals to evaluate their activity and stability against leaching during muconic acid hydrogenation. Catalysts were synthesized using powdered Darco activated carbon (AC) and Davisil silica supports sieved to >270 mesh (<53 μm) to minimize the impact of mass transfer during batch conditions previously studied.[16] Metals precursors were loaded onto their respective supports, and catalysts were reduced in hydrogen prior to characterization to determine their metal loading and dispersion, support surface area, pore volume and pore diameter, and x-ray diffraction (XRD) spectra, as shown in **Table 5.4** and **Figure 5.5**.

High surface areas were observed for both AC (590-971 $m^2 g^{-1}$) and silica (428-480 $m^2 g^{-1}$) supported catalysts, with higher metal loading materials generally showing lower surface areas. Support pore volumes (AC 0.514-0.708 $cm^3 g^{-1}$, silica 0.686-0.811 $cm^3 g^{-1}$) and pore diameters (AC 9.69-9.83 Å, silica 9.74-9.81 Å) were also comparable. Elemental analysis determined metal loadings were near their nominal values and XRD analysis confirmed the absence of sharp prominent peaks due to large metal crystallites. Chemisorption analysis measured dispersions were within the range of 10-62%, likely due to differing metal precursor and support material interactions during synthesis.[50] Due to varying active metal crystallite surface areas, observed catalyst activities for muconic acid hydrogenation were normalized to dispersion values to allow for turn-over-frequency (TOF) comparisons between metals (e.g., moles of compound reacted per second, divided by the moles of surface metal atoms measured by dispersion).

As shown in **Figure 5.6A**, pronounced differences were observed in the muconic acid hydrogenation activity between the platinum group metals tested during batch reactor screening

experiments (see **Figure 5.7**). Pd and Rh displayed highest TOF for muconic acid hydrogenation on both AC and silica supports, with Pd ranging from 14-23 sec^{-1} and Rh ranging from 7-8 sec^{-1}. In comparison, Pt displayed a TOF ranging from 1-3 sec^{-1}, while Ru ranged from 0.4-0.5 sec^{-1}. For batch reactions tested at room temperature, 2-hexenedioic acid was the primary intermediate observed, with trace levels of 3-hexenedioc acid identified on occasion (see **Figure 5.8**). For all catalysts screened in the batch system, mass balance closure was typically within +/-10%, with adipic acid as the only product observed upon completion of the reaction.

In addition to differing hydrogenation activity, catalyst metal leaching also varied significantly based on both the metal and choice of support, as shown in **Figure 5.6B**. Despite exposure to reaction conditions for only 35 min, 1%Pd/SiO_2 displayed the greatest amount of leaching on a percent of initial metal loading basis (8.89%), while 1%Pd/AC leached to a lesser extent (0.93%). Significant leaching was also observed for 5%Ru/AC (2.93%) and 5%Ru/SiO_2 (3.36%) with muconic acid. In contrast, metal leaching for 1%Rh/AC and 1%Rh/SiO_2 was at trace levels, at 0.51% and 0.16%, respectively, while leaching was negligible for both 5%Pt/SiO_2 (0.04%) and 5%Pt/AC (0.03%). Based on the high activity for muconic acid hydrogenation and stability against leaching, Rh/AC was chosen for further time-on-stream testing in a continuous trickle-bed reactor.

5.3.4 Continuous time-on-stream catalyst testing

Based on the activity and stability of Rh during batch reactions, continuous trickle bed reactor studies were conducted to determine its 100-h time-on-stream stability, as shown in **Figure 5.9**. Initially, a 1%Rh/AC catalyst was prepared on Norit AC granules crushed and sieved between 100-80 mesh (150-180 μm) to minimize the catalyst bed pressure drop. The catalyst was

characterized to determine its virgin and post-reaction properties, as shown in **Table 5.5**, **Figure 5.10-12**. Characterization of the virgin 1%Rh/AC catalyst showed high surface area (1029 $m^2 g^{-1}$), with comparable pore volume (0.455 $cm^3 g^{-1}$) and average pore diameter (9.69 Å) to the powder Rh/AC catalyst. XRD analysis confirmed the absence of sharp, prominent peaks due to large metal crystallites. Distinct differences were observed in XRD spectra of the powder and granule AC supports, likely due to different vendor carbon sources and/or activation techniques (**Figure 5.10**). The metal crystallite dispersion of the granule 1%Rh/AC catalyst was also lower (11.2%) compared to the powder catalyst, likely due to differing support-precursor interactions. Lastly, elemental mapping by scanning electron microscopy energy dispersive x-ray spectroscopy (SEM-EDS) confirmed the presence of disperse metal crystallites (**Figure 5.11A-C**), while transmission electron microscopy confirmed their small size (2.81 ± 0.46 nm) (**Figure 5.12A**).

The 100-h time-on-stream stability test of 1%Rh/AC was then evaluated in a sequential fashion, with partial conversion of muconic acid for the first two days to confirm steady state operation,[51] demonstration of complete conversion to adipic acid for days three and four, and lastly a return to partial conversion conditions on day five to observe any changes compared to the initial reactor performance. Sampling of the reactor was not performed during the first 12 h overnight, since preliminary experiments showed comparable time was required to reach steady conversion once the liquid feed was introduced (see **Figure 5.13**).

During the first 48-hours of time-on-stream (50°C, 0.5 mL min^{-1} liquid flow rate), muconic acid was partially converted (57.7 ± 1.9% average molar conversion) to hexenedioic acid (HDA) and adipic acid as the only observed products. Product identities were confirmed by gas chromatography mass spectroscopy, with details provided in **Figure 5.14** and **Table 5.6**. The

moderately higher reaction temperature (50°C) resulted in isomerization to 3-HDA as the predominant species (30.9 ± 1.2% molar yield), in comparison to 2-HDA for room temperature batch screening reactions. Moderate amounts of 2-HDA (19.7 ± 2.9% molar yield) and adipic acid (9.7 ± 1.2% molar yield) were also produced, with an average molar closure of 102.7 ± 4.9%, supporting steady state conversion during the first 48 h. Variability in molar closure was assumed to be primarily due to solvent evaporation and error introduced during the sampling of knockout pot, with concentrations of individual species throughout the 100-h run reported in **Table 5.7**.

Although an in depth study of trickle bed hydrogenation kinetics was beyond the scope of this work, multiple factors can influence the observed rate, including the gas-liquid flow rate ratio, liquid film thickness due to shear, interparticle and intraparticle wetting, and catalyst particle size, shape, and packing geometry.[52] Based on the liquid feed rate flow rate and conversion observed during the first 48 hours, the muconic acid hydrogenation TOF was calculated to be 0.022 sec^{-1} at 50°C, which was ~$1/1000^{th}$ of the rate observed for powder Rh/AC in batch reactor screening experiments at 24°C (TOF 7 sec^{-1}), indicating external and intraparticle diffusion likely influenced the observed rate due to larger particle sizes required for trickle-bed reactor experiments. Varying the catalyst bed temperature from 50-72°C resulted in an apparent activation energy of 60.7 kJ mol^{-1} for the 1%Rh/AC granule catalyst (**Figure 5.15**), well above typical barriers observed under solely mass transfer limiting conditions (<20 kJ mol^{-1})[53] and comparable to past batch reactor results for powder 1%Pd/AC (70 kJ/mol). Although steady state conversion was observed, care should be taken when interpreting these results since deactivation of metal crystallites within the catalyst's pores may be masked by mass and heat transfer effects.

To demonstrate complete conversion of muconic acid to adipic acid, the temperature was increased and liquid flow rate reduced (78°C, 0.2 mL min^{-1}) for day three and four of operation. The reactor was allowed to stabilize overnight before sampling, but deviations were observed in the initial sample mass balance closure (111.6% molar closure). By the second sample, mass balance closure had returned to 100.7% and complete conversion to adipic acid was observed throughout the two-day period. No peaks from HDA were observed by HPLC-DAD, which was highly sensitive to the presence of olefin bonds, supporting near complete conversion of muconic acid to adipic acid.

Lastly, reaction conditions were returned to partial conversion conditions for day five to compare the catalyst conversion and selectivity to the first 48 h of time-on-stream. Mass balance and product distribution perturbations were observed when altering the liquid flow rate, with a trend toward increasing conversion as time continued. For day five, the average muconic acid molar conversion was 55.2 ± 3.6%, comparable to values observed during the first 48 h of time-on-stream (57.7 ± 1.9%). Product distribution molar yields were also comparable, with average molar closure of 103.5 ± 4.6%. Ideally, trickle bed reactor sampling would have continued past day five to ensure steady state conditions had resumed, but limited quantities of biologically derived muconic acid were available for testing beyond the scheduled 100-h run.

5.3.5 Post-reaction catalyst characterization

After 100 h of time on stream testing, the 1%Rh/AC catalyst granules were recovered from the reactor for characterization to determine changes in the support and metal crystallite properties, as shown in **Table 5.4** and **Figures 5.10-12**. Measurement of the support surface area showed a 10% increase (1130 m^2 g^{-1}), potentially due to washing of the pores during the run. A

similar increase was observed in the pore volume (14% increase to 0.52 cm^3 g^{-1}) and average pore diameter (18% increase to 11.43 Å). The reactor effluent was also sampled and filtered daily during the run for elemental analysis to detect leaching. For the first day, trace leaching of Rh was observed at 1 ppb in the ethanol effluent, while for the remaining days leaching was not observed above the detection limit of 1 ppb. XRD analysis of the post-reaction catalyst showed similar spectral features as the virgin catalyst, with a sharp peak observed at ~26° 2θ, outside the major peaks for Rh, but potentially due to modification of the carbon support functional groups. Measurements of the catalyst metal surface area by hydrogen chemisorption after reaction showed a dispersion of 14% for the post reaction catalyst, as opposed to 21% for the fresh catalyst, despite consistent activity observed on day five. Further analysis of the post reaction catalyst by SEM-EDS showed disperse metal crystallites (**Figure 5.11F**), while TEM showed slightly larger crystallites with a diameter of 3.05 ± 0.55 nm, as opposed to 2.81 ± 0.46 nm for the fresh catalyst (**Figure 5.12B**). Collectively, these results suggest that the loss of measurable metal surface area may be due to organic deposition and a moderate increase in particle size, as opposed to dramatic sintering.

5.3.6 Nylon-6,6 polymerization with bio-adipic acid

Bio-adipic acid produced from muconic acid was then polymerized with 1,6-hexanediamine to form nylon-6,6 for comparative material testing to petrochemical adipic acid. Bench-scale condensation polymerizations were conducted using the well-known nylon rope trick reaction, as shown in **Figure 5.16**.[54] After producing nylon fibers from both bio-adipic acid and commercial adipic acid, polymer materials were dried and characterized to determine their thermal and physicochemical properties.

Thermal analysis of both nylon materials by DSC showed comparable melting and glass transition temperatures, similar to values reported in literature for commercial nylon-6,6,[55] as shown in **Table 5.8**. Clean thermal traces for nylon were observed, as highlighted in **Figure 5.16**, with a heat of fusion comparable (50.2 J/g) to literature values for commercial nylon (51.3 J/g).[56] Measurement of the intrinsic viscosity by dilute solution viscometry showed similar values for the two nylon materials, and calculations of the viscosity average MW showed that polymerization had taken place to a comparable extent for bio-adipic acid (1920 ± 20 g/mol) and chemical adipic acid (2230 ± 40 g/mol). However, the limitation of the nylon rope trick was apparent for achieving industrially relevant nylon MW values (40,000-60,000 g/mol).[57]

5.4 Discussion

As demonstrated in this work, the integrated biological and catalytic conversion of muconic acid to adipic acid holds promise for generating monomer precursors suitable for nylon-6,6 production. For the biological conversion of benzoate to muconate, residual benzoate was the only aromatic compound observed. However, upstream non-target metabolites can also result when producing muconic acid from both sugar and aromatic monomer substrates (e.g., p-coumarate), including protocatechuate[35,58] and 4-hydroxybenzoate.[35] Although these molecules were not observed in this work due to the use of benzoic acid as the initial substrate, biological engineering efforts are underway to improve the metabolic flux and minimize the buildup of non-target aromatic compounds during metabolism.[19,20,58–60] Likewise, optimization of the biological conversion process was beyond the scope of this study, but improved bioreactor delivery of substrate and aeration can potentially reduce the accumulation of residual substrate

and non-target metabolites in culture broth, greatly reducing the demand on downstream separation operations.

Following biological conversion, activated carbon was effective at purifying muconic acid culture broth prior to crystallization, as shown previously.[35] Due to the poor solubility of benzoate in solution at low pH, direct crystallization without purification was not viable due to the negative impact of precipitated benzoate on product purity. Although activated carbon was removed residual benzoate, muconate was also lost due to non-selective adsorption (16% observed here). Likely, high titers of muconic acid and low levels of non-target organic substrates will be required for activated carbon treatment to be economically viable at scale. In addition to benzoate adsorption, color compounds were also removed with activated carbon, which may be desirable for the final polymer cosmetically. However, differentiating bio-based material by properties such as color, texture, and transparency may be desirable for increasing consumer adoption.[61]

pH/temperature shift crystallization readily separated muconic acid from purified broth, although significant broth salts were carried over with the crystals. Subsequent dissolution of muconic acid in ethanol greatly reduced elemental impurities due to the poor ethanol solubility of salts, while providing a means for condensed phase catalytic processing. Direct catalytic processing of neat muconic acid in the vapor phase will likely be problematic due to the high boiling point and poor thermal stability. Despite the significant reduction in elemental impurities, the muconic acid nitrogen content of 129 ppm still remained above the specification for polymer grade adipic acid of 20 ppm. Although it was not determined if N was due to inorganic or organic constituents, ultrafiltration may be effective for further reducing nitrogen originating from proteins, while a second stage of crystallization may further reduce inorganic N.[62]

However, early-stage techno-economic analysis will be key for evaluating the potential industrial viability of separation unit at scale for muconic acid production.[63]

Batch catalyst screening reactions observed muconic acid hydrogenation activity in the order of Pd>Rh>Ru>Pt for both silica and activated carbon supports. However, the extent of catalyst metal leaching was both metal and support dependent. Leaching can be a function of temperature, pressure, metal-support interaction, solvent polarity, solution pH, and metal complexation with organic substrates.[64] In this work, silica showed a greater tendency towards leaching compared to activated carbon, potentially due to coordination with activated carbon's diverse surface functional groups.[65] With regards to trends with metal speciation, Pd leached significantly into solution, more so with silica (8.89%) than with activated carbon (0.93%). Pd is known to leach under acidic batch conditions, yet still display homogenous activity.[66] Significant leaching of Ru was also observed, despite Ru being shown to be stable during the hydrogenation of glucose,[67] 3-hydroxypropanal,[68] and lactic acid.[69] The unique dicarboxylic functionality of muconic acid may enhance its chelating abilities, similar to succinic acid,[70] making leaching a greater challenge for catalysis. Although Pt and Rh were both fairly stable, these metals are also among the most costly of platinum group metals.[71] Modification of lower cost Pd by secondary metal addition or support modification may improve its stability while maintaining its activity, similar to strategies applied to other bio-based catalytic systems.[64,72]

In addition to leaching, other catalyst deactivation mechanisms can manifest over longer time scales, such as fouling of active metal sites, pore blockage, sintering, and active metal poisoning.[73] For this work, the 100-h catalyst stability test with 1%Rh/AC showed steady state conversion during the first 48 hours, and comparable values at day five, suggesting significant deactivation had not occurred during this period. Analysis of the virgin and post-reaction catalyst

by TEM a modest 9% increase in average metal crystallite size, suggesting dramatic sintering had not occurred, likely due to the low reaction temperature for this chemistry. Likewise, the catalyst support surface area, pore volume, and pore diameter actually increased slightly, suggesting pore blockage and collapse was not a concern. However, a 33% reduction in active metal surface area was observed, despite comparable hydrogenation activity and modest increase in metal crystallite size. Although the mechanism for active metal area loss is unclear, initial fouling may have occurred during the approach to steady state activity in the first 12 h or when recovering the catalyst after the reaction due to organics remaining in the catalyst pores or bound to the metal surface.

Polymerization of bio-adipic acid to nylon-6,6 demonstrated comparable polymer properties to nylon derived from petrochemical adipic using the same synthetic method. As noted, suitable bio-based monomer purity will be critical for polymer applications. Impurities can result in disruption of the thermal phase transition behavior and intrinsic viscosity due to early polymer chain-termination from mono-functional moieties, incorporation of non-target bifunctional compounds, or entanglement with residual polymeric impurities.[74] Furthermore, impurities can affect the rate and extent of polymerization during synthesis, ultimately determining the applicability of synthetic methods at scale and the final polymer material performance properties.[74] Bio-derived muconic acid purity will also be important for expanding applications beyond nylon-6,6. This can include fully bio-based based nylon-6,5,[75] as well as additional monomer precursors such as diols, diamines, and diesters produced from catalytic upgrading.

Moving forward, efforts are needed to address the challenges when transitioning muconic acid production from model compounds and simple sugars to complex lignocellulosic

feedstocks. Unique impurities can result when deconstructing biomass into monomer streams that greatly differ from those encountered in model compound studies.[36] Lignocellulosic biomass can contain extractives, proteins, minor organics (e.g., carboxylic acids, saccharides, alcohols), and minerals (e.g., silicates, oxides, sulphates, phosphates, nitrates, and others) that vary based on feedstock and origin.[76,77] Furthermore, depending on the depolymerization technology employed, residual mineral acids or caustic salts may remain, as well as non-target organics originating from structural biomass polymers, such as aliphatic acids, furans, phenols, and oxygenated aromatic compounds that are present in monomer, dimer, and oligomer form.[36,78,79]

As a result, integrated solutions are needed to address the impurities generated during biomass depolymerization. With regards to biomass deconstruction, novel solvent systems are being explored to selectively depolymerize and remove sugars, while eliminating the use of mineral acids.[80] Likewise, catalytic systems are being examined for lignin depolymerization to selective aromatic monomers.[81] As improvements reduce the heterogeneity of biomass monomers, biological metabolic pathways can be expanded to convert non-target organics into carbon sources for metabolic functioning to support muconic acid production. This biological utilization of acetic acid produced from lignin depolymerization has been demonstrated during muconic acid production in shake flask experiments,[16] although further efforts are needed to evaluate this approach during fed-batch biological conversion at high titers. Likewise, tailored separation processes will be critical to recover muconic acid in high yield, while leaving behind unwanted inorganic and organic constituents. Ideally, the unique solubility of muconic acid can continue to be leveraged as a recovery strategy. Lastly, robust catalyst formulations can be developed that offer platinum group metal alternatives, while maintaining high activity, selectivity, and stability during acidic process conditions with potential biomass impurities.

5.5 Conclusion

As demonstrated in this work, muconic acid can serve as a biologically derived precursor for high purity adipic acid and nylon-6,6 polymerization through downstream separation and catalysis. The production of value-added chemicals from biomass, in addition to fuels, holds promise for improving the economic and environmental outlook of modern biorefineries. Moving forward, effective strategies are needed to remove impurities generated during biomass depolymerization and biological conversion, while meeting the stringent purity requirements for renewable polymer precursor production through integrated biological conversion, separation, and catalytic unit processes.

5.6 Methods

5.6.1 Biological production of muconic acid

cis,cis-muconic acid was produced biologically with an engineered strain of *Pseudomonas putida,* KT2440-CJ103,[16] using benzoate as the precursor substrate. Seed cultures for cultivation were prepared in 1 L shake flasks containing 200 mL of Luria-Bertani broth and incubated at 30°C at 225 rpm for 14 hours. Subsequently, cells were centrifuged at 5000 rpm for 10 minutes and washed once with 40 mL of modified M9 minimal medium (M9) containing 15 mM glucose. M9 consisted of 13.56 g/L Na_2HPO_4, 6 g/L KH_2PO_4, 1 g/L NaCl, 2.25 g/L $(NH_4)_2SO_4$, 2 mM $MgSO_4$, 100 μM $CaCl_2$, and 18 μM $FeSO_4$. Washed cells were inoculated in a 10-L New Brunswick BioFlo®/CelliGen® 310 bioreactor (Eppendorf), which contained 8 L of M9 media and 15 mM of glucose. The bioreactor started at an initial optical density of 0.1 at 600 nm (OD_{600}). The pH of the medium was automatically controlled and adjusted to 7 with 2 N NaOH and the temperature was maintained at 30°C. Air was sparged at a rate of 8 L/min (1 vol

vol^{-1} min^{-1}) and the agitation was gradually increased from 250 to 450 rpm manually to maintain an average dissolved oxygen (DO) level of ~50%. After 4 hours, drops of antifoam 204 (Sigma Aldich) and 0.5 mM sodium benzoate were added to the culture. When the glucose level was close to depletion at ~7.5 h, 5 mM glucose was supplemented to the bioreactor to maintain an increasing cell density. When the glucose was nearly consumed for the second time (~10.3 h), as indicated by a low DO level and rapid increase, DO-stat control was initiated. The fed-batch feeding solution was composed of 160 g/L sodium benzoate, 100 g/L glucose, and 15 g/L $(NH_4)_2SO_4$. The feed solution was pumped for 36 s intervals (~3.2 mL) when the OD was higher than 65% during the first ~2 h, and 70% thereafter. Glucose levels were tracked with a YSI 7100MBS analyzer (YSI Life Sciences) and muconate and benzoate levels were monitored by HPLC, as described below. The bioreactor was run for 32 h and cells were removed by centrifugation, followed by vacuum filtration (0.2-μm PES).

5.6.2 Separation and purification of muconic acid

Sequential purification of muconic acid was preformed to evaluate the level of impurities after each stage of treatment. Initially, muconic acid culture broth was treated with activated carbon (100 mesh, Darco, Sigma Aldrich) at 2-4% wt/vol to remove residual amounts of benzoate and trace aromatics. Preliminary trials were conducted to minimize the amount of carbon added and resulting muconic acid losses. Activated carbon was removed by vacuum filtration (0.2-μm PES filter assembly, Nalgene). Muconic acid was then separated from solution by pH-temperature shift crystallization. The treated broth was adjusted to pH 2 with concentrated H_2SO_4 to initiate crystallization, and then chilled to 5°C to facilitate further crystal formation. Crystallized solids were recovered by vacuum filtration (0.2-μm PES) and dried in a vacuum

oven for ≥48 h to remove residual moisture. A subsample of crystal was sampled for purity analysis, as described below, and the remaining material was dissolved in 200 proof ethanol (10 g/L, stirring at room temperature for 2 h) to precipitate insoluble salts. The ethanol solution was vacuum filtered (0.2-μm PES) and blown to dryness under nitrogen to collect a final subsample for purity analysis.

5.6.3 Catalyst synthesis and characterization

Platinum group metal catalysts (Pt, Rh, Ru, Pd) were synthesized on powder carbon and silica supports to evaluate their activity and stability for muconic acid hydrogenation. For batch reaction studies, Darco activated carbon (Sigma Aldrich) and Davisil Grade 633 high surface area silica (Sigma Aldrich) were used. Supports were initially sieved >270 mesh (<53 μm) to minimize the impact of mass transfer on observed kinetics. The silica support was calcined at 500°C in air prior to loading metals, while the activated carbon support was used as received. Catalysts were prepared with the following metal salt precursors: palladium acetate (Sigma Aldrich), rhodium nitrate hydrate (Sigma Aldrich), ruthenium chloride hydrate (Sigma Aldrich), chloroplatinic acid (CPA) (Sigma Aldrich), and ammonium tetraammineplatinum nitrate (PTA) (Sigma Aldrich). Pd, Ru, and Rh catalysts were prepared by incipient wetness, while Pt catalysts were prepared by strong electrostatic adsorption (SEA) to improve dispersion due to the low activity. For SEA catalyst synthesis,[82,83] 1.9 g of support was added to 50 mL of DI water, and the pH was adjusted to facilitate protonation/deprotonation of the support (pH 12 with NaOH for silica, pH 2.9 with HCl for AC). In another bottle, the appropriate catalyst precursor was dissolved in 50 mL of DI water (PTA for silica, CPA for activated carbon). The two bottles were mixed together with stirring for 1 h, followed by vacuum filtration to recover the catalyst. The

catalyst was washed twice with 50 mL of DI water and left to dry overnight in air at room temperature. After loading, catalysts were dried at 110°C and reduced in hydrogen flowing at 200 sccm for 2 h at temperature. Due to the sensitivity of Pd dispersion with temperature,[84] Pd catalysts were reduced at 125°C while Pt, Rh, and Ru catalysts were reduced at 250°C.

For flow reactor studies, extruded activated carbon pellets (Norit Rx 3 Extra, Cabot Norit) were initially crushed and sieved between 80-100 mesh (150-180 μm) to allow for a moderate catalyst bed pressure drop (< 5 psig) while still facilitating mass transfer. Rh was loaded onto the support by incipient wetness using ruthenium chloride hydrate (Sigma Aldrich), dried at 110°C, and reduced *ex situ* prior to use at 250°C in flowing hydrogen.

5.6.4 Catalyst testing

For batch reactor activity studies, reactions were performed in using a Parrr 5000 Multi-reactor system (Parr Instruments). Commercial *cis,cis*-muconic acid in the amount of 200 mg (Sigma Aldrich) was dissolved in 19.8 g of 200 proof ethanol. The muconic acid solution and 15 mg of catalyst were then loaded into 75 mL vessels equipped with magnetic stirring. Hydrogenation reactions were performed at 24°C with hydrogen supplied at a constant 24 bar and stirring at 1600 rpm. Duplication reactions were performed at minimum, with error bars indicating sample standard deviations. Samples were collected via an *in situ* sample port, syringe filtered, and analyzed by HPLC, as described below. After the reaction, the reactor contents were vacuum filtered (0.2-μm PES filter assembly, Nalgene) to remove catalyst particles, and subsequently the liquid filtrate was analyzed by ICP-OES to examine active metal leaching.

For flow reactor stability studies, reactions were performed using a Parr Tubular reactor system (Parr Instruments) operated in a down-flow trickle-bed configuration. The system was

outfitted with a HPLC pump to deliver liquid phase reactants (Series III Scientific Instrument), pair of mass flow controllers to control inert and hydrogen gas delivery (Brooks), tube-in-tube heat exchanger for cooling the reactor effluent, high-pressure 1-L stainless steel knockout pot with bottom sampling valve, and a solenoid-controlled backpressure regulator (Tescom) to maintain system pressure. Reactions were performed in trickle down flow configuration, with gas and liquid reagents fed to through the top of a 32" long, 1/4" inner diameter stainless steel reaction tube. The tube temperature was monitored and controlled using an internal thermocouple centered in the catalyst bed and three furnace wall thermocouples. The tube was initially packed halfway with inert 1-mm glass beads (Sigma Aldrich) held in place with quartz wool (Quartz Scientific Inc.). The catalyst bed was then loaded at the tube mid-height. Inert quartz sand (Quartz Scientific Inc.) sieved to <60-mesh (>250 μm) was placed at the base and top of the carbon catalyst packing to serve as a support. The remaining reactor tube void was then filled with inert glass beads and sealed with quartz wool.

Continuous hydrogenation reactions were performed with hydrogen supplied at 200 sccm and a system pressure maintained at 24 bar. Temperature was varied from 50-78°C, as indicated. The mobile phase consisted of biologically derived muconic acid purified with activated carbon, precipitated by temperature-pH shift crystallization, dissolved in 200-proof ethanol (8 g/L), and filtered (0.2-μm PES) to remove insoluble salts. Commercial succinic acid (Sigma Aldrich, ≥99.0% reagent purity) was added as an internal standard (0.8 g/L). The liquid flow rate was varied from 0.2-0.5 mL/min, as indicated. Liquid reactor effluent samples collected from the knockout pot were syringe-filtered, and analyzed by HPLC and GC-MS, as described below. Periodically, the liquid filtrate was analyzed by ICP-MS to detect catalyst metal leaching. After testing, the reactor was cooled to room temperature, depressurized, and 500 mL of ethanol was

flushed through the catalyst bed, followed by drying under 200 sccm nitrogen. The catalyst bed packing solids were then sieved between 80-100 mesh (150-180 μm) to recover the catalyst granules for further analysis.

5.6.5 Analysis of chemical compounds

Chemical substrates and products from biological conversion were monitored by high performance liquid chromatography (HPLC). Concentrations of glucose, *cis,cis*-muconate, and benzoate were determined from filtered sample supernatants on an Agilent1100 series HPLC system utilizing a Phenomenex Rezex RFQ-Fast Fruit H+ column and Bio-Rad Laboratories cation H+ guard cartridge operating at 85°C. Dilute sulfuric acid (0.01 N) was used as the isocratic mobile phase at a flow rate of 1.0 mL/min. Refractive index and diode array detectors were used for compound detection. By-products were identified by co-elution at the same retention time with pure compounds. During fed-batch biological conversion, glucose and nitrogen (as the ammonium ion) was monitored using a YSI MBS 7100 Analyzer (YSI Incorporated Life Sciences). The cell density of the cultures was determined by measuring the optical density at 600 nm (OD600) of the culture against an LB or M9 blank on a Beckman DU640 spectrophotometer. In cultures that had turned dark during growth, the OD was calculated by measuring the OD600 of the culture and subtracting the OD600 of the media following centrifugation to pellet cells.

The purity of muconic acid was measured after varying treatment stages using differential scanning calorimetry and elemental analysis. DSC purity was measured using a TA Q-5000 series Digital Scanning Calorimeter with a Liquid Nitrogen Cooling Systems. All runs were conducted using a ramp rate of 10 °C/min and heating the compounds from 35 °C to above their

melting point. For muconic acid, the purity was determined from the first thermal scan due to stability issues of the compound after the melting point. The purity of adipic acid was determined using the second thermal scan after the compound had recrystallized. Purity was determined by using the TA universal analysis tool in which the purity is determined by the slope at the onset of melting through the use of the van't Hoff equations.[45] Elemental analysis of the samples was outsourced to Huffman-Hazen laboratories for ICP-MS and nitrogen chemiluminescence analysis.

Batch and flow reactor products were monitored by the HPLC method described above, and product identities were confirmed by gas chromatography mass spectroscopy (GC-MS). For product verification, samples were methylate prior to analysis.[85] Briefly, samples dissolved in ethanol were blown to dryness using under nitrogen. Solid acid crystals (~10 mg) were then added to a vial with 0.75 mL of dichloromethane and 1 mL of 3% concentrated sulfuric acid in methanol (vol/vol). Samples were then sealed and heated to 80°C for 20 h. After contents had cooled, ~3 mL of DI water was added to from a biphasic system. The organic phase was removed by pipette, dried with Na_2SO_4, neutralized with Na_2CO_3, and filtered (0.2-μm syringe filter) prior to analysis. Derivatized methyl esters were analyzed using an Agilent 6890A GC equipped with a 5973 mass spectrometer detector (Agilent Technologies) operating in splitless mode. The GC was outfitted with an Agilent DB-Wax column (30 m × 0.25-mm id, 0.25-μm film), and helium (0.8 mL/min column flow) was used as the carrier gas at 1 mL/min. The injector volume was set to 1 μL using an Agilent auto-sampler. The GC/MS method consisted of a front inlet temperature of 260°C, MS transfer line temperature of 260°C, and scan range from 25 m/z to 450 m/z. A starting temperature of 35°C was held for 3 minutes and then ramped at 15°C/min to a temperature of 250°C and held for 5 minutes. The MS was set up with a solvent

delay of 2.5 minutes to collect data after the solvent peak had eluded. HP MSD Chemstation software (Agilent) equipped with NIST11 database Rev. 2.0G (May 19, 2011 build) was used to identity compounds found within the samples.

5.6.6 Polymerization and characterization of nylon-6,6

Adipic acid was initially reacted with thionyl chloride at a 1:1 weight-to-volume ratio. The mixture was heated to 80°C for 1 h and then cooled to room temperature before the top layer of residual thionyl chloride was discarded. The derivatized adipic acid was then added to cyclohexane at 0.25 M. 1,6-Hexanediamine was then prepared at 0.5 M in water containing 0.5 M of NaOH. An equimolar amount of the diamine solution was measured out and poured into an empty beaker, followed by slow pouring of the adipic acid solution to avoid phase mixing. Tweezers where then used to grab the thin layer of polymer formed at the interface of the solution, which was pulled to produce a nylon "rope". The polymer was then dried, rinsed in DI water, and placed in a vacuum oven to dry overnight prior to polymer characterization.

The thermal properties of nylon materials were tested using DSC. The polymers were scanned from -60°C to 200 °C at a rate of 10 °C/minute. The percent crystallinity was determined by taking the heat of fusion for the polymer and dividing it by the heat of fusion for a 100% crystalline Nylon-6,6. The heat of fusion for 100% crystalline Nylon-6,6 has been previously determined to be 189.95 J/g.[56] The results for the thermal properties for both the petrochemical derived nylon and the bio-derived nylon were then compared to literature values.[55] The viscosity average molecular weight, M_v, was determined using dilute solution viscometry.[74] An Ubbelholde viscometer was used with m-cresol as the solvent at 25 °C and polymer solutions ranging in concentration from 0.003 g/mL and 0.015 g/mL. Four different solutions were

prepared for each polymer and tested three times in the viscometer. For these studies with m-cresol at 25 °C, Mark-Houwink parameters were a = 0.61 and K = 0.0024.[57] The resulting viscosity average molecular weight is between the weight average molecular weight, M_w, and the number average molecular weight, M_n.

5.7 References Cited

1. Corma, A., Iborra, S. & Velty, A. Chemical Routes for the Transformation of Biomass into Chemicals. *Chem. Rev.* **107,** 2411–2502 (2007).
2. Gallezot, P. Conversion of biomass to selected chemical products. *Chem. Soc. Rev.* **41,** 1538–1558 (2012).
3. Holladay, J. E., Bozell, J. J., White, J. & Johnson, D. Top Value-Added Chemicals from Biomass. Volume II - Results of Screening for Potential Candidates from Biorefinery Lignin. (2007).
4. Werpy, T. A. & Petersen, G. R. Top Value Added Chemicals from Biomass. Volume I - Results of Screening for Potential Candidates from Sugars and Synthesis Gas. *US Dep. Energy* (2004).
5. Bozell, J. J. & Petersen, G. R. Technology development for the production of biobased products from biorefinery carbohydrates—the US Department of Energy's 'Top 10' revisited. *Green Chem.* **12,** 539 (2010).
6. Chundawat, S. P. S., Beckham, G. T., Himmel, M. E. & Dale, B. E. Deconstruction of Lignocellulosic Biomass to Fuels and Chemicals. *Annu. Rev. Chem. Biomol. Eng.* **2,** 121–145 (2011).
7. Harmsen, P. F. H., Hackmann, M. M. & Bos, H. L. Green building blocks for bio-based plastics. *Biofuels Bioprod. Biorefining* **8,** 306–324 (2014).
8. Zakzeski, J., Bruijnincx, P. C., Jongerius, A. L. & Weckhuysen, B. M. The catalytic valorization of lignin for the production of renewable chemicals. *Chem. Rev.* **110,** 3552–3599 (2010).

9. Ragauskas, A. J. *et al.* Lignin Valorization: Improving Lignin Processing in the Biorefinery. *Science* **344,** 1246843 (2014).

10. Xiong, M. *et al.* A Bio-Catalytic Approach to Aliphatic Ketones. *Sci. Rep.* **2,** (2012).

11. Linger, J. G. *et al.* Lignin valorization through integrated biological funneling and chemical catalysis. *Proc. Natl. Acad. Sci.* **111,** 12013–12018 (2014).

12. Anbarasan, P. *et al.* Integration of chemical catalysis with extractive fermentation to produce fuels. *Nature* **491,** 235–239 (2012).

13. Dusselier, M., Mascal, M. & Sels, B. F. in 1–40 (Springer Berlin Heidelberg, 2014). at <http://link.springer.com/chapter/10.1007/128_2014_544>

14. Draths, K. M. & Frost, J. W. Environmentally compatible synthesis of adipic acid from D-glucose. *J. Am. Chem. Soc.* **116,** 399–400 (1994).

15. Niu, W., Draths, K. M. & Frost, J. W. Benzene-Free Synthesis of Adipic Acid. *Biotechnol. Prog.* **18,** 201–211 (2002).

16. Vardon, D. R. *et al.* Adipic acid production from lignin. *Energy Environ. Sci.* **8,** 617–628 (2015).

17. Draths, K. M. & Frost, J. W. Environmentally compatible synthesis of adipic acid from D-glucose. *J. Am. Chem. Soc.* **116,** 399–400 (1994).

18. Niu, W., Draths, K. M. & Frost, J. W. Benzene-Free Synthesis of Adipic Acid. *Biotechnol. Prog.* **18,** 201–211 (2002).

19. Sun, X., Lin, Y., Huang, Q., Yuan, Q. & Yan, Y. A Novel Muconic Acid Biosynthetic Approach by Shunting Tryptophan Biosynthesis via Anthranilate. *Appl. Environ. Microbiol.* (2013). doi:10.1128/AEM.00859-13

20. Wang, J. & Zheng, P. Muconic acid production from glucose using enterobactin precursors in Escherichia coli. *J. Ind. Microbiol. Biotechnol.* **42,** 701–709 (2015).
21. Fuchs, G., Boll, M. & Heider, J. Microbial degradation of aromatic compounds — from one strategy to four. *Nat. Rev. Microbiol.* **9,** 803–816 (2011).
22. Vyver, S. V. de & Román-Leshkov, Y. Emerging catalytic processes for the production of adipic acid. *Catal. Sci. Technol.* **3,** 1465–1479 (2013).
23. Van Duuren, J. B. J. H. & Wittmann, C. in *Bioprocessing of Renewable Resources to Commodity Bioproducts* (eds. Bisaria, V. S. & Kondo, A.) 519–540 (John Wiley & Sons, Inc., 2014). at <http://onlinelibrary.wiley.com/doi/10.1002/9781118845394.ch19/summary>
24. Davis, R. *et al.* Process design and economics for the conversion of lignocellulosic biomass to hydrocarbons: Dilute-acid and enzymatic deconstruction of biomass to sugars and biological conversion of sugars to hydrocarbons. *NREL Tech. Rep.* 88–101 (2013).
25. Polen, T., Spelberg, M. & Bott, M. Toward biotechnological production of adipic acid and precursors from biorenewables. *J. Biotechnol.* **167,** 75–84 (2013).
26. Reimer, R. A., Slaten, C. S., Seapan, M., Lower, M. W. & Tomlinson, P. E. Abatement of N2O emissions produced in the adipic acid industry. *Environ. Prog.* **13,** 134–137 (1994).
27. Radici Group. Adipic acid. at <www.radicigroup.com/chemicals>
28. Schwartz, T. J., O'Neill, B. J., Shanks, B. H. & Dumesic, J. A. Bridging the Chemical and Biological Catalysis Gap: Challenges and Outlooks for Producing Sustainable Chemicals. *ACS Catal.* **4,** 2060–2069 (2014).
29. Shanks, B. H. Conversion of Biorenewable Feedstocks: New Challenges in Heterogeneous Catalysis. *Ind. Eng. Chem. Res.* **49,** 10212–10217 (2010).

30. Delhomme, C., Goh, S. L. M., Kühn, F. E. & Weuster-Botz, D. Esterification of bio-based succinic acid in biphasic systems: Comparison of chemical and biological catalysts. *J. Mol. Catal. B Enzym.* **80,** 39–47 (2012).
31. Luque, R. *et al.* Chemical transformations of succinic acid recovered from fermentation broths by a novel direct vacuum distillation-crystallisation method. *Green Chem.* **11,** 193–200 (2009).
32. Zhang, Z., Jackson, J. E. & Miller, D. J. Effect of biogenic fermentation impurities on lactic acid hydrogenation to propylene glycol. *Bioresour. Technol.* **99,** 5873–5880 (2008).
33. Roos, J. W., McLaughlin, J. K. & Papoutsakis, E. T. The effect of pH on nitrogen supply, cell lysis, and solvent production in fermentations of Clostridium acetobutylicum. *Biotechnol. Bioeng.* **27,** 681–694 (1985).
34. Linger, J. G. *et al.* Lignin valorization through integrated biological funneling and chemical catalysis. *Proc. Natl. Acad. Sci.* **111,** 12013–12018 (2014).
35. Vardon, D. R. *et al.* Adipic acid production from lignin. *Energy Environ. Sci.* **8,** 617–628 (2015).
36. Klinke, H. B., Thomsen, A. B. & Ahring, B. K. Inhibition of ethanol-producing yeast and bacteria by degradation products produced during pre-treatment of biomass. *Appl. Microbiol. Biotechnol.* **66,** 10–26 (2004).
37. Ramaswamy, S., Huang, H.-J. & Ramarao, B. *Separation and Purification Technologies in Biorefineries*. (John Wiley and Sons Ltd, 2012).
38. Stainer, R. Y. & Ornston, L. N. in *Advances in Microbial Physiology* (ed. Tempest, A. H. R. and D. W.) **9,** 89–151 (Academic Press, 1973).

39. Bang, S.-G. & Choi, C. Y. DO-stat fed-batch production of *cis, cis*-muconic acid from benzoic acid by *Pseudomonas putida* BM014. *J. Ferment. Bioeng.* **79,** 381–383 (1995).
40. Mizuno, S., Yoshikawa, N., Seki, M., Mikawa, T. & Imada, Y. Microbial production of *cis, cis*-muconic acid from benzoic acid. *Appl. Microbiol. Biotechnol.* **28,** 20–25 (1988).
41. Mwangi, G. & Oguntimein, G. Study of an Activated Carbon System for the Treatment of Fermentation Wastewater from a Bioethanol Production Process. *West Indian J. Eng.* **35,** 65–71 (2013).
42. U.S. Army Corps of Engineers. Engineering and Design - Adsorption Design Guide. *DG 1110-1-2* (2001).
43. Creek, D. N. & Davidson, J. M. Treatment Technologies for Removal of Methyl Tertiary Butyl Ether (MTBE) from Drinking Water: Granular Activated Carbon. *Natl. Water Res. Inst.* (2000).
44. Luque, R. *et al.* Chemical transformations of succinic acid recovered from fermentation broths by a novel direct vacuum distillation-crystallisation method. *Green Chem.* **11,** 193–200 (2009).
45. Blaine, R. L. & Schoff, C. K. Purity Determinations by Thermal Methods. (1984).
46. Samant, K. D. & O'Young, L. Understanding crystallization and crystallizers. *Chem. Eng. Prog.* **102,** 28–37 (2006).
47. Bartholomew, C. H. Mechanisms of catalyst deactivation. *Appl. Catal. Gen.* **212,** 17–60 (2001).
48. Moulijn, J. A., van Diepen, A. E. & Kapteijn, F. Catalyst deactivation: is it predictable?: What to do? *Appl. Catal. Gen.* **212,** 3–16 (2001).
49. Forzatti, P. & Lietti, L. Catalyst deactivation. *Catal. Today* **52,** 165–181 (1999).

50. Jiao, L., Zha, Y., Hao, X. & Regalbuto, J. R. in *Studies in Surface Science and Catalysis* (ed. E.M. Gaigneaux, M. D., D. E. De Vos, S. Hermans, P. A. Jacobs, J. A. Martens and P. Ruiz) **162,** 211–218 (Elsevier, 2006).
51. Davis, R. J. Reaction Engineering Concepts for the Catalytic Conversion of Biorenewable Molecules. (2013). at <http://www.edition-open-access.de/proceedings/2/10/index.html>
52. Ranade, V. V., Chaudhari, R. & Gunjal, P. R. *Trickle Bed Reactors: Reactor Engineering & Applications*. (Elsevier, 2011).
53. Fogler, H. S. *Elements of Chemical Reaction Engineering*. (Prentice Hall, 2005).
54. Morgan, P. W. & Kwolek, S. L. The nylon rope trick: Demonstration of condensation polymerization. *J. Chem. Educ.* **36,** 182 (1959).
55. Brandrup, J., Immergut, E. H. & Grulke, E. A. *Polymer Handbook, 2 Volumes Set*. (Wiley, 2003).
56. Starkweather, H. W., Zoller, P. & Jones, G. A. The heat of fusion of 66 nylon. *J. Polym. Sci. B Polym. Phys.* **22,** 1615–1621 (1984).
57. Burke, J. J. & Orofino, T. A. Nylon 66 polymers. I. Molecular weight and compositional distribution. *J. Polym. Sci. Part -2 Polym. Phys.* **7,** 1–25 (1969).
58. Weber, C. *et al.* Biosynthesis of *cis,cis*-Muconic Acid and Its Aromatic Precursors, Catechol and Protocatechuic Acid, from Renewable Feedstocks by *Saccharomyces cerevisiae*. *Appl. Environ. Microbiol.* **78,** 8421–8430 (2012).
59. Curran, K. A., Leavitt, J. M., Karim, A. S. & Alper, H. S. Metabolic engineering of muconic acid production in *Saccharomyces cerevisiae*. *Metab. Eng.* **15,** 55–66 (2013).

60. Lin, Y., Sun, X., Yuan, Q. & Yan, Y. Extending shikimate pathway for the production of muconic acid and its precursor salicylic acid in Escherichia coli. *Metab. Eng.* **23,** 62–69 (2014).

61. Karana, E. Characterization of 'natural' and 'high-quality' materials to improve perception of bio-plastics. *J. Clean. Prod.* **37,** 316–325 (2012).

62. Ramaswamy, S., Huang, H.-J. & Ramarao, B. *Separation and Purification Technologies in Biorefineries*. (John Wiley and Sons Ltd, 2012).

63. Claypool, J. T. & Raman, D. R. Development and validation of a technoeconomic analysis tool for early-stage evaluation of bio-based chemical production processes. *Bioresour. Technol.* **150,** 486–495 (2013).

64. Sádaba, I., Granados, M. L., Riisager, A. & Taarning, E. Deactivation of solid catalysts in liquid media: the case of leaching of active sites in biomass conversion reactions. *Green Chem.* (2015). doi:10.1039/C5GC00804B

65. Rodríguez-reinoso, F. The role of carbon materials in heterogeneous catalysis. *Carbon* **36,** 159–175 (1998).

66. Novák, Z., Szabó, A., Répási, J. & Kotschy, A. Sonogashira Coupling of Aryl Halides Catalyzed by Palladium on Charcoal. *J. Org. Chem.* **68,** 3327–3329 (2003).

67. Hoffer, B. W. *et al.* Carbon supported Ru catalysts as promising alternative for Raney-type Ni in the selective hydrogenation of d-glucose. *Catal. Today* **79–80,** 35–41 (2003).

68. Besson, M., Gallezot, P., Pigamo, A. & Reifsnyder, S. Development of an improved continuous hydrogenation process for the production of 1,3-propanediol using titania supported ruthenium catalysts. *Appl. Catal. Gen.* **250,** 117–124 (2003).

69. Besson, M., Gallezot, P. & Pinel, C. Conversion of Biomass into Chemicals over Metal Catalysts. *Chem. Rev.* **114,** 1827–1870 (2014).

70. Li, L. *et al.* Succinic acid-based leaching system: A sustainable process for recovery of valuable metals from spent Li-ion batteries. *J. Power Sources* **282,** 544–551 (2015).

71. BASF. Metal Price History Charts. *BASF* (2015). at <http://apps.catalysts.basf.com/apps/eibprices/mp/DPCharts.aspx>

72. Alonso, D. M., Wettstein, S. G. & Dumesic, J. A. Bimetallic catalysts for upgrading of biomass to fuels and chemicals. *Chem. Soc. Rev.* **41,** 8075–8098 (2012).

73. Besson, M. & Gallezot, P. Deactivation of metal catalysts in liquid phase organic reactions. *Catal. Today* **81,** 547–559 (2003).

74. Hiemenz, P. C. & Lodge, T. P. *Polymer Chemistry, Second Edition*. (CRC Press, 2007).

75. Kind, S. *et al.* From zero to hero – Production of bio-based nylon from renewable resources using engineered Corynebacterium glutamicum. *Metab. Eng.* **25,** 113–123 (2014).

76. Vassilev, S. V., Baxter, D., Andersen, L. K., Vassileva, C. G. & Morgan, T. J. An overview of the organic and inorganic phase composition of biomass. *Fuel* **94,** 1–33 (2012).

77. Vassilev, S. V., Baxter, D., Andersen, L. K. & Vassileva, C. G. An overview of the chemical composition of biomass. *Fuel* **89,** 913–933 (2010).

78. Zakzeski, J., Bruijnincx, P. C., Jongerius, A. L. & Weckhuysen, B. M. The catalytic valorization of lignin for the production of renewable chemicals. *Chem. Rev.* **110,** 3552–3599 (2010).

79. Pandey, M. P. & Kim, C. S. Lignin Depolymerization and Conversion: A Review of Thermochemical Methods. *Chem. Eng. Technol.* **34,** 29–41 (2011).

80. Luterbacher, J. S. *et al.* Nonenzymatic Sugar Production from Biomass Using Biomass-Derived γ-Valerolactone. *Science* **343,** 277–280 (2014).

81. Schutyser, W. *et al.* Selective Nickel-Catalyzed Conversion of Model and Lignin-Derived Phenolic Compounds to Cyclohexanone-Based Polymer Building Blocks. *ChemSusChem* **8,** 1805–1818 (2015).

82. Miller, J. T., Schreier, M., Kropf, A. J. & Regalbuto, J. R. A fundamental study of platinum tetraammine impregnation of silica: 2. The effect of method of preparation, loading, and calcination temperature on (reduced) particle size. *J. Catal.* **225,** 203–212 (2004).

83. Hao, X., Barnes, S. & Regalbuto, J. R. A fundamental study of Pt impregnation of carbon: Adsorption equilibrium and particle synthesis. *J. Catal.* **279,** 48–65 (2011).

84. Gurrath, M. *et al.* Palladium catalysts on activated carbon supports: Influence of reduction temperature, origin of the support and pretreatments of the carbon surface. *Carbon* **38,** 1241–1255 (2000).

85. Shen, X.-W., Yang, Y., Jian, J., Wu, Q. & Chen, G.-Q. Production and characterization of homopolymer poly(3-hydroxyvalerate) (PHV) accumulated by wild type and recombinant Aeromonas hydrophila strain 4AK4. *Bioresour. Technol.* **100,** 4296–4299 (2009).

5.8 Figures and Tables

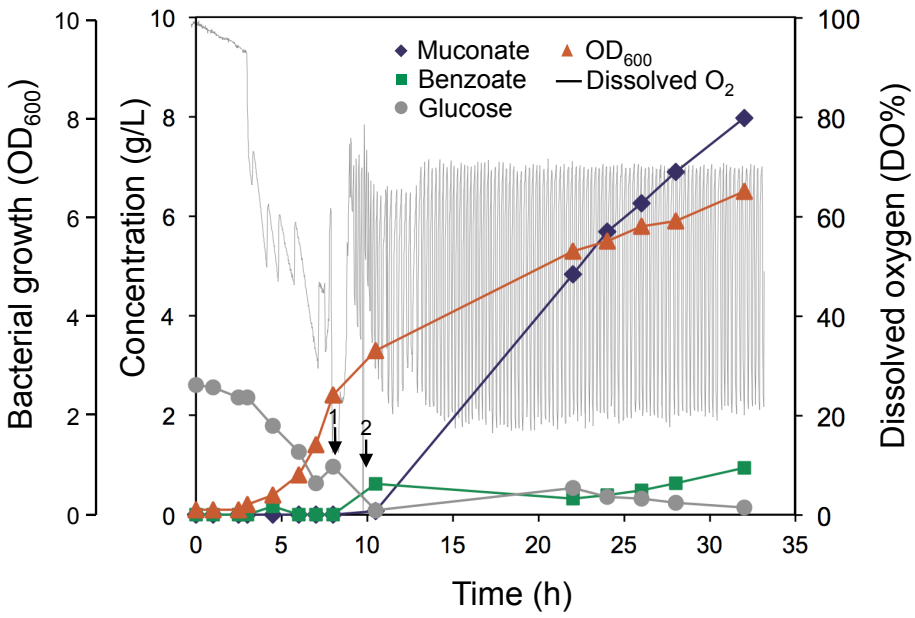

Figure 5.1. Fed-batch biological conversion of benzoate to muconate by *P. putida* KT2440 using glucose as a carbon source and dissolved oxygen (DO) control.

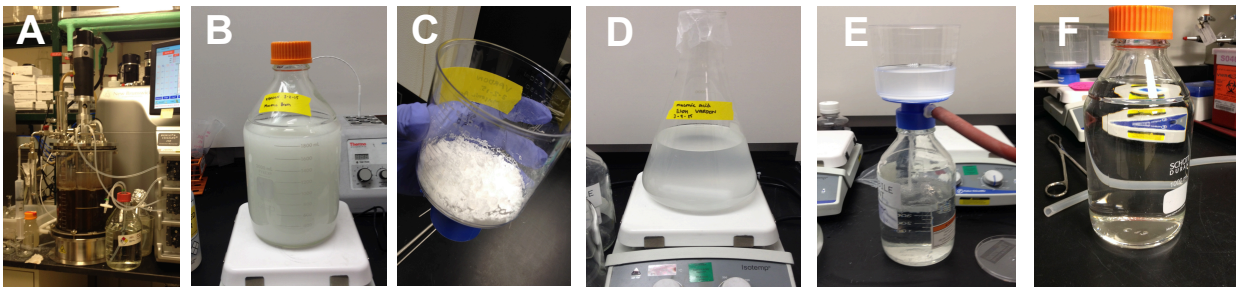

Figure 5.2. Purification of muconic acid biological culture media by activated carbon treatment, pH/temperature shift crystallization, and ethanol dissolution with microfiltration. The initial muconic acid culture broth appeared dark coffee colored (A). Activated carbon treatment of the broth significantly removed color compounds, while adjustment to pH 2 initiated crystal formation (B). Filtration and drying of the purified broth produced a white crystal solid, with a purity of 97.86 ± 0.05% by DSC melting point analysis (C). Muconic acid crystals dissolved in ethanol resulted in a cloudy solution (D), that upon 0.2-µm microfiltration (E) resulted in a clear solution (F) with a final muconic acid purity of 99.76 ± 0.04% upon drying.

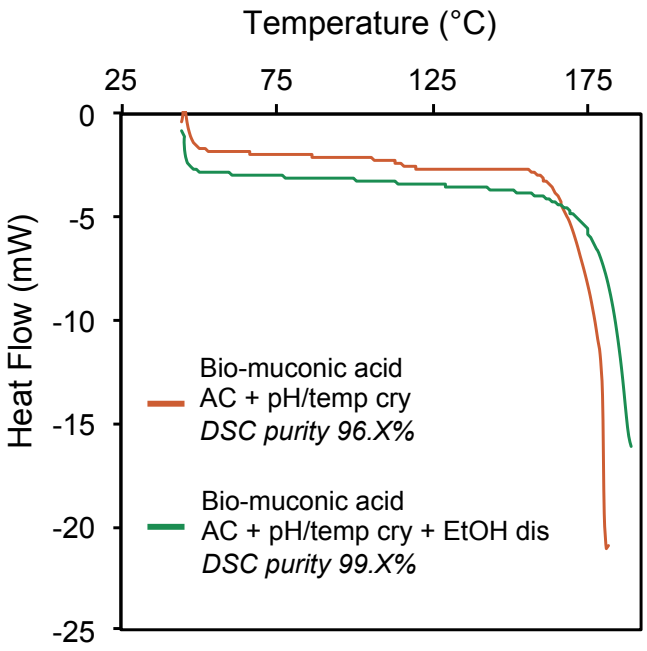

Figure 5.3. DSC purity analysis of bio-muconic acid after sequential treatment. Muconic acid was produced from the fed-batch fermentation of benzoate and subsequently treated with activated carbon (AC) to remove organic impurities from the broth. Muconic acid was then precipitated from solution by pH/temperature shift crystallization (pH/temp cry), resulting in a crystal purity of 97.86% by DSC melting point analysis. Subsequently, the recovered muconic acid crystals were dissolved in ethanol (EtOH dis) to precipitate inorganic salts, resulting in a crystal purity of 99.76% by DSC melting point analysis.

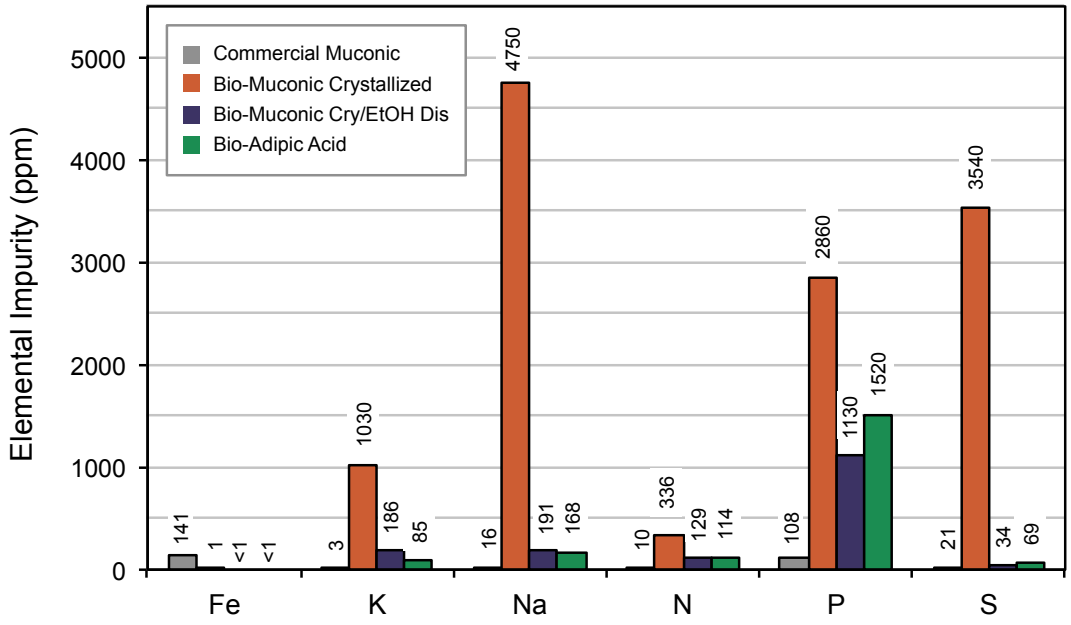

Figure 5.4. Elemental impurities present at >100 ppm in commercial muconic acid (chemical origin), biologically derived muconic acid following crystallization, biologically derived muconic acid following crystallization and ethanol dissolution (Cry/EtOH Dis), and biological derived adipic acid produced from muconic acid hydrogenation. A full listing of screened elements provided in **Table 5.3.** Due to the large sample requirements for trace analysis, only single batch samples were analyzed.

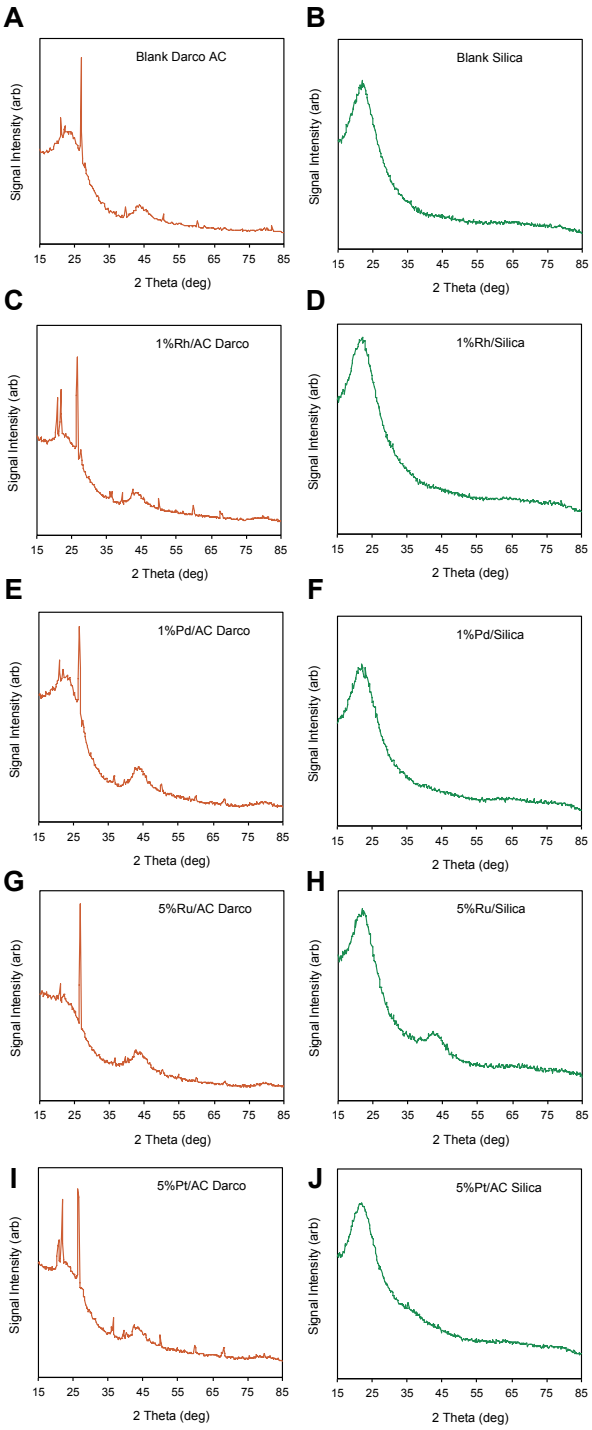

Figure 5.5. XRD spectra of virgin catalysts used for batch reactor screening experiments. XRD spectra were collected after metal loading and catalyst reduction. Spectra were also provided for blank powdered silica and activated carbon supports for reference (A, B).

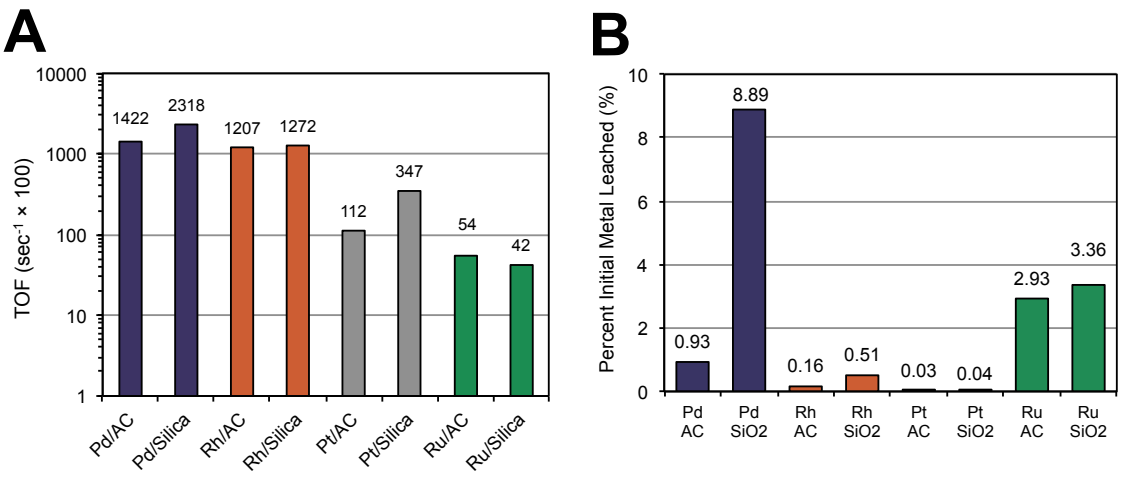

Figure 5.6. Muconic acid hydrogenation activity for platinum group metals (PGM) on powder activated carbon and silica supports in batch (A), and PGM leaching after 35 min exposure to reaction conditions (B). Reaction conditions were as follows: muconic acid 1 wt% in ethanol, temperature 24°C, H_2 pressure 24 bar, catalyst loading 15 mg, stirring 1600 rpm. Reactions were performed in a minimum of duplicate reactors. Turn over frequencies (TOF) were calculated based on pseudo-first order rate constants fitted for duplicate reactions, with moles reacted after 10% conversion and metal crystallite active surface area determined by chemisorption. Error bars indicate TOF standard deviation. Metal leaching was based on a single leaching measurement from combined solutions of duplicate reactors.

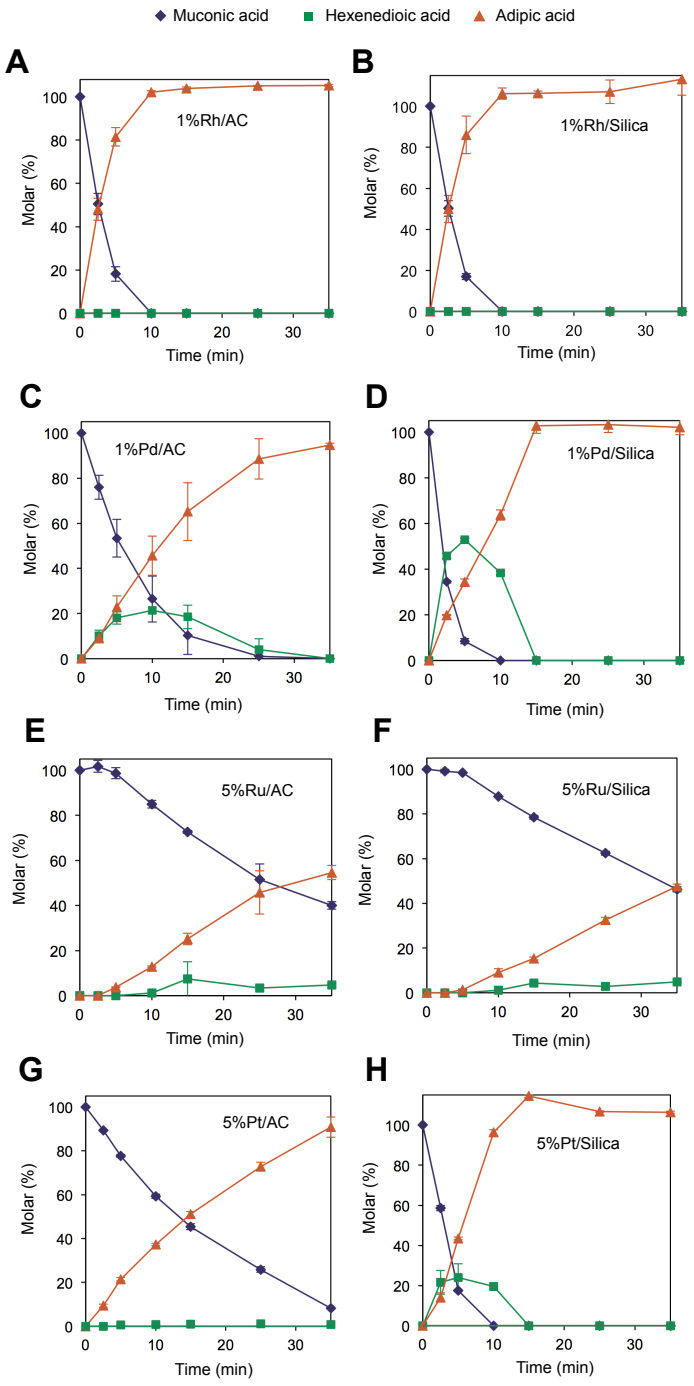

Figure 5.7 Batch reactor catalyst activity screening for muconic acid hydrogenation. Reactions were performed in a minimum of duplicate batch reactors, with error bars indicating standard deviations. Typical mass closure was ±10%. Reaction conditions were as follows: temperature 24°C, muconic acid 200 mg, catalyst loading 15 mg, H_2 pressure 24 bar, EtOH solvent 19.8 g.

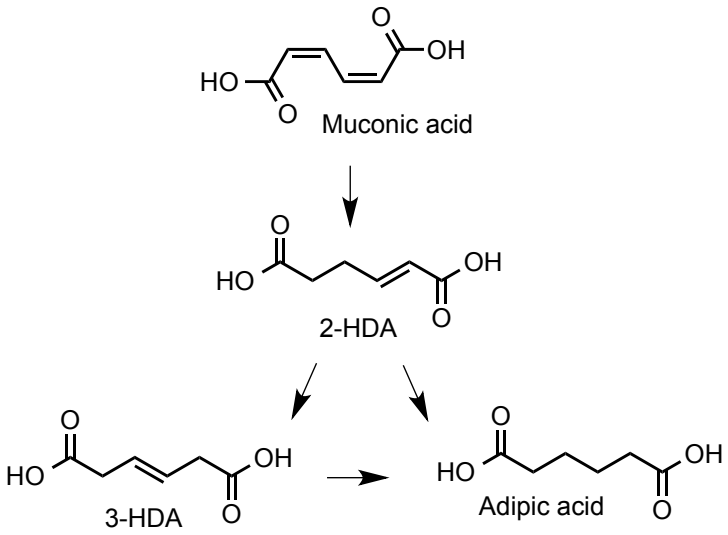

Figure 5.8. Reaction network for the hydrogenation of muconic acid via the intermediate hexenedioic acid (HDA) to produce adipic acid. For room temperature batch reactions, 2-HDA was the primary intermediate, while for higher temperature (≥50°C) 3-HDA was observed as the primary intermediate.

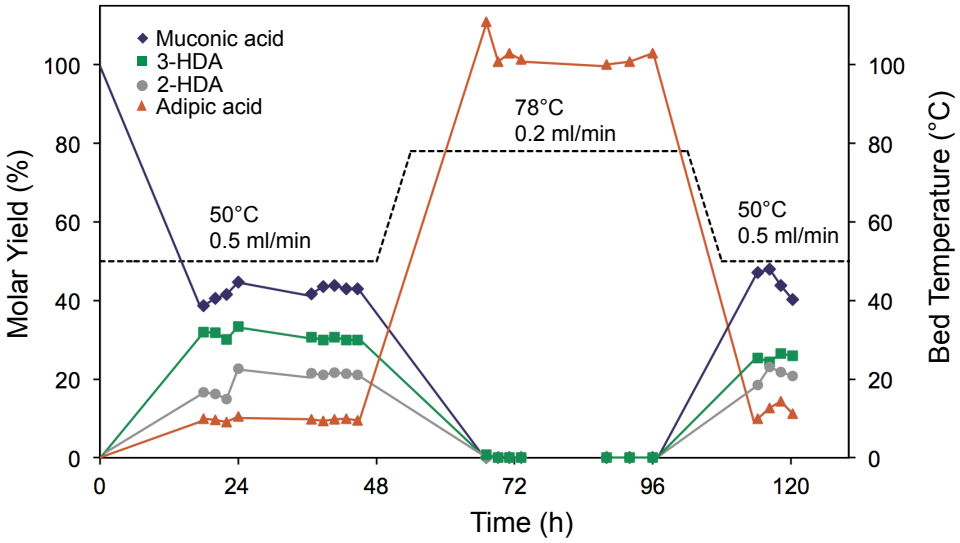

Figure 5.9. Product molar yields, catalyst bed temperature, and liquid feed rate during the 100-h time-on-stream stability test of 1%Rh/AC for muconic acid hydrogenation. Reaction conditions were as follows: muconic acid 1 wt% in ethanol, temperature and liquid flow rate as indicated, H_2 200 sccm at 24 bar, catalyst loading 1100 mg.

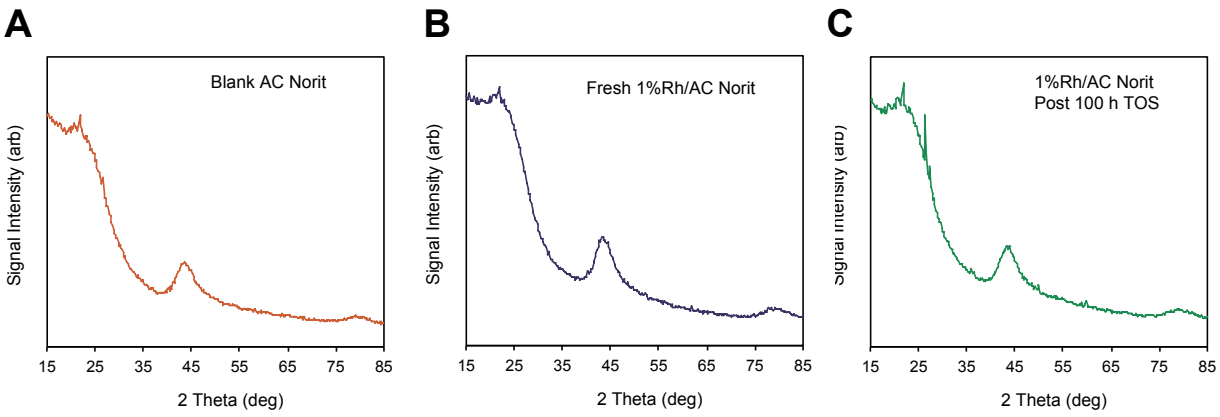

Figure 5.10. XRD spectra of blank AC support and 1% Rh/AC catalyst granules used for the trickle bed hydrogenation of muconic acid. Major XRD peaks for rhodium occur at 2θ values of 40.99°, 47.83°, 69.58°, and 84.10°. Spectra of the blank Norit activated carbon granule support provided for comparison (A). The virgin catalyst spectra was collected after metal loading and reduction (B), while the post reaction catalyst was collected after > 100 h time-on-stream testing (C).

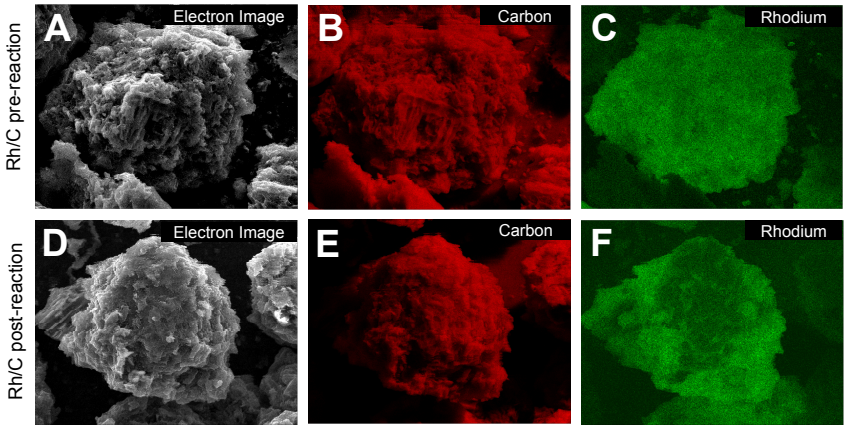

Figure 5.11. Characterization by SEM-EDS of the virgin (A-C) and post-reaction (D-F) 1% Rh/AC granule catalyst used in the 100-h time-on-stream stability test for muconic acid hydrogenation.

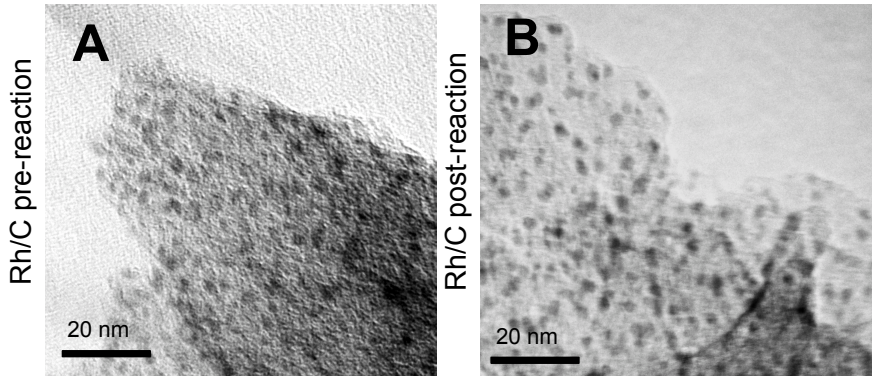

Figure 5.12. Characterization by TEM of the virgin and post-reaction 1% Rh/AC granule catalyst used in the 100-h time-on-stream stability test for muconic acid hydrogenation.

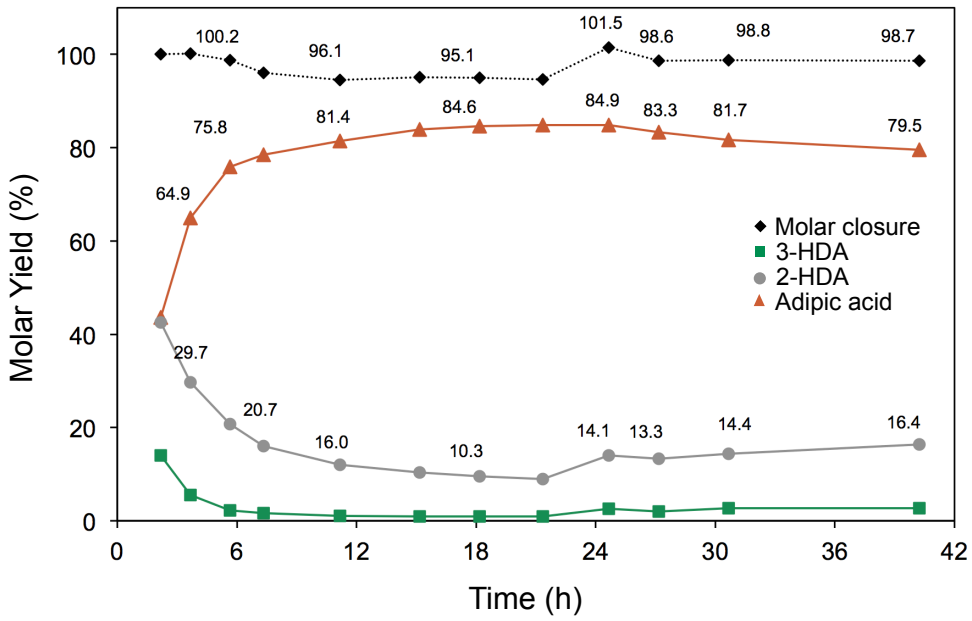

Figure 5.13. Preliminary trickle bed reactor run with 1%Pd/AC granules, demonstrating ~12 h to reach stead-state activity. Reaction conditions were as follows: muconic acid 1 wt% in ethanol, liquid flow rate 0.5 mL/min, catalyst bed temperature 72°C, H_2 200 sccm at 24 bar, and catalyst loading 200 mg 1%Pd/AC granules.

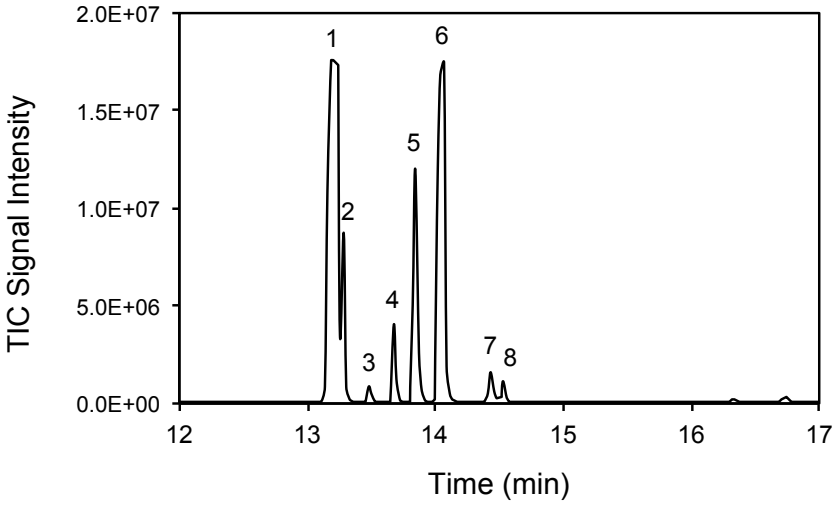

Figure 5.14. GC-MS TIC of methylated acids produced during the trickle bed hydrogenation of muconic acid at partial conversion conditions. Identified compounds are listed in Table S1. Reaction conditions were as follows: muconic acid 1 wt% in ethanol, liquid flow rate 0.5 mL/min, temperature 50°C, H_2 200 sccm at 24 bar, and catalyst loading 1100 mg 1% Rh/AC granules.

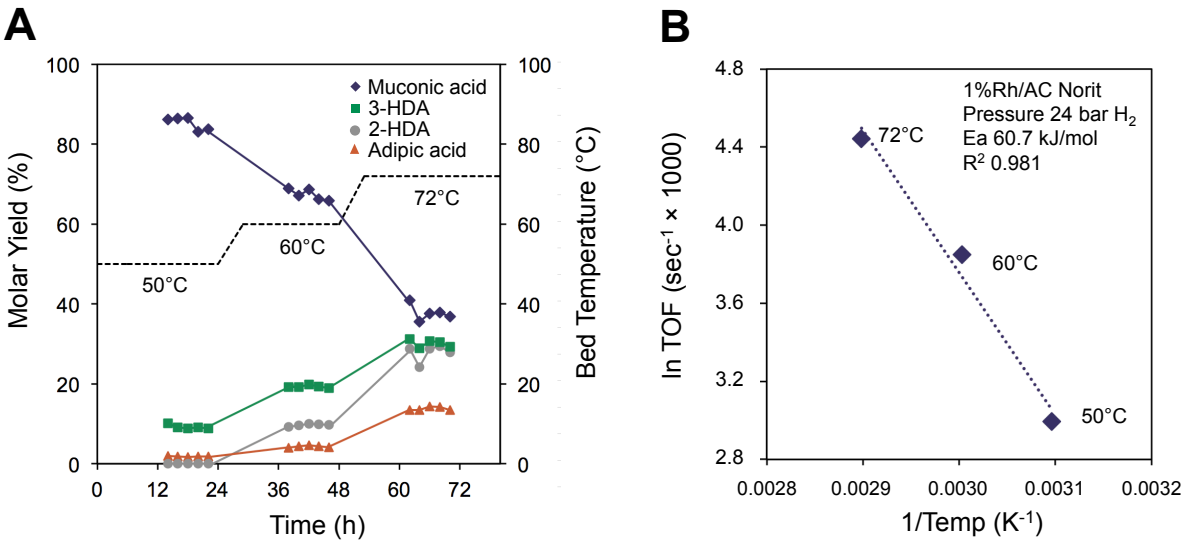

Figure 5.15. Influence of catalyst bed temperature during the trickle bed hydrogenation of muconic acid with 1% Rh/AC granules. Product distribution with varying reaction temperature (A). Apparent activation energy for the hydrogenation of muconic acid based on the Arrhenius equation (B). Reaction conditions were as follows: muconic acid 1 wt% in ethanol, liquid flow rate 0.5 mL/min, temperature as indicated, H_2 200 sccm at 24 bar, and catalyst loading 300 mg.

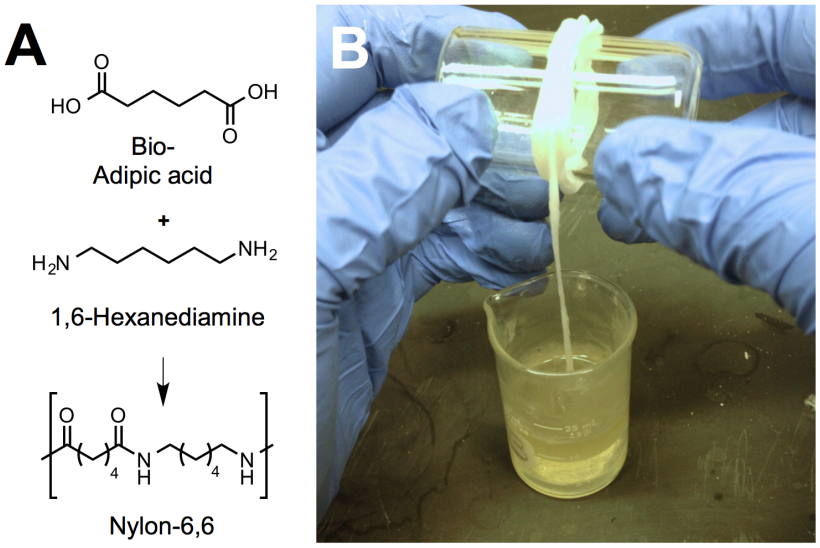

Figure 5.16. Polymerization scheme for reacting bio-adipic acid with 1,6-hexanediamine to produce Nylon-6,6 (A). Nylon "rope trick" using bio-adipic acid produced from the catalytic hydrogenation of muconic acid (B). Adipic acid was initially reacted with thionyl chloride and dissolved to cyclohexane, prior to adding the solution to a basic 1,6-hexanediamine aqueous solution. Nylon "rope" was then pulled from the biphasic solution interface for subsequent characterization.

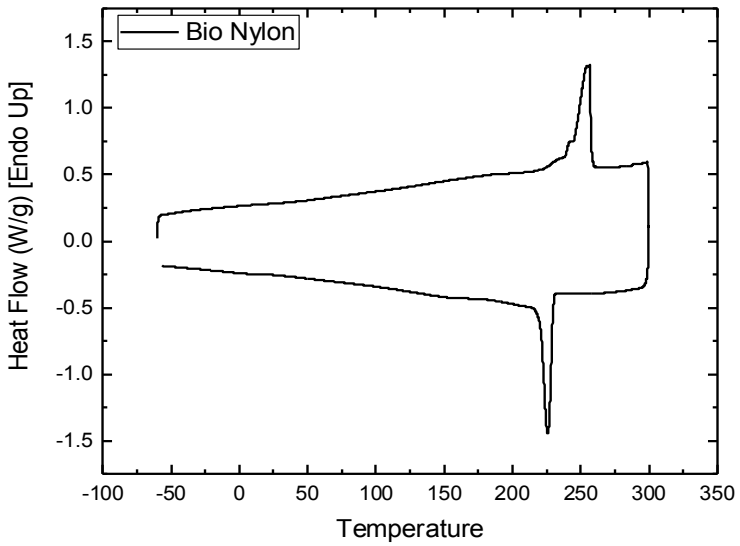

Figure 5.17. DSC thermal analysis of nylon-6,6 produced from biologically derived adipic acid. The polymer was scanned from -60°C to 200 °C at a rate of 10 °C/minute.

Table 5.1. Purity requirements for polymer-grade adipic acid specified by Radici group.

Polymer-Grade Adipic Acid	Specification
Purity	99.8% min
Total N	20 ppm max
Iron	0.2 ppm max
Crystallization	152 +/- 0.5 °C
Moisture	0.2% max

Table 5.2. Purity of commercial muconic acid (chemical origin) and biologically derived muconic acid after sequential treatment.

Sample Origin	AC Treated	pH 2 Crystallized	EtOH Dissolved	Purity (%)
Commercial Chemical	N	N	N	97.83 ± 0.07%
Biological Conversion	Y	Y	N	97.86 ± 0.05%
Biological Conversion	Y	Y	Y	99.76 ± 0.04%

[a]Standard deviation values reported for triplicate sample measurements.

Table 5.3. Elemental impurities screened by ICP-MS in muconic acid of chemical and biological origin, as well as in adipic acid produced from the catalytic hydrogenation of muconic acid.

Elemental Impurity	Commercial Muconic Acid *(chemical origin)*	Crystallized Muconic Acid *(biological origin)*	EtOH Dissolved Muconic Acid *(biological origin)*	Bio-Adipic Acid *(muconic derived)*
Al	11	10	5	8
Ca	42	5	4	6
Cl	<10	34	<10	<10
Cu	0.2	<0.1	<0.1	0.1
Fe	141	1	<1	<1
K	3	1030	186	85
Mg	7	21	4	1
Mn	0.1	<0.1	<0.1	0.1
Na	16	16	191	168
N	10	336	129	114
P		2860	1130	1520
S	21	3540	34	69
Si	10	10	<10	<10

Table 5.4. Properties of virgin activated carbon (AC) and silica powdered catalysts used in batch screening reactions for muconic acid hydrogenation.

Catalyst (nominal)	S_{BET} ($m^2\ g^{-1}$)	Pore vol. [a] ($cm^3\ g^{-1}$)	Pore dia. [a] (Å)	Dispersion [b] (%)
1% Pd/AC	768	0.514	9.71	13
1% Rh/AC	971	0.708	9.83	69
5% Ru/AC	590	0.588	9.69	10
5% Pt/AC	882	0.657	9.71	60
1% Pd/SiO_2	466	0.774	9.74	28
1% Rh/SiO_2	480	0.804	9.81	62
5% Ru/SiO_2	428	0.686	9.75	17
5% Pt/SiO_2	454	0.811	9.79	47

[a]Pore volume and average micropore diameter determined by BJH adsorption. [b]Dispersion calculated based on chemisorption and ICP measured metal loading.

Table 5.5. Properties of virgin and post-reaction 1%Rh/AC granule catalyst used in the 100-h time-on-stream stability test for muconic acid hydrogenation.

Catalyst (nominal)	ICP (%)	S_{BET} (m^2 g^{-1})	Pore vol. [a] (cm^3 g^{-1})	Pore dia. [a] (Å)	Dispersion [b] (%)
Virgin 1% Rh/AC	0.8	1029	0.46	9.69	14%
Post Reaction 1% Rh/AC	0.9	1130	0.52	11.43	21%

[a] Pore volume and pore diameter (average) determined by BJH desorption. [b] Dispersion calculated based on chemisorption and ICP measured metal loading.

Table 5.6. Volatile components identified by GC-MS for the trickle bed hydrogenation of muconic acid under partial conversion conditions.[a] Compounds were methylated prior to analysis.

Peak No.	Ret. Time (min)	Compound Identified
1	13.22	Dimethyl Adipate
2	13.31	Dimethyl 2-Hexenedioate (Z)
3	13.51	Dimethyl Muconate
4	13.70	Dimethyl 3-Hexenedioate (Z)
5	13.87	Dimethyl 3-Hexenedioate (E)
6	14.09	Dimethyl 2-Hexenedioate (E)
7	14.46	Dimethyl Hexanedioate, 3-Methoxy
8	14.56	Dimethyl Muconate

[a]Reaction conditions were as follows: Muconic acid 1 wt% in ethanol, liquid flow rate 0.5 mL/min, 50°C, H_2 flow 200 sccm, system pressure 24 bar, 300 mg 1% Rh/AC granules.

Table 5.7. Time-on-stream results for the trickle bed hydrogenation of muconic acid.[a] Compounds were monitored by HPLC-RID.

Time (h)	Temp (°C)	Liq. flow (mL/min)	Muconic (g/L)	2-HDA (g/L)	3-HDA (g/L)	Adipic (g/L)
18	50	0.5	2.98	1.30	2.50	0.79
20	50	0.5	3.12	1.26	2.48	0.77
22	50	0.5	3.20	1.16	2.35	0.72
24	50	0.5	3.44	1.78	2.60	0.83
37	50	0.5	3.21	1.68	2.40	0.78
39	50	0.5	3.36	1.64	2.34	0.74
41	50	0.5	3.38	1.69	2.40	0.77
43	50	0.5	3.31	1.67	2.34	0.79
45	50	0.5	3.31	1.65	2.34	0.75
67	78	0.2	0.00	0.00	0.00	8.78
69	78	0.2	0.00	0.00	0.00	7.97
71	78	0.2	0.00	0.00	0.00	8.14
73	78	0.2	0.00	0.00	0.00	8.02
88	78	0.2	0.00	0.00	0.00	7.92
92	78	0.2	0.00	0.00	0.00	7.97
96	78	0.2	0.00	0.00	0.00	8.14
114	50	0.5	3.63	1.45	1.99	0.78
116	50	0.5	3.70	1.80	1.91	1.00
118	50	0.5	3.38	1.71	2.07	1.14
120	50	0.5	3.10	1.63	2.03	0.89

[a]Reaction conditions were as follows: Muconic acid 1 wt% in ethanol, liquid flow rate and temperature as indicated, H_2 flow 200 sccm, system pressure 24 bar, 1100 mg 1% Rh/AC granules.

Table 5.8. Properties of nylon-6,6 produced using commercial adipic acid of chemical origin and bio-adipic acid generated in this work from the catalytic hydrogenation of muconic acid.

Nylon-6,6 Properties	Adipic Acid *Chemical*	Adipic Acid *Biological*	Literature for Nylon-6,6
Melting Temp (°C)	258	264	262[55]
Glass Transition (°C)[a]	55	46	50[55]
Heat of fusion (J/g)	37.8	50.2	51.3[56]
Crystallinity (%)	19.9	26.4	27.0[55]
Intrinsic Viscosity (mL/g)[b]	26.5 ± 0.9	24.1 ± 0.6	79-174[57]
Viscosity Avg. MW (g/mol)[b]	2,230 ± 40	1,920 ± 20	40,000-60,000[57]

[a]T_g determined from literature for 27% crystallinity and is known to vary. [b]Standard deviation values reported for four solutions tested in triplicate.

CHAPTER 6

PRELIMINARY TECHNO-ECONOMIC ANALYSIS FOR THE DOWNSTREAM PROCESSING OF BIO-BASED MUCONIC ACID TO ADIPIC ACID

6.1 Abstract

Adipic acid is the most widely manufactured dicarboxylic acid derived from petroleum, with significant potential for renewable production from lignocellulosic biomass via integrated biological and chemo-catalytic processing. However, downstream processing of biologically derived acids can represent over half of the final product cost, requiring identification and reduction of key cost drivers. To that end, this study presents a techno-economic analysis for the downstream separation and catalytic hydrogenation of bio-based muconic acid to adipic acid. The technical basis for the model is as follows: For the base-case downstream plant design, an n^{th}-generation plant was modeled to produce 75 million kg of adipic acid per year. Cell-free broth, containing 50 g/L muconate and 2 g/L non-target of aromatic compounds, was initially treated with activated carbon to achieve a muconate organic purity of >99%. Muconic acid was then separated by low temperature/pH crystallization, followed by rotary filtration and drying to recover 93% of muconic acid post-purification. Crystallized muconic acid was dissolved in ethanol to precipitate inorganic Na_2SO_4, and muconic acid was catalytically converted to adipic acid in trickle bed reactor packed with 2%Rh/C, operating at 350 psig and 75°C. The hydrogenation yield was assumed to be nearly quantitative, with a reactor weight hourly space velocity (WHSV) of 5 h^{-1}. To recover adipic acid, a second train of evaporative crystallization with rotary filtration and drying was modeled, with an adipic acid recovery of 98%. For the base-case design, discounted cash flow rate of return analysis predicts a minimum selling price (MSP)

of $1.90/kg (2014 USD) for bio-adipic acid, within the historical range for petro-derived adipic acid ($1.75-2.50/kg). Single point sensitivity analysis was then performed to determine the impact associated with inaccuracy in total equipment capital cost (± 50%), incoming muconate broth cost ($0.90-1.70/kg dissolved muconate), muconate titer (20-100 g/L muconic acid), level of non-target aromatics (0.5-10 g/L non-target aromatics), and hydrogenation reactor throughput (WHSV 0.6-10 h^{-1}). In addition, bivariate analysis was performed to determine the joint impact of broth price and broth titer on the adipic acid MSP. Overall, multiple process scenarios were identified that result in an adipic acid MSP of < $2.50/kg, demonstrating the potential for economically competitive pathways for renewable adipic acid production.

6.2 Introduction

Integrated biological and chemo-catalytic processing of lignocellulosic biomass holds significant potential for displacing fuels and chemicals derived from petroleum.[1–6] Recent analysis of next-generation biorefineries has shown that by targeting value-added chemicals, in addition to fuels, premiums can result that help offset the economic cost and environmental impact of renewable fuel production.[7] Advances in biotechnology have greatly expanded the slate of molecules that can be produced by engineered microorganisms,[8–10] with subsequent separation and catalytic processing steps under development to diversify applicable markets and product applications.[11–13] *cis,cis*-Muconic acid is one such promising biologically-derived molecule that can be catalytically hydrogenated to adipic acid, the latter molecule being the most widely manufactured dicarboxylic acid derived from petroleum.

Adipic acid currently has a global market of ~2.5 billion kg per year, with the primary application as a nylon-6,6 precursor, consuming 85% of production.[14,15] The market price of

adipic acid has varied significantly, ranging from ~$1.75-2.50/kg, due to its dependence on petroleum. Applications for adipic acid are expected to grow, including use for polyesters and polyurethanes, and as an additive in pharmaceuticals, cosmetics, and agrochemicals.[14,15] However, conventional adipic acid production is conducted via nitric acid oxidation of cyclohexanone and cyclohexanol, which generates significant NO_x emissions and depends on volatile petroleum markets. As a result, alternative "green" pathways are being examined for the production of adipic acid,[14,16–19] including through the production of muconic acid as a bio-derived precursor.[15,20–23]

Muconic acid can be produced extracellularly with engineered organisms using multiple substrates, including glucose[24] and lignin-derived aromatics,[3] as shown in **Figure 6.1**. The potential to produce muconate from non-food feedstocks, particularly lignocellulosic biomass, has been proposed to have significant environmental and economic promise.[25,26] Glucose is converted to muconic acid by rerouting aromatic amino acid synthesis pathways, with demonstrated molar yields of 22-30%,[24,27] and theoretical yields, depending on the metabolic pathway, ranging from 69-86%.[28] However, as noted above, the high price and societal impacts of utilizing glucose derived from food resources will likely necessitate utilization of cellulose-derived sugars, which have been estimated at $0.39/kg.[15] Based on this value and theoretical molar yields, the cost of glucose derived substrate could potentially range between $0.57-0.72 per kg of muconic acid (**Table 6.1**).

In comparison, small MW oxygenated aromatics derived from lignin depolymerization, such as *p*-coumarate, ferulate, catechol, and phenol, can also be used as starting substrates for muconic acid. These oxygenated aromatics can be routed through the β-ketoadipate pathway, with demonstrated muconate molar yields ranging from 14 to ≤100% that vary significantly

depending on the substrate and cultivation conditions. For aromatic catabolism, theoretical muconic acid molar yields are 100% from ring opened monomers.[3,29,30] Furthermore, the cost of using lignin as a substrate for aromatic monomers has been estimated at $0.17/kg.[15] Based on this value and theoretical molar yields, the cost of lignin derived substrate could potentially range between $0.11-0.20 per kg of muconic acid (**Table 6.1**). High broth titers with oxygenated aromatics have also been demonstrated during fed-batch biological conversion, including 13.5 g/L from *p*-coumarate [3], 44.0 g/L from benzoate [29], and 59.0 g/L from catechol.[30] Efforts to improve muconate yields, titers, and productivities are ongoing through both metabolic pathway optimization,[31–35] bioreactor engineering,[27,36,37] and co-optimization of the upstream lignin isolation/conditioning strategies and microbial host selection.

Despite the significant potential for the producing muconic acid from sugars, aromatic compounds, and other renewable feedstocks, the downstream processing costs for biologically derived acids can account for over half of the final product cost.[38,39] Recently, our group demonstrated bench-scale fed-batch biological conversion of *p*-coumarate to muconic acid, followed by activated carbon purification, low pH/temperature crystallization, and catalytic hydrogenation to adipic acid.[3] Despite the technical feasibility of this approach, the downstream economic prospects remain speculative. Early-stage techno-economic analysis can potentially provide key insight into major cost drivers and energy consumptive processes, as well as identifying targets for future technology development.[40] As such, this study presents a techno-economic analysis focused on the downstream separation and catalytic hydrogenation of biologically derived muconic acid to adipic acid.

6.3 Results and Discussion

6.3.1 Base case process model

In order to evaluate the economic viability of renewable adipic acid production via muconic acid as an intermediate, an n^{th}-generation plant was modeled to produce 75 million kg of adipic acid per year. For this work, boundary conditions excluded upstream biomass deconstruction and biological conversion processes due to the rapid and ongoing efforts with both sugar and lignin-derived feedstocks, as noted above. Cell free muconic acid culture media was assumed to contain 50 g/L muconate and 2 g/L non-target aromatic metabolites, requiring an incoming broth flow rate of 208,392 L/h. Cooling needs for downstream plant operations were supplied with freshwater (incoming 28°C, with 9°C rise) and chill water (incoming 7°C, with 5°C rise), depending on the required final temperature. Heat loads were supplied with medium pressure steam (216°C, 300 psig). The process model was divided into two sections, Area 100 and Area 200 (**Figure 6.2**), with their respective design bases and performance assumptions summarized in **Table 6.2**.

Area 100 of the process model focused on purification and recovery of muconic acid from biological conversion broth. Muconate broth was purified over parallel activated carbon treatment beds to remove non-target aromatic impurities and achieve a final purity of 99% on a dissolved organics basis, with a safety factor of 1.2 (final purity >99%). Based on an assumed activated carbon adsorption capacity of 0.10 g/g_{AC} for muconic acid and 0.15 g/g_{AC} for aromatics, 7.2% of muconic acid was lost during treatment due to non-specific adsorption. Spent activated carbon from purification was thermally regenerated onsite by kiln combustion due to the high boiling point of adsorbed organics. During regeneration, it was assumed that 5% of activated carbon was lost per combustion cycle [41].

After purification, low pH and low temperature crystallization was employed to recover muconic acid based on a solubility of 3.5 g/L at pH 2 and 10°C. Concentrated sulfuric acid was used for pH adjustment, producing Na_2SO_4 (2 g of Na_2SO_4 per 1 g of muconic acid solid) that co-crystallized at a solubility limit of 82.8 g/L at 10°C.[42] Rotary filtration and rotary drying was then employed to recover mixed solid crystals, with the filter broth effluent treated as wastewater. Mixed solid crystals were added to ethanol in a heated stirred tank at 70°C to dissolve muconic acid to a level of 100 g/L, while insoluble Na_2SO_4 was separated by rotary filtration and treated as solid waste. Following purification, the net recovery of muconic acid was 92.8%.

Area 200 of the model focused on the purification and catalytic conversion of muconic acid to adipic acid, with subsequent product recovery. Muconic acid in ethanol was initially pressurized to 350 psig using a positive-displacement pump for feeding to the reactor. On site hydrogen was supplied at ambient temperature and pressure, requiring a 3-stage compression train with inter-stage cooling to deliver hydrogen at 350 psig, with a 10:1 molar flow ratio to muconic acid. Muconic acid, ethanol, and hydrogen were mixed and introduced to a trickle bed reactor operating at 70°C with a weight hour space velocity (WHSV), defined as the weight of liquid solution processed per hour divided by the weight of catalyst material, of 5 h^{-1}. Hydrogenation of muconic acid was assumed to be quantitative over a 2% Rh/C catalyst, with adipic acid as the only product. The catalyst was assumed to be stable during operation, requiring $1/5^{th}$ of the bed to be regenerated every year at a cost of $40/kg of catalyst, with an assumed 3% precious metal loss.

Following hydrogenation, adipic acid was recovered from solution by ethanol evaporation and crystallization. The stream of adipic acid in ethanol exiting the reactor was

mixed with the crystallizer recycle stream and concentrated to 360 g/L at 82°C, below the adipic acid/ethanol solubility limit of 363 g/L at 60°C.[43] The solution was then cooled to 10°C to partially crystallize adipic acid based on a solubility limit of ~67 g/L at 10°C,[43] with the remaining solution recycled to the inlet of the evaporator. Rotary filtration and drying was then employed to dry crystals, with an assumed net adipic acid recovery of 98% post-hydrogenation.

6.3.2 Installed equipment costs

Based on the base-case model design scenario, capital equipment costs with installation were estimated, as shown in **Figure 6.3A,** with detailed equipment design bases, materials of construction, and installation factors described in the **Supplementary Information**. Installed equipment costs totaled to $57.4E6, with the largest contributors being the activated carbon regeneration kilns in Area 100 and the packed hydrogenation reactor in Area 200.

In Area 100, the cost of onsite kilns to regenerate spent activated carbon ($14.6E6) was primarily a function of the concentration of non-target aromatics in the incoming broth media. Non-target aromatics can result from incomplete conversion of lignin-derived aromatic substrates, as well as from buildup of upstream metabolic intermediates prior to muconic acid, such as protocatechuate and 4-hydroxybenzoate.[3] During fed-batch bioconversion, controlled substrate feeding based on broth pH or dissolved oxygen levels has been shown to effectively prevent buildup of model feed compounds,[3,36,37] but significant work remains to demonstrate this approach with mixed hydrolyzate sugars and aromatic monomers obtained from biomass depolymerization. Likewise, engineered enhancement of metabolic bottlenecks holds promise for alleviating the buildup of upstream aromatic intermediates.

It should be emphasized that high purity muconic acid will likely be a key requirement for meeting the stringent specification of polymer-grade adipic acid (**Table 6.3**).[44] As noted, 85% of adipic acid is used for nylon-6,6 production, making separation and purification a key consideration. Numerous alternative strategies to recover dicarboxylic acids are in varying stages of development and industrial readiness, including carboxylate absorption and adsorption, reactive extraction, electrochemical crystallization, electrodialysis, membrane filtration, ion exchange, chromatography, and reactive distillation to name a few;[39,45–50] however, economic analysis of these technologies was beyond the scope of this study.

In Area 200, the largest capital investment was the packed bed catalytic reactor ($16.9E6), primarily due to the use of 2% Rh/C as the catalyst, which represented 76% of the installed cost. Bench-scale experimentation by our group has been shown the Rh/C is highly active and stable during continuous catalytic conversion of muconic acid. The high catalytic activity of Rh can allow for high process flow rates (WHSV of 5 h^{-1} assumed for this study), greatly reducing the size and capital requirements of reactor components. However, Rh is one of the most expensive platinum group metals, with an average price in 2014 of $37.78/g, compared to Ru at $2.09/g, Pd at $26.08/g, and Pt at $44.66/k).[51] As such, this provides significant motivation for exploring non-platinum group metals that are highly active and stable under acidic liquid-phase conditions.[52] Activated carbon was chosen as the metal support due its known stability and relatively low cost (~$0.50-3.00/kg) under liquid-phase catalytic conditions.

Hydrogen compression also represented a significant capital cost ($4.2E6) due to the high pressure employed (375 psig) and need for gas recycle. High hydrogen pressures can be necessary at industrial process scales due to mass transfer limitations which result when dissolved hydrogen is depleted in the condensed phase,[53] limiting the potential for significant

capital reduction with conventional packed bed reactor configurations. Alternative reactor configurations have been examined for catalytic hydrogenation, including inorganic membrane doped with catalytic sites to facilitate hydrogen mass transfer,[54] immobilized enzyme transfer hydrogenation,[55] and electrochemical reduction under mild reaction conditions,[56] but similar to the alternative separation strategies listed above, their technological readiness and economic impacts were beyond the scope of this study.

Crystallization in Area 100 ($5.2E6) and Area 200 ($5.4E6) also contributed significantly to the capital cost. As noted, the solubility of muconic acid in water is highly sensitive to pH due to protonation/deprotonation, providing a facile option for recovery through pH-shift crystallization at low temperature; however, aromatic acids derived from lignin depolymerization (e.g., *p*-coumaric acid) are also highly susceptible to crystallization at low pH, necessitating upstream purification. Trace impurities can greatly impact crystallization performance of biologically derived compounds,[57,58] requiring a stable stream composition for optimum continuous performance. Na_2SO_4 produced during pH adjustment of muconate was also assumed to partially co-precipitate due to its low solubility at 10°C (82.8 g/L),[42] requiring dissolution in ethanol for selective removal. Insoluble Na_2SO_4 was removed and prepared for disposal by rotary filtration ($3.1E6) and drying ($1.0E6). Lastly, temperature-shift crystallization was employed for adipic acid recovery, similar to the approach with petrol-derived adipic acid.(*54*) Adipic acid displays a near exponential solubility in alcohols and water,[43] providing a facile recovery method at low temperature. Lastly, a second train of rotary filtration ($0.6E6) and drying ($0.8E6) was incorporated to produce dry adipic acid as the final product.

6.3.3 Variable operating costs

Annual operating expenses were estimated based on process requirements and demands from installed equipment, as shown in **Figure 6.3B**. Excluding labor and overhead (**Table 6.4**), operational expenses totaled to $118.6E6/y, with unit cost parameters and consumption rates summarized in **Table 6.5**. By far the most significant operational expense was the incoming muconate culture media, with an assumed unit cost of $1.00/kg of dissolved muconic acid. The cost of muconic acid broth is highly dependent on a number of factors, including initial substrate costs (e.g., glucose, lignin-derived aromatics), biological productivity, titer, bioreactor configuration, media sterilization, broth neutralization, and cell removal.[7,47] As noted, cost estimates for consumables that impact broth cost include aromatic substrate, reported at $0.17/kg [15] and NaOH at $0.21/kg ($0.18/kg 2013 USD).[7] In comparison, costs for succinic acid in culture broth, a dicarboxylic acid derived from glucose, have been estimated at $0.69/kg ($0.66/kg 2013 USD).[46] To address the economic implications of broth cost uncertainty, a range of values ($0.90-$1.70/kg) were evaluated, as described in the **Model Sensitivity Analysis** section below.

In Area 100, several operational costs were of comparable magnitude, including sulfuric acid ($6.8E6) and chill water ($5.6E6) to lower the pH and temperature during muconic acid crystallization, waste treatment ($3.2E6) to dispose of post-crystallization broth and Na_2SO_4, and make-up ethanol ($4.3E6) due to losses during muconic acid dissolution and Na_2SO_4 drying (ethanol recovery assumed to be 98%). Ethanol was chosen as a solvent since it displays near-exponential temperature solubility dependence with dicarboxylic acids,[43,59] while being sparingly soluble with salts.[60] Further, ethanol can be derived from renewable resources and it displays a greatly reduced specific heat capacity compared to water. In contrast, the production of Na_2SO_4 as a waste product is a well-known problem for biological conversion processes that require pH control.[61,62] Alternative neutralization agents, such as ammonia, have been evaluated due to the

potential recovery of labile ammonia.[61,62] Alternatively, electrochemical methods can be used to regenerate free acid and base for recycle,[48] but the associated energy costs and scalability require further evaluation.

It should be noted that in Area 100, evaporative concentration of muconic acid prior to crystallization was also evaluated for the base-case model to improve muconic acid recovery yields; however, the high heat duty for the evaporator, subsequent increased cooling demand, and increase in Na_2SO_4 filtration and solid waste disposal costs made pre-concentration cost prohibitive.

In Area 200, several operational costs were also of comparable magnitude, including hydrogen ($3.1E6), electricity ($2.4E6), freshwater ($3.3E6), steam ($2.6E6), and chill water ($2.0E6). Hydrogen was consumed during the quantitative catalytic conversion of muconic acid to adipic, with stoichiometry of 2:1. The primary consumption of electricity was due to hydrogen recompression during recycle, which required 3.3 MW of electricity. Reductions in hydrogen pressure and fluid temperature were necessary to facilitate gas-liquid separation after exiting the reactor, resulting in significant freshwater demand for cooling (11.0 MW). Efforts to minimize excess hydrogen requirements during the reaction, while still facilitating high conversion and substrate flow rates, have the potential to greatly reduce associated operational costs. Evaporative concentration of adipic acid in ethanol at 82°C required significant steam demand (19.8 MW) that may be provided within an integrated biorefinery through the combustion of a portion of lignin stream.[7] Lastly, crystallization of adipic acid at 10°C resulted in significant chill water demand (2.0 MW), in part due to the added volumetric throughput from recycle.

6.3.4 Minimum selling price for adipic acid

For the base-case design scenario described above, discounted case flow analysis determined a minimum selling price (MSP) of $1.90/kg of adipic acid, after accounting for remaining financial expenditures (e.g., fixed operational costs, indirect capital costs, working capital), with details provided in the Supplementary Information. Compared to the incoming muconate broth price of $1.00/kg, downstream processing added $0.90/kg to the MSP, representing 47% of the product cost, inline with other bioprocess derived chemicals.[38,39] Although early stage techno-economic analysis only provides an order of magnitude estimate of process costs,[63] the integrated biological and chemo-catalytic production of adipic acid shows potential for further development due to the parity with market prices for petroleum-derived adipic acid ($1.75-2.50/kg). Further research and development, as well as detailed evaluation of the environmental impact is warranted, with previous studies highlighting the potential for reductions in cumulative energy demand and greenhouse gas reductions compared to conventional adipic acid production.[7,15,64]

6.3.5 Model single point sensitivity analysis

To provide insight into the impact of base-case design assumptions on the MSP of adipic acid, single point sensitivity analysis of major process variables was performed, as shown in **Figure 6.4** and **Tables 6.6-6.7**. Design variables for sensitivity analysis included: (1) equipment capital expenditures, (2) incoming broth cost, (3) muconate titer in the initial broth, (4) concentration of non-target aromatic acids, (5) hydrogenation reactor weight hourly space velocity (WHSV), (6) catalyst cost, and (7) catalyst replacement frequency. Parameter values were varied independently to determine the impact on equipment capital and variable operating

expenses, with subsequent discounted cash flow rate of return analysis to calculate the new MSP of adipic acid.

For single point sensitivity analysis, errors in estimating the capital cost of equipment (±50%) had a minimal effect on the MSP of adipic acid. As noted, preliminary techno-economic analysis provides an order of magnitude estimate of equipment expenditures.[63] Even with capital equipment costs evaluated at -50% of the base case value, the MSP of adipic acid only decreased by $0.09/kg. Similarly, a +50% increase only raised the MSP by $0.09/kg. The impact of equipment costs on the MSP was relatively minor, primarily due to financing capital expenditures over the 30-year lifetime of the plant.

Varying the cost of incoming muconate broth resulted in a linear impact on the MSP of adipic acid, since it was assumed to be a fixed increase throughout the life of the plant. For each $0.10/kg increase in the incoming broth price, the MSP of adipic acid increased by $0.11/kg. As a noted, the initial substrate costs for biological conversion will likely account for a significant fraction of the broth cost, highlighting the potential for utilizing low-cost feedstocks, such as lignocellulosic biomass. In addition, significant environmental and societal benefits may be afforded through the use of next generation feedstocks that do not compete with food resources,[65,66] particularly with regards to lignin.[67]

Interestingly, varying the concentration of muconate in the incoming broth resulted in a nonlinear impact on the MSP of adipic acid. The nonlinearity was partially due to the assumed fixed concentration of non-target aromatics (2 g/L) during sensitivity analysis. Lower ratios of muconate-to-aromatics increased purification process demands, resulting in greater capital and operational expenses for activated carbon regeneration, as well as non-selective losses of muconate due to activated carbon adsorption. Increased incoming broth flow rates were also

necessary to maintain a fixed adipic acid output of 75 million kg per year, and muconic acid crystallization yields were reduced since recovery was a function of the broth titer compared to the solubility at 10°C and pH 2 (3.5 g/L). Likewise, muconate titers above the base-case design of 50 g/L resulted in decreasing improvements for the MSP. Even when the broth titer was doubled to 100 g/L, the MSP was only reduced by 5% from $1.90/kg to $1.80/kg. Yield improvements during purification and crystallization at high titers were less impactful, suggesting that a target titer of ≥50 g/L is desirable. This is promising from a state-of-technology perspective since comparable titers have been demonstrated values with model aromatic monomers (e.g., 44.0 g/L from benzoate,[29] 59.0 g/L from catechol[30]).

Varying the concentration of non-target aromatics in the incoming broth also had a significant impact on the MSP, and likely represents the most challenging technological hurdle for further development. Within the range of 1-10 g/L, each additional gram per liter of non-target aromatic compound added an average of $0.09/kg to the MSP, increasing in magnitude at higher concentrations. At non-target aromatic concentrations >8 g/L, the MSP of adipic acid exceeded the upper limit for the 5-year historical price range of petroleum-derived adipic acid. As noted, biological engineering efforts will be key to reduce non-target upstream metabolites while maintaining low levels of residual biomass-derived substrates during fed-batch cultivation. Alternative separation strategies for selective recovery of muconic acid may needed if biological advancements cannot overcome this challenge with complex feedstocks.

With regards to catalysis, varying the hydrogenation reactor throughput resulted in a nonlinear impact on the MSP. At reactor WHSVs less than 3 h^{-1} (weight of liquid solution processed per hour, divided by the weight of catalyst), the increase in MSP was increasingly pronounced, due to the inversely proportional change in reactor capital cost. As noted, the

hydrogenation reactor was the most costly piece of installed equipment ($16.7E6) due to the high cost of the 2% Rh/C catalyst. Lowering the WHSV by a factor of two effectively doubled the catalyst cost, which quickly impacted the MSP despite the offset of 30-year financing.

Varying the initial catalyst cost and replacement frequency also significantly impacted the MSP, depending on the reactor WHSV, as shown in **Table 6.6** and **Table 6.7**. For the base case reactor throughput (WHSV 5 h^{-1}), reductions in the catalyst cost showed a minor improvement in the MSP, even at $1/100^{th}$ of the initial catalyst price. Such a reduction would be expected if Rh was replaced with a low cost, earth abundant metal alternative. A similar trend was observed for catalyst replacement frequency. As noted, the short reactor residence time of the base case model masks potential MSP reductions due to the relatively low catalyst capital investment over the 30-year period. However, at slow reactor throughputs (e.g., WHSV 1 h^{-1}), the impact of catalyst cost and replacement frequency quickly becomes dramatic, as shown in **Table 6.6** and **6.7**. As such, additional catalyst performance validation efforts are to accurately assign catalyst reactor throughput values and stability lifetimes for muconic acid hydrogenation.

6.3.6 Bivariate sensitivity analysis for broth price and broth titer

Due to the joint impact of broth titer and broth cost on the MSP of adipic acid, bivariate analysis was performed to generate an adipic acid MSP surface response plot for both parameters, as shown in **Figure 6.5**. The broth price was varied from $0.60-$1.50/kg of muconate, while the broth titer was varied between 10-100 g/L of muconate. With regards to the broth price, increasing the price above the base-case design of $1.00/kg of muconate quickly reduced the acceptable range of titers that would provide an adipic acid MSP of less than $2.50/kg, resulting in a minimum broth titer of 40 g/L at the maximum broth price of $1.50/kg of

muconate. In contrast, reducing the broth price below the base-case design of $1.00/kg showed a negligible impact on the necessary titer, allowing for a minimum broth titer of ~20 g/L to maintain the adipic acid MSP below $2.50/kg.

With regards to broth titer, increasing the titer above 40 g/L for a given broth price showed a negligible impact on the adipic acid MSP. However, for titer values between 20-40 g/L of muconate, the codependence of broth titer and price was significant, requiring a narrower range of pair values to maintain the adipic acid MSP below $2.50/kg. Lastly, at broth titers below 18 g/L, the adipic acid MSP was above $2.50/kg for all broth price analyzed ($0.60-$1.50/kg of muconate), identifying a minimum titer value within this parameter space.

6.4 Conclusion

The integrated biological and chemo-catalytic production of adipic acid from muconic acid shows potential for being economically competitive with conventional adipic acid. Discounted cash flow analysis determined that for the base-case downstream process model, an adipic acid MSP of $1.90/kg can be achieved, within the 5-year historical range for petroleum-derived adipic acid of ~$1.75-2.50/kg. The two major equipment capital costs were: (1) activated carbon regeneration kilns ($14.6E6), whose cost was a function of the concentration of non-target aromatic metabolites and residual aromatics, and (2) the hydrogenation catalyst reactor ($16.7E6), due to the use of 2% Rh/C as the active material. Operationally, the annual expense of incoming muconate broth ($82.1E6) far outweighed all other variable expenses combined ($36.4E6), pointing to the significant weight of initial substrate costs on the MSP of adipic acid. Single point sensitivity analysis of major design variables further revealed that the MSP of adipic acid was impacted in a linear fashion by the incoming muconate broth price, and nearly linear by

the concentration of broth non-target aromatics within that range of 1-10 g/L. In contrast, the broth muconate titer and hydrogenation reactor throughput impacted the adipic acid MSP in a nonlinear fashion, identifying technical targets for muconate titer ≥50 g/L and hydrogenation reactor WHSV >3 h^{-1}. Bivariate analysis of the muconate broth price and broth titer determined that broth prices below $1.00/kg allowed for a minimum acceptable titer of ~20 g/L to maintain an adipic acid MSP below $2.50/kg, while higher broth prices quickly reduced the acceptable range of titers. In comparison, increasing the broth titer above 40 g/L showed a minimum impact on the adipic acid MSP for a given broth price. The codependence of both parameters was significant for broth titers ranging between 20-40 g/L, requiring a narrower range of acceptable broth price and titer values to maintain an adipic acid MSP below $2.50/kg. Overall, this preliminary techno-economic analysis determined that further research and development is warranted to reduce key cost bottlenecks and demonstrate technical targets for bio-derived muconic acid and adipic acid produced from complex, biomass-derived feedstocks.

6.5 Methods

6.5.1. Unit operation design and capital cost

Unit operation design parameters and performance assumptions were based on reported values from literature, computational simulations, and assumed when specified. Detailed descriptions for each unit process are provided in the Supplementary Information. Aspen Plus modeling software was used to compute heat duty, mass balance, and power requirements for the hydrogen compression and recycle train, as well as for the ethanol-adipic acid evaporative crystallization unit operations. Quotes and installation factors were then tabulated to provide an order-of-magnitude cost estimate for equipment, and normalized to 2014USD based on chemical

engineering plant equipment indices (**Table 6.8** and **Table 6.9**). Other capital costs (e.g. direct, indirect, working capital) were a function of the total cost for inside battery limits equipment (**Table 6.9**), following previous NREL techno-economic design studies.[7,68]

6.5.2. Operating expense estimation

Annual operating expenses were based on the desired plant throughput, consumption of chemicals and utilities, and production of waste. Unit consumption costs were based on values reported in literature and assumed when specified (**Table 6.5**). Variable operational costs were normalized to 2014 USD based on chemical indices (**Table 6.8**). Other operating costs (e.g. manpower, insurance, tax) were modeled after following previous NREL techno-economic design studies (**Table 6.4**).[7,68]

6.5.3. Minimum selling price calculation

The minimum selling price (MSP) of adipic acid was calculated by discounted cash flow analysis of a 30-year plant to result in a net present worth of zero dollars (**Table 6.10**), following previous NREL techno-economic design studies.[7,68] The plant land requirement was assumed to be 32 acres, at a cost of $14k per acre. Equity for the plant was assumed to be 40% from a parent company, with a 10 year loan at 8% APR. Principal costs were taken out during the first 3 years of construction, but principal was not paid during this period due to the n^{th}-plant assumption that the cash flow originates from the parent company until startup. The construction period was set to 3 years, with capital costs and start-up revenues varying accordingly. Income taxes were levied at 35% with state taxes not accounted for due to variability between states (0-12% state income tax rates). Plant depreciation was based on the IRS Modified Accelerated Cost Recovery

System (MACRS), which allows for the shortest recovery period and largest tax deductions over a 7-year period under the Asset Class 49.5, "Waste Reduction and Resource Recovery Plants". The discount rate, which was also the internal rate of return for this analysis, was assumed to be 10% after tax based on recommendations for DOE renewable energy technologies.[69]

6.5.4. Sensitivity analysis

For single point sensitivity analysis, the base-case model parameters were varied independently to determine the impact on plant capital and operating expenses. Discounted cash flow analysis was then performed to calculate the new MSP of adipic acid. Plant values were restored to the base-case design before each new parameter was varied. A focus was place on the incoming broth composition due to the impact on downstream unit process performance, as well as the hydrogenation reactor due to its significant capital and operating cost with unknown performance at scale. Crystallization was not examined for sensitivity analysis since performance parameters were based on literature solubility parameters.[3,43] Likewise, rotary filtration and drying were not evaluated since performance parameters were based on literature and technical handbook values.[70,71]

For bivariate analysis, the impact of broth price and broth titer was evaluated to determine the impact on the MSP of adipic acid. Both parameters were varied jointly, with broth price ranging from \$0.60-1.50/kg of muconate and broth titer ranging from 10-100 g/L of muconate. To generate a MSP surface response plot, each parameter was varied in 10% increments within the range boundaries to generate a 100-pair simulation space, with discounted cash flow analysis performed at each pair value to calculate the MSP of adipic acid.

6.6 Supplemental Information

6.6.1. Heat transfer calculations

Heat transfer calculations were performed to determine equipment heat transfer area sizing, heat transfer fluid mass flow rates, and natural gas consumption. Counter current fluid flow was assumed when calculating the log mean temperature difference, ΔT_{lm} (°C), for heat transfer equipment, as shown in **Eqn. 6.1**. Equipment heat transfer areas, A (m^2), were calculated based on the required heat duty, Q (kW), equipment heat transfer coefficient, U ($kW/m^2/°C$), and log mean temperature difference, as shown in **Eqn. 6.2**. Cooling fluid mass flow rates, $\dot{m}_{cool}$ (kg/s), for a given unit process were calculated based on the required heat duty, Q (kW), allowed temperature rise, ΔT (°C), and the specific heat capacity of the cooling fluid, c (kJ/kg/K), as shown in **Eqn. 6.3**. Medium pressure steam (300 psig, 216°C) mass flow rates, $\dot{m}_{stm}$ (kg/s), were determined by enthalpy balance, using saturated steam enthalpy values for steam, h_{stm} (2,799 kJ/kg), and condensate, h_{cond} (927 kJ/kg), under those conditions, as shown in **Eqn. 6.4**. For unit operations that utilized natural gas (e.g., rotary driers), a natural gas combustion efficiency of 90% was assumed, with a natural gas energy density of 54 MJ/kg.

Eqn 6.1 $$\Delta T_{LM} = \frac{\left[T_{hot,in} - T_{cold,out}\right] - \left[T_{hot,out} - T_{cold,in}\right]}{\ln\left[\frac{T_{hot,in} - T_{cold,out}}{T_{hot,out} - T_{cold,in}}\right]}$$

Eqn 6.2 $$A = \frac{Q}{U\Delta T_{LM}}$$

Eqn 6.3 $$\dot{m}_{cool} = \frac{Q}{\Delta T c}$$

Eqn 6.4 $$\dot{m}_{stm} = \frac{Q}{h_{stm} - h_{cond}}$$

6.6.2 Process model design basis

6.6.2.1 Activated carbon treatment & regeneration

Activated carbon treatment was modeled for muconic acid purification. The mass of activated carbon required for treatment was based on an assumed carbon adsorption capacity of 0.100 g/g_{AC} for muconic acid, and 0.150 g/g_{AC} for 4-hydroxybenzoic acid, a model non-target aromatic acid.[72] A target purity of 99% for muconic acid was assumed, with a safety factor of 1.2 to ensure high purity adipic acid as the final product. This resulted in an non-target muconic acid concentration of 48.8 g/L. Representative treatment bed parameters were modeled, with an empty bed contact time of 0.5 h using 3 reactor units in series, each containing 9,071 kg of activated carbon.[41] Parallel operating lines were used ensure continuous output, and treatment trains were replicated in triplicate to provide redundancy and sufficient time for bed regeneration, resulting in 6 parallel treatment units, each containing 3 reactors in series.

On site regeneration of activated carbon with fired kiln hearths was used to continuously produce fresh activated carbon. Combustion of adsorbed organics was chosen due to the high boiling point of muconic acid and non-target aromatic acids. Single hearth capacity was assumed to be 227 kg/h.[41] Natural gas consumption for regenerating 1 kg of activated carbon was assumed to be 0.436 m^3, with 5% of the activated carbon lost during combustion,[41] resulting in a natural gas consumption rate of 729 kg/h and makeup activated carbon rate of 105 kg/h.

6.6.2.2 Broth evaporative concentration

As noted, evaporative concentration was initially evaluated to increase the recovery yield of muconic acid during crystallization, but determined to be cost prohibitive. The evaporator was modeled as a horizontal tube forced circulation evaporator made of 316SS, with evaporated

water sent to wastewater treatment. The evaporator heat duty was based on water's latent heat of vaporization (2,257 kJ/kg), specific heat capacity (4.18 kJ/kg/°C), and incoming temperature of 24°C. The evaporator tubes had an assumed heat transfer coefficient of 1.25 kW/m^2/°C.[47] Medium pressure steam (216°C, 300 psig) was used as the heat transfer agent. Following evaporation, an external shell-and-tube heat exchanger made of 316SS was used to cool the broth to 50°C prior to entering the crystallizer due to the large heat duty. The external heat exchanger used fresh water as the heat transfer agent (28°C incoming with 9°C rise), with an assumed heat transfer coefficient of 1.30 kW/m^2/°C.[47].

6.6.2.3 Muconic acid crystallization

Crystallization at low pH/temperature was used to recover muconic acid from solution using an external, forced circulation crystallizer constructed of 304SS. Upon entering the crystallizer, sulfuric acid (93%) was added to the incoming broth at stoichiometric levels at an anhydrous rate of 7,023 kg/h. Internal jacketed cooling coils were used to remove the of heat generated during acid dissolution (766 kJ/kg)[73] and cool the broth to a temperature of 10°C, with a net heat duty of 5.6 MW. Chill water used as the internal crystallizer cooling medium (7°C incoming with 5°C rise), resulting in a chill water consumption rate of 962,126 kg/h. It was assumed that Na_2SO_4 was formed stoichiometrically as a by-product, with a solubility limit of 82.8 g/L at 10°C.[42] This resulted in a Na_2SO_4 formation rate of 3,082 kg/h. The combined solid crystals were assumed to have 5% residual moisture content, resulting in 13,181 kg/h of moist crystal production, within the typical range of a single external forced circulation crystallizer unit (4,545-45,454 kg/h).[71]

6.6.2.4 Muconic acid rotary vacuum filtration and drying

Following crystallization, a rotary vacuum belt filter constructed of 316SS was incorporated to recover crystals from the broth solution. An average filter flux value of 400 $L/m^2/h$ was assumed,[47] which resulted in a filter design area of 521 m^2, within the typical range of a single rotary filter (1-74 m^2).[71] A filter motor power consumption of 0.8 kw/m^2 of filter area was assumed,[74] resulting in an electricity consumption rate of 417 kWh/h.

Following filtration, a rotary dryer, constructed of 304 SS and heated indirectly with combustion gas, was utilized to remove trace moisture from the recovered crystals. The drier was assumed to have a removal flux capacity of 33 kg of water per m^2 per h [70], resulting in a total drier area of 20 m^2, within the typical range of a single drier (9-372 m^2).[71] The drier was modeled with a heat duty requirement of 5.8 MJ/kg of evaporate,[70] resulting in a heat duty of 1.1 MW. Natural gas combustion was used to supply the drier heat duty, resulting in a natural gas consumption rate of 79 kg/h. A blower fan was used to circulate hot air, with an assumed power requirement of 0.04 kWh per kg/h of evaporate,[70] resulting in an electricity consumption rate of 28 kWh/h.

6.6.2.5 Muconic acid dissolution and Na_2SO_4 removal

To remove Na_2SO_4 and facilitate downstream catalytic processing, dried mixed crystals of muconic acid and Na_2SO_4 were dissolved in ethanol at 70°C using a heated mixing vessel constructed of 316 SS. The volume of the dissolution tank was specified to allow for a 10 min retention time and 20% vessel head volume. The vessel was designed to operate at 70°C with a 10 wt% muconic acid loading,[43] resulting in a heat duty of 2.6 MW. Medium pressure steam was used as the heat transfer agent, with a consumption rate of 4,303 kg/h. Stirring was constantly

applied using a head-mounted mounted agitator. The power consumption of the agitator was assumed to be 2 kW per 1000 L, resulting in an electricity consumption of 43 kWh/h.

Due to the insolubility of Na_2SO_4 in ethanol, residual Na_2SO_4 crystals were removed from the tank effluent by a second pair of rotary filtration and dryer units. Identical filter and dryer performance parameters were assumed, as described above. This resulted in a filter area of 236 m^2, filter electricity consumption rate of 67 kWh/h, dryer area of 5 m^2, dryer natural gas consumption rate of 28 kg/h, and dryer electricity consumption rate of 10 kWh/h. Recovered ethanol from drying Na_2SO_4 was recycled back to the dissolution tank, while solid Na_2SO_4 crystals were sent for solid waste disposal.

6.6.2.6 Packed bed flow hydrogenation reactor

Hydrogen for downstream processing was assumed to be initially available at ambient pressure and temperature, and was pressurized prior to entering the reactor using a three-stage compressor system constructed from carbon steel. Hydrogen was delivered with a molar flow ratio to muconic acid of 10:1. Isentropic compressors were assumed, with each compressor operating at 72% efficiency and having a maximum compression ratio of 3.5. The compressor train power requirement of 633 kW was calculated using Aspen Plus.

Muconic acid in ethanol was delivered to the reactor using a large head, positive displacement pump constructed of 316 SS. The pump operated with an efficiency of 68.7% and pumped 1,806 lpm, resulting in a power consumption of 266 kWh/h, calculated in Aspen Plus.

Hydrogenation of muconic acid to adipic acid was modeled using a packed bed catalytic reactor constructed of 316 SS. The reactor itself was packed with a 2% Rh/C catalyst that had a density of 0.5 kg/L. For the base case model, the catalyst was assumed to be stable during

operation, requiring 1/5th of the bed to be regenerated every year at a cost of $40/kg of catalyst for processing and an assumed 3% precious metal loss. Regeneration was treated as a annual variable operating cost. For sensitivity analysis, catalyst bed replacement was assumed to recover 35% of the initial catalyst cost due to reclaiming precious metal.

The catalyst was packed inside of heat exchanger tubes (0.0508 m diameter, 6.096 m long)[63] with cooling water flowing within the shell to remove heat released from hydrogenation ($\Delta H°_{rxn}$ ~ 254 kJ/mol). The reactor was operated at 70°C and 350 psig, with an assumed liquid hourly space velocity (LHSV) of 5 h^{-1}, requiring 16,515 kg of catalyst. Complete conversion of muconic acid resulted in a heat duty of 4.4 MW, requiring 234,944 kg/h of cooling water to maintain a constant temperature. The molar yield of adipic acid was assumed to be near quantitative, requiring 268 kg/h of makeup hydrogen.

6.6.2.7 Hydrogen recovery and recycle

Excess hydrogen was recovered from the reactor effluent after cooling the stream with an external heat exchanger. The heat exchanger cooled the reactor effluent to 40°C and reduced the pressure for efficient downstream gas-liquid separation. The exchanger cooling duty was 11.0 MW was calculated in Aspen Plus. The heat exchanger used fresh water as the heat transfer agent (28°C incoming with 9°C rise), with an assumed heat transfer coefficient of 1.30 kW/m^2/°C.[47] This resulted in a cooling heat transfer area of 425 m^2 and fresh water demand of 1,055,451 kg/h.

Gas-liquid separation was then performed using two flash tanks operating in series and at pressure. The flash tanks were each modeled as a vertical, semi-elliptical head vessel, with a length-to-diameter ratio of 3:1, fill level-to-cylinder length ratio of 1:3, and a hold-up time of

0.08 h. These design parameters resulted in a tank inside diameter of 2.62 m and a cylinder length of 7.85 m. A wall thickness of 0.0127 m was assumed, resulting in a tank weight of 7,916 kg of steel. Vapor-liquid separation performance was calculated in Aspen Plus.

The vapor phase from both flash tanks was then routed to a pressure swing adsorption (PSA) unit to remove trace ethanol in the vapor phase. The incoming gas mass flow rate was 6,337 kg/h, resulting in a power consumption of 22 kWh/h. Performance values were scaled based on previous NREL design reports.[7] In order to scale PSA equipment costs from previously reported flow rates, scaling exponents were used per **Eqn. 6.5** for adjusting equipment costs. Lastly, purified recycle hydrogen was recompressed to 350 psig using a single stage compressor. Recycle compressor design assumptions were identical to the hydrogen feed compressor train, resulting in a cooling duty of 3.2 MW, fresh water consumption of 1,055,451 kg/h, and power consumption of 3,292 kWh/h.

$$\textbf{Eqn 6.5} \qquad \text{Scaled cost} = \text{Base cost} \times \left[\frac{\text{Scaled size}}{\text{Base size}}\right]^{n}$$

6.6.2.8 Ethanol evaporative concentration

Adipic acid in ethanol was then concentrated using a horizontal tube, forced circulation evaporator constructed of 316 SS. The incoming reactor effluent solution was mixed with recycled crystallizer effluent, and concentrated to 360 g/L at 80°C, below the solubility limit of adipic acid at 60°C (~363 g/L).[43] This resulted in an ethanol evaporation rate of 74,476 kg/h and evaporator heat duty of 19.8 MW, calculated in Aspen Plus. The evaporator design incorporated horizontal tubes with an assumed heat transfer coefficient of 1.25 kW/m^2/°C.[47] Medium pressure steam (216°C, 300 psig) was used as the heat transfer agent, with a consumption rate of 37,996

kg/h. The evaporator required a heat transfer area of 103 m^2, within the typical range of a single forced circulation evaporator (14-743 m^2).[71]

6.6.2.9 Adipic acid crystallization

Following evaporation, adipic acid was recovered by temperature-shift crystallization using an external forced circulation crystallizer constructed of 304 SS. At 10°C, adipic acid has a solubility of 67.4 g/L in ethanol, requiring recycle back to the evaporator for efficient recovery. Internal jacketed cooling coils were used to reduce the temperature, with a net heat duty of 2.0 MW. Chill water used as the cooling medium (7°C incoming with 5°C rise), resulting in a chill water consumption rate of 342,327 kg/h. Solid crystals were assumed to have 5% residual ethanol content, resulting in 9,251 kg/h of crystal production.

6.6.2.10 Adipic acid rotary filtration and drying

Lastly, dry adipic acid crystals were produced with third pair of rotary filtration and dryer units with identical parameters assumed, as described above. For the filter, this resulted in filter liquid flow rate of 33,416 L/h, area of 84 m^2, and electricity consumption of 67 kWh/h. For the dryer, this resulted in an evaporate rate of 618 kg/h, dyer area of 19 m^2, heat duty of 1.0 MW, natural gas consumption of 74 kg/h, and electricity consumption of 26 kWh/h.

6.6.3 Economic modeling

To account for costs reported for varying years, indices for equipment, chemicals, and labor were used to normalize prices to 2014USD using **Eqn. 6.8**, with index values listed in **Table 6.8**. All capital costs were normalized to 2014 USD based on the Chemical Engineering

Plant Cost Index. The total direct cost (TDC) for support facilities was estimated based on a percentage of installed equipment inside battery limits (ISBL). The total indirect cost (TIC) for contingencies, field expenses, and other related items was estimated based on a percentage of total direct costs (TDC). Lastly, working capital was estimated based on a percentage of the fixed capital investment (FCI), the sum of total direct costs and indirect costs.

Capital costs for equipment inside battery limits (ISBL) were based on unit process design and performance parameters, described above, with quotes scaled to the current year and total installed costs based on installation factors from literature (**Table 6.9**).[71] Direct costs, indirect costs, land, and working capital were ultimately a function of the ISBL, with percentages based on previous NREL design reports (**Table 6.9**).[7,68] The total direct cost (TDC) for support facilities was estimated based on a percentage of installed equipment inside battery limits (ISBL). The total indirect cost (TIC) for contingencies, field expenses, and other related items was estimated based on a percentage of total direct costs (TDC). Lastly, working capital was estimated based on a percentage of the fixed capital investment (FCI), the sum of total direct costs and indirect costs.

Variable expenses are described in the manuscript main text, with fixed operational costs for manpower salaries, labor burden, maintenance, property insurance, and taxes were based on previous NREL design reports (**Table 6.4**).[7,68] Salaries were based on price estimates for labor, assuming a high degree of plant automation to determine the number of positions.

Eqn 6.6 $$\text{Cost 2014 USD} = \text{Base cost} \times \frac{\text{2014 cost index}}{\text{Base year cost index}}$$

6.7 References Cited

1. Linger, J. G. *et al.* Lignin valorization through integrated biological funneling and chemical catalysis. *Proc. Natl. Acad. Sci.* **111,** 12013–12018 (2014).
2. Tuck, C. O., Pérez, E., Horváth, I. T., Sheldon, R. A. & Poliakoff, M. Valorization of Biomass: Deriving More Value from Waste. *Science* **337,** 695–699 (2012).
3. Vardon, D. R. *et al.* Adipic acid production from lignin. *Energy Environ. Sci.* **8,** 617–628 (2015).
4. Koutinas, A. A. *et al.* Valorization of industrial waste and by-product streams via fermentation for the production of chemicals and biopolymers. *Chem. Soc. Rev.* **43,** 2587–2627 (2014).
5. Anbarasan, P. *et al.* Integration of chemical catalysis with extractive fermentation to produce fuels. *Nature* **491,** 235–239 (2012).
6. Xiong, M. *et al.* A Bio-Catalytic Approach to Aliphatic Ketones. *Sci. Rep.* **2,** (2012).
7. Davis, R. *et al.* Process design and economics for the conversion of lignocellulosic biomass to hydrocarbons: Dilute-acid and enzymatic deconstruction of biomass to sugars and biological conversion of sugars to hydrocarbons. *NREL Tech. Rep.* 88–101 (2013).
8. Wen, M., Bond-Watts, B. B. & Chang, M. C. Production of advanced biofuels in engineered *E. coli*. *Curr. Opin. Chem. Biol.* **17,** 472–479 (2013).
9. Jang, Y.-S. *et al.* Bio-based production of C2–C6 platform chemicals. *Biotechnol. Bioeng.* **109,** 2437–2459 (2012).
10. Peralta-Yahya, P. P., Zhang, F., del Cardayre, S. B. & Keasling, J. D. Microbial engineering for the production of advanced biofuels. *Nature* **488,** 320–328 (2012).
11. Besson, M., Gallezot, P. & Pinel, C. Conversion of Biomass into Chemicals over Metal Catalysts. *Chem. Rev.* **114,** 1827–1870 (2014).

12. Dapsens, P. Y., Mondelli, C. & Pérez-Ramírez, J. Biobased Chemicals from Conception toward Industrial Reality: Lessons Learned and To Be Learned. *ACS Catal.* **2,** 1487–1499 (2012).
13. Sheldon, R. A. Green and sustainable manufacture of chemicals from biomass: state of the art. *Green Chem.* **16,** 950–963 (2014).
14. Vyver, S. V. de & Román-Leshkov, Y. Emerging catalytic processes for the production of adipic acid. *Catal. Sci. Technol.* **3,** 1465–1479 (2013).
15. Van Duuren, J. B. J. H. & Wittmann, C. in *Bioprocessing of Renewable Resources to Commodity Bioproducts* (eds. Bisaria, V. S. & Kondo, A.) 519–540 (John Wiley & Sons, Inc., 2014). at <http://onlinelibrary.wiley.com/doi/10.1002/9781118845394.ch19/summary>
16. Wang, Q., Vural Gürsel, I., Shang, M. & Hessel, V. Life cycle assessment for the direct synthesis of adipic acid in microreactors and benchmarking to the commercial process. *Chem. Eng. J.* **234,** 300–311 (2013).
17. Sato, K., Aoki, M. & Noyori, R. A 'Green' Route to Adipic Acid: Direct Oxidation of Cyclohexenes with 30 Percent Hydrogen Peroxide. *Science* **281,** 1646–1647 (1998).
18. Beardslee, T. & Picataggio, S. Bio-based adipic acid from renewable oils. *Lipid Technol.* **24,** 223–225 (2012).
19. Yu, J.-L., Xia, X.-X., Zhong, J.-J. & Qian, Z.-G. Direct biosynthesis of adipic acid from a synthetic pathway in recombinant Escherichia coli. *Biotechnol. Bioeng.* **111,** 2580–2586 (2014).
20. Curran, K. A., Leavitt, J. M., Karim, A. S. & Alper, H. S. Metabolic engineering of muconic acid production in *Saccharomyces cerevisiae*. *Metab. Eng.* **15,** 55–66 (2013).

21. Xie, N.-Z., Liang, H., Huang, R.-B. & Xu, P. Biotechnological production of muconic acid: current status and future prospects. *Biotechnol. Adv.* **32,** 615–622 (2014).

22. Vardon, D. R. *et al.* Adipic acid production from lignin. *Energy Environ. Sci.* **8,** 617–628 (2015).

23. Draths, K. M. & Frost, J. W. Environmentally compatible synthesis of adipic acid from D-glucose. *J. Am. Chem. Soc.* **116,** 399–400 (1994).

24. Draths, K. M. & Frost, J. W. Environmentally compatible synthesis of adipic acid from D-glucose. *J. Am. Chem. Soc.* **116,** 399–400 (1994).

25. Davis, R. *et al.* Process design and economics for the conversion of lignocellulosic biomass to hydrocarbons: Dilute-acid and enzymatic deconstruction of biomass to sugars and biological conversion of sugars to hydrocarbons. *NREL Tech. Rep.* 88–101 (2013).

26. Van Duuren, J. B. J. H. & Wittmann, C. in *Bioprocessing of Renewable Resources to Commodity Bioproducts* (eds. Bisaria, V. S. & Kondo, A.) 519–540 (John Wiley & Sons, Inc., 2014). at <http://onlinelibrary.wiley.com/doi/10.1002/9781118845394.ch19/summary>

27. Niu, W., Draths, K. M. & Frost, J. W. Benzene-Free Synthesis of Adipic Acid. *Biotechnol. Prog.* **18,** 201–211 (2002).

28. Averesch, N. J. H. & Krömer, J. O. Tailoring strain construction strategies for muconic acid production in *S. cerevisiae* and *E. coli*. *Metab. Eng. Commun.* **1,** 19–28 (2014).

29. Mizuno, S., Yoshikawa, N., Seki, M., Mikawa, T. & Imada, Y. Microbial production of *cis, cis*-muconic acid from benzoic acid. *Appl. Microbiol. Biotechnol.* **28,** 20–25 (1988).

30. Kaneko, A., Ishii, Y. & Kirimura, K. High-yield Production of *cis*,*cis*-Muconic Acid from Catechol in Aqueous Solution by Biocatalyst. *Chem. Lett.* **40,** 381–383 (2011).

31. Averesch, N. J. H. & Krömer, J. O. Tailoring strain construction strategies for muconic acid production in *S. cerevisiae* and *E. coli*. *Metab. Eng. Commun.* **1,** 19–28 (2014).

32. Weber, C. *et al.* Biosynthesis of *cis,cis*-Muconic Acid and Its Aromatic Precursors, Catechol and Protocatechuic Acid, from Renewable Feedstocks by *Saccharomyces cerevisiae*. *Appl. Environ. Microbiol.* **78,** 8421–8430 (2012).

33. Sonoki, T. *et al.* Enhancement of protocatechuate decarboxylase activity for the effective production of muconate from lignin-related aromatic compounds. *J. Biotechnol.* **192, Part A,** 71–77 (2014).

34. Curran, K. A., Leavitt, J. M., Karim, A. S. & Alper, H. S. Metabolic engineering of muconic acid production in *Saccharomyces cerevisiae*. *Metab. Eng.* **15,** 55–66 (2013).

35. Sun, X., Lin, Y., Huang, Q., Yuan, Q. & Yan, Y. A Novel Muconic Acid Biosynthetic Approach by Shunting Tryptophan Biosynthesis via Anthranilate. *Appl. Environ. Microbiol.* (2013). doi:10.1128/AEM.00859-13

36. Bang, S.-G. & Choi, C. Y. DO-stat fed-batch production of *cis, cis*-muconic acid from benzoic acid by *Pseudomonas putida* BM014. *J. Ferment. Bioeng.* **79,** 381–383 (1995).

37. Van Duuren, J. B. J. H. *et al.* pH-stat fed-batch process to enhance the production of *cis,cis*-muconate from benzoate by *Pseudomonas putida* KT2440-JD1. *Biotechnol. Prog.* **28,** 85–92 (2012).

38. Bechthold, I., Bretz, K., Kabasci, S., Kopitzky, R. & Springer, A. Succinic Acid: A New Platform Chemical for Biobased Polymers from Renewable Resources. *Chem. Eng. Technol.* **31,** 647–654 (2008).

39. Ramaswamy, S., Huang, H.-J. & Ramarao, B. *Separation and Purification Technologies in Biorefineries*. (John Wiley and Sons Ltd, 2012).

40. Claypool, J. T. & Raman, D. R. Development and validation of a technoeconomic analysis tool for early-stage evaluation of bio-based chemical production processes. *Bioresour. Technol.* **150,** 486–495 (2013).
41. U.S. Army Corps of Engineers. Engineering and Design - Adsorption Design Guide. *DG 1110-1-2* (2001).
42. Okorafor, O. C. Solubility and Density Isotherms for the Sodium Sulfate−Water−Methanol System. *J. Chem. Eng. Data* **44,** 488–490 (1999).
43. Gaivoronskii, A. N. & Granzhan, V. A. Solubility of Adipic Acid in Organic Solvents and Water. *Russ. J. Appl. Chem.* **78,** 404–408 (2005).
44. Radici Group. Adipic acid. at <www.radicigroup.com/chemicals>
45. Gorden, J., Zeiner, T. & Brandenbusch, C. Reactive extraction of *cis,cis*-muconic acid. *Fluid Phase Equilibria* **393,** 78–84 (2015).
46. Orjuela, A., Orjuela, A., Lira, C. T. & Miller, D. J. A novel process for recovery of fermentation-derived succinic acid: Process design and economic analysis. *Bioresour. Technol.* **139,** 235–241 (2013).
47. Efe, Ç., van der Wielen, L. A. M. & Straathof, A. J. J. Techno-economic analysis of succinic acid production using adsorption from fermentation medium. *Biomass Bioenergy* **56,** 479–492 (2013).
48. Urbanus, J. *et al.* Integrated product removal of slightly water-soluble carboxylates from fermentation by electrochemically induced crystallization. *J. Membr. Sci.* **363,** 36–47 (2010).
49. Nasrollahnejad, T., Urbanus, J., ter Horst, J. H., Verdoes, D. & Roelands, C. P. M. Electrochemically Induced Crystallization as a Sustainable Method for Product Recovery of

Building Block Chemicals: Techno-Economic Evaluation of Fumaric Acid Separation. *Ind. Biotechnol.* **8,** 133–151 (2012).

50. Cok, B., Tsiropoulos, I., Roes, A. L. & Patel, M. K. Succinic acid production derived from carbohydrates: An energy and greenhouse gas assessment of a platform chemical toward a bio-based economy. *Biofuels Bioprod. Biorefining* 16–29 (2014). doi:10.1002/bbb.1427
51. BASF. Metal Price History Charts. *BASF* (2015). at <http://apps.catalysts.basf.com/apps/eibprices/mp/DPCharts.aspx>
52. Besson, M. & Gallezot, P. Deactivation of metal catalysts in liquid phase organic reactions. *Catal. Today* **81,** 547–559 (2003).
53. Bartholomew, C. H. & Farrauto, R. J. *Fundamentals of Industrial Catalytic Processes*. (Wiley-AIChE, 2011).
54. Armor, J. N. Applications of catalytic inorganic membrane reactors to refinery products. *J. Membr. Sci.* **147,** 217–233 (1998).
55. Laue, S., Greiner, L., Wöltinger, J. & Liese, A. Continuous Application of Chemzymes in a Membrane Reactor: Asymmetric Transfer Hydrogenation of Acetophenone. *Adv. Synth. Catal.* **343,** 711–720 (2001).
56. An, W., Hong, J. K., Pintauro, P. N., Warner, K. & Neff, W. The electrochemical hydrogenation of edible oils in a solid polymer electrolyte reactor. I. Reactor design and operation. *J. Am. Oil Chem. Soc.* **75,** 917–925 (1998).
57. Feng, L. & Berglund, K. A. ATR-FTIR for Determining Optimal Cooling Curves for Batch Crystallization of Succinic Acid. *Cryst. Growth Des.* **2,** 449–452 (2002).
58. Sano, C., Kashiwagi, T., Nagashima, N. & Kawakita, T. Effects of additives on the growth of L-glutamic acid crystals (β-form). *J. Cryst. Growth* **178,** 568–574 (1997).

59. Yu, Q., Black, S. & Wei, H. Solubility of Butanedioic Acid in Different Solvents at Temperatures between 283 K and 333 K. *J. Chem. Eng. Data* **54,** 2123–2125 (2009).

60. Pinho, S. P. & Macedo, E. A. Solubility of NaCl, NaBr, and KCl in Water, Methanol, Ethanol, and Their Mixed Solvents. *J. Chem. Eng. Data* **50,** 29–32 (2005).

61. Cheng, K.-K. *et al.* Downstream processing of biotechnological produced succinic acid. *Appl. Microbiol. Biotechnol.* **95,** 841–850 (2012).

62. Rodriguez, B. A., Stowers, C. C., Pham, V. & Cox, B. M. The production of propionic acid, propanol and propylene via sugar fermentation: an industrial perspective on the progress, technical challenges and future outlook. *Green Chem.* (2013). doi:10.1039/C3GC42000K

63. Peters, M., Timmerhaus, K. & West, R. *Plant Design and Economics for Chemical Engineers*. (McGraw-Hill Science/Engineering/Math, 2002).

64. Van Duuren, J. B. J. H. *et al.* A limited LCA of bio-adipic acid: Manufacturing the nylon-6,6 precursor adipic acid using the benzoic acid degradation pathway from different feedstocks. *Biotechnol. Bioeng.* **108,** 1298–1306 (2011).

65. Menon, V. & Rao, M. Trends in bioconversion of lignocellulose: Biofuels, platform chemicals & biorefinery concept. *Prog. Energy Combust. Sci.* **38,** 522–550 (2012).

66. Valentine, J. *et al.* Food vs. fuel: the use of land for lignocellulosic 'next generation' energy crops that minimize competition with primary food production. *GCB Bioenergy* **4,** 1–19 (2012).

67. Ragauskas, A. J. *et al.* Lignin Valorization: Improving Lignin Processing in the Biorefinery. *Science* **344,** 1246843 (2014).

68. Humbird, D. *et al.* Process design and economics for biochemical conversion of lignocellulosic biomass to ethanol: Dilute-acid pretreatment and enzymatic hydrolysis of corn stove. (2011).
69. Short, W., Packey, D. J. & Holt, T. A manual for the economic evaluation and energy efficiency and renewable energy technologies. *NREL Tech. Rep.* (2005).
70. APV Ltd. APV Dryer Handbook. (2000).
71. Couper, J. R., Penney, W. R. & Fair, J. *Chemical Process Equipment, Third Edition: Selection and Design*. (Butterworth-Heinemann, 2012).
72. García-Araya, J. F., Beltrán, F. J., Álvarez, P. & Masa, F. J. Activated Carbon Adsorption of Some Phenolic Compounds Present in Agroindustrial Wastewater. *Adsorption* **9,** 107–115 (2003).
73. General Chemical. Heat of dilution, sulfuric acid with water (liq.) at 77°F. (1991).
74. Hugot, E. *Handbook of Cane Sugar Engineering*. (Elsevier Science Ltd, 1972).
75. Bang, S.-G. & Choi, C. Y. DO-stat fed-batch production of *cis, cis*-muconic acid from benzoic acid by *Pseudomonas putida* BM014. *J. Ferment. Bioeng.* **79,** 381–383 (1995).
76. Van Duuren, J. B. J. H. *et al.* pH-stat fed-batch process to enhance the production of *cis,cis*-muconate from benzoate by *Pseudomonas putida* KT2440-JD1. *Biotechnol. Prog.* **28,** 85–92 (2012).
77. Kaneko, A., Ishii, Y. & Kirimura, K. High-yield Production of *cis*,*cis*-Muconic Acid from Catechol in Aqueous Solution by Biocatalyst. *Chem. Lett.* **40,** 381–383 (2011).
78. U.S. Energy Information Administration. Electric Power Monthly. (2015).
79. U.S. Energy Information Administration. Annual Energy Outlook 2015. (2015).
80. Chemical Engineering Magazine. Chemical Engineering's Plant Cost Index. (2013).

81. SRI. International Chemical Economics Handbook, Economic Environment of the Chemical Industry. (2006).
82. Bureau of Labor Statistics. Average Hourly Earnings of Production Workers. Series ID: CEU3232500008 Chemicals.
83. Creek, D. N. & Davidson, J. M. Treatment Technologies for Removal of Methyl Tertiary Butyl Ether (MTBE) from Drinking Water: Granular Activated Carbon. *Natl. Water Res. Inst.* (2000).
84. Matches. Matches' process equipment cost estimates. (2014). at <http://www.matche.com/equipcost/Default.html>

6.8 Figures and Tables

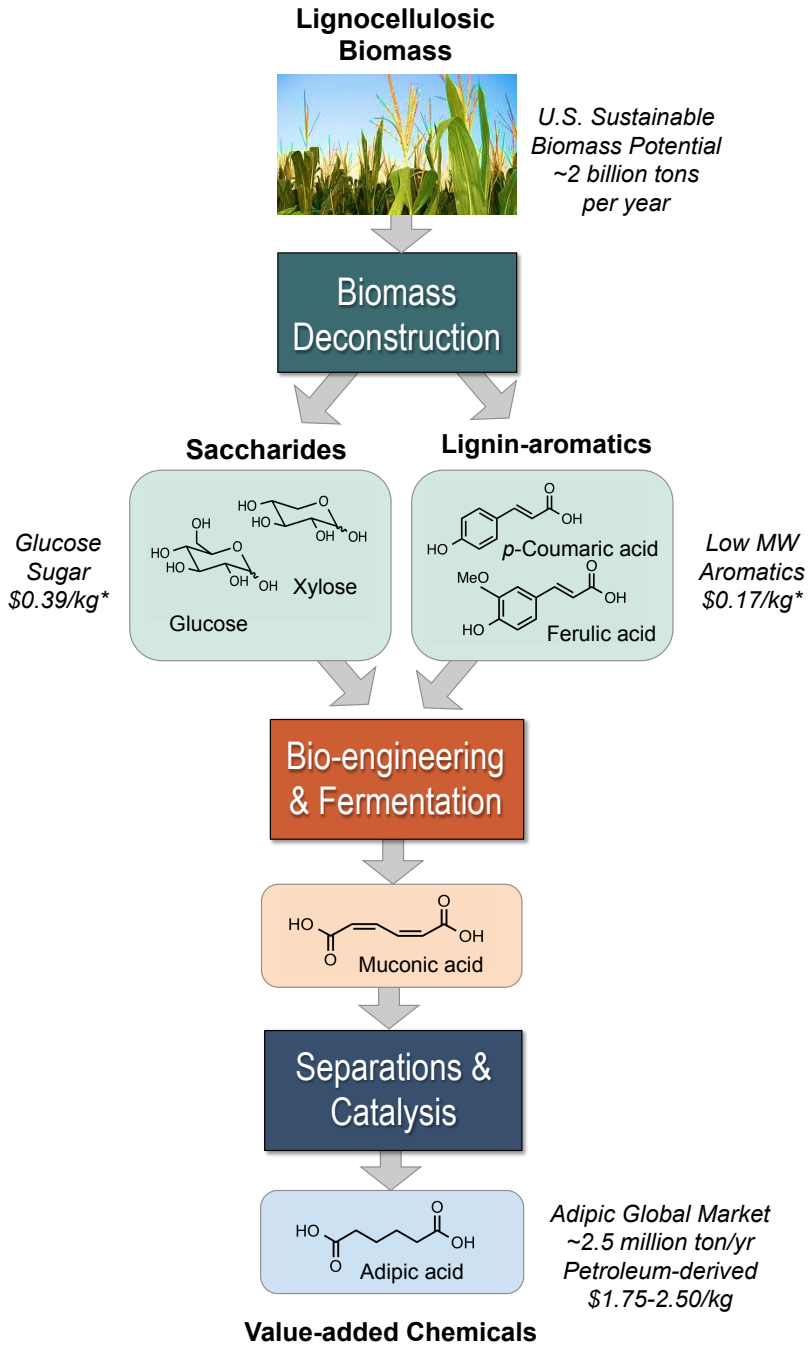

Figure 6.1 Integrated biological and chemical conversion of lignocellulosic biomass to muconic and adipic acid utilizing glucose and aromatic monomer substrates. *Estimate of monomer cost.[15]

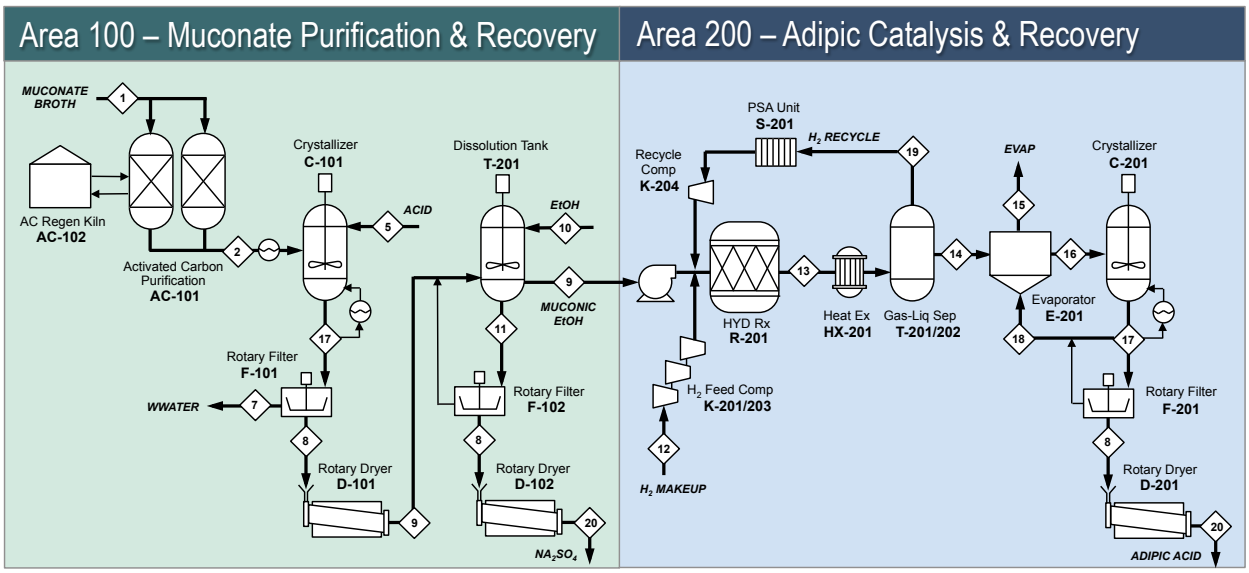

Figure 6.2 Process model diagram for muconic acid purification and separation (Area 100), with subsequent catalytic hydrogenation to produce and recover adipic acid (Area 200).

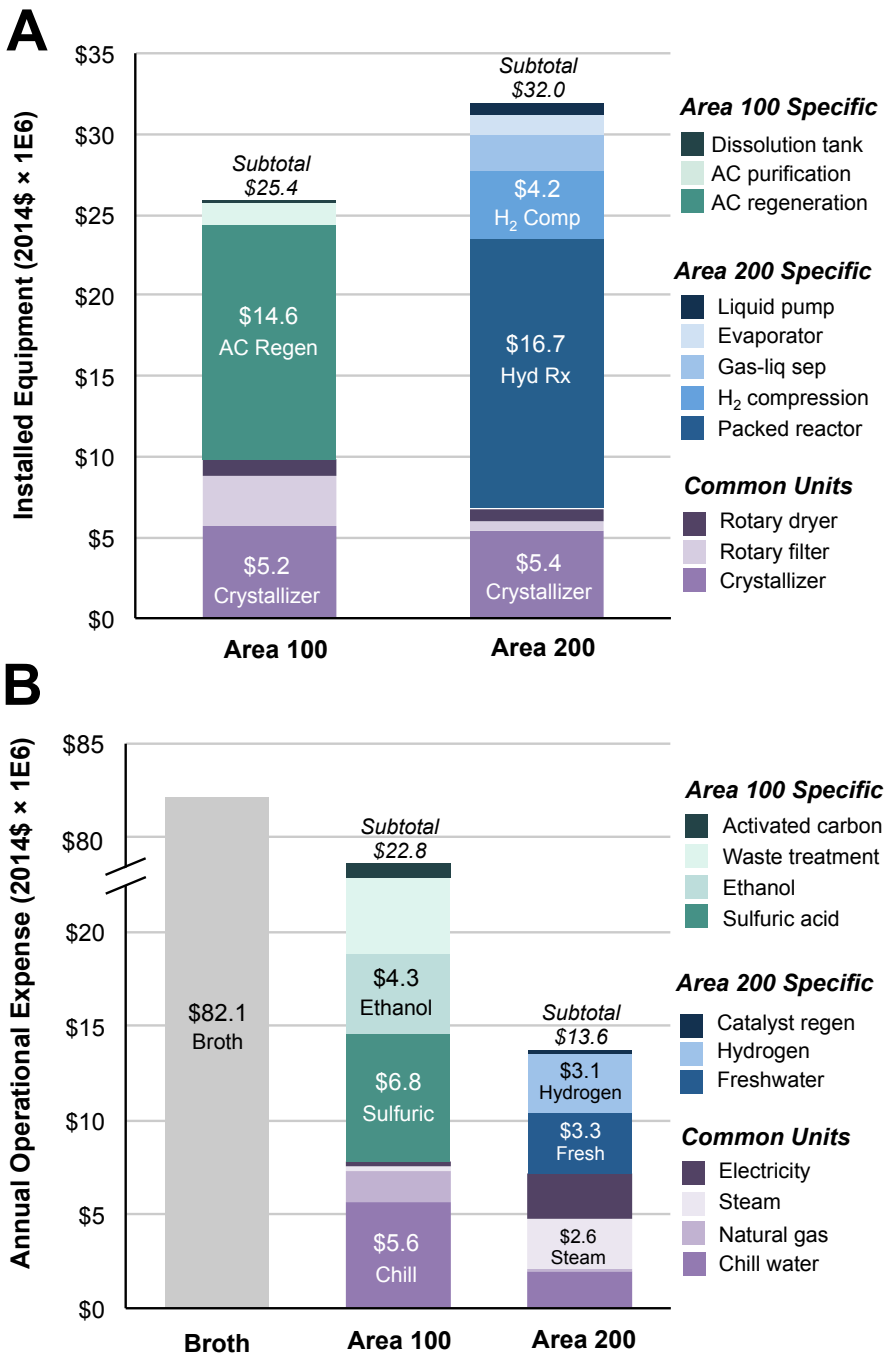

Figure 6.3 Installed equipment costs (A) and annual operating expenses (B) for the base-case process model.

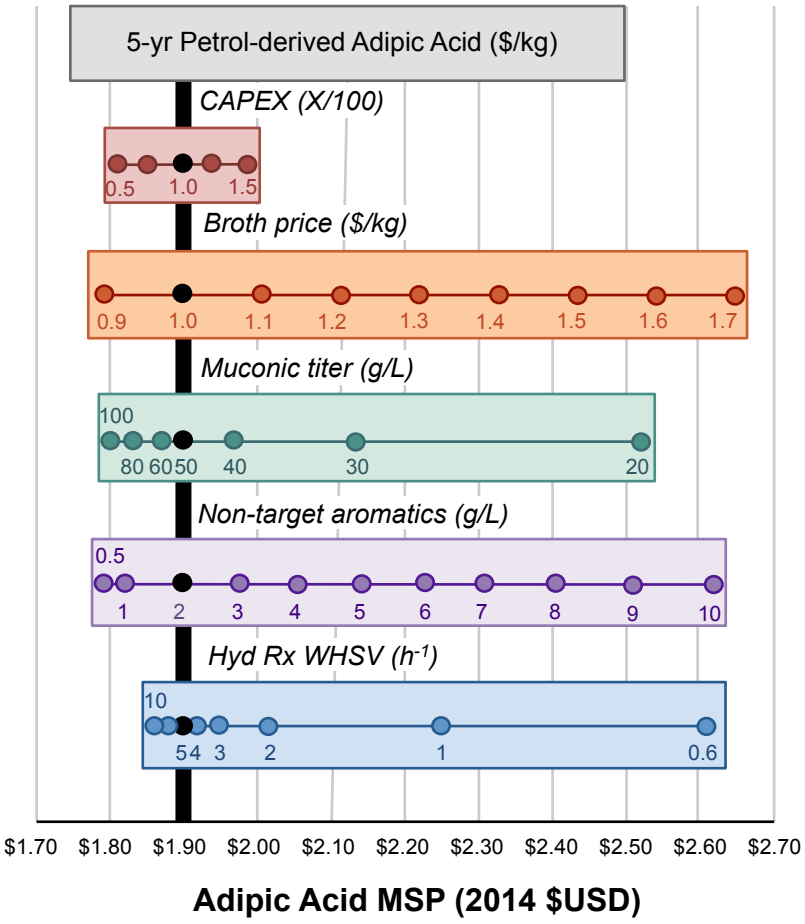

Figure 6.4 Single point sensitivity analysis for the base case model process parameters (black marker) with regards to adipic acid minimum selling price (MSP) of $1.90.

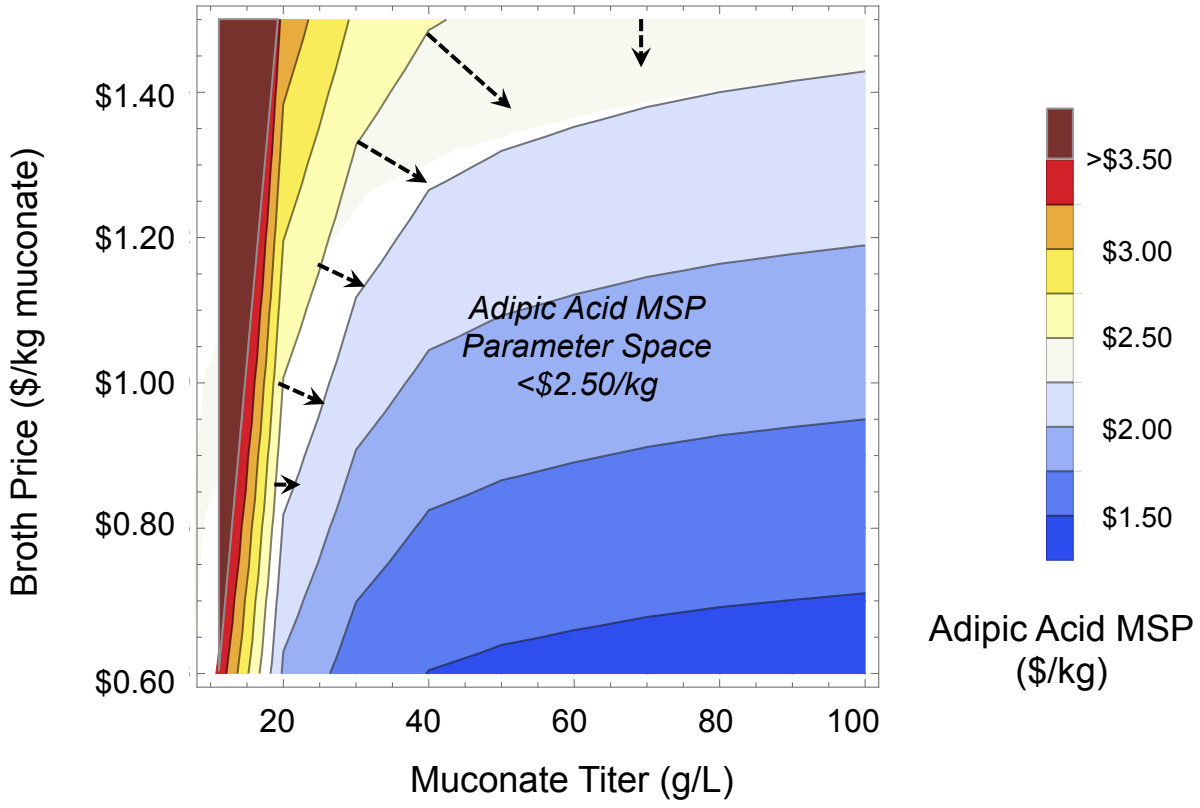

Figure 6.5 Bivariate sensitivity analysis to determine the joint impact of broth price ($0.60-$1.50/kg of muconate) and broth titer (10-100 g/L of muconate) on the minimum selling price (MSP) of adipic acid. Dashed arrows indicate the parameter space that provides an adipic acid MSP <$2.50/kg.

Table 6.1 Demonstrated and theoretical molar yields and substrate mass and cost requirements to produce 1 kg of muconic acid.

Bio-based Substrate	Substrate MW (g/mol)	Demonstrated molar yield of MA (%)	Demonstrated substrate mass required per kg MA (kg/kg)	Demonstrated substrate cost per kg of MA ($/kg)	Theoretical molar yield of MA (%)	Theoretical substrate mass required per kg MA (kg/kg)	Theoretical substrate cost per kg of MA ($/kg)
Glucose[24,27]	180.16	22-30%	4.23-5.76	$1.65-2.25	69-86%[28]	1.47-1.84	$0.57-0.72
4-HBA[3]	138.12	53%	1.83	$0.31	100%	0.97	$0.17
p-Coumaric acid[3]	164.16	67%	1.72	$0.29	100%	1.16	$0.20
Phenol[3]	94.11	64%	1.03	$0.18	100%	0.66	$0.11
Benzoic acid[3,75,76]	122.12	93-100%	0.92	$0.16	100%	0.86	$0.15
Catechol[77]	110.11	100%	0.77	$0.13	100%	0.77	$0.13

*MA = muconic acid, ** = substrate cost assumes $0.39/kg glucose and $0.17/kg aromatics, with a Euro exchange rate of 1.2[15]

Table 6.2 Base-case model design summary.

Parameter	Model bases
Overall plant	Adipic acid 75E6 kg/y Operational time 7,884 h/y
Clarified broth properties	$1.00/kg muconate (in solution) Na-muconate (50 g/L muconic acid-basis) Non-target aromatics 2 g/L Flow rate 478,146 L/h
AC purification & regeneration	Post-AC muconic purity 99% Purity engineering factor 1.2 Muconic loss during purification 7.2% AC loss during regen 5%
Muconic acid crystallization	Crystallization at pH 2/10°C Protonated muconic acid solubility 3.5 g/L Na_2SO_4 produced 2:1 during acidification Na_2SO_4 solubility 90 g/L at 10°C Solids removal by rotary filtration
Muconic EtOH dissolution	EtOH dissolution temp 70°C Muconic acid loading 100 g/L Na_2SO_4 negligible EtOH solubility Na_2SO_4 removal by rotary filtration/drying
Catalytic hydrogenation	Trickle bed HYD Rx using 2%Rh/C Temp 75°C, pressure 350 psig, WHSV 5 h^{-1} Adipic acid 100% molar yield 3-stage H_2 compression with recycle
Evaporative crystallization	EtOH evaporation to 360 g/L adipic acid Crystallization at 10°C with recycle Adipic EtOH solubility 67.4 g/L at 10°C Crystallization adipic losses 2%
Adipic acid recovery	Rotary filtration w/drying

Table 6.3 Purity requirements for polymer-grade adipic acid specified by Radici group.

Polymer-Grade Adipic Acid	Specification
Purity	99.8% min
Total N	20 ppm max
Iron	0.2 ppm max
Crystallization	152 +/- 0.5 °C
Moisture	0.2% max

Table 6.4 Operating labor expense summary for base-case design.

Position	Salary	Quote Year	2014 Salary	# Required	Annual Cost
Plant Manager	$147,000	2009	$161,917	1	$161,917
Plant Engineer	$70,000	2009	$77,103	2	$154,207
Maintenance Supr	$57,000	2009	$62,784	1	$62,784
Maintenance Tech	$40,000	2009	$44,059	12	$528,709
Lab Manager	$56,000	2009	$61,683	1	$61,683
Lab Technician	$40,000	2009	$44,059	2	$88,118
Shift Supervisor	$48,000	2009	$52,871	4	$211,484
Shift Operators	$40,000	2009	$44,059	20	$881,182
Yard Employees	$28,000	2009	$30,841	4	$123,366
Clerks & Secretaries	$36,000	2009	$39,653	3	$118,960
Total Salaries					$2,392,410
Labor Burden	90% of Salary				$2,153,169
Maintenance	3.0% of ISBL				$1,732,006
Property Ins. & Tax	0.7% of FCI				$810,698
Plant Variable					$118,346,793
Total Operating					**$125,435,076**

Table 6.5 Base case model variable operational unit costs.

Area 100 Component	Unit cost	Ref	Usage
Muconic acid broth	$1.00/kg	Assumed	10,420
Activated carbon	$1.00/kg	[40]	105
Sulfuric acid	$0.1140/kg	[7]	1,582
Ethanol	$0.7309/kg	[46]	745
Na_2SO_4 solid disposal	$0.0693/kg	[49]	1,582
Wastewater treatment	$0.0014/kg	[49]	208,392
Area 200 Component			
Catalyst regeneration	$62.99/kg	Assumed	0.21
Hydrogen	$1.50/kg	[7]	266
Freshwater	$0.14/ton	[63]	1,653,014
Common Utilities			
Electricity	$0.0694/kWh	[78]	4,757
Steam	$0.0078/kg	[63]	47,571
Natural gas	$0.2460/kg	[79]	900
Chill water	$0.0007/kg	[63]	1,304,453

Table 6.6 Influence of the fractional change in catalyst cost on the minimum selling price of adipic acid.

Catalyst Cost Change (1/X)	WHSV 5 h^{-1} Adipic MSP ($/kg)	WHSV 1 h^{-1} Adipic MSP ($/kg)
1/100	$1.84	$1.99
1/2	$1.87	$2.13
1	$1.90	$2.26
2	$1.95	$2.53
10	$2.38	$4.68

Table 6.7 Influence of catalyst bed replacement frequency on the minimum selling price of adipic acid.*

Replacement Freq. (years)	WHSV 5 h^{-1} Adipic MSP ($/kg)	WHSV 1 h^{-1} Adipic MSP ($/kg)
Never	$1.90	$2.26
10	$1.91	$2.32
5	$1.92	$2.37
2	$1.95	$2.54
1	$2.01	$2.81
0.5	$2.12	$3.37
0.2	$2.45	$5.03

*Assumes 35% recovery of the catalyst cost due to precious metal reclamation.

Table 6.8 Cost indices for installed equipment, chemicals, and labor.

Year	Chemical Engineering Plant Index [80]	Inorganic Chemical Index [81]	Chemicals Labor Index [82]
2001	394.3	158.4	17.57
2002	395.6	157.3	17.97
2003	402.0	164.6	18.50
2004	444.2	172.8	19.17
2005	468.2	187.3	19.67
2006	499.6	196.8	19.60
2007	525.4	203.3	19.55
2008	575.4	228.2	19.50
2009	521.9	224.7	20.30
2010	550.8	233.7	21.07
2011	585.7	249.3	21.46
2012	584.6	259.6	21.76
2013	567.3	269.9	22.06
2014	573.9	280.2	22.36

Table 6.9 Total capital investment summary for base case plant design.

Equipment	# Units	Unit Quote	Quote Year	Unit Cost 2014	Total Cost 2014	Install Factor [71]	Installed Cost	Quote Ref
AREA 100 – Muconic acid recovery								
AC purification (AC-101)	6	$154,245	1999	$226,629	$1,359,773	1.0	$1,359,773	[83]
AC regeneration (AC-102)	10	$1,000,000	2001	$1,455,491	$14,554,907	1.0	$14,554,907	[41]
Crystallizer (C-101)	1	$2,088,033	2003	$2,980,901	$2,980,901	1.9	$5,663,711	[71]
Rotary filter (F-101)	1	$1,011,614	2003	$1,444,193	$1,444,193	1.9	$2,021,870	[71]
Rotary drier (D-101)	1	$298,191	2003	$425,701	$425,701	1.4	$595,982	[70,71]
Dissolution tank (T-101)	1	$50,971	2002	$73,944	$73,944	1.4	$147,888	[63]
Rotary filter (F-102)	1	$562,229	2003	$802,645	$802,645	2.0	$1,123,703	[71]
Rotary drier (D-102)	1	$201,057	2003	$287,032	$287,032	1.4	$401,845	[70,71]
Area 200 – Catalytic adipic acid production and recovery								
Liquid pump (P-201)	1	$491,800	2014	$491,800	$491,800	1.4	$688,520	[84]
H2 feed compressor (K-201/202/203)	1	$410,347	2002	$595,174	$595,174	1.3	$773,726	[63]
Hydrogenation Rx (R-201)	1	$1,754,172	2003	$2,504,276	$2,504,276	1.6	$4,006,842	[71]
Catalyst 1% Rh/AC (S-201)	1	$12,698,061	2014	$12,698,061	$12,698,061	1.0	$12,698,061	[51]
Gas-liquid separator (T-201/202)	2	$118,582	2003	$169,289	$338,578	1.8	$609,441	[71]
PSA unit (S-201)	1	$150,710	2003	$215,156	$215,156	1.9	$408,796	[7]
H2 recycle compressor (K-204)	1	$620,509	2013	$627,728	$627,728	1.9	$1,192,683	[63]
Evaporator (E-201)	1	$1,827,559	2002	$2,650,718	$2,650,718	1.3	$3,445,934	[71]
Crystallizer (C-201)	1	$451,491	2003	$644,554	$644,554	1.9	$1,224,653	[71]
Rotary filter (F-201)	1	$1,998,419	2003	$2,852,967	$2,852,967	1.9	$5,420,637	[71]
Rotary drier (D-201)	1	$290,984	2003	$415,412	$415,412	1.4	$581,576	[70,71]
Total ISBL					**$46,544,233**		**$57,733,546**	
Warehouse		4% of ISBL					$2,309,342	
Site development		9% of ISBL					$5,196,019	
Additional piping		4.5% of ISBL					$2,598,010	
Total Direct Costs							**$67,836,917**	
Prorateable expenses		10% of TDC					$6,783,692	
Filed expenses		10% of TDC					$6,783,692	
Home office & fees		20% of TDC					$13,567,383	
Project contingency		10% of TDC					$6,783,692	
Other costs		10% of TDC					$6,783,692	
Total Indirect Costs							**$40,702,150**	
Fixed Capital Investment							**$108,539,067**	
Land							$1,848,000	
Working capital		5% of FCI					$5,426,953	
Total Capital Investment							**$115,814,00**	

Table 6.10 Process model economic finance parameters.

Cost year	2014 USD
Profit analysis	Discounted cash flow analysis
Plant lifetime	30 y
Land requirement	32 acres at $14k per acre
Equity	40%
Loan interest	8%
Construction period	3 year construction period · 8% spent in year -2 · 60% spent in year -1 · 32% spent in year 0
Startup revenues	0.25 year start-up · 50% production capacity · 75% variable costs · 100% fixed costs
Working capital	5% fixed capital investment
Loan term	10 y at 8% APR
Internal rate of return	10%
Net present worth	$0
Income tax rate	35%
Depreciation	7 y MACRS

CHAPTER 7

SUMMARY AND CONCLUSIONS

7.1 Summary and Conclusions

This thesis examined the integrated catalytic conversion of microbial acids to both fuels and chemicals in order to achieve the following objectives: (1) investigate hydrothermal catalysis for deoxygenating monocarboxylic acids to diesel-grade hydrocarbons with *in situ* hydrogen production from renewable donors, (2) examine downstream separation and catalysis for converting *cis,cis*-muconic acid to adipic acid, the latter compound being a high-value polymer precursor for nylon-6,6 production, and (3) identify key economic drivers and technical targets the downstream processing of muconic acid to adipic acid using preliminary techno-economic analysis. Findings from these efforts are as follows:

Hydrothermal catalysis was shown to rapidly convert saturated and unsaturated monocarboxylic acids to linear hydrocarbons using a Pt-Re catalyst supported on activated carbon (AC). The reaction produced hydrocarbons with chain lengths one carbon shorter than their parent fatty acid, suggesting decarboxylation/decarbonylation was the primary reaction pathway. The addition of Re to Pt/AC enhanced the rate of deoxygenation, and characterization of the catalyst by chemisorption showed that the bimetallic CO:H uptake ratio was greatly modified compared to the monometallic counterpart, suggesting alloy formation. The addition of hydrogen to the system maintained the bimetallic catalyst in a reduced oxidation state when exposed to hydrothermal media, while also increasing the rate of deoxygenation. Furthermore, glycerol was effective as an *in situ* hydrogen donor, meeting process hydrogen demands when converting unsaturated fatty acids.

The hydrothermal Pt-Re/AC catalytic system was then employed to convert complex alkenoic acids to hydrocarbons, the former substrate originating from depolymerized lignin. The microorganism *Pseudomonas putida* KT2440 provided a biological route to "funnel" complex model and corn stover lignin derived monomers to intracellular medium chain length polyhydroxyalkanoates (*mcl*-PHAs). Extraction and analysis of *mcl*-PHA polymers confirmed lignin monomers were assimilated in the presence of residual sugars and acetate resulting from biomass depolymerization. *mcl*-PHA polymers derived from lignin monomers also displayed comparable properties to those derived from clean sugar. Thermal depolymerization of *mcl*-PHAs produced alkenoic acids reflective of their parent hydroxyacid, while hydrothermal catalytic deoxygenation with Pt-Re/AC produced hydrocarbons with chain lengths one carbon shorter than their parent alkenoic acid, as demonstrated with model saturated and unsaturated fatty acids described above.

In order to target value-added chemicals in addition to fuels, downstream separation and catalysis was applied to the dicarboxylic acid *cis,cis*-muconic acid for producing adipic acid, the latter molecule being the most widely manufactured dicarboxylic acid from petroleum. Expanding on previous efforts, an engineered strain of *P. putida* KT2240 was used to biologically convert model and complex lignin derived monomers to extracellular muconic acid. Fed-batch biological conversion of *p*-coumaric acid produced muconic acid in sufficient titers for downstream processing. Activated carbon purification of cell-free broth readily removed residual aromatic and upstream non-target metabolites, while pH/temperature shift crystallization effectively recovered muconic acid from purified broth media. Screening of commercial Pd, Pt, and Ru catalysts supported on activated carbon determined that Pd was the most active by far, although leaching was observed from the acidic reaction conditions.

Follow-up efforts were conducted to improve the separation purity, evaluate continuous time-on-stream catalyst stability, and polymerize bio-adipic acid to nylon-6,6. To improve the purity after crystallization, dissolution of muconic acid crystals in ethanol with filtration removed insoluble inorganic salts and produced muconic acid with a purity of 99.8%, on par with polymer precursor specifications. Catalyst activity and leaching stability screening of Pd, Pt, Ru, and Rh prepared on carbon and silica supports determined that Pd and Rh were both highly active, regardless of support; however, Pd leached significantly, more so on silica, under batch reaction conditions. Continuous time-on-stream catalytic testing with Rh supported on granular AC confirmed stable conversion after 100 h, with minor losses in catalyst active metal surface area. Lastly, polymerization of bio-adipic acid derived from muconic acid produced nylon-6,6 with comparable polymer properties to its petrochemical counterpart.

Preliminary techno-economic modeling then assessed key cost drivers and technical targets for the downstream processing of muconic acid to adipic acid. An n^{th}-generation downstream plant was modeled to produce 75 million kg of adipic acid per year, and the base-case process model estimated an adipic acid minimum selling price of $1.90/kg, within the 5-year range for petroleum derived adipic acid ($1.75-2.50/kg). The largest capital costs were activated carbon regeneration kilns and the packed bed hydrogenation reactor, while variable operating costs were comparable throughout, excluding the cost of incoming muconate broth which was the largest expense by far. High muconic acid-to-impurity broth ratios were deemed critical for economical activated carbon purification, while muconate broth titers above 50 g/L were shown to provide minor economic benefits. The high cost of Rh as a hydrogenation catalyst required high reactor space velocities in order to be economical, while the application of lower cost metal

combinations showed significant potential to reduce the minimum selling price of adipic acid if long residence times are required due to mass transfer limitations.

7.2 Implications for Future Research

Based on the work conducted in this thesis, implications for future research directions are described below:

- *Hydrothermal catalysis for converting mono-carboxylic acids to hydrocarbon fuels.* The aqueous biological conversion environment and high boiling points of medium and long-chain carboxylates presents a unique opportunity to utilize water as the reaction medium for catalysis. Although hydrothermal media facilitates mono-carboxylate deoxygenation and renewable hydrogen donor conversion, further work is needed to evaluate the long-term catalyst stability during continuous processing due to the harsh conditions employed and potential for biogenic impurities. As noted, non-target inorganic and organic constituents can dramatically impact catalyst performance when transitioning to complex carboxylate streams, requiring tailored separation processes and robust catalysts. Likewise, alternatives to platinum group metals (PGM) may further improve the economic viability of carboxylate deoxygenation in hydrothermal media. The unique bimetallic performance observed in this work may also be possible with non-PGM materials active for hydrogen dissociation and C-C bond cleavage. For both material classes, further efforts are needed to understand the nature of bimetallic enhancement from a mechanistic, synthetic, and applied perspective.

- *Downstream separation and catalysis for converting muconic acid to adipic acid for polymer applications.* As shown in this work, *cis,cis*-muconic acid is a promising platform chemical for polymer precursor production due its ability to be produced biologically from both sugar and lignin derived monomers, facile separation through pH/temperature shift crystallization, and ready catalytic conversion to adipic acid at modest temperature and pressures. Moving forward, efforts are needed to transition fed-batch muconic acid production at high titers from model aromatic compounds and clean sugar substrates to complex lignocellulose derived monomers. Engineered biological conversion pathways can be incorporated to expand the number of substrates that can be utilized, particularly for non-target compounds generated during biomass depolymerization, and reduce the gap between demonstrated and theoretical yields. With regards to broth purification, upstream biological optimization will play a key role in maximizing the substrate titers compared to the level of non-target impurities, ideally allowing the economical implementation of activated carbon treatment. With regards to separation, the unique solubility of muconic acid should continue to be leveraged with rigorous characterization of non-target complex broth constituents. Lastly, low-cost PGM alternatives should be explored for upgrading of muconic acid to acid, with a focus on leaching stability and potential deactivation mechanisms. The sustained performance of promising catalytic materials can then be tested at higher muconic acid and hydrogen concentrations to minimize the impact of mass transfer and provide relevant parameters for techno-economic process modeling.

- *Preliminary techno-economic analysis for evaluating separation and catalytic unit process configurations with microbial acids.* Understanding the scalability and limitations of technologies at the bench-scale will be key to designing economically viable unit process configurations for valorizing microbial acids. As shown with muconic acid, the use of complex lignocellulosic monomers will have dramatic economic implications, as well as the dictate the performance criteria for biological conversion and separation unit processes. Lignin derived aromatic monomers are a promising substrate due to their potential low cost and high demonstrated and theoretical biological conversion yields, although further research is needed to show comparable yields in fed-batch biological conversion experiments. Increased broth titers compared to impurity levels may also facilitate low-cost separation strategies, although further study is needed to evaluate the performance and stability under continuous process conditions, as well as develop comparative economic process models for alternative separation trains (e.g., membrane treatment, reactive extraction, biphasic esterification). Likewise, efforts to replace PGM for catalytic upgrading can greatly impact the final selling price of products derived from microbial acids, indicating a key area for further investigation, as echoed above. Lastly, close coupling of techno-economic modeling and experimental design can potentially improve the rigor of unit process performance and cost estimates, while identifying linear and nonlinear economic impact factors to facilitate the selection of future research objectives.